MICROSTRUCTURE ENGINEERING WITH QUINOA PROTEIN FOR THE DESIGN OF PLANT-BASED SOFT MATERIALS

by

MARINA CAMPOS ASSUMPCAO DE AMARANTE

A thesis submitted to the University of Birmingham and the University of Melbourne for the degree of

DOCTOR OF PHILOSOPHY

School of Chemical Engineering

College of Engineering and Physical Sciences

University of Birmingham

March 2024

Abstract

The movement towards the reduction in production and consumption of animal proteins combined with the increase in world population has prompted the food industry to consider more sustainable protein sources. Quinoa is a pseudocereal that has recently gained popularity worldwide as an alternative to rice due to its higher protein content and to its complete essential amino acid profile. Quinoa protein isolate (QPI) is a protein mixture commonly extracted from quinoa flour by wet fractionation, consisting of alkalinisation of the flour suspension at pH 8 – 11 followed by acid precipitation by HCl addition to pH 4 – 5. Its physico-chemical and functional properties have been increasingly investigated in the last few years, however, there are a few gaps in literature regarding its potential to create microstructures in food systems. Thus, this study aimed to explore different approaches to enable the use of QPI in the microstructure engineering of plant-based foods.

Firstly, the phase behaviour of mixtures of QPI and maltodextrin (MD) was investigated as a function of MD dextrose equivalent, protein heat pre-treatment and salt conditions. It was found that the mixtures phase separated by depletion flocculation, where fractions of MD were entrapped within the aggregated QPI network. This behaviour does not allow for structure formation by droplet deformation under shear and limits the application of these mixtures in microstructure design. Thus, in the following steps of this research, the focus was shifted to the adjustment of the physico-chemical and technofunctional properties of QPI through the modification of its extraction conditions.

Improved soluble protein content, thermal properties and gelation properties were achieved by substituting HCl for the more kosmotropic acids acetic acid and citric acid during the acid precipitation step of QPI extraction. It was also found that the functional

properties of QPI could be further modulated by the dispersion conditions. A longer dispersion time improved the functional properties of QPI precipitated with HCl, while dispersion in 0.1 M NaCl and dialysis before dispersion resulted in extensive protein aggregation and hindered gel formation in the QPI extracts.

Results further showed that QPI can be extracted with a significant content of lipids, which are originally found in quinoa seeds in the form of oil bodies. These natural oil droplets have interesting applicability in the formulation of plant-based foods to confer desired textures and improve organoleptic properties, especially due to their naturally emulsified structure, but there is a gap in literature pertaining those sourced from quinoa. Thus, a strategy was developed to recover quinoa oil bodies (OB) before QPI extraction from cryo-milled quinoa seeds. OB of good stability against acid treatment were obtained, while a further improvement in the gelation properties of QPI precipitated with citric acid was observed. Overall, this thesis provided insights on the phase behaviour of QPI, as well as processing routes for the modulation of its properties for the design of a range of plant-based products of different textures. It also presented a combined strategy to recover two highly functional ingredients for plant-based food formulations.

Declaration of authorship

I, Marina Campos Assumpcao de Amarante, declare that:

- This thesis comprises only my original work towards the Doctor of Philosophy degree, except where indicated in the preface;
- Due acknowledgement has been made in the text to all other material used; and
- This thesis is fewer than the maximum word limit in length, exclusive of tables, maps, bibliographies and appendices.

Signed: Marina Campos Assumpcao de Amarante

Date: 25/03/2024

Preface

This thesis comprises chapters presented in article format with the following status:

Chapter 4: Atypical phase behaviour of quinoa protein isolate in mixture with maltodextrin

- Published by Food Research International on 16 October 2022;
- Author contributions: **Marina Campos Assumpcao de Amarante** (70%): Conceptualisation of study, all experiments, except for molecular weight distribution analysis, writing of original draft. **Thomas MacCalman** (2.5%): Molecular weight distribution analysis. **Stephen E. Harding** (2.5%): Development of the methodology for molecular weight distribution analysis. **Fotis Spyropoulos** (5%): Supervision and review of original draft. **Sally Gras** (10%): Conceptualisation of study, funding acquisition, project administration, supervision and review of original draft. **Bettina Wolf** (10%): Conceptualisation of study, funding acquisition, project administration, supervision and review of original draft.
- Source of funding: Priestley Joint PhD Scholarship from the University of Birmingham (UK) and The University of Melbourne (Australia).

Chapter 5: Modulation of physico-chemical and technofunctional properties of quinoa protein isolate: Effect of precipitation acid

- Published by Food Chemistry on 7 July 2024;

- Author contributions: **Marina Campos Assumpcao de Amarante** (70%): Conceptualisation of study, all experiments, writing of original draft. **Lydia Ong** (5%): Supervision and review of original draft. **Fotis Spyropoulos** (5%): Supervision and review of original draft. **Sally Gras** (10%): Conceptualisation of study, funding acquisition, project administration, supervision and review of original draft. **Bettina Wolf** (10%): Conceptualisation of study, funding acquisition, project administration, supervision and review of original draft.
- Source of funding: Priestley Joint PhD Scholarship from the University of Birmingham (UK) and The University of Melbourne (Australia).

Chapter 6: Modulation of physico-chemical and technofunctional properties of quinoa protein isolate: Effect of dispersion conditions on isolates precipitated with different acids

- Unpublished material not submitted for publication at the time of submission of this thesis;
- Author contributions: **Marina Campos Assumpcao de Amarante** (70%): Conceptualisation of study, all experiments, writing of original draft. **Lydia Ong** (5%): Supervision and review of original draft. **Fotis Spyropoulos** (5%): Supervision and review of original draft. **Sally Gras** (10%): Conceptualisation of study, funding acquisition, project administration, supervision and review of original draft. **Bettina Wolf** (10%): Conceptualisation of study, funding acquisition, project administration, supervision and review of original draft.
- Source of funding: Priestley Joint PhD Scholarship from the University of Birmingham (UK) and The University of Melbourne (Australia).

Chapter 7: Characterisation of oil bodies and protein isolates extracted from cryo-milled quinoa seeds

- Unpublished material not submitted for publication at the time of submission of this thesis;
- Author contributions: **Marina Campos Assumpcao de Amarante** (70%): Conceptualisation of study, all experiments, except for fatty acid composition analysis, writing of original draft. **Thomas Holt** (2.5%): Development and performance of fatty acid composition analysis. **Lydia Ong** (5%): Supervision and review of original draft. **Fotis Spyropoulos** (2.5%): Supervision and review of original draft. **Bettina Wolf** (10%): Conceptualisation of study, funding acquisition, project administration, supervision and review of original draft. **Sally Gras** (10%): Conceptualisation of study, funding acquisition, project administration, supervision and review of original draft.
- Source of funding: Priestley Joint PhD Scholarship from the University of Birmingham (UK) and The University of Melbourne (Australia).

Acknowledgements

As my PhD journey comes to an end, I need to thank everyone who was a part of this experience and that helped and supported me during this time.

I would first like to thank my supervisors Prof Bettina Wolf and Prof Sally Gras for their guidance throughout this project, the countless scientific discussions and meetings and for sharing all their knowledge with me. Thank you for the many opportunities you both have given me along the way and the constant professional and personal support. I am truly grateful for the opportunity to learn from both of you. A huge thank you also to my co-supervisors Dr Lydia Ong and Dr Fotis Spyropoulos for all the support, meetings, training and feedback, and most importantly for all the time invested in helping me improve my work even more.

I would also like to thank everyone from the Food Microstructure group in Birmingham for their support throughout the years and everyone from the Gras group in Melbourne for welcoming me so warmly during the last year of my PhD.

Thank you to my mentors Prof Susana Kalil, Dr Luisa Sala and Prof Anna Rafaela Braga for their friendship and constant support and encouragement. I can truly say I would not have come to this stage if it wasn't for you and the opportunities you have given me throughout my academic career.

Many thanks to all my friends for being my comic relief and/or therapists, no matter where we are in the world: Bruna, Claudia, Guilherme, Laura, Leonardo and Victoria. Thank you to my chosen family Gabrielle and Henrique for always being there for me, be it for good times or bad, for scientific theories of all kinds and amazing memories. Especial thanks also to our support network in Birmingham: Ikram, Jo, Niko, Thais and

Vitor – I can safely say Vini and I would be lost without you, thanks for answering every distress signal and for always being there for us. Finally, thank you to my very magical friends, otherwise known as Veggie's Mighty Heroes: Adam, Charlotte (your chaos is inspiring), Thomas Marie and, of course, Jo – I never imagined I would find myself a sister during all this. Thank you for all the weekends spent in the lab/office or eating pizza and playing games, the venting sessions and for giving me my dear nephew Freddie (a.k.a. Fredderick).

Thank you to all my favourite bands for translating my feelings so accurately. In especial, thank you to Fall Out Boy for being the soundtrack of my time in Australia and to Mcfly for being the soundtrack of my life.

Thank you to my family for always picking me up, for understanding my absences and for bearing with me during this time: my brothers Rafael and Vitor, my sister-in-law Tatiana, my Aunt Fatima, my dear baby nieces Sofia and Eloisa and, of course, Vinicius – you are my family and my best friend. Thank you for being with me every step of the way and for giving me a second family in your grandparents, mother and sister. Thank you for celebrating all my victories and for sharing the burden when it becomes too heavy to carry.

Lastly, I would like to dedicate this thesis to my parents, Nadia and Marcos. Thank you for your endless love and support and for all the sacrifices you made so that my brothers and I could follow our dreams. Words are not enough to express my love and gratitude.

Table of Contents

List of Tables

List of Figures

Abbreviations

3D	three-dimensional
ATPS	aqueous two-phase systems
ATR	attenuated total reflectance
B	bottom phase after phase separation
CLSM	confocal laser scanning microscopy
DE	dextrose equivalent
DP	degree of polymerization
DSC	differential scanning calorimetry
DSF	differential scanning fluorimetry
DT400	dextran of average molecular weight of 400,000 g/mol
DT5000	dextran of average molecular weight of 5,000,000 g/mol
DTT	dithiothreitol
dw	dry weight
eq	equivalent(s)
FAO	Food and Agriculture Organization of the United Nations
FTIR	Fourier transform infrared spectroscopy
HCl	hydrochloric acid
HD-SPI	heat denatured soy protein isolate
HTQPI	heat treated quinoa protein isolate
I	initial mixture
IR	infrared
κ-car	κ-carrageenan
LAr	liquid argon

LA-SPI	large soy protein isolate aggregates
Leg	legumin
LN_2	liquid nitrogen
LVE	linear viscoelastic region
MD	maltodextrin
NaOH	sodium hydroxide
Native-PAGE	Native-polyacrylamide gel electrophoresis
N-SPI	native soy protein isolate
OB	oil bodies
PAGE	polyacrylamide gel electrophoresis
pI	isoelectric point
PPDF	pea protein isolate produced by ultrafiltration
PPI	pea protein isolate
PPP	pea protein isolate produced by precipitation
QPC	quinoa protein concentrate
QPI	quinoa protein isolate
QPI-A	quinoa protein isolate precipitated by acetic acid
QPI-C	quinoa protein isolate precipitated by citric acid
QPI-H	quinoa protein isolate precipitated by hydrochloric acid
SA	sodium alginate
SA-SPI	small soy protein isolate aggregates
SDS-PAGE	sodium dodecyl sulfate-polyacrylamide gel electrophoresis
SPI	soy protein isolate
S-S	disulfide bond
STL	slope of the tie-line

T	top phase after phase separation
TAG	triacylglycerol(s)
UNU	United Nations University
WHO	World Health Organization
WPI	whey protein isolate
W/W	water-in-water

Symbols

A	area (m^2)
a	best fit parameter describing the shape of the binodal (1)
A_{11}	second virial coefficient for biopolymer 1-biopolymer 1 (cm^3/mol)
A_{12}	second virial coefficient for biopolymer 1-biopolymer 2 (cm^3/mol)
A_{22}	second virial coefficient for biopolymer 2-biopolymer 2 (cm^3/mol)
B	length of the shorter principal axis of an ellipsoid (m)
b	best fit parameter describing the shape of the binodal (1)
C	shear rate (1/s) for shear flow fields and extension rate (1/s) for extensional flow fields
D	droplet deformation (1)
δ	phase shift (°)
ΔG_{mix}	Gibbs free energy of mixing (J/mol)
ΔH	enthalpy of denaturation (J/g)
ΔH_{mix}	enthalpy of mixing (J/mol)
Δ_{ratio}	difference between the initial and final 350 nm/330 nm ratio (1)
ΔS_{mix}	entropy of mixing (J/(mol.K))
ΔT	differential temperature (°C)
$\dot{\varepsilon}$	extension rate (1/s)
F	force (N)
g	acceleration due to gravity (m/s^2)
G'	storage or elastic modulus (Pa)
G'_{20}	final gel strength (Pa) at 20 °C
G"	loss or viscous modulus (Pa)
G^*	complex shear modulus (Pa)

h	shear gap (m)
k'	calibration factor in differential scanning calorimetry (1)
L	length of the longer principal axis of an ellipsoid (m)
λ	viscosity ratio (1)
Mn	number-average molecular weight (g/mol)
Mw	molecular weight (g/mol)
n	slope of the frequency dependence of G' (1)
η_c	viscosity of the continuous phase (Pa.s)
η_d	viscosity of the dispersed phase (Pa.s)
ω	angular frequency (rad/s)
φ	deflection angle (°)
Φ_m	measured heat flow rate (W)
Φ_r	heat flow rates to the reference sample (W)
Φ_s	heat flow rate to the sample (W)
r	droplet radius (m)
ρ_1	density of the dispersed phase (kg/m^3)
ρ_2	density of the continuous phase (kg/m^3)
s	deflection path (m)
σ	interfacial tension (mN/m)
T	temperature (°C or K in Equation 2-1)
t	time (s)
τ	shear stress (Pa)
tan δ	loss factor (1)
τ_y	yield point or yield stress (Pa)
T_d	denaturation temperature (°C)

T_e	endset temperature (°C)
T_{gel}	gelation temperature or gel point (°C)
T_i	inflection temperature (°C)
T_o	onset temperature (°C)
T_p	peak temperature (°C)
v or *v*	velocity (m/s) or creaming velocity (m/s)
Vf_B	volume fraction of the bottom phase (1)
Vf_T	volume fraction of the top phase (1)
x	droplet diameter (m)
χ_{12}	Flory interaction parameter for biopolymer 1-biopolymer 2 (1)
χ_{1s}	Flory interaction parameter for biopolymer 1-solvent (1)
χ_{2s}	Flory interaction parameter for biopolymer 2-solvent (1)
γ	shear strain (%)
$\dot{\gamma}$	shear rate (1/s)

Copyrights declaration

Citation Information for Third party copyright material	Location of item in thesis	Permission granted Y/N
Figure 1a from Norton, I.T. and Frith, W.J. (2001) 'Microstructure design in mixed biopolymer composites', *Food Hydrocolloids*, 15 (4–6), pp. 543–553. doi:10.1016/S0268-005X(01)00062-5.	p. 24	Y
Figure 18 from Prego, I., Maldonado, S. and Otegui, M. (1998) 'Seed structure and localization of reserves in *Chenopodium quinoa*', *Annals of Botany*, 82 (4), pp. 481–488. doi:10.1006/anbo.1998.0704.	p. 40	Y
Figures 4.2, 8.1, 9.3 and 9.6 from Anton Paar, Educational resources (no date) *Basics of rheology*. Available at: https://wiki.anton-paar.com/en/basics-of-rheology/ (Accessed: 13 January 2024).	p. 63	Y

Chapter 1. Introduction

1.1 Research background and motivation

Proteins of animal origin, such as milk, egg and meat proteins, are of high quality due to their complete essential amino acid content, which cannot be synthesised by humans and can only be obtained through diet. These proteins greatly contribute to the overall properties of food products, including texture, appearance and mouthfeel, due to their specific functional properties, such as emulsification and water holding capacity, as well as the ability to form gels (Damodaran, Parkin and Fennema, 2008; Asgar et al., 2010; Xiong, 2018). However, there is a recent movement towards the reduction in production and consumption of animal proteins, which is motivated by three main issues. Firstly, animal welfare has been a pressing concern of consumers, who are susceptible to animal cruelty and their unethical treatment during rearing, transportation and slaughter (Kumar et al., 2017). Secondly, the overconsumption of animal products, particularly red meat, has been associated with public health issues, such as increase in the incidence of cardiovascular disease, diabetes and colorectal cancer (Post, 2012). Finally, the production of poultry and livestock, including beef, pig, lamb and mutton, requires large amounts of water (total of 5,700 L/kg of food) and land space (725 m^2/kg food) and it is accountable for 46% of the global emissions of greenhouse gases (161 kg CO_2eq/kg food), greatly contributing to climate change (Ritchie, Rosado and Roser, 2020).

The food industry is thus considering more sustainable sources of protein to address these issues, as well as to ensure food and nutrition security for an increasing world population (Asgar et al., 2010; United Nations Department of Economic and Social affairs, 2015; Lonnie et al., 2018; Augustin and Cole, 2022). Plant proteins have recently attracted attention from the scientific community because, compared to animal proteins, plant

protein production is cheaper (Asgar et al., 2010), requires a fraction of the water and land space (Mattice and Marangoni, 2019) and emits lower levels of greenhouse gases (Scarborough et al., 2014). Moreover, plant protein consumption is reported to lower the risk of diabetes, cardiovascular disease, hypertension and some types of cancer (Huang et al., 2012; Yokoyama et al., 2014; Wang et al., 2015). However, it should be noted that plant proteins may show a few health and nutritional limitations compared to animal proteins, including a lower average essential amino acid content, lower protein digestibility and lower protein content per serving. These drawbacks can be overcome by combining different food groups to ensure adequate essential amino acid intake, as well as by applying processing techniques to improve protein digestibility and by increasing the serving sizes of plant proteins (Gorissen et al., 2018; Nichele, Phillips and Boaventura, 2022).

A keyword search (January/2024) in the Scopus database has shown that the number of publications per year containing the term “plant protein” or “plant-based protein” increased from 762 papers in 1993 to 5,339 papers in 2020, which was the year with the most publications in the field so far (Figure 1-1). Since then, there has been a decrease in the number of papers published, reaching 3,824 in 2023. However, the enthusiasm towards plant proteins is still growing, as projections show that the market for plant-based foods can reach USD 162 billion by 2030, a significant growth from USD 29 billion in 2020 (Bartashus and Srinivasan, 2021).

Food microstructure is defined as the arrangement of different material phases, visible at microscopic scale, arising from the organisation and interaction of each food component or ingredient, including proteins, polysaccharides and oils/fats (Aguilera, 2005; Verboven, Defraeye and Nicolai, 2018). Proteins are one of the most important

ingredients used to create microstructures in many food products due to their unique physico-chemical and technofunctional properties, also referred to as "functionality". These include the ability to stay dissolved or suspended, to emulsify oils/fats and to create foams and soft-solid gels (Loveday, 2020; McClements and Grossmann, 2021).

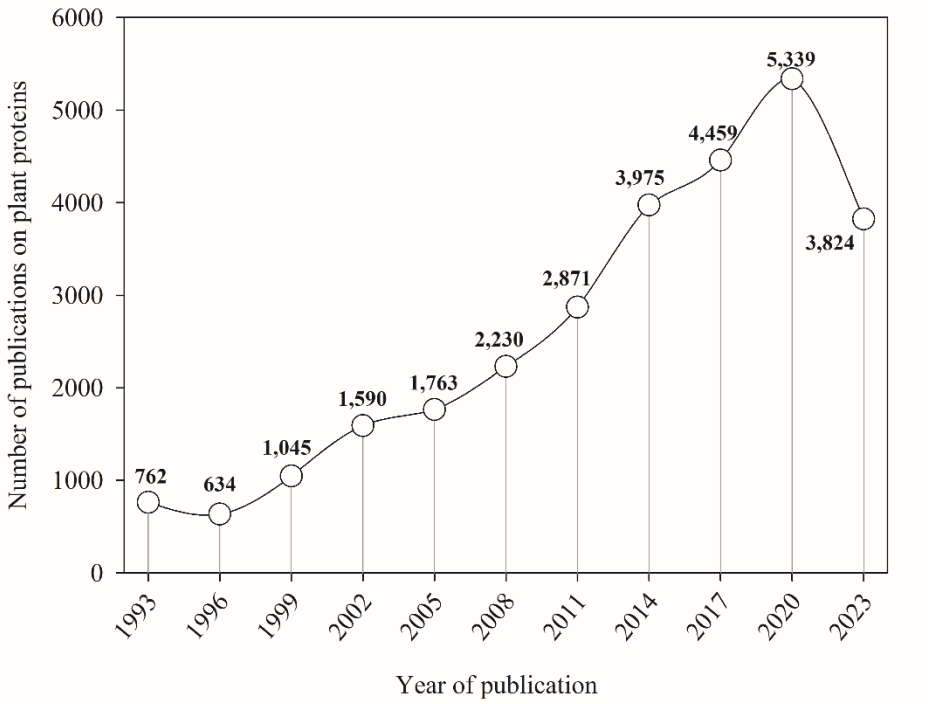

Figure 1-1. Number of publications containing the term "plant protein" or "plant-based protein" over the last 30 years (1993 – 2023). Data extracted from Scopus in January/2024.

Most plant proteins, however, have reduced functionality compared to animal proteins, such as low solubility and poor foaming, emulsifying and gelation properties, which limits their ability to fully replace animal proteins in the creation of desirable and predictable microstructures in food products (Loveday, 2020; McClements and Grossmann, 2021). This arises from fundamental structural differences between animal and plant proteins (McClements and Grossmann, 2021). Additionally, the most

commonly applied method for plant protein extraction from different sources is wet fractionation, which is reported to cause protein denaturation and impairment of some of the protein functionality due to harsh solvent conditions (Schutyser and van der Goot, 2011; Opazo-Navarrete et al., 2018a; Kumar et al., 2021; Hopf, Dehghani and Buckow, 2023; Lie-Piang et al., 2023). Several approaches can be applied to overcome these drawbacks, though, including mixing plant proteins with other biopolymers to adjust structural and functional properties and modifying the conditions used for their extraction from the plant matrix (Nasrabadi, Doost and Mezzenga, 2021; Sim et al., 2021).

Plant proteins can be recovered from a variety of sources, including cereals and pseudocereals, legumes, seeds and tubers (Schmitt et al., 2021). Currently, according to another keyword search (January/2024) in the Scopus database, the most investigated plant proteins are soy protein (Grabowska et al., 2016; Chiang et al., 2019; Chantanuson et al., 2022), pea protein (Yin, Zhang and Yao, 2015; Lan, Chen and Rao, 2018; Kornet et al., 2021) and wheat protein (Pietsch, Emin and Schuchmann, 2017; Samard, Gu and Ryu, 2019) (Figure 1-2). Soy has been used in Asian countries for centuries as a protein source for texturised products such as tofu and tempeh (Felix et al., 2021). Due to its complete essential amino acid composition and its ability to provide a desired texture and appearance to the final product, it is currently the most commonly used protein in the formulation of plant-based foods, especially meat analogues (Akdogan, 1999; Chen et al., 2010; Fang, Zhang and Wei, 2014; Samard and Ryu, 2019). Although it lacks in essential amino acid content, wheat protein is also extensively applied in plant-based foods due to its unique texturisation properties (Veraverbeke and Delcour, 2002; Ruiz-Capillas and Herrero, 2024). Both of these proteins are sources of food allergens though, which is a limitation from a consumer acceptance and safety point of view (Sun et al., 2021). Pea

protein is increasingly explored as a substitute to soy protein (Figure 1-2), as it also shows a complete essential amino acid content, as well as comparable functional properties, while displaying low allergenicity (Gorissen et al., 2018; Lam et al., 2018; Liu et al., 2022).

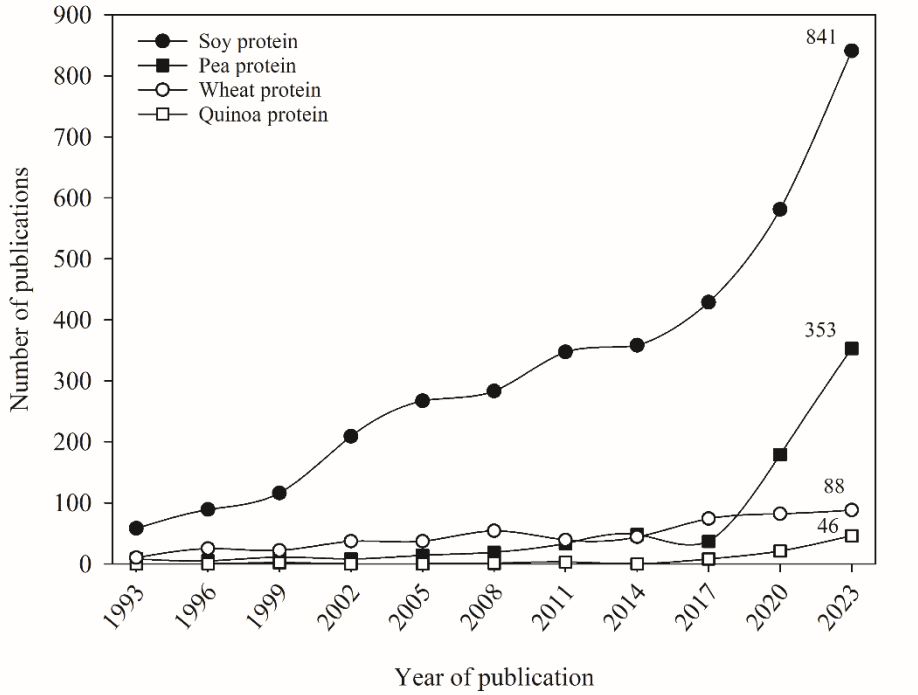

Figure 1-2. Number of publications containing the term "soy protein" (●), "pea protein" (■), "wheat protein" (○) or "quinoa protein" (□) in the last 30 years (1993 – 2023). Data extracted from Scopus in January/2024.

Nonetheless, there is still the need for diversifying plant protein sources to ensure food security through the implementation of sustainable, equitable and resilient diets, in which unconventional crops may play a fundamental role (Granado-Rodríguez et al., 2022; Bogueva and McClements, 2023; Chaudhary, Walia and Kumar, 2023). Thus, other protein sources such as chickpea (Boye et al., 2010), beans (Tang, 2008), lentils (Quintero

et al., 2022), faba bean (Johansson et al., 2022) and quinoa (Ruiz et al., 2016b) have begun to attract the attention of researchers.

Quinoa is a pseudocereal that has good endurance to the challenges imposed by climate change, including resistance to heat, drought and high salinity soils, and thus shows great potential to contribute to worldwide food security in the upcoming years (Chaudhary, Walia and Kumar, 2023). Its seeds contain 12 – 19% (w/w) of high quality protein with a complete essential amino acid profile, including 2.4 – 8.3 g/100 g protein of histidine, 3.2 – 4.6 g/100 g protein of isoleucine, 4.5 – 7.9 g/100 g protein of leucine, 5.1 – 13.5 g/100 g protein of lysine, 1.4 – 2.6 g/100 g protein of methionine, 3.4 – 4.8 g/100 g protein of phenylalanine, 3.4 – 7.8 g/100 g protein of threonine, 0.4 – 1.7 g/100 g protein of tryptophan and 3.7 – 6.4 g/100 g protein of valine (Ruales and Nair, 1992; de Bock et al., 2021; Gómez et al., 2021).

Quinoa protein isolate (QPI) is a protein mixture extracted from quinoa flour by wet or dry fractionation (Opazo-Navarrete et al., 2018a). It is an emerging protein source for protein-rich foods due to its complete essential amino acid composition (Abugoch et al., 2008; Luo et al., 2022a). Thus, its physico-chemical and technofunctional properties, including solubility, foaming and emulsifying capacity, water and oil holding capacity, thermal properties and gelation properties, have been increasingly investigated in the last few years (Figure 1-2) (Abugoch et al., 2008; Ruiz et al., 2016b; Steffolani et al., 2016; Mir, Riar and Singh, 2019a, 2019b, 2021a, 2021b, 2023; Vera et al., 2019; Luo et al., 2022a).

There are, however, several gaps in the understanding of quinoa protein isolate. There are a few reports on the phase behaviour of segregative mixtures of QPI with polysaccharides, including carrageenan, guar gum, locust bean gum and xanthan gum (Duran et al., 2018b;

Patole, Cheng and Yang, 2022; Agarwal et al., 2023); nonetheless, there are no studies on the creation of phase diagrams of these systems. Biopolymer mixtures can be used to create structures, textures and appearances that cannot be achieved by a single polymer, and the understanding of their phase behaviour through the construction of phase diagrams is central for the design of predictable microstructures for food applications, as it allows for the determination of workable phase volumes, compositions and mixture microstructures (Norton and Frith, 2001). Further, while one previous work has shown that precipitation with HCl, citric acid and malic acid has diverse effects on some structural and functional properties of okara protein isolate (Cai et al., 2020), there are no reports on the impact of precipitation with different acids on the thermal properties and gelation behaviour of plant proteins. As these properties are determining factors in the application of these proteins in the structuring of food products, the study of the acid used during QPI extraction may offer opportunities to improve the functionality of these proteins and further expand their applications.

Quinoa seeds also have a lipid content of 6.5 – 6.8% (w/w) (Elsohaimy, Refaay and Zaytoun, 2015; Alonso-Miravalles and O'Mahony, 2018), higher than that of other emerging plant protein sources, such as pea and lentil, which have a lipid content of less than 3.0% (w/w) (Chung et al., 2008). In seeds, lipids are present in the form of oil bodies, which are stabilised by a monolayer of phospholipids anchored at the interface with the hydrophobic region of oil body-associated proteins. Due to their naturally-emulsified structure, plant oil bodies can be used in emulsion-based food formulations to build structure and improve the organoleptic properties of the products without the need for additional emulsifiers and homogenisation steps (Iwanaga et al., 2007, 2008; White et al.,

2008; de Chirico et al., 2018). However, there is a gap in the literature concerning the isolation and characterisation of quinoa oil bodies and their associated proteins.

Considering the need to diversify the plant protein sources currently in use and the identified gaps in the literature regarding the structuring potential of quinoa protein, the overall aim of this thesis was to explore the use of quinoa protein isolate in the microstructure engineering of plant-based foods. Firstly, the phase behaviour of QPI and maltodextrin mixtures was studied as a function of maltodextrin dextrose equivalent, protein heat pre-treatment and salt conditions. This study aimed to assess whether these mixtures could be used in the creation of tailored microstructures for the design of plant-based products, such as gel particles and fibres formed by droplet deformation and gelation of the protein phase under shear, which has not yet been reported for biopolymer mixtures involving plant proteins. Maltodextrin was chosen because it has been widely applied as a phase separating polysaccharide, mainly in mixture with refined animal proteins, such as gelatine and caseinate (Kasapis et al., 1993b; Manoj, Kasapis and Chronakis, 1996; Williams et al., 2001; Loret et al., 2005; Beldengrün et al., 2018). This allows the comparison between its phase behaviour with both types of proteins. Secondly, different acids were used during the precipitation step of wet fractionation for QPI extraction aiming at modulating or improving the protein's physico-chemical and functional properties. For the first time, the impact of the different acid treatments on the thermal properties and gelation behaviour of QPI was evaluated at different protein concentrations and dispersion conditions. Finally, after identifying quinoa seeds as a potential source of natural oil bodies, a novel strategy to recover these structures before QPI extraction was developed to obtain two highly functional ingredients for the microstructure engineering of plant-based foods.

1.2 Thesis outline

This thesis consists of 8 chapters. In the current **Chapter 1**, a general introduction to the research is presented, including the context and motivation of the study, overall aim, thesis layout and a list of publications and presentations. In **Chapter 2**, the relevant and current literature related to this research is reviewed and the specific objectives of the thesis are presented. In **Chapter 3**, the main analytical techniques used in this thesis are reviewed. Chapters 4 to 7 are publication-style chapters. **Chapter 4** is based on a published paper, reformatted as a thesis chapter, where the phase behaviour of mixtures of quinoa protein isolate and maltodextrin is investigated as a function of maltodextrin dextrose equivalent, protein heat pre-treatment and salt concentration. In **Chapter 5** the influence of the precipitation acid on the physico-chemical and technofunctional properties of quinoa protein isolate is reported. In **Chapter 6** the impact of the dispersion conditions of quinoa protein isolate extracted with different acids is further explored. In **Chapter 7** oil bodies were recovered from cryo-milled quinoa seeds before quinoa protein isolate extraction and evaluation of its functional properties. Lastly, in **Chapter 8** the main conclusions of this research and recommendations for future work are presented. The list of references used throughout the thesis is also presented, as well as four appendices comprising the supplementary materials of the publication-style chapters, as published, submitted or prepared for submission to peer reviewed journals.

1.3 Dissemination of research work

Publications in scientific journals

1. Amarante, M.C.A., MacCalman, T., Harding, S.E., Spyropoulos, F., Gras, S. and Wolf, B. (2022) 'Atypical phase behaviour of quinoa protein isolate in mixture with maltodextrin', *Food Research International*, 162, pp. 112064. doi:10.1016/j.foodres.2022.112064.

2. Amarante, M.C.A., Ong, L., Spyropoulos, F., Gras, S. and Wolf, B. (2024) 'Modulation of physico-chemical and technofunctional properties of quinoa protein isolate: Effect of precipitation acid', *Food Chemistry*, 457, pp. 140399. doi:10.1016/j.foodchem.2024.140399

Presentations at scientific conferences

1. Amarante, M.C.A., Spyropoulos, F., Gras, S. and Wolf, B. (2021) 'Phase behaviour and microstructure of quinoa protein isolates and maltodextrin mixtures', oral presentation at the International Conference on Formulations in Food and Healthcare, online event, 8 – 11 March, 2021.

2. Amarante, M.C.A., Spyropoulos, F., Gras, S. and Wolf, B. (2021) 'Phase behaviour of quinoa protein isolates and maltodextrin for the microstructure engineering of plant-based foods', poster presentation (online) at the 35th Conference of the European Colloid & Interface Society, Athens, Greece, 5 – 10 September, 2021.

3. Amarante, M.C.A., Gras, S. and Wolf, B. (2022) 'Effect of acid precipitation on the gelation properties of quinoa protein isolate', oral presentation at the Annual European Rheology Conference, Seville, Spain, 26 – 28 April, 2022.
4. Amarante, M.C.A., Gras, S. and Wolf, B. (2022) 'Atypical phase behaviour of quinoa protein isolate-maltodextrin mixtures', oral presentation at the Total Food 2022 conference, Nottingham, UK, 13 – 14 July, 2022.
5. Amarante, M.C.A., Spyropoulos, F., Gras, S. and Wolf, B. (2022) 'Microstructure engineering with quinoa protein isolate', poster presentation at the 36th European Federation of Food Science and Technology International Conference, Dublin, Ireland, 7 – 9 November, 2022.
6. Amarante, M.C.A., Ong, L., Wolf, B. and Gras, S. (2023) 'Impact of cryo-milling of quinoa seeds in quinoa protein isolate gelation: a microstructure engineering strategy for the design of meat analogues', oral presentation at the Delivery of Functionality in Complex Food Systems, Melbourne, Australia, 25 – 27 October, 2023.

Chapter 2. Literature review

2.1. The challenge of food structure creation with plant proteins

Plant proteins have recently attracted a lot of interest from the research community as more sustainable, cheaper and healthier alternatives to animal proteins (Nasrabadi, Doost and Mezzenga, 2021). The first step for their utilisation is the extraction from the plant matrix by an appropriate method. Plant proteins are rarely studied as purified protein fractions and are more often found as concentrates or isolates composed of different proteins in mixture, which are extracted together from the raw material (Loveday, 2020). Many different extraction methods can be applied, including wet fractionation (Ruiz et al., 2016b), dry fractionation (Opazo-Navarrete et al., 2018b), salt extraction (Sun and Arntfield, 2010), enzyme-assisted extraction (Houde et al., 2018), ultrasound-assisted extraction (Quintero et al., 2022), microwave-assisted extraction (Ochoa-Rivas et al., 2017) and pulsed electric fields-assisted extraction (Sarkis et al., 2015).

Plant protein extracts tend to be a mixture of native (soluble monomers or oligomers) and denatured (mostly insoluble aggregates) proteins, while the balance between these two states depends on the physico-chemical changes imposed during their recovery from the plant source. These two colloidal states of protein influence the functional properties of the concentrates or isolates (Schmitt et al., 2021; Grossmann and McClements, 2023).

Due to fundamental structural differences arising from distinct physiological functions and polypeptide sequences, plant proteins usually show reduced functionality compared to animal proteins. The main proteins in plants are globular, which are approximately spherical colloids of relatively rigid structure. Plant globular proteins are more hydrophobic than animal proteins, due to their function as inert and compact protein

storage in seeds, and thus show lower solubility in water and consequently lower foaming, emulsifying and gelation properties. As such, their capacity to replace animal proteins in the creation of desirable and predictable food structures is limited (Loveday, 2020; Nasrabadi, Doost and Mezzenga, 2021; Sim et al., 2021; Day, Cakebread and Loveday, 2022; Grossmann and McClements, 2023). Further, many of the proteins from animal sources have unique structural characteristics that set them apart from globular proteins. For example, muscle meat is composed of a complex structural hierarchy containing the fibrous proteins actin and myosin at its core, while milk contains the highly flexible casein in the form of micelles that are disrupted and coagulate in cheese and yoghurt production. Thus, the key challenge in the production of plant-based foods that mimic animal-based products is to assemble the plant proteins into structures that result in physico-chemical and textural properties that are similar to those offered by animal proteins (McClements and Grossmann, 2021). Several approaches have been developed to overcome this challenge, including the mixture with other biopolymers, the modification of plant protein extraction conditions and the modification of their structure and functionality after extraction by different physical, chemical or biological treatments, including heat treatment, high pressure homogenisation, extrusion, glycation, phosphorylation and fermentation (Akharume, Aluko and Adedeji, 2021; McClements and Grossmann, 2021; Nasrabadi, Doost and Mezzenga, 2021; Sim et al., 2021). This thesis covers two of these approaches: biopolymer mixtures between plant proteins and polysaccharides and the modification of plant protein extraction conditions, envisaging the creation of tailored microstructures for food formulations. Both approaches are reviewed in detail in the following.

2.1.1 Heat-induced gelation of globular proteins

Before going into detail on the microstructure engineering approaches explored in this thesis, it is necessary to discuss protein gelation, as it is one of the most important mechanisms for developing structure in food systems and it is relevant in the context of both approaches studied. Protein gelation may be induced by several processes, such as increase in ionic strength, acidification, enzymatic hydrolysis and/or pressure, but the most common method is by thermal treatment, that is, heating or cooling (Nicolai, 2019). The gelation mechanism and the type of network formed will confer different textures and influence the sensory properties of the product. Examples of food products formed by different protein gelation mechanisms include cheese (enzymatic hydrolysis), yoghurt (acidification) and meat analogues (shear and thermal treatment) (Norton et al., 2015; Dekkers, Nikiforidis and van der Goot, 2016; Nicolai, 2019; McClements and Grossmann, 2022). This section introduces the heat-induced gelation of globular proteins.

The native (folded) structure of globular proteins in aqueous solution is stabilised by the electrostatic repulsion between protein molecules and maintained by their net charge. Most proteins show a negative net charge at alkaline pH values and positive net charge at acidic pH values. These states are separated by the pH where the protein's net charge is zero, called the isoelectric point (pI). Nonetheless, proteins still contain both negatively- and positively charged amino acids at their surface over a wide pH range, independently from their net charge.

When heated, the structure of globular proteins denatures (unfolds), exposing amino acids previously located in the interior of the folded structure, which become available to interact with other proteins by covalent disulfide bridges, hydrogen bonds and hydrophobic interactions, triggering protein aggregation (Kharlamova et al., 2016;

Nicolai, 2019). Depending on the strength of the electrostatic repulsions between the proteins, the aggregates can form either strands or spherical microgels and, at critical concentrations, filamentous or particulate gels are formed, respectively, in a process called heat-induced gelation (Figure 2-1) (Kharlamova et al., 2016; Duran, Spelzini and Boeris, 2019).

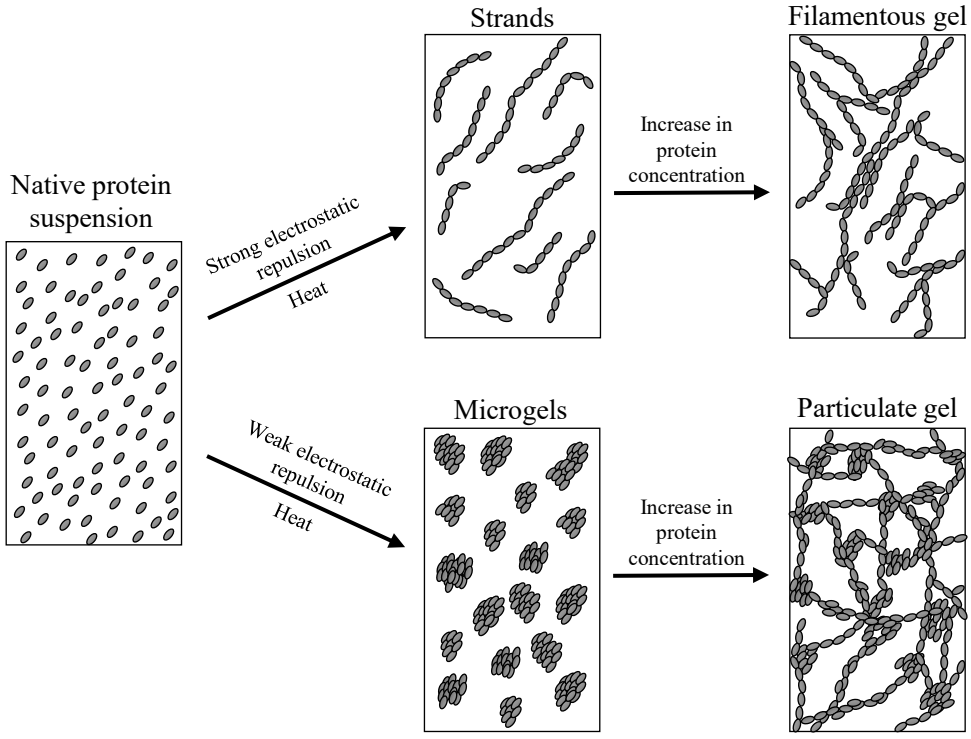

Figure 2-1. Gel formation of globular proteins. Adapted from Bryant and McClements (1998).

If the electrostatic repulsion between protein molecules is strong, protein-protein interactions form only at certain points of the protein surface and the aggregates tend to organise in strands; whereas if the electrostatic repulsion between protein molecules is weak, protein-protein interactions form at any point of the protein surface, leading to the formation of spherical aggregates, so-called microgels (Figure 2-1) (Bryant and McClements, 1998; Nicolai, 2019). As more protein denatures and aggregates, both types

of aggregates are strengthened by inter- and intramolecular disulfide bonds resulting from sulfhydryl-disulfide interchange or sulfhydryl oxidation (McSwiney, Singh and Campanella, 1994). As the protein concentration reaches a critical value, or the ionic strength increases, a three-dimensional network of strands or fractal aggregates is formed, resulting in either a filamentous or a particulate (network of crosslinked microgels) gel, respectively (Figure 2-1) (Bryant and McClements, 1998). Then, as the heat-induced protein gels are cooled, the gel network may undergo restructuring and reinforcement as a consequence of the strengthening of hydrogen bonds and electrostatic forces upon cooling (Chen and Dickinson, 1999; Nicolai, 2019). Based on confocal laser scanning microscopy (CLSM, Section 3.3) evidence, it has been reported that filamentous gels appear as a homogeneous network, while particulate gels appear as an aggregated network of microgels, although clear distinction between the two structures is not always straightforward. Further, a mixture of these two types of gel microstructures can be found at intermediate electrostatic repulsions between protein molecules (Bryant and McClements, 1998; Nicolai, 2019).

The heat-induced gelation of globular proteins, as with most other functional properties, is dictated by the initial content of native (soluble) proteins in suspension, as it is the unfolding of the protein structure during heat treatment that triggers irreversible aggregation and network formation (Brodkorb et al., 2016; Nicolai, 2019). For this reason, proteins that undergo extensive denaturation during extraction and processing, such as most commercial plant protein products, usually show a low content of soluble protein and poor heat-induced gelation capacity, as has been reported for pea protein isolate (Ben-Harb et al., 2018; Schmitt et al., 2021; Moll et al., 2023). Thus, to promote the wider application of plant proteins as food ingredients for microstructure creation, it

is crucial to design the extraction process in order to maximise protein yield while preserving the native protein structure and, consequently, its gelation capacity (Schmitt et al., 2021).

2.2 Biopolymer mixtures

Biopolymer mixtures are extensively applied in the food and allied industries to create product microstructures, rheologies, textures and appearances which cannot be achieved by the use of a single biopolymer (Norton and Frith, 2001). The design of products containing these systems relies on the understanding of their interaction mechanisms, phase behaviours and microstructure-rheology relationships, all of which influence the physico-chemical and functional properties of these mixtures, consequently defining their possible applications (Frith, 2010). The mixing of two biopolymers in a common solvent can lead to a one-phase or two-phase system, depending on the characteristics of the biopolymers and the solvent conditions. In one-phase systems, the biopolymers either form soluble complexes or are co-soluble, while in two-phase systems the mixture separates into phases of different biopolymer compositions (Matalanis, Jones and McClements, 2011). These types of phase behaviours are encountered for protein-protein, protein-polysaccharide and polysaccharide-polysaccharide mixtures.

2.2.1 Phase behaviours

The phase behaviour of biopolymer mixtures is classified into two types: associative and segregative. In the context of this thesis, Figure 2-2 depicts the general phase behaviours of biopolymer mixtures on the example of globular proteins and polysaccharides.

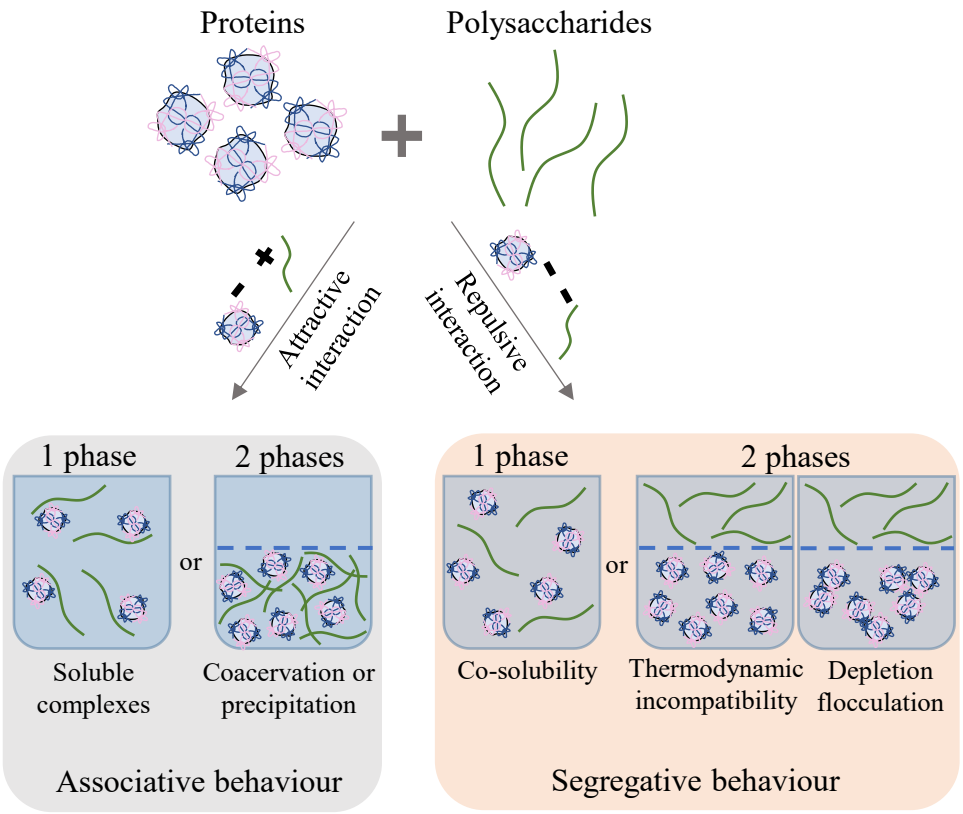

Figure 2-2. Phase behaviour resulting from the attractive or repulsive interactions between globular proteins and polysaccharides in an aqueous system. Adapted from Matalanis, Jones and McClements (2011).

Associative phase behaviour is most frequently encountered in mixtures of oppositely charged biopolymers. The polymers associate by electrostatic interactions, forming either a one-phase system of soluble complexes at low concentrations, or a two-phase system at high concentrations where one of the phases is rich in coacervates or precipitates of the associated biopolymers while the other phase is rich in solvent (Figure 2-2) (Matalanis, Jones and McClements, 2011). The formation of a coacervate or a precipitate depends on the characteristics of the polymers and the nature of their interaction; coacervates are spherical insoluble complexes where charge neutrality is achieved, while precipitates are amorphous solid-like particles formed by strong electrostatic attraction between densely-charged neighbouring molecules (Moschakis and Biliaderis, 2017).

When the system is composed of two similarly charged polymers, or of a charged and a neutral polymer which show repulsive interaction in solution, segregative phase behaviour is observed. Generally, at concentrations below the phase separation threshold, defined as the minimum overall biopolymer concentration in the mixture required for phase separation (Tolstoguzov, 2002), the system displays one phase where the components are co-soluble. At concentrations equal or above the phase separation threshold, the mixture separates into two phases, where each phase is rich in one of the polymers and depleted of the other (Figure 2-2) (Matalanis, Jones and McClements, 2011). Phase segregation is enhanced, that is, the phase separation threshold decreases, by an increase in the molecular weight of at least one of the polymers, increase in ionic strength and/or increase in temperature. In mixtures containing proteins, the separation is also affected by the pH value as it affects the protein charge, solubility and aggregation state (Tolstoguzov, 2000b). Further, segregative phase separation may occur by two different mechanisms: (1) thermodynamic incompatibility or (2) depletion flocculation.

2.2.1.1 Thermodynamic incompatibility

Thermodynamic incompatibility refers to the limited miscibility exhibited by biopolymer mixtures. It is determined by the Gibbs free energy of mixing (ΔG_{mix}, J/mol), which is given by the balance between the enthalpy (ΔH_{mix}, J/mol) and entropy (ΔS_{mix}, J/(mol.K)) of mixing at varying temperature (T, K), as shown in Equation 2-1.

$$\Delta G_{mix} = \Delta H_{mix} - T\Delta S_{mix} \quad (2\text{-}1)$$

The mixture is miscible if ΔG_{mix} is negative and demixes into two phases if ΔG_{mix} is positive, while ΔH_{mix} is a measure of the total energy of the system and is always positive, favouring demixing. The mixing entropy of polymers is small, so biopolymer mixtures tend to phase separate ($\Delta G_{mix} > 0$) (Tolstoguzov, 2000b).

The molecular origin of thermodynamic incompatibility arises from the fact that the macromolecules in the mixture cannot occupy the same volume, the so-called excluded volume effect. It reflects the competition between the molecules for solvent space, leading to small repulsive interactions between the two biopolymers (Tolstoguzov, 2000b). These interactions in biopolymer mixtures displaying thermodynamic incompatibility can be predicted by theoretical models, such as the Flory-Huggins model or the second virial coefficient model (Doublier et al., 2000).

The Flory-Huggins model expands Equation 2-1 to consider the molecular volume of the polymers and the solvent and includes the Flory interaction parameters for biopolymer 1-solvent (χ_{1s}), biopolymer 2-solvent (χ_{2s}) and biopolymer 1-biopolymer 2 (χ_{12}) (Zaslavsky, 1995). When χ_{12} is large and positive, the polymers display mutual repulsion and interactions between each of the biopolymers and the solvent are favourable, which results in the demixing of the system into two phases, each phase rich in one of the biopolymers (Figure 2-2). Alternatively, if χ_{12} is negative, interactions between the polymers are favourable, to the detriment of biopolymers-solvent interactions, leading to associative phase behaviour (Doublier et al., 2000).

The second virial coefficient approach, on the other hand, expands the chemical potential expression of each component of the mixture to include the second virial coefficients representing the interactions between biopolymer 1-biopolymer 2 (A_{12}), biopolymer 1-biopolymer 1 (A_{11}) and biopolymer 2-biopolymer 2 (A_{22}) (Zaslavsky, 1995). A positive

value for A_{12} indicates a thermodynamically unfavourable interaction between the biopolymers, leading to an increase in their chemical potentials, which represents the increase of their effective concentration in the mixture. Thus, biopolymer-solvent interactions are favourable, leading to segregative phase separation. Oppositely, a negative value for A_{12} indicates a thermodynamically favourable interaction between the biopolymers, leading to associative phase separation (Semenova, 2007; Dickinson, 2019).

Segregative systems displaying thermodynamic incompatibility are often referred to as aqueous two-phase systems (ATPS) and water-in-water (W/W) emulsions can be formed in these systems (Esquena, 2016). W/W emulsions are colloidal dispersions where droplets of the phase with the smaller phase volume are dispersed in the other phase (Tolstoguzov, 2003). This droplet microstructure indicates the existence of interfacial energy between the two liquid phases (Norton and Frith, 2001). However, due to the dispersion of both phases in a common solvent (typically water), interfacial tension values of W/W emulsions are low, ranging between 0.5×10^{-3} mN/m and 500×10^{-3} mN/m (Ding et al., 2002), while typical values for oil/water systems are ~30 mN/m in the absence of surfactants (Esquena, 2016).

W/W emulsions can be directly added to food formulations to confer structure stability or specific textural properties (Wolf et al., 2001), combined with other materials to improve their droplet stability prior to application (Matalanis, Jones and McClements, 2011; Esquena, 2023), or further processed to create other microstructures (Norton and Frith, 2001). The latter approach will be further discussed in Section 2.2.3.

2.2.1.2 Depletion flocculation

The Flory-Huggins model or the second virial coefficient model are only valid to analyse protein-polysaccharide phase behaviours when the dissolved protein behaves similarly to a polysaccharide, as is the case for gelatin, for example. In systems involving globular proteins and polysaccharides, depletion flocculation may occur (Doublier et al., 2000). Polysaccharides lose conformational entropy when confined between two neighbouring globular proteins resulting in a depletion of polymers in the region between the colloidal entities. In this so-called depleted region, the concentration of polymer is lower than in the bulk solution, creating a difference in osmotic pressure, which favours the displacement of solvent from the depleted region to the bulk and induces attractive interactions between the globular proteins (Tuinier, Dhont and de Kruif, 2000). This effect is similar to the observed when polysaccharides are added to oil-in-water emulsions (McClements, 2000).

Although depletion flocculation also results in segregative phase separation, it differs from the thermodynamic incompatibility mechanism displayed by biopolymers in solution because it involves a suspension of colloidal entities, which are thermodynamically unstable. The change from a solution to a colloidal suspension decreases the phase separation threshold of the system. As a result, based on the study of many different mixtures in literature, including mixtures between two polysaccharides (e.g., dextran and polyethylene glycol, and dextran and methylcellulose), between two proteins (e.g., ovalbumin and soybean globulins), or between a protein and a polysaccharide (e.g., gelatin and alginate, and casein and dextran), it is generally reported that systems displaying thermodynamic incompatibility require a phase separation

threshold of above 4%, while systems displaying depletion flocculation require biopolymer concentrations of less than 1% (Doublier et al., 2000; Tolstoguzov, 2000b).

Segregative systems displaying depletion flocculation show a microstructure of protein aggregates dispersed in the polysaccharide continuous phase (Figure 2-2) (de Bont, van Kempen and Vreeker, 2002). In these systems, the protein aggregates may form a volume-spanning network containing domains of polysaccharide entrapped within the network (de Bont, van Kempen and Vreeker, 2002; Li et al., 2008b; Mession et al., 2012b).

2.2.2 Phase diagrams of segregative phase behaviours

The phase behaviour of biopolymer mixtures, independent of phase separation mechanism, can be investigated by the construction of phase diagrams. For two-biopolymer mixtures, these usually show the weight fraction of each biopolymer on either axis, while the concentration of the solvent (typically water) is given by difference. The phase diagram in Figure 2-3a represents a segregative system where the two phases have a similar overall concentration of polymer, resulting in a symmetrical diagram. However, phase diagrams of biopolymer mixtures are often asymmetric regarding the overall compositions of the separated phases (Figure 2-3b) (Tolstoguzov, 2000a).

In phase diagrams, a binodal curve (solid curve in Figure 2-3a) separates the one-phase region, located below the curve, from the two-phase region, located above the curve. Tie-lines (line TB in Figure 2-3a) connect the binodal points corresponding to the compositions of the co-existing phases of a same mixture. The phase volume ratio corresponds to the ratio between the tie-line segments between the top phase composition (T) and the initial mixture and between the bottom phase composition (B) and the initial

mixture. Mixtures of composition given by any point located on a particular tie-line are likely to separate into two equilibrated phases of polymer compositions given by points T and B, although the phase volume ratios are different (Dickinson, 2019).

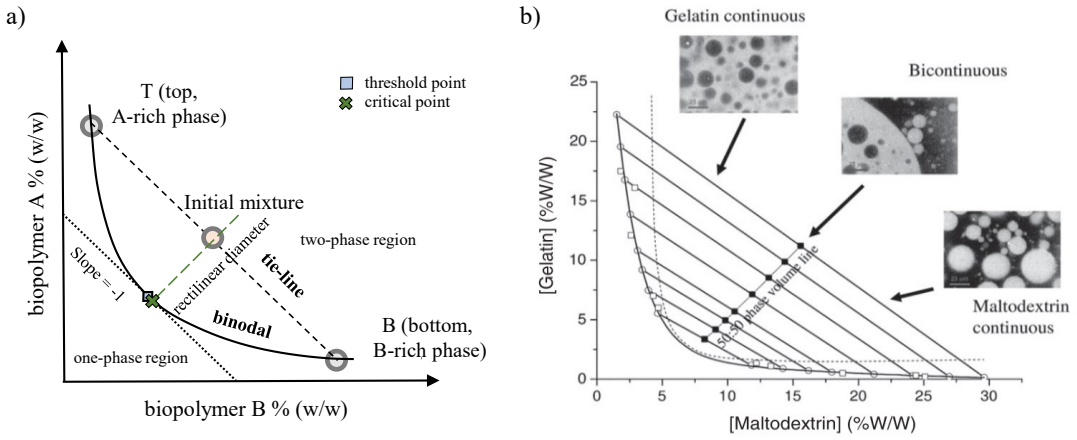

Figure 2-3. Typical phase diagram for a segregative phase behaviour of two biopolymers in aqueous solution: a) schematic and b) experimental phase diagram between gelatin and maltodextrin, the insets show examples of water-in-water emulsion microstructures found according to the system's volume ratio (reproduced from Norton and Frith (2001) with permission from Elsevier).

Phase diagrams also usually display the threshold point and the critical point of the phase separated systems (Figure 2-3a). The phase separation threshold of the system is determined as the intercept between a tangent line with a slope of −1 that crosses equal segments of both axes and the binodal (Antonov et al., 1996). The rectilinear diameter is a straight line that connects the composition of the system at the centre of each tie-line, denoting equal phase volumes for each phase. The point of interception of the binodal with the rectilinear diameter defines the critical point which gives the composition of the system that demixes into phases of the same volume and composition (Tolstoguzov, 2002). Tie-lines become shorter as the weight fractions of both polymers are reduced in

the initial mixture until they reach the critical point. The critical and threshold points are unique characteristics of a phase separated system and they coincide in symmetrical phase diagrams (Figure 2-3a). Alternatively, as the distance between the critical and threshold points increases, the phase diagram becomes increasingly asymmetrical (Zaslavsky, 1995).

Figure 2-3b shows an experimental phase diagram of a segregative mixture between gelatin and maltodextrin and the respective microstructures found according to the system's phase volume ratio along a same tie-line (Norton and Frith, 2001). At high phase volume of the gelatin-rich phase, this system formed W/W emulsions composed of maltodextrin droplets dispersed in a gelatin continuous phase; whereas at high phase volume of the maltodextrin-rich phase, W/W emulsions composed of gelatin droplets dispersed in a maltodextrin continuous phase were formed. At the centre point of a tie line, bicontinuity may occur (Norton and Frith, 2001). Bicontinous microstructures are transient in nature and, depending on the characteristics of each system, may show different morphologies, such as the formation of regions of alternating continuity, as exemplified in Figure 2-3b, or the lack of formation of a defined droplet microstructure (Frith, 2010).

The phase behaviour of most biopolymer mixtures is studied at pH 6.0 – 7.0, room temperature (20 – 25 °C) and at low ionic strength (0.05 – 0.50 M NaCl) (Tolstoguzov, 2002). At pH 6.0 – 7.0, most proteins have a negative net charge and will show repulsive interaction with anionic or neutral polysaccharides. Further, the incompatibility between proteins and polysaccharides increases with salt concentration, due to shielding of electrostatic repulsion between proteins molecules and enhancement of protein-protein interactions (Grinberg and Tolstoguzov, 1997).

Several methods have been used to construct the phase diagrams of segregated biopolymer mixtures, such as turbidometric titration (Albertsson and Tjerneld, 1994), chromatographic methods (Planas et al., 1997), mathematical models (Croll et al., 2003; Spyropoulos, Portsch and Norton, 2010), interfacial tension measurements (Forciniti, Hall and Kula, 1990), microfluidics (Silva et al., 2014) and mass balance using phase volume and density measurements (Atefi et al., 2016). The most common method, chosen to be carried out in this research due to its simplicity and accuracy, is the direct determination of each phase composition (Antonov et al., 1980; Kasapis et al., 1993c; Albertsson and Tjerneld, 1994). In this method, several mixtures of different initial biopolymer compositions are created and, when phase separation occurs, two bulk phases are visually observed. The phase volumes are measured using a graduated cylinder and the compositions of each phase are directly determined by appropriate experimental methods according to the polymers involved in the mixture (Kasapis et al., 1993c). In the present research, protein concentration was determined by measurement at 280 nm using an UV-Vis spectrophotometer, utilising solutions of known concentrations of QPI for the calibration curve, while polysaccharide concentration was determined in each phase by the sulfuric acid-UV method (Albalasmeh, Berhe and Ghezzehei, 2013), used for the determination of monosaccharides, disaccharides and polysaccharides of high molecular weight. This method for phase diagram construction is advantageous as it relies on simple and direct methods for biopolymer concentration determination in each phase; however, it can be laborious due to the analysis of many samples to ensure the accuracy of the phase diagram.

2.2.3 Kinetically trapped anisotropic microstructures from biopolymer mixtures

W/W emulsions behave similarly to oil-in-water emulsions and, thus, also display droplet deformation, break-up and coalescence under shear. Gelation of at least one of the biopolymers in the mixture is often used to create kinetically trapped anisotropic microstructures and, depending on the extent of droplet deformation and the gelation behaviour of the biopolymers in the mixture, a range of different microstructures can be formed, such as deformed gel particles (Norton et al., 2000; Wolf et al., 2000; Beldengrün et al., 2018), phase separated mixed gels (Norton et al., 2000; Ben-Harb et al., 2018) or fibres (Wolf et al., 2000; Tolstoguzov, 2002; Wolf and Frith, 2003).

Deformation of a single droplet subjected to a two-dimensional flow field can be defined as D in Equation 2-2, where L and B are the length (m) of the longer and shorter principal axis of an ellipsoid, respectively (Figure 2-4).

$$D = \frac{L - B}{L + B} \tag{2-2}$$

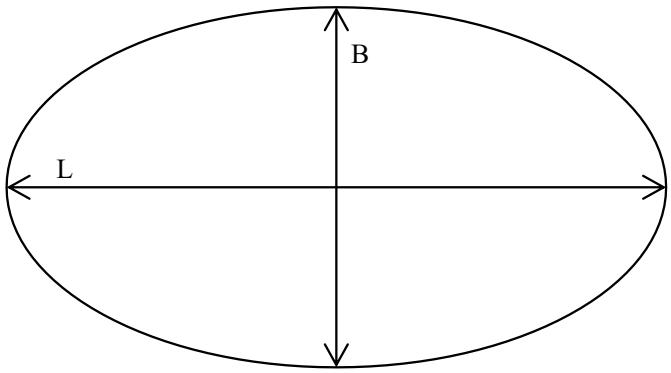

Figure 2-4. Single droplet deformation in a two-dimensional flow field.

The droplet deformation (D) under a flow field is dependent on the interfacial tension, droplet diameter and viscosity ratio (λ) between the dispersed phase (η_d, Pa.s) and the continuous phase (η_c, Pa.s), as defined by Equation 2-3 (Taylor, 1934).

$$\lambda = \frac{\eta_d}{\eta_c} \tag{2-3}$$

The viscosity ratio limits the degree of droplet deformation before break-up given by Equation 2-4, where a λ value of ≤ 3.5 is required to induce significant droplet deformation (Taylor, 1934; Grace, 1982). Of course, as gelation of one or both phases occur, the viscosity ratio changes and the prediction of droplet deformation becomes more complex (Wolf et al., 2000; Wolf, Frith and Norton, 2001).

$$D = \frac{C\, x\, \eta_c}{\sigma} f(\lambda) \tag{2-4}$$

Where $C = \dot{\gamma}/2$ for shear flow fields or $C = \dot{\varepsilon}$ for extensional flow fields, $\dot{\gamma}$ is the shear rate (1/s), $\dot{\varepsilon}$ is the extension rate (1/s), x is the droplet diameter (m), σ is the interfacial tension (mN/m) and $f(\lambda)$ is a function of the viscosity ratio (λ) given by Equation 2-5, which only varies between 1 – 1.2 for λ varying from 0 to ∞ (Taylor, 1934; Grace, 1982).

$$f(\lambda) = \frac{19\lambda + 16}{16\lambda + 16} \tag{2-5}$$

W/W emulsion droplets are more easily deformed than oil-in-water emulsion droplets due to their comparatively lower interfacial tensions, as aforementioned (Section 2.2.1.1) and consequently lower resistance to deformation forces (Scholten et al., 2002; Simeone, Alfani and Guido, 2004; Frith, 2010). Thus, the application of a simple shear flow before or during gelation of one or both phases can be used to manipulate the microstructure of W/W emulsions, creating kinetically trapped anisotropic structures. If only the biopolymer contained in the dispersed phase gels, spherical gel particles are formed at rest or under low shear, whereas elongated particles or fibres are formed under higher shear (Wolf et al., 2000, 2001). If only the biopolymer contained in the continuous phase gels, phase inversion may occur at rest or under low shear, as there is a high tendency for the lower viscosity phase (dispersed phase as the continuous phase gels) to become the continuous phase (Kasapis et al., 1993a; Brown et al., 1995; Norton et al., 2000; Frith, 2010). Under sufficiently high shear and rapid gelation of the continuous phase, gels filled with elongated liquid droplets, so-called capillary fibres, can be formed (Tolstoguzov, Mzhel'sky and Gulov, 1974). If both phases undergo gelation, phase separated mixed gels with spheroidal particles can be created at rest or under low shear (Morris, 1986; Kasapis et al., 1993a; Ben-Harb et al., 2018), while gels filled with ellipsoidal particles or fibres are formed under high shear (Antonov et al., 1980; Tolstoguzov, 2002).

The formation of fibres by deformation and alignment of phase separated biopolymer mixtures under shear and gelation (Figure 2-5) was pioneered by Tolstoguzov and co-workers (Tolstoguzov, Mzhel'sky and Gulov, 1974; Antonov et al., 1980; Tolstoguzov, 2002), who mainly concentrated on devices employing orifice flow, such as extruders. The same principle was later applied in rheometric flow fields, as cited above (Brown et al., 1995; Wolf et al., 2000). More recently, researchers from Wageningen University

(Manski, van der Goot and Boom, 2007; Krintiras et al., 2015; Geerts et al., 2018; Schreuders et al., 2019) scaled-up the rheometric flow field approach and developed shearing devices inspired by rheometers, so-called shear cells, fitted with a cone-in-cone or concentric cylinder/Couette geometry. These devices were developed to create fibrous structures from plant proteins and plant protein-polysaccharide mixtures of high solids concentration, aiming at the production of meat analogues.

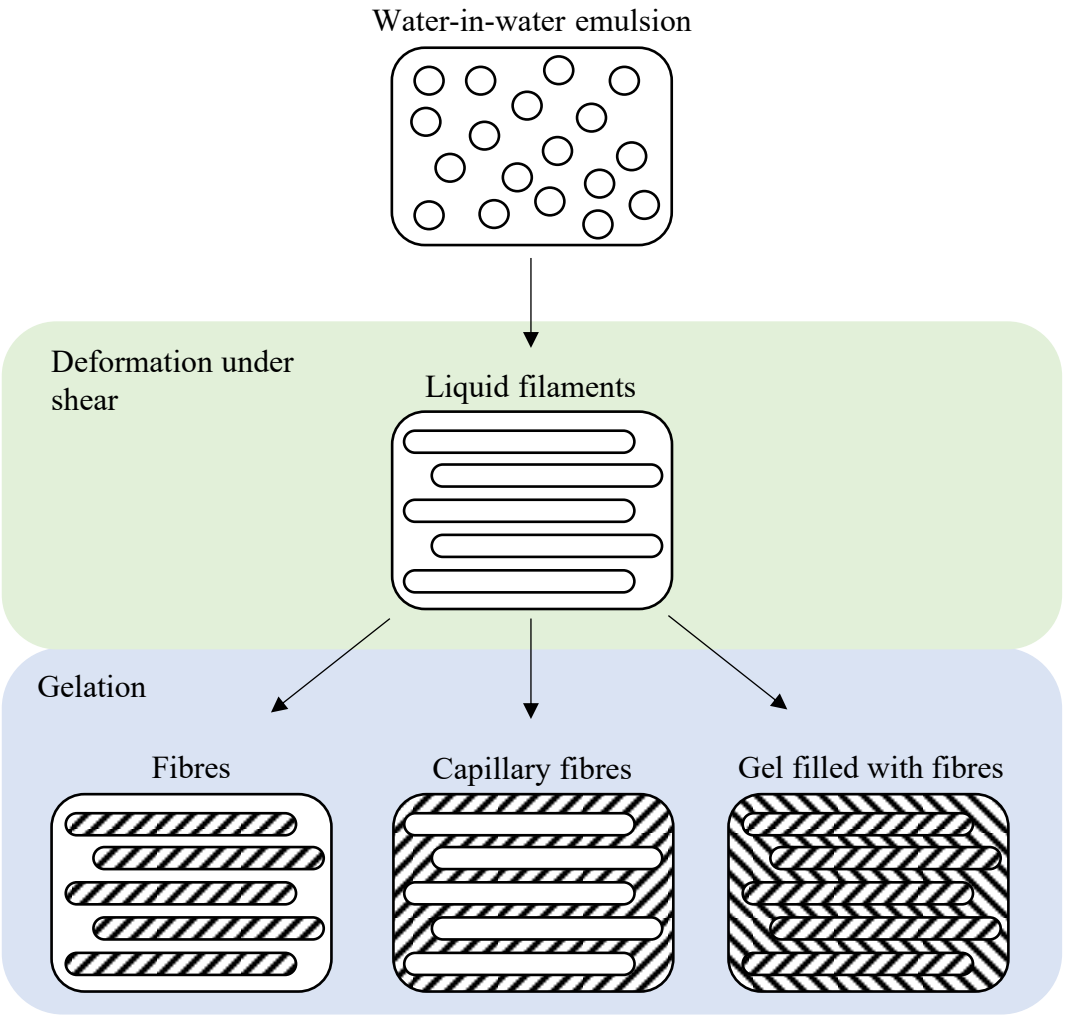

Figure 2-5. Kinetically trapped fibrous microstructures formed through shear and gelation of at least one of the phases of a water-in-water emulsion. Adapted from Tolstoguzov, Grinberg and Gurov (1985).

2.2.4 Phase behaviours and microstructures of segregated plant protein biopolymer mixtures

The phase behaviour of many biopolymer mixtures involving proteins and polysaccharides has been extensively studied since 1910 (Esquena, 2016). Grinberg and Tolstoguzov (1997) listed 86 protein-polysaccharide combinations showing segregative phase separation and their respective incompatibility conditions, where most systems contained gelatin, casein, purified globulin from soy or sunflower, gluten or bovine serum albumin as the protein phase.

The phase behaviour of biopolymer mixtures containing plant proteins has also been investigated, although to a lesser extent. The first studies on the phase behaviour of polysaccharides and plant proteins were reported for highly purified protein fractions of plant origin, including globulin and rubisco (Antonov et al., 1979; Antonov and Soshinsky, 2000; Antonov, Dmitrochenko and Leontiev, 2006). More recently, biopolymer mixtures involving plant protein isolates have been explored. As aforementioned (Section 2.1), protein isolates represent mixtures of more than one protein and the majority of the reports focuses on the association between the plant proteins and the other biopolymer (another protein or a polysaccharide) to improve protein solubility and gelation or to develop bioactive encapsulation systems (Gharsallaoui et al., 2010; Abugoch et al., 2011; Caro et al., 2016; Lan, Chen and Rao, 2018; Duran et al., 2018a, 2018b; Medina et al., 2019; Duran, Spelzini and Boeris, 2019; Guo et al., 2019; Lan et al., 2020b; Li et al., 2020b; Lan et al., 2020a; Alrosan et al., 2022; Salminen et al., 2022; Alrosan et al., 2023). Very few studies report on the phase diagrams of segregative systems involving plant protein isolates and polysaccharides (Li et al., 2008b, 2008a; Mession et al., 2012a, 2012b) (Table 2-1).

Table 2-1. Phase behaviour-microstructure relationship of segregated biopolymer mixtures involving plant protein isolates.

Biopolymer system	System conditions	Phase separation mechanism	Microstructure	Reference
Pea protein isolate (PPI) + sodium alginate (SA)	20 °C, pH 7.2 and 0.1 M NaCl; Both biopolymers have negative net charge under these conditions; PPIs were produced by precipitation (PPP), ultrafiltration (PPDF) and ion exchange chromatography (legumin fraction, Leg)	PPP + SA: depletion-flocculation PPDF + SA: depletion-flocculation Leg + SA: thermodynamic incompatibility	5.5% PPP + 0.7% SA: PPP aggregates dispersed in SA-continuous phase; 11% PPP + 0.38% SA: SA droplets dispersed in PPP-continuous phase 12% PPDF + 0.8% SA: PPDF aggregates dispersed in SA-continuous phase; 6% PPDF + 0.3%SA: SA droplets dispersed in PPDF-continuous phase Leg + SA: all mixtures showed Leg droplets dispersed in SA-continuous phase	(Mession et al., 2012a, 2012b)
Native and heat denatured soy protein isolates (N-SPI and HD-SPI) + κ-carrageenan (κ-car)	25 °C, pH 7.0 and 0.1 M NaCl; Both biopolymers show net negative charge under these conditions	HD-SPI+κ-car: depletion-flocculation N-SPI+κ-car: thermodynamic incompatibility	4% HD-SPI+ 0.35% κ-car: interconnected large SPI aggregates in κ-car-continuous phase 4% N-SPI + 0.35% k-car: isolated SPI aggregates in κ-car-continuous phase	(Li et al., 2008b)

Continuation of Table 2-1. Phase behaviour-microstructure relationship of segregated biopolymer mixtures involving plant protein isolates.

Biopolymer system	System conditions	Phase separation mechanism	Microstructure	Reference
Small and large soy protein isolate aggregates (SA-SPI and LA-SPI) + dextran of average molecular weight of 400,000 and 5,000,000 g/mol (DT400 and DT5000)	25 °C and pH 7.0; Dextran is a neutral polysaccharide and SPI shows a net negative charge under these conditions	Depletion-flocculation	4% SA-SPI + 1% DT400: small SPI aggregates in a dextran continuous phase 4% LA-SPI + 1% DT400: large SPI aggregates in a dextran continuous phase 4% SA-SPI + 1% DT5000: small SPI aggregates in a dextran continuous phase 4% LA-SPI + 1% DT5000: dextran entrapped withing a volume-spanning SPI network	(Li et al., 2008a)

The microstructure displayed by the segregated systems described in Table 2-1 depends on the phase separation mechanism, as previously discussed (Sections 2.2.1.1 and 2.2.1.2). In the case of thermodynamic incompatibility, the microstructure is usually that of W/W emulsions: protein- or polysaccharide-continuous (depending on the phase volumes) with dispersed droplets of the other phase. However, when the separation mechanism is depletion-flocculation, the microstructure is that of protein aggregates dispersed in a continuous phase of the other biopolymer (Li et al., 2008b, 2008a; Mession et al., 2012a, 2012b).

2.3 Quinoa

Quinoa (*Chenopodium quinoa* Willd.) is a pseudocereal from the *Amaranthaceae* family, *Chenopodiaceae* subfamily and *Chenopodium* genus. The term pseudocereal is used to differentiate non-grass plants, such as quinoa, amaranth and buckwheat, from cereals, such as wheat and rice, which are botanically classified as grass plants (Contreras-Jiménez, Torres-Vargas and Rodríguez-García, 2019). According to the Whole Grains Council (2020), there are many known varieties of quinoa, where white, red and black quinoa are the most common and commercialised types.

Quinoa is mainly cultivated in the Andes mountains region of South America (Murphy et al., 2019). Peru is the main producer, with a production of more than 78.6 thousand tonnes of quinoa in 2017, which represented ~54% of the total world production of this crop in the same year (FAO, 2020). However, quinoa is currently cultivated in many countries across the world including China, USA, India, Japan, Poland, Canada, United Kingdom and Australia (Piñuel et al., 2019).

Quinoa is a dicotyledonous grain, meaning that its seeds have two cotyledons (embryonic leaves), while most cereals, such as rice, wheat and barley, are monocotyledonous (Alvarez-Jubete, Arendt and Gallagher, 2009). Quinoa seeds are small and spherical, with a diameter of 1.0 – 2.5 mm (Figure 2-6). The bran fraction, composed of the seed coat and embryo, surrounds the starch-rich perisperm (Alvarez-Jubete, Arendt and Gallagher, 2010; Alonso-Miravalles and O'Mahony, 2018). The embryo contains the two cotyledons and is composed of oblong-shaped cells containing spherical protein bodies (~0.5 – 3 μm in diameter) and oil bodies (~0.2 – 0.5 μm in diameter). The perisperm is composed of uniform thin-walled cells containing compound starch granules, which are oval aggregates of simple starch granules, of 20 – 25 μm (Prego, Maldonado and Otegui, 1998).

Quinoa seeds are composed of 13.0 – 14.0% (w/w) protein, 6.5 – 6.8% (w/w) lipid, 69.0 – 72.0% (w/w) carbohydrate, 60.0% (w/w) starch, 4.0 – 11.0% (w/w) total fibres, 9.0 – 9.7% (w/w) moisture and 2.3 – 2.9% (w/w) ash (Elsohaimy, Refaay and Zaytoun, 2015; Alonso-Miravalles and O'Mahony, 2018). It is a gluten-free pseudocereal, thus it can be safely consumed by patients of celiac disease (Koziol, 1992; Janssen et al., 2017). The digestibility, defined as the availability for absorption after digestion, of protein from quinoa seeds or flour is reported to be of 76.3 – 96.7% based on in vitro studies (Ruales and Nair, 1992; Repo-Carrasco-Valencia and Serna, 2011; Zhu and Li, 2019; Cao et al., 2022) and ~92% based on an in vivo study (Ruales and Nair, 1992). These values are within the range of 75.0 – 94.0% digestibility based on in vitro and in vivo studies reported for other plant protein sources, such as pea and soy (Nosworthy et al., 2017; Berrazaga et al., 2019; Corgneau et al., 2019). Moreover, quinoa seeds, flour and protein extracts contain many bioactive compounds, such as phenolic acids, flavonoids,

carotenoids and tocopherols, which are reported to have health-promoting properties, including anti-cancer, anti-diabetic, anti-inflammatory and antioxidant properties (Tang et al., 2015; Tang and Tsao, 2017; Mudgil et al., 2019; Chen et al., 2022; Estivi et al., 2022; Jan et al., 2023).

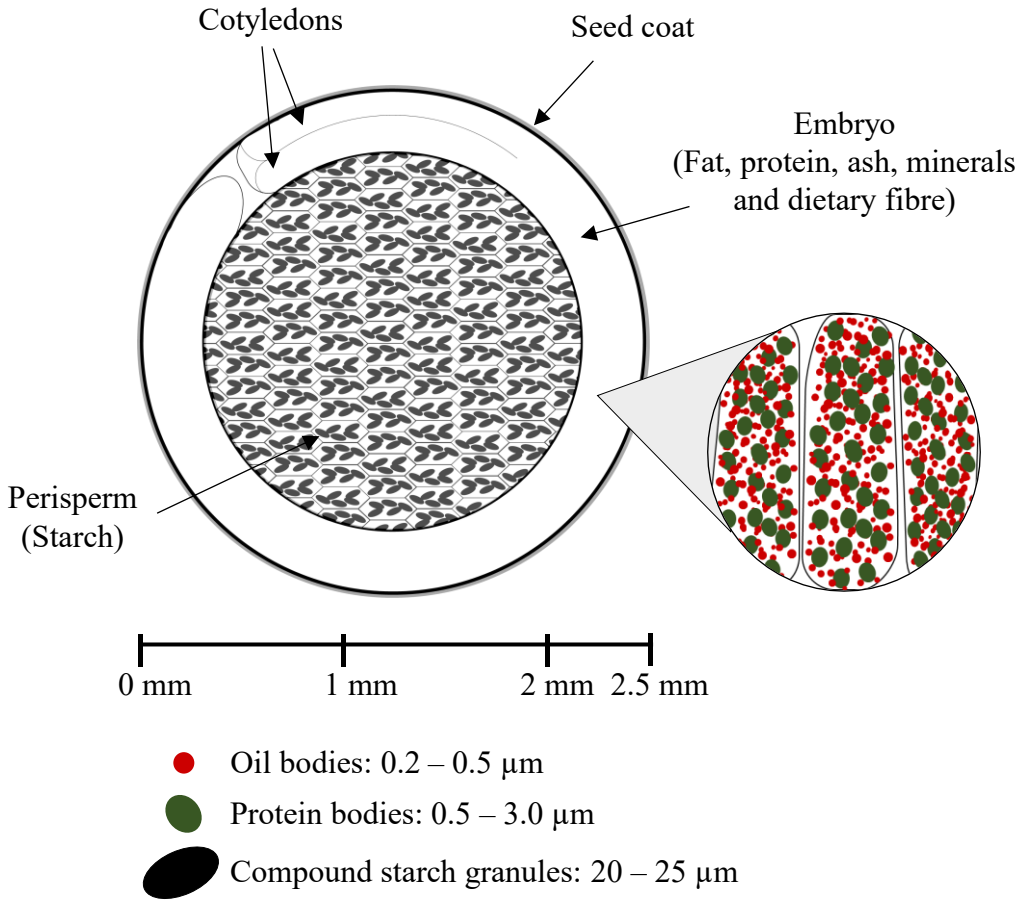

Figure 2-6. Schematic representation of a quinoa seed. Adapted from Alonso-Miravalles and O'Mahony (2018).

2.3.1 Carbohydrate fraction of quinoa

Of the carbohydrate content of quinoa (69 – 72%, w/w), starch is the major component representing about 60% of the whole grain composition (~85% of the carbohydrate content), followed by ~3.2% of pentosans, ~2.5% of crude fibres, ~2.5% of non-reducing

sugars and ~2.0% of reducing sugars (Koziol, 1992). Quinoa starch granules have a polygonal shape with a narrow size distribution of 0.5 – 3.0 μm, which is smaller than those of rice, maize and barley (Matos et al., 2013; Timgren et al., 2013). The starch granules are aggregated into oval compound starch granules of around 20 – 25 μm located in the perisperm of the seeds (Figure 2-6) (Prego, Maldonado and Otegui, 1998).

Quinoa starch has a large fraction of amylopectin (~90%), which contributes to interesting physico-chemical properties, such as slow retrogradation, low gelatinisation temperature, high swelling power and susceptibility to enzymes. Thus, quinoa starch is emerging as a novel starch source with potential application in several industries (Li and Zhu, 2018; Li, Xu and Zhu, 2019). For example, the use of chemically modified quinoa starch granules as Pickering emulsifiers has been widely explored in the past 10 years. Their small size and unimodal size distribution favours the stabilisation of emulsions with small droplets and low creaming index (Rayner et al., 2012; Matos et al., 2013; Li et al., 2019a, 2019b, 2020a; Li, Xu and Zhu, 2019; Kierulf et al., 2020; Lin et al., 2020).

2.3.2 Lipid fraction of quinoa

There is little information in literature on the composition of lipids in quinoa seeds. Przybylski, Chauhan and Eskin (1994) reported that quinoa lipids are composed by 55.9 ± 0.6% of neutral lipids, 25.2 ± 0.3% of polar lipids, which are almost entirely composed of phospholipids, and 18.9 ± 0.2% of free fatty acids. Triacylglycerols (TAG) account for 73.7 ± 0.6% of the neutral lipids, followed by 20.5 ± 0.2% of diacylglycerols, 3.1 ± 0.1% of monoacylglycerols and 2.7 ± 0.1% of waxes (Przybylski, Chauhan and Eskin, 1994). The high level of free fatty acids reported by these authors (~20%) is

unusual in plant tissues (Damodaran, Parkin and Fennema, 2008) and suggests that the material may have suffered lipolytic activity during preparation or lipid extraction for quantification. Conversely, Wood et al. (1993) reported that neutral lipids account for ~90% of the total lipid from quinoa seeds, suggesting a different lipid composition than the previously described. No other reports on the complete composition of quinoa lipids were found, however, it is reported that TAG are stored in the form of oil bodies located in the embryo in quinoa seeds (Figure 2-6) (Prego, Maldonado and Otegui, 1998).

The fatty acid composition of quinoa seeds, on the other hand, is more often reported. About 80% of the total fatty acids are unsaturated, where linoleic acid (C18:2, Ω6), oleic acid (C18:1) and α-linolenic (C18:3, Ω3) correspond to about 52%, 25% and 5% of the total fatty acid content, respectively. Eicosenoic acid (C20:1) and docosenoic acid (C22:1) are also present in a lower concentration of about 1.5% each, while squalene (C30:6) is found at a concentration of ~3.4%. As for saturated fatty acids, palmitic acid (C16:0) corresponds to about 10% of the total fatty acid content, while tetradecanoic acid (C14:0), stearic acid (C18:0), icosanoic acid (C20:0), docosanoic (C22:0) and tetracosanoic acid (C24:0) can also occur in concentrations of less than 1% each (Koziol, 1992; Ruales and Nair, 1993; Jahaniaval, Kakuda and Marcone, 2000; Alvarez-Jubete, Arendt and Gallagher, 2009, 2010).

2.3.2.1 Quinoa oil bodies

Oil bodies, also called oleosomes, are the reserves of triacylglycerols (TAG) in plants and occur in the form of TAG droplets stabilised by a monolayer of phospholipids anchored at the interface with the hydrophobic region of amphiphilic proteins, called oleosins or

oil body-associated proteins (Figure 2-7) (Tzen et al., 1993; White, Fisk and Gray, 2006). Oil bodies can be found in many plant tissues, including roots (Jayaram and Bal, 1991) and leaves (Shimada and Hara-Nishimura, 2015) but they are more abundant in seeds (Tzen et al., 1993). Due to their phospholipid and protein membrane, plant oil bodies are stable against fatty acid oxidation (Gray et al., 2010) and can act as carriers for flavour molecules (Fisk et al., 2011) and bioactives (White et al., 2009; Zheng et al., 2019). Further, owing to their naturally emulsified structure, plant oil bodies can be used directly in the formulation of emulsion-based products, eliminating the need for an oil homogenisation step during processing (Iwanaga et al., 2007, 2008; White et al., 2008; de Chirico et al., 2018).

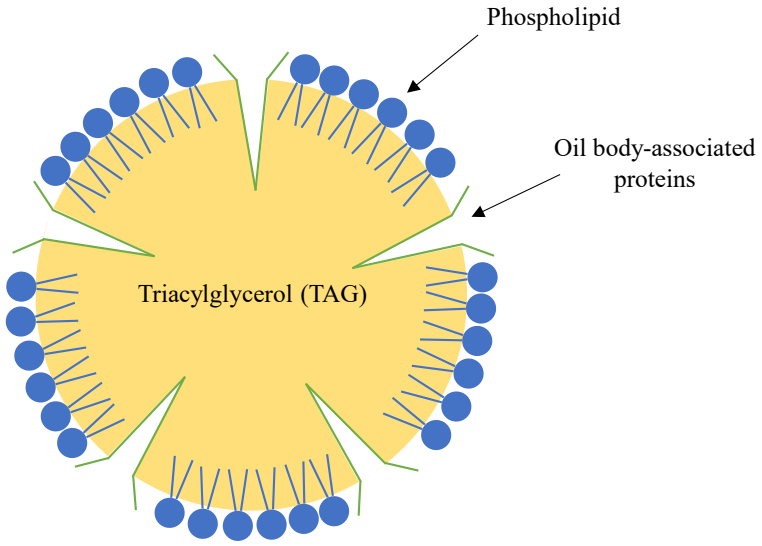

Figure 2-7. Schematic of an oil body structure. Adapted from Yang et al. (2022a).

Quinoa oil bodies are reported to be 0.2 – 0.5 µm in diameter and are mainly located in the embryo fraction of the seed (Figure 2-8) (Prego, Maldonado and Otegui, 1998). A few recent proteomics studies have confirmed the presence of oil body-associated proteins in

quinoa seeds (van de Vondel, Lambrecht and Delcour, 2020; Shen et al., 2022). No further studies focusing on the extraction and characterisation of quinoa oil bodies, or their associated proteins, were found.

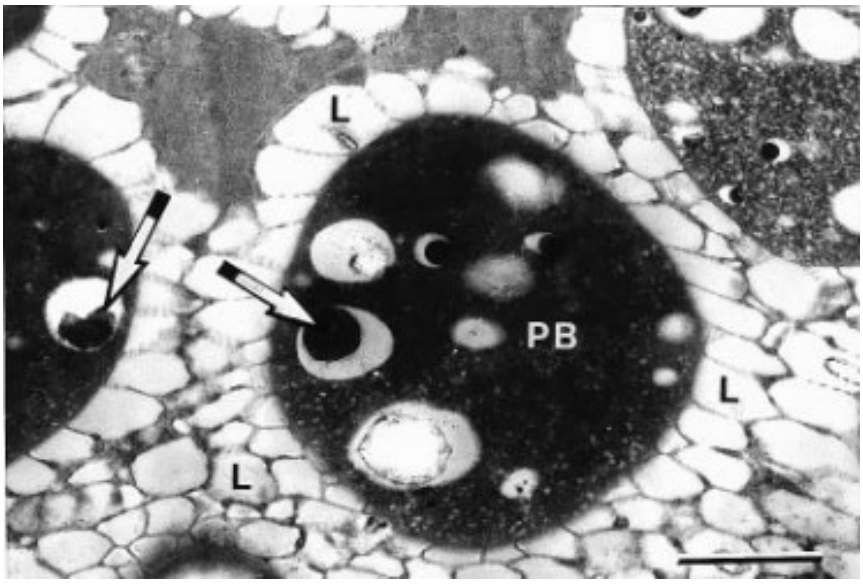

Figure 2-8. Section of a cell of the embryo of quinoa seed showing oil bodies (L – for lipid bodies or oil bodies, black letters in white background) and protein bodies (PB, white letters in black background), one of them with a globoid crystal (white arrow, see Section 2.3.3). The scale bar represents 1 μm (reproduced from Prego, Maldonado and Otegui (1998) with permission from Academic Press and Oxford University Press).

Several methods can be applied for the extraction of oil bodies from seeds, including aqueous extraction followed by mechanical disruption of the seeds with a blender (Romero-Guzmán et al., 2020b) or a twin-screw press (Romero-Guzmán et al., 2020a), ultrasound-assisted extraction (Al Loman et al., 2018) and enzyme-assisted extraction (Zhou et al., 2019). The most common approach involves the soaking of seeds in an aqueous solution (usually at pH 7.0 – 9.5) followed by grinding, typically with a blender to disrupt the seeds' cell walls. The oil bodies are then collected in the form of an emulsion cream layer after centrifugation (Tzen et al., 1997; Grundy et al., 2016; Qi et al., 2017;

de Chirico et al., 2018, 2020; Romero-Guzmán et al., 2020b; Yang et al., 2022a). Although this method has been extensively used, it can negatively affect the stabilising membrane of the oil bodies, leading to aggregation and coalescence (Karefyllakis, van der Goot and Nikiforidis, 2019). Thus, it is essential to develop oil body extraction methods that do not affect their membrane and consequent stability (Nikiforidis, 2019).

Cryo-milling, or cryogenic grinding, has recently received some attention from researchers. It consists in the griding of materials at temperatures below −150 °C in the presence of liquid nitrogen (LN_2) or liquid argon (LAr) (Katiyar, Biswas and Tiwary, 2021). Cryo-milling has been suggested as a good alternative to conventional seed milling methods, such as jet, pin or ball milling, as it solidifies the oil and increases the brittleness of seed particles allowing for an easier break up into smaller fragments (Schutyser and van der Goot, 2011; Sharma et al., 2016; de Bondt et al., 2020). It has been mainly applied in the grinding of spices to protect oils against heat damage by maintaining a low temperature while absorbing the heat generated during grinding (Singh and Goswami, 1999; Mékaoui et al., 2016; Sharma et al., 2016; Katiyar, Biswas and Tiwary, 2021). More recently it was used as a pre-treatment to extract oils from pumpkin seeds (Balbino et al., 2019) and fennel seeds (Marčac et al., 2023) resulting in improved oil extraction yield. There is one report on the recovery of intact oil bodies from rapeseeds by cryo-milling with liquid nitrogen (di Bari et al., 2018), but no reports on quinoa seeds were identified.

2.3.3 Protein fraction of quinoa

Within quinoa seeds, proteins are located mainly in the bran fraction (seed coat and embryo) in the form of protein bodies of 0.5 – 3.0 μm in diameter, composed of a

proteinaceous matrix that occasionally contains globoid crystals (Figure 2-8). Globoid crystals are spherical crystalline structures that contain mineral nutrients necessary for plant growth, which in the case of quinoa seeds are phosphorus, potassium and magnesium (Prego, Maldonado and Otegui, 1998). Apart from this information, there is very little literature on the structure of quinoa protein bodies, also referred to as protein storage vacuoles (Burrieza, López-Fernández and Maldonado, 2014). In cereals and legumes, protein bodies are described as small organelles composed of a homogeneous proteinaceous matrix, containing storage proteins, bound by an external single membrane. The protein matrix may contain inclusions of globoid crystals, as is the case of quinoa (Prego, Maldonado and Otegui, 1998), or of proteinaceous crystals (Pernollet, 1978; Zhou et al., 2012).

The different protein fractions in a plant matrix or protein mixture can be classified by Osborne fractionation according to their solubility, and consequent extractability, in different media. Albumins are extractable in water, globulins are extractable in low ionic strength solutions, prolamins are extractable in aqueous alcohol and insoluble glutelins are partially extractable in dilute acids or bases (Osborne, 1907). It is reported that the protein bodies in the embryo of quinoa seeds contain 57% of the whole seed protein and, of those, ~36% are water-soluble proteins (albumins), ~33% are NaCl-soluble proteins (globulins), around 3% are propanol-soluble proteins (prolamins), 2% are lactic acid-soluble proteins (glutelins) and ~26% are insoluble proteins (Ando et al., 2002).

Globulins and albumins are the main proteins in quinoa seeds. Globulin 11S (Figure 2-9), also known as chenopodin, corresponds to about 37% of the total protein in quinoa (Brinegar, Sine and Nwokocha, 1996). It is composed of subunits of 45 – 60 kDa in size, which are associated into hexameric units of 300 – 360 kDa (Brinegar and

Goundan, 1993; Mäkinen, Zannini and Arendt, 2015; Liu et al., 2023). Each subunit contains an α-chain (also called acidic chain) of 30 – 39 kDa and a β-chain (also called basic chain) of 20 – 25 kDa, which are linked by disulfide bonds (Brinegar and Goundan, 1993; Abugoch et al., 2008; Yang et al., 2022b). Albumin 2S is a small globular protein corresponding to about 35% of the total protein in quinoa, with a molecular weight of around 8 – 16 kDa (Brinegar, Sine and Nwokocha, 1996; Shen et al., 2022).

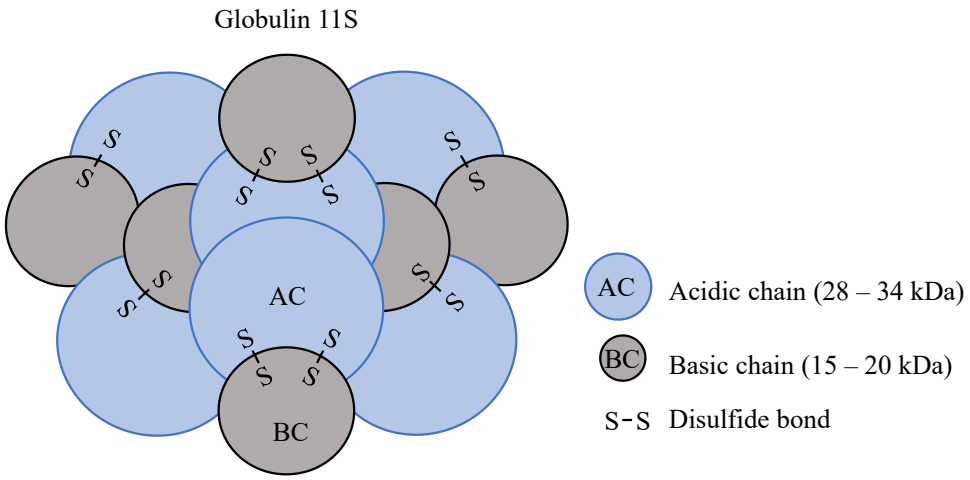

Figure 2-9. Schematic representation of globulin 11S, the main protein in quinoa.

Recently, two other globulins, globulin 13S and globulin 7S, were identified in quinoa seeds proteomics (Burrieza et al., 2019; Shen et al., 2022). While neither have been structurally characterised in quinoa yet, similar proteins have been described in other pseudocereals. Globulin 13S is very similar to globulin 11S in terms of structure and size in buckwheat (*Fagopyrum spp.*) (Maksimovic et al., 1996; Janssen et al., 2017), while globulin 7S is reported to occur as a tetrameric unit of ~200 kDa, with subunits of 16 kDa, 38 kDa, 52 kDa and 66 kDa in size in amaranth (*Amaranthus hypochondriacus*) (Quiroga et al., 2010).

Glutelins and prolamins are also present in quinoa seeds but in lower quantities, representing around 12.7% and 7.2% of the total protein content, respectively. Gluten is formed by the reaction between glutelins and prolamins, however, the content of the latter in quinoa is too low to react and form the gluten complex, hence quinoa's gluten-free classification (Koziol, 1992).

Quinoa protein is typically obtained from quinoa seeds or quinoa flour by either dry or wet fractionation. In dry fractionation, mechanical techniques, such as milling and air or size classification, are applied, usually resulting in quinoa protein concentrate (QPC). In wet fractionation, a liquid solvent is used to solubilise the proteins and facilitate their extraction from the matrix, resulting in quinoa protein isolate (QPI) (Alonso-Miravalles and O'Mahony, 2018).

2.3.3.1 Dry fractionation

Dry fractionation for quinoa protein extraction involves the coarse milling of seeds, which causes the embryo to break into small fragments releasing the perisperm. The milled seeds are then sieved, where several fractions of different sizes can be collected. The composition of each fraction is different and can vary between quinoa varieties (Opazo-Navarrete et al., 2018b, 2018a).

Compared to wet fractionation, dry fractionation has a lower energy and water consumption and it is reported to protect a few functional properties of proteins, such as solubility and water holding capacity (Schutyser and van der Goot, 2011; Pelgrom et al., 2013; Hopf, Dehghani and Buckow, 2023). However, it usually results in protein

concentrates of low protein content, ranging 28 – 33% (w/w) (Opazo-Navarrete et al., 2018a, 2018b).

2.3.3.2 Wet fractionation

Wet fractionation is currently the most commonly applied method for plant protein extraction from different sources, including quinoa (Mession et al., 2012a; Ruiz et al., 2016b; Janssen et al., 2017; Geerts et al., 2018; Tanger, Engel and Kulozik, 2020; Kumar et al., 2021). In wet fractionation, quinoa seeds are milled into flour which is often defatted using organic solvents, such as hexane or petroleum ether. The flour is then suspended in water and the pH of the suspension is adjusted with NaOH to values between 8 and 11 (Ruiz et al., 2016b; Mir, Riar and Singh, 2019b). The pH value during this step strongly influences the functional properties of the resulting quinoa protein isolate (QPI) and this influence will be discussed in further detail in Sections 2.4.1 and 2.4.2. The flour suspension is kept under stirring for anytime between 1 and 16 h (Ruiz et al., 2016a, 2016b), centrifuged and the supernatant containing the soluble protein is collected. Wet fractionation may end at this step with the freeze-drying of the supernatant to obtain quinoa protein isolate (QPI) powder (Valenzuela et al., 2013; Guerreo-Ochoa, Pedreschi and Chirinos, 2015; Vera et al., 2019). However, further purification of the isolate is usually carried out by acid precipitation of the globulins at their isoelectric point through adjustment of the pH, typically with HCl, to values between 4 and 5, followed by centrifugation. The precipitate is then rinsed to remove remaining salts and contaminants, neutralised with NaOH and freeze-dried (Abugoch et al., 2008; Ruiz et al., 2016b).

Wet fractionation uses large quantities of water and energy, and some of the protein functionality, such as solubility and water holding capacity, can be compromised due to the severe solvent conditions (Schutyser and van der Goot, 2011; Alonso-Miravalles and O'Mahony, 2018; Opazo-Navarrete et al., 2018a). However, compared to dry fractionation, wet fractionation is well stablished in both industry and laboratory-scale, provides a high degree of process control and usually results in QPI with a higher protein content of > 70% (w/w) (Ruiz et al., 2016b; Steffolani et al., 2016; Mir, Riar and Singh, 2019a; Kumar et al., 2021; Sim et al., 2021). In this research, wet fractionation was chosen as the extraction method to obtain QPI from quinoa flour.

2.4 Quinoa protein isolate

The conditions applied during quinoa protein isolate (QPI) extraction strongly influence the physico-chemical and functional properties of the isolate, which in turn also affect its potential applications (Abugoch et al., 2008). Literature has especially focused on the impact of the alkalinisation pH used during wet fractionation, which will be discussed in the following sections.

2.4.1 Physico-chemical properties

Table 2-2 shows the variation of the physico-chemical properties of QPI, including chemical composition, protein yield and thermal properties parameters, according with the alkalinisation pH during wet fractionation. The highest variability in all physico-chemical properties seems to occur for alkalinisation at pH 9. This variability may arise from slight differences in extraction conditions, including alkalinisation times, strength

of the base and acid used during extraction, as well as centrifugation speeds and times (Guerreo-Ochoa, Pedreschi and Chirinos, 2015; Nongonierma et al., 2015; Ruiz et al., 2016b, 2016a; Sánchez-Reséndiz et al., 2019). Results have also been shown to depend on quinoa variety/cultivar (Steffolani et al., 2016).

Table 2-2. Variation in chemical composition, protein yield, denaturation temperature (T_d) and denaturation enthalpy (ΔH) of quinoa protein isolate according to the alkalinisation pH during wet fractionation.

	Alkalinisation pH			
	pH 8	pH 9	pH 10	pH 11
Protein (%, w/w, dw)	87.1 – 91.6	40.7 – 95.7	84.0 – 94.0	75.3 – 83.5
Carbohydrates* (%, w/w, dw)	1.6	2.3 – 18.8	1.4	11.9
Lipid (%, w/w, dw)	0 – 4.9	-	-	-
Ash (%, w/w, dw)	2.2 – 2.8	0.9 – 3.0	4.59	3.5
Protein yield (%, w/w)	16.5 – 36.3	9.2 – 46.0	10.5 – 40.0	11.4 – 52.0
T_d (°C)	82.0 – 101.1	96.0 – 99.2	92.4 – 96.3	-
ΔH (J/g)	10.2	2.0 – 12.4	2.0	-

References: Abugoch et al. (2008); Nongonierma et al. (2015); Ruiz et al. (2016b); Steffolani et al. (2016); Kaspchak et al. (2017); Mir, Riar and Singh (2019a); Sánchez-Reséndiz et al. (2019); Vera et al. (2019); Yang et al. (2022b); Liu et al. (2023). *Fibre and non-fibre. Dw: dry weight.

Protein content (also referred to as protein purity) is typically > 70% (w/w), although values as low as 40.7% (w/w) have been reported for extraction at pH 9 (Nongonierma et al., 2015). Protein yield, calculated as the percentage mass ratio between the protein in the extracted QPI and the protein in the flour used for extraction, varies between 9.2% and 52.0% (w/w) (Nongonierma et al., 2015; Ruiz et al., 2016b) but it tends to be higher for extraction at pH 10 – 11. Alkalinisation leads to deprotonation of amine groups and ionisation of carboxyl groups. As a consequence, the net charge of proteins becomes increasingly negative, increasing repulsive interactions between protein molecules and favouring protein-solvent interactions. Thus, proteins are typically more soluble in

increasingly alkaline pH values, which favours their aqueous extraction (Valenzuela et al., 2013; Ruiz et al., 2016b; van de Vondel, Lambrecht and Delcour, 2020). As for other components, QPI usually has low lipid and carbohydrate contents, however, these may be present depending on the extraction protocol applied (Table 2-2).

Thermal properties of QPI measured by differential scanning calorimetry (DSC, Section 3.2) have also been reported. The thermograms typically show a single endothermic peak with peak denaturation temperatures (T_d) of 82 – 101 °C for QPI extracted at pH 8 – 9. Contrarily, QPI extracted at higher pH values (10 – 11) show a loss of thermal stability, signalled by a decrease in denaturation enthalpy (ΔH) values, and a reduction in peak size or even absence of peaks during DSC analysis (Abugoch et al., 2008; Ruiz et al., 2016b; Steffolani et al., 2016; Vera et al., 2019; Liu et al., 2023). Strong alkalinisation at pH 10 – 11 followed by isoelectric precipitation may disrupt the secondary structure of proteins to a certain extent, breaking hydrogen bonds and hydrophobic interactions, which may lead to irreversible changes in conformation, protein denaturation and subsequent loss of thermal stability (Martínez and Añón, 1996; Ruiz et al., 2016b). Similarly to protein content and yield, though, ΔH values seem to be strongly dependent on quinoa variety/cultivar, with values spanning from 2.0 J/g to 12.4 J/g for QPI extracted at pH 9.

Also relevant for this research is the amino acid profile of QPI. Although it has been shown to vary slightly with alkalinisation pH, QPI has a similar amino acid profile to that of soy protein isolate and casein (Abugoch et al., 2008; Elsohaimy, Refaay and Zaytoun, 2015). It also shows a complete composition of essential amino acids, which meets the amino acid requirements for adults suggested by FAO; while only lysine and leucine contents are limited when compared to the recommended for children between

1 and 5 years old (WHO/FAO/UNU, 2007; Abugoch et al., 2008; Vilcacundo and Hernández-Ledesma, 2017). Thus, proteins in QPI are considered to be of high nutritional value (Damodaran, Parkin and Fennema, 2008), contributing to its application potential in the formulation of nutritious protein-rich foods.

Further, literature reports that the protein and amino acid profile and the thermal properties of QPI have a high similarity to that of isolated globulin 11S. This indicates that globulin 11S is the most important protein in QPI, governing the physico-chemical properties of the whole isolate (Ruiz et al., 2016b; Vera et al., 2019). This is an interesting observation because QPI is most commonly extracted using water as solvent during wet fractionation (Abugoch et al., 2008; Ruiz et al., 2016b, 2016a; Vera et al., 2019), thus, according to the principle of Osborne fractionation, it would be expected that these protein isolates are rich in water-extractable albumins; while globulins are extractable at low ionic strength solutions (Osborne, 1907). However, recent research (van de Vondel, Lambrecht and Delcour, 2020; van de Vondel et al., 2021) has shown that aqueous extracts of quinoa protein contained both albumins and globulins in high quantities, due to the a relatively high mineral content of quinoa flour (~3.4 – 4.2%, w/w) inducing globulin extraction.

2.4.2 Technofunctional properties

The technofunctional properties of QPI, including water holding capacity, foaming capacity, solubility, emulsifying capacity and gelation capacity, have been increasingly studied in the last few years (Abugoch et al., 2008; Ruiz et al., 2016b; Kaspchak et al., 2017; Cerdán-Leal et al., 2020; Shen, Tang and Li, 2021; Zhao et al., 2023). Only

solubility and heat-induced gelation of QPI are reviewed as relevant in the context of this thesis. Like the physico-chemical properties previously discussed (Section 2.4.1), both solubility and gelation capacity have been shown to vary with the alkalinisation pH and values fluctuate even for the same pH across different studies (Table 2-3).

Abugoch et al. (2008) reported that QPI extracted at pH 9 had a high solubility (> 80%) at the wide pH range of 6 – 11, while QPI obtained at pH 11 had low solubility (< 40%) at the whole pH range studied (pH 3 – 11). Contrarily, Ruiz et al. (2016b) reported that the solubility curves of QPI extracted at pH 8, 9, 10 and 11 showed an inversed bell shape, where all samples showed reduced solubility (< 10%) at pH 4 – 6. QPI extracted at pH 8 had the highest solubility at pH 3 – 4 (around 60%), while QPI extracted at pH 9 showed the highest solubility at pH 7 – 8 (> 60%) (Ruiz et al., 2016b). Further, Liu et al. (2023) reported that the solubility at pH 7 of QPI decreased with the increase in alkalinisation pH during wet fractionation, with ~63% for QPI extracted at pH 7 to ~47% for QPI extracted at pH 11 (Table 2-3).

Table 2-3. Solubility and gel strength of quinoa protein isolates according to alkalinisation pH during wet fractionation.

Alkalinisation pH	Solubility (%, w/w)	Gel strength*	Reference
pH 9	pH 3 – 4: ~15% pH 5 – 11: ~80 – 95%	-	Abugoch et al. (2008)
pH 11	pH 3 – 4: ~12% pH 5 – 11: ~20 – 40%		
pH 9	pH 7: 60.2%	-	Mir et al. (2019a)
pH 10	pH 7: 75.3%		
pH 11	pH 7: 73.5%		
pH 12	pH 7: 70.8%		
		10% (w/w) QPI:	(Ruiz et al., 2016b)
pH 8	pH 3: ~60% pH 5: ~10% pH 9: ~60%	~3000 Pa	
pH 9	pH 3: ~40% pH 5: ~5% pH 9: ~70%	~5000 Pa	
pH 10	pH 3: ~25% pH 5: ~5% pH 9: ~60%	~1000 Pa	
pH 11	pH 3: ~20% pH 5: ~5% pH 9: ~70%	~500 Pa	
		15% (w/w) QPI:	(Liu et al., 2023)
pH 7	pH 7: ~63%	~570 Pa	
pH 8	pH 7: ~62%	~800 Pa	
pH 9	pH 7: ~55%	~3000 Pa	
pH 10	pH 7: ~55%	~4000 Pa	
pH 11	pH 7: ~47%	~9000 Pa	

*Determined as the final elastic modulus (G') at the end of temperature sweeps conducted under small amplitude oscillatory deformation in a rheometer.

As for heat-induced gelation capacity, QPI follows the gelation behaviour of globular proteins: unfolding of protein structure and aggregation under heating followed by

network reinforcement under cooling (Section 2.1.1). This gelation behaviour is usually measured by small amplitude oscillatory rheometry, more specifically by temperature sweeps, where the storage and loss moduli (G' and G", respectively) are measured as the temperature is gradually increased and decreased (Section 3.1). The final G' at the end of the temperature sweep is used as a measure of gel strength of QPI heat-induced gels (Table 2-3). Ruiz et al. (2016b) reported that QPI extracted at pH 10 – 11 did not gel during heating due to near complete protein denaturation during extraction under these conditions. The microstructure of these gels, analysed by confocal laser scanning microscopy (CLSM, Section 3.3), was highly inhomogeneous, with no evidence of network formation. On the other hand, QPI extracted at pH 8 – 9 formed protein networks during heat treatment, resulting in strong gels (Ruiz et al., 2016b). Conversely, Liu et al. (2023) reported an increase in gel strength with increasing alkalinisation pH. The microstructure of these gels featured large and irregular protein aggregates, where only QPI extracted at pH 11 showed indication of gel network formation (Table 2-3).

Although the data for physico-chemical and technofunctional properties is highly variable across different studies, the reports by Abugoch et al. (2008) and Ruiz et al. (2016b) both suggest that the functionality of QPI is preserved by milder alkalinisation conditions during extraction. In these studies, QPI extracted by alkalinisation at pH 9 showed higher protein content, solubility, thermal stability and final gel strength than alkalinisation at pH 8 or at pH 10 – 11.

2.5 Modification of wet fractionation conditions: the Hofmeister's series

As shown in the previous sections (2.4.1 and 2.4.2), the conditions imposed during extraction strongly influence the structural stability and, consequently, the functionality

of proteins. During wet fractionation, the ions added to the system during the alkalinisation and precipitation steps become increasingly relevant, as their interactions with the protein structure dictate the extraction yield and colloidal state of the protein (Okur et al., 2017; Schmitt et al., 2021).

The Hofmeister's series, formulated by Franz Hofmeister in 1888, describes the effect of ions during the salting in or salting out of proteins, providing a range of ions that could be considered for protein extraction studies. The series classifies anions and cations into kosmotropes or chaotropes (Hofmeister, 1888; Kunz, Henle and Ninham, 2004). Ions that facilitate the precipitation of proteins and prevent unfolding through the salting out effect (decrease of protein solubility with the increase in salt concentration) are conventionally referred to as kosmotropic; whereas ions that promote salting in (increase of protein solubility with the increase in salt concentration), while increasing structure unfolding, are referred to as chaotropic (Wilson, 2007; Metrick and MacDonald, 2015). Generally, the effect of anions on protein stability is stronger than that of cations and the anionic Hofmeister series follows the order (from more kosmotropic to more chaotropic): SO_4^{2-} > HPO_4^{2-} > $Acetate^-$ > $Citrate^-$ > Cl^- > NO^{3-} > ClO^{3-} > I^- > ClO^{4-} > SCN^-, with Cl^- generally considered as the dividing line between the kosmotropic and chaotropic effects (Ries-Kautt and Ducruix, 1989; Kumar and Venkatesu, 2014; Okur et al., 2017).

The mechanism behind the kosmotropic or chaotropic effect was initially thought to be related to interactions between the ions and the bulk water structure; however, this was later refuted by showing that ions have no effect on water beyond the first layer of molecules of their own solvation shell (Omta et al., 2003; Wilson, 2007; Okur et al., 2017). Recent research (Okur et al., 2017) suggests that the acting mechanism of anions and cations in the Hofmeister series is related to interactions in solution between the ions

and the protein's amide backbone or side chain groups of charged amino acids. Anions follow the order of the series when the effect of the protein backbone is stronger than that of the positively charged side chains, that is, at pH values at or above their isoelectric point where the protein net charge is negative. This is because chaotropic anions are weakly hydrated and become attracted to the amide backbone, , interacting with the N-H end of the peptide bond and the neighbouring methylene groups, which leads to salting in and consequent destabilisation and unfolding of the protein structure to allow interaction; while kosmotropic anions, which are strongly hydrated, are excluded from the backbone and promote the salting out effect, stabilising and protecting the protein structure against unfolding (Okur et al., 2017).

The Hofmeister series and the effects of different ions on the properties of proteins extracted from different sources have been extensively studied. However, results vary in that the order of the stabilisation effect of the ions established by the series is not always followed (Damodaran, 1988; Ries-Kautt and Ducruix, 1989; Bowland, Allen Foegeding and Hamann, 1995; Zhang and Cremer, 2009; Sun and Arntfield, 2012; Metrick and MacDonald, 2015; Kaspchak et al., 2017; van de Vondel, Lambrecht and Delcour, 2020; Wang et al., 2021b; Liu et al., 2022; Yang et al., 2022b). Specifically in wet fractionation for plant protein extraction, HCl is invariably used during the acid precipitation step (Mession et al., 2012a; Ruiz et al., 2016b; Janssen et al., 2017; Geerts et al., 2018; Kumar et al., 2021). Only isolated studies have reported on the use of other acids and the effects on the extracted protein (Salt et al., 1982; Cai et al., 2020). Salt et al. (1982) studied the effect of precipitation with different acids on soy protein recovery, showing that sulfuric acid and phosphoric acid resulted in a lower extent of protein denaturation than HCl, in agreement with the Hofmeister series. However, results also showed that nitric acid

induced less protein changes during precipitation than HCl, which is contrary to the expected from the Hofmeister series (Hofmeister, 1888; Kunz, Henle and Ninham, 2004; Okur et al., 2017). More recently, Cai et al. (2020) reported that the precipitation acid can alter the structural and functional properties of proteins extracted from okara (pulp resultant from soy milk production). Precipitation with HCl improved the solubility, water holding capacity, foaming capacity and stability of okara protein, whereas precipitation with citric acid contributed to oil holding capacity and emulsifying stability, and precipitation with malic acid resulted in a higher surface hydrophobicity (Cai et al., 2020). Based on the results reported in the cited study, the different precipitation acids affected protein functionality in different ways and no clear correlation to the Hofmeister series could be established. Nonetheless, this approach is promising and the effects of precipitation with acids other than HCl on the functional properties of QPI have not yet been reported.

2.6 Maltodextrin

Maltodextrin (MD) is a neutral polysaccharide derived from the hydrolysis of starch via acidic or enzymatic routes. Its chemical structure (Figure 2-10) consists of D-glucose monomers linearly-linked by α-1,4 glucosidic bonds, originating from the amylose portion of starch (Zheng, Jin and Zhang, 2007; Klinjapo and Krasaekoopt, 2018) and it may contain α-1,6 branch points arising from the amylopectin portion of starch (Chronakis, 1998). Maltodextrins are characterised by the dextrose equivalent (DE), which refers to the extent of starch hydrolysis and represents the percentage of reducing sugars (free glucose groups), which define this polysaccharide's reducing power.

Maltodextrins can have DE values ranging from 3 to 20, while hydrolysates with DE values higher than 20 are called glucose syrups (Saavedra-Leos et al., 2015).

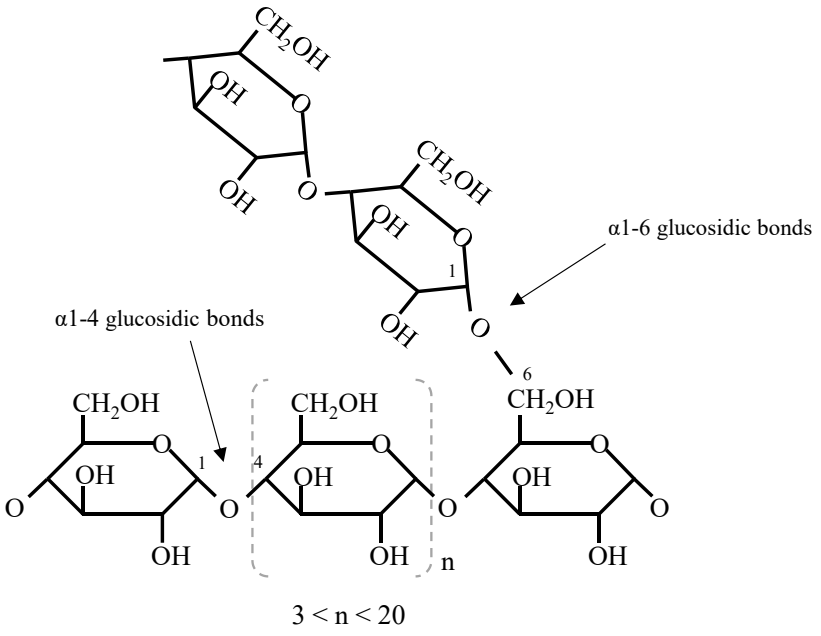

Figure 2-10. Chemical structure of maltodextrin.

A few general properties of MD are solubility in cold water, water-holding capacity, low or no sweetness, absence of odour and moderate viscosity. Due to its range of properties, it is commonly applied in the food industry to confer texture and bulk, replace fat, assist in the spray-drying of flavours and seasonings and in the encapsulation of flavour compounds (Chronakis, 1998; Wang and Wang, 2000; Zheng, Jin and Zhang, 2007). The applicability of maltodextrins of different DE to create structures for food applications, especially as a component of two-phase biopolymer mixtures with refined animal proteins, such as gelatin and caseinate, has been demonstrated in several studies (Kasapis et al., 1993b; Manoj, Kasapis and Chronakis, 1996; Lorén and Hermansson, 2000; Norton and Frith, 2001; Williams et al., 2001; Beldengrün et al., 2018, 2020; Wang et al., 2019b).

There is limited information, however, on the phase-separating behaviour of mixtures of MD and plant proteins (Nguyen et al., 2014). Thus, maltodextrin was chosen to be investigated as the phase separating polysaccharide in this research because a comparison can be established between its phase behaviour in mixtures with plant proteins and animal proteins.

2.6.1 Physico-chemical and functional properties of maltodextrin

The functional properties of a specific maltodextrin are dependent on the DE value, which is inversely correlated to the degree of polymerization (DP) and the number-average molecular weight (Mn), values commonly used to describe the size distribution of polysaccharide polymer chains (Saavedra-Leos et al., 2015). Solubility, hygroscopicity and the capacity to decrease the freezing point of solutions increase with increasing DE. In contrast, the viscosity, cohesiveness and the prevention of coarse-crystal formation increase with decreasing DE (Chronakis, 1998).

Usually, starches from corn, potato or rice are used for the production of commercial maltodextrins (Wang and Wang, 2000), however, the source of the starch influences the properties of the resulting maltodextrin, since the ratio between linear-chain amylose and branched-chain amylopectin varies across different sources (Chronakis, 1998). Thus, maltodextrins from different sources may have the same DE value, but different proportions of high and low molecular weight chains. The proportion of high molecular weight chains (amylopectin) influences the solubility and stability of the solutions, while the amount of low molecular weight chains (amylose) influences the crystallization, viscosity and sweetness of MD solutions (Chronakis, 1998).

Maltodextrin solutions are prepared by dispersion in water under high temperatures, usually 90 – 95 °C, to promote hydration of the polysaccharide chains (Kasapis et al., 1993b; Kanyuck et al., 2019). Depending on maltodextrin concentration and DE, the maltodextrin solution may form gels as the temperature is lowered (Chronakis, 1998). The mechanism of maltodextrin gelation is similar to that of starch and involves the creation, at sufficiently high concentrations (so-called critical gelation concentration), of double helices by the α-1,4-linked amylose chains and long chains of branched amylopectin. The double helices then aggregate to form crystallised regions, which are connected to other crystallised regions by long chains at multiple aggregation points (Reuther et al., 1984; Chronakis, 1998; Loret et al., 2004). The critical gelation concentration of maltodextrin varies between 10 – 25% (w/w), where higher concentrations result in stronger and more solid gels, while lower concentrations result in softer gels (Schierbaum et al., 1992; Loret et al., 2004; Kanyuck et al., 2019). Holding temperature also influences gel formation, where gels formed at lower temperatures (10 °C) showed to be stronger and more brittle than gels formed at higher temperatures (60 °C) (Kanyuck et al., 2019). Further, maltodextrin gels show increasing gel strength with time for up to 12 days (Chronakis and Kasapis, 1995; Loret, Frith and Fryer, 2004; Kanyuck et al., 2019).

2.7 Concluding remarks

Quinoa protein isolate (QPI) has been shown to have a broad range of physico-chemical and technofunctional properties with potential applications in food formulations. However, this literature review has uncovered a few gaps regarding its ability to create microstructures in food systems.

There are limited reports on the phase behaviour of segregative mixtures of QPI with polysaccharides (Duran et al., 2018b; Patole, Cheng and Yang, 2022; Agarwal et al., 2023) and there are no studies focusing specifically on the creation of phase diagrams of these mixtures. Understanding the phase behaviour and interaction mechanisms of biopolymer mixtures is fundamental in the design of tailored microstructures for food applications. Maltodextrin is a neutral polysaccharide, while QPI has a negative net charge above its isoelectric point (pH 4.5), thus, it was hypothesised that aqueous mixtures of QPI and maltodextrin would display a segregative phase behaviour at pH 7, allowing the creation of phase diagrams to study the different microstructures that can be achieved by this system.

Further, previous studies have shown that the alkalinisation step of the wet fractionation of QPI should be performed at pH 8 – 9, to preserve the functional properties of the isolate. However, there is evidence in the literature that the acid used during the isoelectric precipitation step of wet fractionation also potentially affects the functionality of proteins and this has been scarcely investigated in the context of plant proteins extraction. In the case of QPI, there are no studies evaluating the effects of extraction with different acids other than HCl on its physico-chemical and technofunctional properties. Considering the Hofmeister series, it was hypothesised that acids with a higher kosmotropic effect, such as acetic acid and citric acid, would protect the protein structure during wet fractionation, preventing protein unfolding. The protection of the protein's native structure would likely positively affect its solubility, thermal properties and heat-induced gelation properties, expanding the possible applications of QPI in food systems.

During the experimental development of this thesis, it was revealed that the QPI extraction process applied was also efficient in recovering lipids from quinoa flour. Lipids

are stored in the form of emulsified oil bodies in plant seeds and show potential application in the formulation of emulsion-based food products, however, there is limited information available regarding quinoa oil bodies. Cryo-milling of plant seeds is a promising approach to recover oil bodies as it solidifies the oil during grinding. Thus, it was hypothesised that cryo-milling would promote the solidification of oil bodies in quinoa, preserving their structural stability and allowing their aqueous extraction via creaming and centrifugation to study their properties.

2.8 Aims and objectives

The overall aim of this PhD research was to explore different approaches to enable the use of quinoa protein isolate in the microstructure engineering of plant-based foods, as well as to develop a strategy to extract and characterise quinoa oil bodies. To achieve this aim, the following specific objectives were developed:

1. To investigate the phase behaviour and microstructure of mixtures between quinoa protein isolate and maltodextrin;
2. To evaluate the effect of different precipitation acids on the physico-chemical and technofunctional properties of quinoa protein isolate at different concentrations and dispersion conditions;
3. To recover and characterise quinoa oil bodies before the extraction of quinoa protein isolate from cryo-milled quinoa seeds.

Chapter 3. Analytical techniques

This chapter provides a summary of the main analytical techniques used throughout this thesis, including their principles and applications.

3.1 Rheological methods to assess heat-induced gelation of aqueous protein samples

Rheology is the science of flow and deformation, giving information on the flow behaviour of liquids and deformation behaviour of solids. Ideal rheological behaviours are divided into the viscous flow behaviour of ideal liquids, governed by Newton's law, and the elastic deformation behaviour of ideal solids, governed by Hooke's law; whereas the rheological behaviour of most real materials can be described as viscoelastic, as it is a combination between a viscous and an elastic portion. To evaluate the viscoelastic behaviour, creep, relaxation and/or oscillatory tests can be performed in shear rheometers (Mezger, 2014).

The two-plates model is typically used to define the rheological parameters that describe the flow and deformation behaviour of materials. Unidirectional shear is applied to a sample contained between two plates. The top plate with a shear area is set in motion by an applied shear force, while the bottom plate is stationary (Figure 3-1a). The shear stress, τ (Pa), is defined as the ratio between the shear force applied (F, N) and the shear area (A, m^2). The shear rate, $\dot{\gamma}$ (1/s), is defined as the ratio between the velocity (v, m/s) of the top plate and the shear gap (h, m) between the top and bottom geometries. In this research, small amplitude oscillatory rheometry with a parallel plate configuration was used to measure the viscoelastic behaviour of samples. In these tests, the top plate oscillates parallel to the bottom plate, shearing the sample back and forth, while the bottom plate is

stationary. The defection path is measured and rheologically determined as the shear strain or shear deformation, γ (%), defined as the ratio between the deflection path (s, m) and the shear gap (h) (Figure 3-1b). In oscillatory tests, a sinusoidal oscillation of a known shear stress is applied while the shear strain is measured, or vice versa. Each sine curve is described by the amplitude of the oscillatory shear, either γ or τ (shown as the green arrow in Figure 3-1c), and its angular frequency (ω, rad/s), that is, the number of oscillation cycles per second (one oscillation cycle is shown as the blue arrow in Figure 3-1c). For viscoelastic behaviours, the sine curves of the preset oscillatory shear (either γ or τ) and of the measured result have a time lag for the response signal, the so-called phase shift (δ), given by angles between 0° and 90° (Figure 3-1d) (Mezger, 2014).

The complex shear modulus (G^*, Pa) describes the viscoelastic behaviour of the material by the ration between the shear stress amplitude (τ_A) and the shear strain amplitude (γ_A). G^* is split into the storage (elastic) and loss (viscous) moduli, G' and G" (Pa), which are measures of the deformation energy stored and dissipated by the sample during shear, respectively. This relationship can be illustrated by a vector diagram (inset in Figure 3-1d), where G^* is the vector sum; the phase shift (δ) determines the position of the x-axis vector representing G' and the perpendicular y-axis vector represents G". The loss factor, tan δ, is then defined as the ratio between the viscous and elastic portions of the material, G"/G' (Mezger, 2014).

As G' and G" are susceptible to changes in the physico-chemical attributes of the material, small amplitude oscillatory tests can be used to assess the gelation properties of polymers (Figure 3-2) (Ross-Murphy, 1994). The sol-gel transition of materials that gel upon the application of heat followed by cooling, such as heat-induced protein gels, can be measured by temperature sweeps (Figure 3-2a), that is, the gradual increase and decrease

in temperature, where the amplitude of the oscillatory shear (either γ or τ) and the angular frequency are kept constant while recording G' and G" (Westphalen, Briggs and Lonergan, 2005). G' > G" values during and at the end of the temperature sweep are characteristic of a strong intermolecular network (Uruakpa and Arntfield, 2004; Sun and Arntfield, 2010). The gelation temperature (T_{gel}) or gel point is determined as the temperature of the cross-over between the viscoelastic moduli (G' = G" and tan δ = 1) (Mezger, 2014), or as the temperature given by the intercept between a linear extrapolation of the rapidly rising G' and the temperature axis (Sun and Arntfield, 2010; Ruiz et al., 2016b).

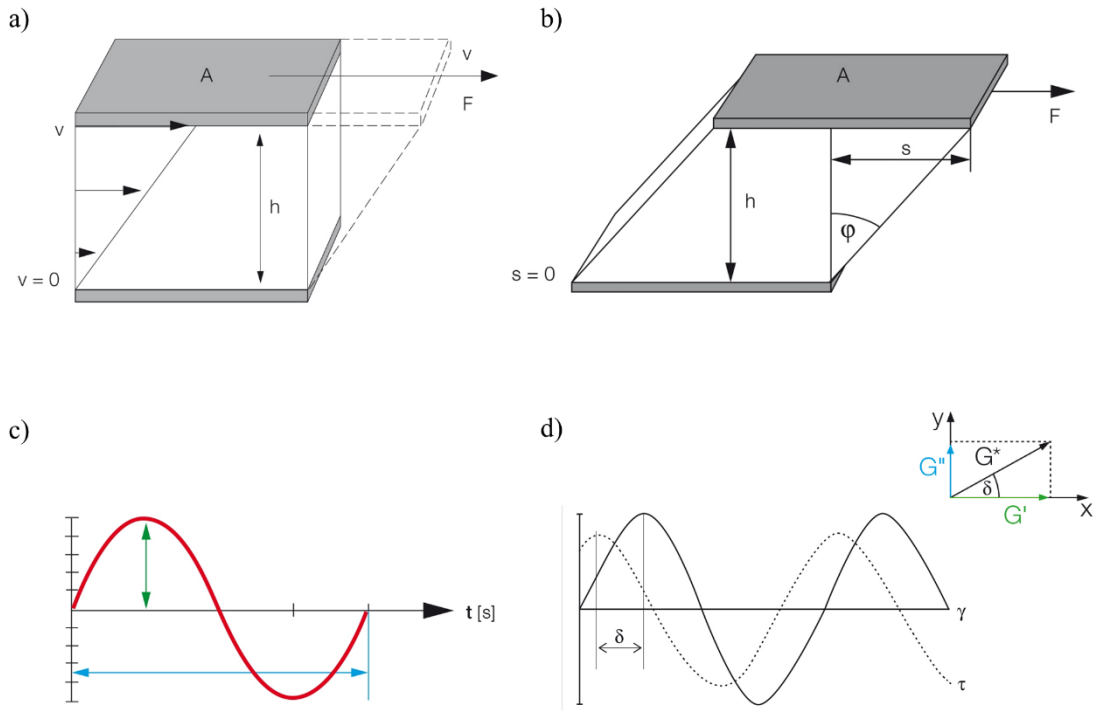

Figure 3-1. Two-plates model used to define rheological parameters for applied a) unidirectional shear and b) oscillatory deformation; c) sine curve described by the amplitude (green arrow) and angular frequency (blue arrow represents one oscillation cycle); d) oscillatory test for a viscoelastic behaviour shown as the sine curves of the preset oscillatory shear and of the measured result, the curves are offset by a phase shift (δ). The inset in d shows a vector diagram representing the relationship between the complex shear modulus (G^*), storage modulus (G') and loss modulus (G") (reproduced from Anton Paar's educational resources with permission from Anton Paar).

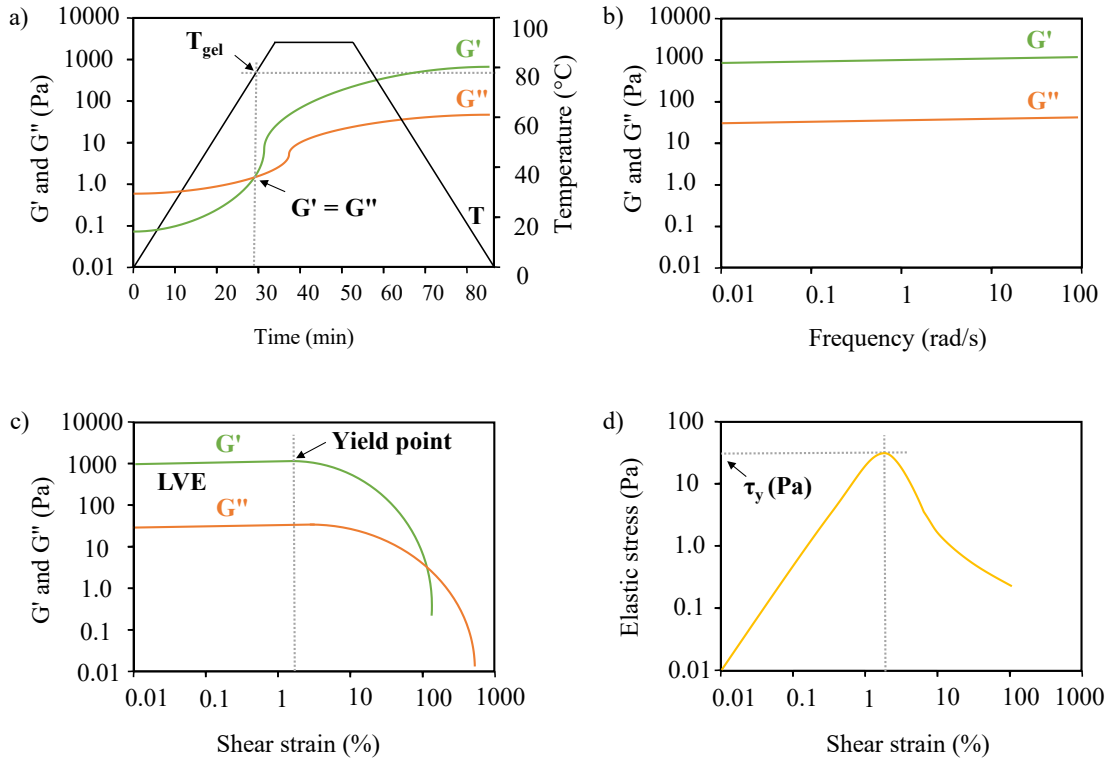

Figure 3-2. Typical rheological assessment of heat-induced gelation of aqueous protein samples: a) temperature sweep, b) frequency sweep, c) amplitude sweep and d) determination of yield stress by a plot of elastic stress versus shear strain.

Time sweeps can be applied following temperature sweeps to investigate the change in structural strength of gels at isothermal conditions where the amplitude of the oscillatory shear (either γ or τ) and the angular frequency are kept constant. If the structure of the gelled material is not time-dependent, G' and G" values will remain unchanged during time sweeps; equally, the viscoelastic moduli may increase or decrease as a result of re-enforcement or softening, respectively (Mezger, 2014).

Frequency sweeps are applied to investigate the time-dependency of the deformation behaviour of materials. These tests are performed at increasing or decreasing frequencies and constant amplitude of oscillatory shear (either γ or τ) while recording G' and G". Gelled materials are three-dimensional networks composed of stable intermolecular

interactions and thus show elastic behaviour (G' > G") and almost parallel data traces of G' and G" of very small slopes in the frequency range usually applied in oscillatory shear rheology (Figure 3-2b) (Mezger, 2014).

So-called amplitude sweeps are applied to determine the linear viscoelastic (LVE) region of the material and its yield behaviour. These tests are performed at increasing amplitude of oscillatory shear (either γ or τ) and constant angular frequencies while recording G' and G". In the LVE region (Figure 3-2c) the preset and measured parameters are proportional and the increasing amplitude or deformation is small enough that there is no change in the structure of the material, so G' and G" are constant, with G' > G" for gelled materials. G' and G" remain constant up to the yield point (γ_y or τ_y), where the deformation amplitude affects the microstructure of the material, reversibly or irreversibly, represented by a decrease in the G' value (Figure 3-2c). The γ_y or τ_y values are taken as the maximum permissible deformation amplitude and, thus, amplitude sweeps should always be carried out as a first-step characterisation of every unknown sample in small amplitude oscillatory rheometry, to ensure that the working oscillatory shear (either γ or τ) is selected from within the LVE region of the material. The yield point in terms of shear stress, the so-called yield stress (τ_y, Pa) can be used to characterise the structural strength of materials, including gels. τ_y values can be determined by a few methods, including visual analysis of the amplitude sweep graph or data table or by fitting a straight line to the G' plateau and determining the stress value at which the data starts to deviate from the fit (Mezger, 2014). Some authors report the determination of τ_y with a higher accuracy as the maximum value of elastic stress, defined as the product of storage modulus and shear strain ($G' \times \gamma$), when plotted as a function of shear strain (Figure 3-2d) (Yang, Scriven and Macosko, 1986; Walls et al., 2003).

3.2 Differential scanning calorimetry to determine thermal properties of aqueous protein samples

Calorimetry is the universal method for the investigation of chemical reactions and physical transitions in which there is generation or consumption of heat. Differential scanning calorimetry (DSC) refers to the measurement of the difference in the heat flow rate of a sample against a reference sample. Heat only flows if there is a temperature difference present, thus DSC subjects the sample and a reference sample, such as water, air or solvent/buffer, to a controlled temperature program. Additionally, DSC can give information on the heat capacity and the characteristic temperatures of the reactions or thermal transitions of a sample (Höhne, Hemminger and Flammersheim, 2003).

There are different types of DSC measuring systems but, generally, a sample and a reference sample are loaded into the equipment in parallel. When the equipment furnace is heated, heat flows to the sample and reference and the differential temperature signal (ΔT) is recorded in the form of electric voltage. When neither the sample nor reference undergo any thermal transitions, ΔT is zero. When this equilibrium is disturbed by a temperature-induced transition in the sample, a ΔT is generated, which is proportional to the difference between the heat flow rates to the sample (Φ_s, W) and to the reference sample (Φ_r, W) (Equation 3-1). The output measurement signal is the measured heat flow rate (Φ_m, W), which is related to the ΔT signal by Equation 3-2, using a factory-installed calibration factor (k') in the equipment (Höhne, Hemminger and Flammersheim, 2003).

$$\Delta T \sim \Phi_r - \Phi_s \tag{3-1}$$

$$\Phi_m = -k' \times \Delta T \tag{3-2}$$

The DSC curve shows the heat flow rate (W) on the y-axis, which can be expressed as heat flow rate per gram of sample (W/g), versus the temperature or time on the x-axis (Figure 3-3). Characteristically, the DSC curve gives information on the baseline and thermal transition peaks and temperatures of the sample. The baseline is the heat flow rate produced in the absence of reactions or thermal transitions. A peak occurs when there is a disturbance caused by heat release or consumption in the sample, that is, exothermic or endothermic transitions, respectively (Höhne, Hemminger and Flammersheim, 2003). Exothermic or endothermic peaks in DSC curves can be assigned positive ("upwards") or negative ("downwards") peaks, depending on equipment; thus, the adopted convention should always be indicated.

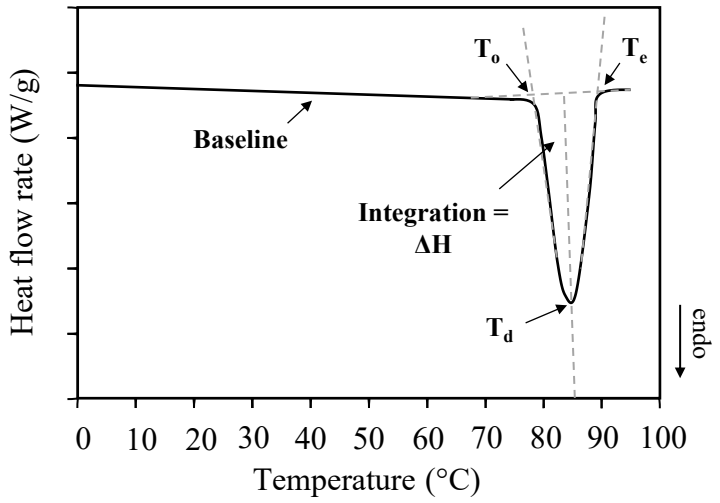

Figure 3-3. Typical DSC thermogram of an endothermic reaction, such as protein denaturation.

The area under the peak can be integrated to give the enthalpy (ΔH, J/g), which is the amount of energy released or consumed during the exothermic or endothermic reactions, respectively. Crystallisation of fats or polymerisation reactions are examples of

exothermic reactions, showing conventionally negative enthalpy values (Höhne, Hemminger and Flammersheim, 2003); whereas protein denaturation is an example of endothermic reaction showing conventionally positive enthalpy values (Figure 3-3). The integration of the area under the endothermic peaks gives the enthalpy of denaturation of proteins, which is related to their thermal stability. Higher ΔH values denote higher resistance to thermal denaturation as more energy is needed (consumed) to cause denaturation (Damodaran, 1988).

The DSC curve also gives information on characteristic thermal transition temperatures. The onset temperature (T_o) is the temperature where the peak initiates, that is, where there is a first deviation from the baseline, obtained by the intersection between the extrapolated ascending (or descending) peak slope and the baseline. The peak temperature (T_p), also denoted as the denaturation temperature (T_d) for endothermic protein denaturation processes, is the temperature where the peak reaches its maximum (or minimum) value. The endset temperature (T_e) is the temperature where the peak is completed, obtained similarly to T_o (Figure 3-3) (Höhne, Hemminger and Flammersheim, 2003).

3.3 Confocal scanning laser microscopy for microstructure assessment

Confocal laser scanning microscopy (CLSM) is a widely used technique for the visualisation of a variety of samples in the biomedical and material sciences, being especially useful to acquire high resolution images of thin sections of thick samples. Basic components of a confocal microscope are shown in Figure 3-4a. Light from a laser beam source is passed through a dichroic mirror and reflected to the objective, which focuses the laser beam to a point in the sample. Scanning mirrors then sweep the laser beam over

the sample point by point in the x and y directions of the single field of view (Figure 3-4b).

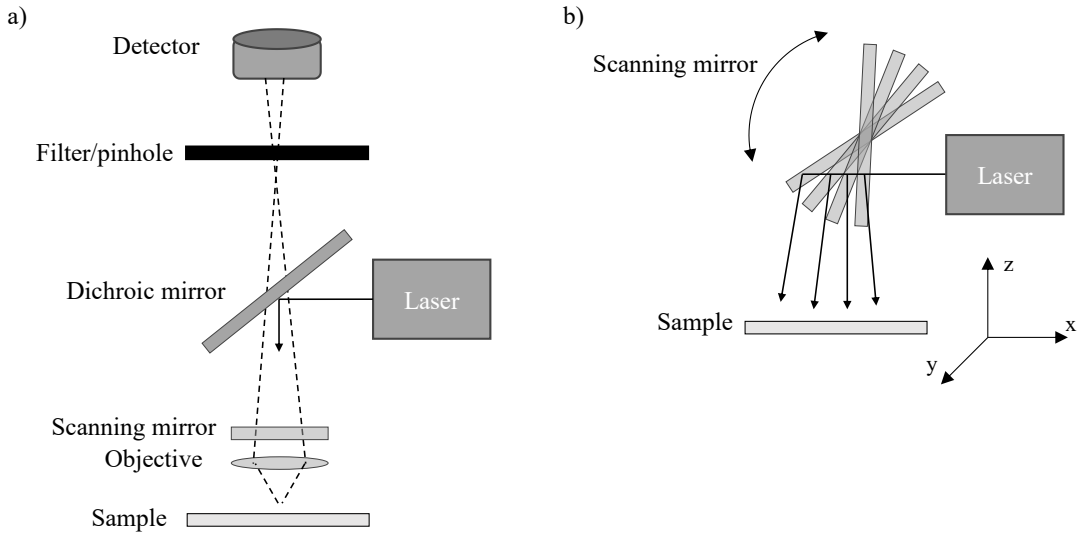

Figure 3-4. a) Basic components of a confocal microscope; b) scanning mirrors used to sweep the laser beam over the sample. Adapted from Elliott (2020).

The excitation of the fluorochrome molecules in the sample results in the emission of fluorescent light, which passes through the microscope's objective and is collected by the detector to form the image. The laser scanning can also be moved incrementally across the sample in the z direction to produce a three-dimensional (3D) image. A filter (commonly called a pinhole) is placed in front of the detector to block out-of-focus light arising from planes above and below the focal plane, which allows for the acquisition of high resolution images of thick samples (Sheppard and Shotton, 1997; Elliott, 2020).

Samples in CLSM often need to be treated with fluorescent dyes or stains which can be molecule-specific. This feature is especially advantageous in the visualisation of multi-component microstructures as it allows for the localisation and differentiation of the

different components, as long as the stains applied have different emission wavelengths (Elliott, 2020). For the visualisation of samples containing both protein and lipid components, for example, the protein-specific stain Fast Green FCF (excitation at 638 nm and emission at 660 – 710 nm) and the lipid-specific stain Nile Red (excitation at 488 nm and emission at 550 – 620 nm) can be used (Ong et al., 2011). Quantitative data, such as gel porosity and particle size (Ong et al., 2020), can also be collected from CLSM images by image analysis software (Nechyporuk-Zloy, 2022).

3.4 Gel electrophoresis for protein separation

Polyacrylamide gel electrophoresis (PAGE) is a widely applied technique for protein separation on the basis of surface charge and molecular weight, and thus gives information about the protein profile of a sample. It consists of the migration of charged protein molecules through a gel, driven by an applied electric field. The migration of the protein molecules through the gel depends on several factors, including size, shape, surface charge, the presence of aggregates and buffer pH. The PAGE matrix is a gel formed by the copolymerisation of acrylamide and a cross-linking agent, such as N,N-methylenebis(acrylamide), and the gel's pore size can be controlled by the ratio between acrylamide and cross-linker, allowing the separation of proteins of a wide range of charges or molecular weights (Kurien and Scofield, 2019).

In PAGE, the separating gel is placed between two electrodes of opposite charges and immersed in buffer. Upon loading into the gel, negatively charged proteins migrate to the cathode and once the separation is completed, the gel is stained/destained by appropriate methods to reveal bands identifying the retained proteins (Kurien and Scofield, 2019).

Native-PAGE refers to the electrophoresis technique where the proteins in the sample maintain their surface charge and native (folded) structure, thus the separation is dependent not only on their charge but also size and shape. This technique is useful to identify different native protein molecules in the sample or when recovery of proteins after separation is desired (Arndt et al., 2019), however, it shows low separation efficiency of complexes, isoforms and small proteins (Eubel, Braun and Millar, 2005).

A much more common electrophoretic technique is SDS-PAGE, consisting of the use of sodium dodecyl sulfate (SDS), a detergent that forms negatively charged micelles around the protein molecule, minimising the influence of protein surface charge. Further, the proteins are usually denatured under heat before loading into the gel, minimising the influence of protein structure (Arndt et al., 2019). The separation of the proteins in the gel upon the application of the electric field is then solely dependent on their size, with small proteins moving faster through the gel than larger proteins which are likely to retain in the gel. Molecular weight protein markers are loaded onto the gel alongside the sample to serve as a reference for the migration profile and allow the determination of the molecular weight profile of the sample (Matsumoto, Haniu and Komori, 2019).

SDS-PAGE can be performed under reducing or non-reducing conditions. Under reducing conditions, a reducing agent is added, normally β-mercaptoethanol or dithiothreitol (DTT), which breaks disulfide bonds. Thus, protein subunits that are linked by disulfide bonds are expected to separate into different bands in the gel. Under non-reducing conditions, no further reducing agents are added, so disulfide bonds remain intact and proteins subunits remain linked, moving as one through the gel (Kurien and Scofield, 2019).

3.5 Fourier transform infrared spectroscopy for protein secondary structure assessment

Infrared (IR) spectroscopy is the study of the interaction of infrared light with matter, giving information on which molecules are present in a sample and at which concentrations (Smith, 2011). An IR spectrum is obtained by passing an IR source through the sample and determining what fraction of the radiation is absorbed at a particular wavelength. Each peak in an IR spectrum corresponds to the vibrational frequency of specific functional groups, which must have a dipole moment in order to absorb infrared radiation, such as CH_2 and C=O. The modes of vibration of functional groups can be either stretching (change in bond length) or bending (change in bond angle) and are dependent of mass of the atoms, molecule shape and bond stiffness (Che Man, Syahariza and Rohman, 2010; Karoui, 2018). Peak positions in infrared spectra correlate with molecular structure and peak positions of known molecules can be used as reference to identify unknown samples (Smith, 2011).

Fourier transform infrared spectroscopy (FTIR) is based on interferometry. The Michelson interferometer is employed in most FTIR instruments, which uses a beam splitter to divide the IR source into two beams travelling two different paths, one reflected to a fixed mirror and the other reflected to a moving mirror (Figure 3-5). The two beams are then recombined at the beam splitter, but, due to their different paths, they each undergo constructive or destructive interferences so that the superposition of the beams results in a final amplitude that is higher or lower than the amplitude of each beam, respectively. The recombined beam is then passed through the sample and the light that is transmitted, reflected or absorbed is measured by the detector. The moving mirror is gradually moved away from the beam splitter to scan the sample multiple times. The

output signal is an interferogram, which is the sum of cosine waves consisting of the intensity of the energy measured versus the position of the moving mirror. According to the Fourier's theorem, any superposition of sine or cosine waves can be expressed as a mathematical function. Thus, the Fourier transform of an interferogram gives a function known as the conventional IR spectra (Smith, 2011; Karoui, 2018).

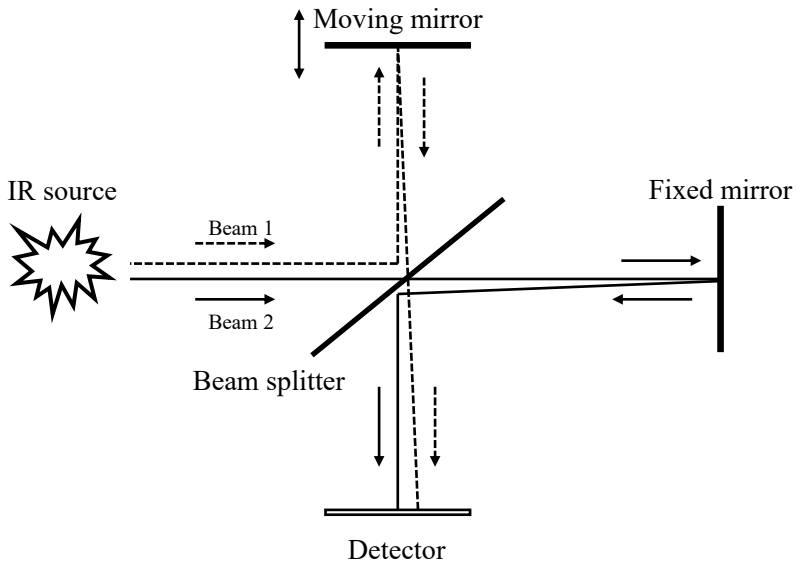

Figure 3-5. Basic components of an interferometer, part of most FTIR spectrometers. Adapted from Karoui (2018).

Most FTIR spectrometers work in the mid-infrared region (400 – 4000 cm^{-1}), where molecular vibrations can be measured. Attenuated total reflectance (ATR) is one of the most important sampling techniques for FTIR, in which the sample is put in contact with a crystal of high refraction index made of zinc selenide (ZnSe), germanium (Ge) or diamond. ATR is based on internal reflectance of the IR beam, where the radiation originating from the beam splitter is reflected in the surface of the crystal one or more times. This creates an evanescence wave, that is, penetrating electromagnetic fields which decrease in intensity as they move away from the source. The evanescence wave passes

through the sample, generating the IR spectrum. ATR is a useful FTIR technique to acquire spectra of materials that are either too thick or too opaque to be used in other sampling techniques, such as transmission IR measurement (Che Man, Syahariza and Rohman, 2010; Karoui, 2018). Thus, FTIR-ATR spectroscopy can be used with variety of materials, including gels, powders and liquids (Yuan et al., 2017; Andrade et al., 2019; Pax et al., 2019; Ong et al., 2020).

IR spectroscopy gives information on the secondary structure of proteins, including ligand interactions and unfolding events. The main spectral signals that are related to protein structures are the Amide A and B and Amides I – VII. Amide I, located in the region of 1600 – 1700 cm^{-1} of the IR spectra, gives information on the protein backbone and it is often the most intense peak of protein spectra. It is related to the presence of C=O and C-N bonds and characterised by a high sensitivity to small changes in molecular geometry (Khanmohammadi and Garmarudi, 2010). The contribution of each conformation of secondary structure to the overall protein structure can be determined by the application of the second derivative of the Amide I peak followed by deconvolution by appropriate software. Peaks at ~1625 cm^{-1} (range 1580 – 1680 cm^{-1}) are related to β-sheet conformations, at ~1650 cm^{-1} (1640 – 1660 cm^{-1}) correspond to random coil structures, at ~1670 cm^{-1} (1645 – 1690 cm^{-1}) correspond to α-helix confomations and at ~1690 cm^{-1} (1670 – 1700 cm^{-1}) are related to β-turns structures (Figueroa-González et al., 2022).

Chapter 4. Atypical phase behaviour of quinoa protein isolate in mixture with maltodextrin

Published article in Food Research International.

Amarante, M.C.A., MacCalman, T., Harding, S.E., Spyropoulos, F., Gras, S. and Wolf, B. (2022) 'Atypical phase behaviour of quinoa protein isolate in mixture with maltodextrin', *Food Research International*, 162, pp. 112064. doi:10.1016/j.foodres.2022.112064.

Authorship contribution statement:

Marina Campos Assumpcao de Amarante: Conceptualisation, Formal analysis, Investigation, Methodology, Software, Validation, Visualization, Writing – original draft, Writing – review & editing. **Thomas MacCalman:** Methodology, Investigation. **Stephen E. Harding:** Methodology. **Fotis Spyropoulos:** Supervision, Writing – review & editing. **Sally Gras:** Conceptualisation, Funding acquisition, Project administration, Resources, Supervision, Writing – review & editing. **Bettina Wolf:** Conceptualisation, Funding acquisition, Project administration, Resources, Supervision, Writing – review & editing.

Acknowledgements: This work was supported by the Priestley Joint PhD Scholarship from the University of Birmingham (UK) and The University of Melbourne (Australia).

Abstract

Consumers are increasingly looking for new plant-based alternatives to substitute animal proteins in their diets but for some applications it can be difficult to achieve the desired product microstructure using only plant proteins. One approach to facilitate structuring is to mix these plant-based ingredients with a polysaccharide. Here, the phase behaviour and microstructure of quinoa protein isolate (QPI) in mixture with maltodextrin (MD) of two dextrose equivalents (DE 7 and 2) were investigated. The binodals of both QPI-MD phase diagrams showed an atypical shape, where the concentration of MD in the QPI-rich phase and of QPI in the MD-rich phase increased with overall biopolymer concentration. Molecular weight distribution and microstructure analyses revealed that both maltodextrins fractionated between the phases and were probably entrapped within the volume-spanning protein network in the QPI-rich phase, indicating a depletion flocculation mechanism of phase separation. The pre-heating of QPI and the removal of salt from the systems resulted in similarly atypical phase diagrams. The approach presented contributes to our understanding of the phase behaviour of mixtures between plant proteins and polysaccharides, while the results suggest that the formulation of plant-based products of predictable properties may be more challenging than anticipated.

Keywords: biopolymer mixture, phase diagram, depletion flocculation, plant protein, microstructure, molecular weight distribution.

4.1 Introduction

Biopolymer mixtures, mainly those composed of a protein and a polysaccharide, have been extensively applied in the creation of a wide range of microstructures in the food and healthcare industries. Polymer-polymer and polymer-solvent interactions influence the physico-chemical properties of these mixtures, consequently defining their possible applications. The design of new products containing these systems relies on an understanding of the mechanism by which these components interact and the relationship between microstructure and product rheology (Frith, 2010).

Traditionally, studies on biopolymer mixtures have mainly focused on systems composed of polysaccharides and animal-based proteins, such as whey protein (Kim, Decker and McClements, 2006), bovine serum albumin (Antonov and Wolf, 2006) and gelatine (Kasapis et al., 1993b). Over the last decade, though, the research community and industry have paid increasing attention to plant proteins due to consumer concerns with the sustainability of the animal protein industry (Mattice and Marangoni, 2019). At first, studies emerged on the phase behaviour of polysaccharides and isolated protein fractions of plant origin, i.e., globulin fraction or rubisco (Antonov et al., 1979; Antonov and Soshinsky, 2000; Antonov, Dmitrochenko and Leontiev, 2006). More recently, protein mixtures (referred to as protein concentrate or isolate with no clear differentiation in terms of protein content in the mixtures among the publications cited further on) containing more than one isolated plant protein, have been progressively explored. Soy and pea protein appear to be the most studied plant proteins for the creation of biopolymer mixtures with polysaccharides, although very few studies on phase behaviour can be found (Li et al., 2008b; Mession et al., 2012a, 2012b), where the majority focuses on the

association between the biopolymers (Gharsallaoui et al., 2010; Lan, Chen and Rao, 2018; Guo et al., 2019; Lan et al., 2020b, 2020a).

Quinoa (*Chenopodium quinoa* Willd.) is considered an attractive non-animal protein source due to its high nutritional value and absence of gluten (Föste et al., 2015). Its global consumption has recently become very popular and its production expanded from the traditional Andes region of South America to a wide range of different cultivation areas worldwide (Murphy et al., 2019). Quinoa protein isolate (QPI) is a protein mixture prepared via a fractionation process from quinoa and has been increasingly investigated in the last few years, especially due to its complete essential amino acid profile (Steffolani et al., 2016; Mir, Riar and Singh, 2019a; Cerdán-Leal et al., 2020), which meets the amino acid requirements for adults suggested by the Food and Agriculture Organization of the United Nations (FAO), the World Health Organization (WHO) and the United Nations University (UNU) (WHO/FAO/UNU, 2007; Vilcacundo and Hernández-Ledesma, 2017). QPI has been shown to present a range of potential applications in the food industry due to its functional properties, which are largely affected by extraction pH, including thermal stability and gel formation (Abugoch et al., 2008; Ruiz et al., 2016b). However, to the best of the authors' knowledge, there are no studies on the phase behaviour of QPI in mixture with polysaccharides aiming at the design of microstructures for food applications.

Maltodextrin (MD) is a polysaccharide derived from the acidic or enzymatic hydrolysis of starch (Saavedra-Leos et al., 2015). Its chemical structure consists of D-glucose monomers linearly linked by α-1,4 glucosidic bonds (Zheng, Jin and Zhang, 2007; Klinjapo and Krasaekoopt, 2018) and it may contain branch points arising from α-1,6 bonds (Chronakis, 1998). Maltodextrins are characterised by their dextrose

equivalent (DE), which refers to the extent of starch hydrolysis and represents the percentage of reducing sugars, i.e., free glucose groups that define the reducing power of starch-derived polysaccharides (Wang and Wang, 2000). Generally, the higher the DE value, the greater the extent of starch hydrolysis and the lower the number-average molecular weight (Saavedra-Leos et al., 2015). The general properties of MD include low sweetness, the absence of odour and moderate viscosity and solubility in cold water. Therefore, maltodextrins are widely applied in the food industry to confer texture and bulk, or to replace fat in food products, as well as to assist in the spray-drying of flavours and seasonings (Wang and Wang, 2000; Zheng, Jin and Zhang, 2007). The use of MD as a phase separating polysaccharide has been widely explored, mainly in a mixture with refined animal proteins, such as gelatine and caseinate (Kasapis et al., 1993b; Manoj, Kasapis and Chronakis, 1996; Williams et al., 2001; Loret et al., 2005; Beldengrün et al., 2018). There is limited information, however, on the phase-separating behaviour of mixtures of MD and plant proteins (Nguyen et al., 2014).

The aim of this study was to investigate the relationship between the phase behaviour of QPI and MD and the microstructure of these systems, envisaging the creation of tailored microstructures for the design of plant protein-enriched products. MD is a neutral polysaccharide and QPI has a negative net charge above its isoelectric point, i.e., pH 4.5 (Mir, Riar and Singh, 2019a). Thus, aqueous mixtures of QPI and MD should be expected to separate into co-existing QPI- and MD-rich phases at pH 7.0, also known as segregative phase behaviour. These mixtures could be processed to create kinetically trapped anisotropic structures, where, depending on the gelation behaviour of the biopolymers in the mixture and the extent of shear applied, a range of different microstructures can be formed, such as deformed gel particles (Norton et al., 2000; Wolf et al., 2000; Beldengrün

et al., 2018), phase separated mixed gels (Norton et al., 2000; Ben-Harb et al., 2018) or fibres (Wolf et al., 2000; Tolstoguzov, 2002; Wolf and Frith, 2003). Phase diagrams were constructed to represent the segregative phase behaviour of the mixtures, where a binodal curve separates the one- and two-phase regions, located below and above the curve, respectively. Parallel tie-lines connect the binodal points corresponding to the compositions of the co-existing phases (top and bottom) with the initial mixture composition (Dickinson, 2019).

In this study, the phase behaviour of QPI was investigated in mixture with maltodextrins of two different DE values, DE 2 and 7, i.e., different molecular weights, since the molecular weight of the polysaccharide is a key factor influencing the incompatibility of biopolymer mixtures (Tolstoguzov, 2000b). Molecular weight distributions of the MDs and micrographs of the separated phases were acquired in aid of understanding the observed phase behaviour. Additionally, the partial denaturation through heat treatment has been previously shown to affect the phase behaviour of other proteins (Kim, Decker and McClements, 2006; Chun et al., 2014). Therefore, the influence of heat pre-treatment on the phase diagram of QPI and MD of DE 2 was also investigated, as MD of DE 2 has been reported to show segregative phase behaviour with other proteins (Manoj, Kasapis and Chronakis, 1996; Beldengrün et al., 2018). Moreover, ionic strength affects protein structure and protein-polysaccharide interactions, consequently influencing the phase behaviour of the mixtures. Thus, the absence of salt in the QPI-MD systems was also studied in order to build a better understanding of these mixtures.

4.2 Materials and methods

4.2.1 Materials

The quinoa flour, produced from white quinoa seeds, was purchased from The British Quinoa Company® (Ellesmere, UK). The white quinoa seeds were grown on Shropshire farm (Ellesmere, UK), harvested in 2015, cleaned, selected, sorted and stored in 2016 – 2017. The seeds were then flaked and milled into flour in the first trimester of 2019. According to the manufacturer, the flour contained, on a dry weight basis, 14.3% protein, 65.7% carbohydrate (of which 2.6% was sugar), 6.8% fat and 6.8% fibre. Maltodextrin (MD) with a dextrose equivalent (DE) of 7 produced from corn starch (C*Dry MD) was purchased from Cargill® (USA). MD of DE 2 produced from potato starch (Paselli SA-2) was purchased from Avebe® (Netherlands). NaOH pellets (≥ 97%) and NaCl (≥ 99.5%) were purchased from Fisher Scientific® (UK). HCl (≥ 32%) was purchased from Honeywell® (UK). Sodium azide (≥ 99.5%) and starch assay kit were purchased from Sigma-Aldrich® (UK). Double distilled water with a resistivity of 15.0 MΩ.cm (Millipore®, UK) was used in all experiments.

4.2.2 Quinoa protein isolate extraction and characterisation

4.2.2.1 Extraction from quinoa flour

Quinoa protein isolate was extracted from quinoa flour using the method of Ruiz et al. (2016b), except that the flour defatting step was omitted to avoid the use of organic solvents and the centrifugal speed was modified. Briefly, the flour was sieved through a 250 μm aperture sieve and suspended in water (10%, w/w). The pH was adjusted to 9.0 using 1 M NaOH and the suspension was agitated at 22 °C for 4 h, then stored at 4 °C for

16 h. Afterwards, the suspension was centrifuged for 30 min at 10 °C and 8228 × g and the supernatant poured through a cheesecloth to separate the cream layer (Geerts et al., 2018). The precipitate and cream layer were discarded. The pH of the supernatant was adjusted to 4.5 using 1 M HCl to induce isoelectric precipitation of the protein, followed by centrifugation as described above. The precipitate was rinsed by re-suspending in distilled water and centrifuged once more. Finally, the precipitate was re-suspended in distilled water, neutralised using 1 M NaOH and freeze-dried for 72 h (Labogene®, Scanvac Coolsafe, Denmark). The lyophilised quinoa protein isolate (QPI) was kept at 4 °C until use.

4.2.2.2 Compositional analysis and protein yield

The total protein content of the prepared QPI and quinoa flour was determined as total nitrogen content, via elemental analysis (Thermo Flash EA 1112, ThermoFisher Scientific®, UK) and converted to total protein using a conversion factor of 5.85 (Abugoch et al., 2008; Ruiz et al., 2016b). Moisture, ash and fat were assayed through methods from the Association of Official Analytical Chemists (AOAC, 2002), i.e., method numbers 934.01, 923.03 and 920.39 (using hexane as solvent), respectively. Carbohydrate content was determined by difference. Starch content was determined using a starch assay kit (Supelco™ Analytical, Sigma Aldrich®, USA), where starch is hydrolysed to glucose by amyloglucosidase and glucose concentration measured by the change in absorbance at 340 nm.

Protein yield was calculated considering the total protein content of QPI and of quinoa flour, using Equation 4-1.

$$\text{Protein yield (\%)} = \frac{\text{total protein content in QPI (\%)} \times \text{QPI weight (g)}}{\text{total protein content in quinoa flour (\%)} \times \text{flour weight (g)}} \times 100\% \quad (4\text{-}1)$$

4.2.3 Acquisition of phase diagrams

For the acquisition of QPI-MD phase diagrams, stock solutions of both polymers were prepared in 0.1 M NaCl solution, as salt promotes phase separation (Grinberg and Tolstoguzov, 1997) and mixed at different ratios. The QPI-MD mixtures were then centrifuged to obtain two phases and the biopolymer composition in each phase was determined to construct phase diagrams. Mathematical approximations of the phase diagrams were also undertaken.

4.2.3.1 Preparation of stock solutions

A QPI stock solution (10%, w/w) was prepared by dissolving the lyophilised QPI in 0.1 M NaCl containing 0.03% (w/w) sodium azide to prevent microbial growth. The solution was stirred constantly for 2 h at pH 9.0 (adjusted with 1 M NaOH). The pH was adjusted to 7.0 (with 1 M HCl) and the stock solution was kept stirring overnight on a magnetic stirrer at 22 °C. To remove any insoluble material, the QPI stock solution was centrifuged for 1 h at 10 °C and 2400 × g and used immediately.

Stock solutions of maltodextrin of DE 7 and DE 2 were prepared by dissolving the powders in 0.1 M NaCl (containing 0.03% (w/w) sodium azide) at 90 °C under constant stirring. After the powders appeared to be completely dissolved, the solutions were cooled

to room temperature (22 °C) and used immediately after pH adjustment to 7.0 using 1 M NaOH.

4.2.3.2 Preparation of phase-separated QPI and MD mixtures

Mixtures (10 g) of QPI and MD of DE 7 and 2, respectively, containing different concentrations of both polymers were prepared by mixing weighted amounts of QPI and MD stock solutions with 0.1 M NaCl (containing 0.03% (w/w) sodium azide). Four mixtures of each system were studied, in concentration ranges of 0.2 – 4.3% QPI (w/w) and 0.4 – 5.7% MD (w/w). The mixtures were stirred for 2 h at 22 °C, then transferred to graduated centrifuge tubes and kept for approximately 16 h at 22 °C to allow for phase separation. The mixtures were then centrifuged for 1 h at 10 °C and 2400 × g and the equilibrium phases were separated with a pipette.

4.2.3.3 Experimentally determined phase diagrams

Phase volume fractions were determined using a graduated cylinder and phase densities were calculated from the weight of samples of known volume to obtain the phase compositions in w/w. QPI concentration (x-axis of phase diagrams) was determined by measurement at 280 nm using an UV-Vis spectrophotometer (Orion AquaMate 8000, Thermo-Scientific®, UK), utilising solutions of known concentrations of lyophilised QPI for the calibration curve. Maltodextrin concentration (y-axis of phase diagrams) was determined in each phase by the sulfuric acid-UV method (Albalasmeh, Berhe and Ghezzehei, 2013), used for the determination of monosaccharides, disaccharides and polysaccharides of high molecular weight. Briefly, 1 mL of sample was acidified with

3 mL of concentrated sulfuric acid, then agitated in a vortex for 30 s and cooled to room temperature (22 °C) in an ice bath before measuring the absorption of the samples using an UV-Vis spectrophotometer at 315 nm. MD concentrations were calculated from calibration curves acquired for each MD.

Finally, the experimental phase diagrams were constructed by plotting the tie-lines and manually fitting the binodals to the equilibrium phases points. The phase separation threshold corresponds to the minimum overall biopolymer concentration in the mixture required for phase separation (Tolstoguzov, 2002) and it was calculated as the point of contact between a tangent line with a slope of −1 that crosses equal segments of both axes and the binodal (Antonov et al., 1996). The critical point gives the composition of the system that demixes into phases of the same volume and composition and it was calculated as the point of interception of the binodal with the rectilinear diameter, i.e., a straight line that connects the composition of the system at the centre of each tie-line, i.e., at 50:50 phase volume (Tolstoguzov, 2002). The critical point and threshold point are unique characteristics of a phase diagram and if they coincide, the phase diagram is symmetrical. On the other hand, as the distance between the critical and threshold points increases, the phase diagram becomes increasingly asymmetrical (Zaslavsky, 1995). Several mixtures of each experimental phase diagram were prepared and analysed twice to verify reproducibility.

4.2.3.4 Mathematical approximations of the phase diagrams

The phase diagrams were also mathematically approximated, using the volume fraction method suggested by Spyropoulos, Portsch and Norton (2010). The method consists of

the determination of the approximate composition of the equilibrium phases of a given aqueous two-phase system (ATPS) using the initial concentration of both biopolymers in the mixture and the volume fraction of each phase after phase separation. The following assumptions were made: (1) both biopolymers are pure and consist of one species of constant molecular weight, (2) the mixtures display classical segregative phase separation behaviour and (3) the tie-lines of the phase diagrams are parallel, i.e., of the same slope.

A two-parameter exponential decay function (Equation 4-2) was fitted to the top and bottom phases concentration data to give the binodals of the phase diagrams.

$$[\mathrm{MD}] = a \times e^{-b \times [\mathrm{QPI}]} \tag{4-2}$$

where [MD] and [QPI] correspond to the concentration of MD and QPI, respectively, and *a* and *b* are best fit parameters that describe the shape of the binodal. Tie-lines were calculated using Equations 4-3a-c:

$$[\mathrm{MD}]_{\mathrm{I}} = [\mathrm{MD}]^{0} + \mathrm{STL} \times [\mathrm{QPI}]_{\mathrm{I}} \tag{4-3a}$$

$$[\mathrm{MD}]_{\mathrm{T}} = [\mathrm{MD}]^{0} + \mathrm{STL} \times [\mathrm{QPI}]_{\mathrm{T}} \tag{4-3b}$$

$$[\mathrm{MD}]_{\mathrm{B}} = [\mathrm{MD}]^{0} + \mathrm{STL} \times [\mathrm{QPI}]_{\mathrm{B}} \tag{4-3c}$$

where subscripts I, T and B relate to the initial mixture, the top and bottom phase after phase separation, respectively. $[\mathrm{MD}]^{0}$ corresponds to the intercept between the y-axis of the phase diagram and the tie-line, and STL corresponds to the slope of the tie-line. Combining Equations 4-3a, 4-3b and 4-3c and consequently eliminating $[\mathrm{MD}]^{0}$ and STL, gives Equation 4-4:

$$\frac{[MD]_T - [MD]_I}{[MD]_B - [MD]_I} = \frac{[QPI]_T - [QPI]_I}{[QPI]_B - [QPI]_I} \quad (4\text{-}4)$$

The compositions of the top and bottom phases must lie on the binodal described by Equation 4-2. For maltodextrin this concentration is:

$$[MD]_T = a \times e^{-b \times [QPI]_T} \quad (4\text{-}5a)$$

$$[MD]_B = a \times e^{-b \times [QPI]_B} \quad (4\text{-}5b)$$

Finally, each tie-line is divided into two segments: $\overline{TI}$ and $\overline{BI}$, where I, T and B correspond to the initial, top and bottom phase composition, respectively. As pointed out by Spyropoulos, Portsch and Norton (2010), Zaslavsky (1995) has shown that the ratio between the length of each of these segments and the length of the entire tie-line $\overline{TB}$ corresponds to the volume fraction of the top (Vf_T) and bottom (Vf_B) phases at equilibrium:

$$Vf_T = \frac{\overline{TI}}{\overline{TB}} = \frac{[QPI]_I - [QPI]_B}{[QPI]_B - [QPI]_T} \quad (4\text{-}6a)$$

$$Vf_B = \frac{\overline{BI}}{\overline{TB}} = \frac{[QPI]_I - [QPI]_T}{[QPI]_B - [QPI]_T} \quad (4\text{-}6b)$$

Therefore, the QPI and MD concentrations in the top and bottom phases ($[QPI]_T$, $[QPI]_B$, $[MD]_T$, $[MD]_B$) can be calculated based on the initial biopolymer concentration in the mixtures and the experimentally determined volume fractions of the top and bottom phases after phase separation, by numerically solving Equations 4-4, 4-5a (or 4-5b) and 4-6a (or 4-6b). Fitting Equation 4-2 to the resulting data set then allows the determination of the binodal. The phase separation thresholds for the mathematical approximations were determined as described for the experimentally determined phase diagrams (Section 4.2.3.3).

4.2.4 Microstructure visualisation

The microstructure of initial mixtures and equilibrium phases was visualised at 22 °C using an optical microscope (DM 2500 LED, Leica®, CH) in phase contrast mode (Sarbon, Badii and Howell, 2015). A droplet of sample was added to each slide (not diluted) and covered with a cover slip.

4.2.5 Determination of molecular weight distribution of MD

The molecular weight distribution of both MD samples was determined by size exclusion chromatography coupled with multi angle laser light scattering (SEC-MALS), consisting of a Postnova Analytics® PN7505 degassing unit (Germany), a Shimadzu® LC-10 AD HPLC Pump (UK), a Spark-Holland® Marathon Basic autosampler (Netherlands), a Shodex™ LB-G 6B guard column (USA) and a Shodex™ LB-805 column (USA) connected in series. Light scattering intensities were measured simultaneously at 18 angles as a function of elution volume using a DAWN® HELEOS™ II light scattering

photometer, connected in series to a ViscoStar® II on-line differential viscometer and an Optilab® rEX refractive index detector (Wyatt Technology Corporation, USA). Samples were filtered using 0.2 μm polyvinylidene difluoride (PVDF) Whatman® Puradisc 25 syringe filters. Aliquots of 50 μL of each MD stock solution were injected onto the columns at 22 °C. The eluent used was 0.1 M NaCl with 0.01% ProClin™ 150 (Sigma-Aldrich®) at a flow rate of 0.5 mL/min. The laser was used at a wavelength of 633 nm and the refractive increment for maltodextrin was 0.155 mL/g. ASTRA™ (Version 6) software was used to calculate the weight average molecular weight (M_w). Thermodynamic non-ideality effects were assumed to be negligible, due to low sample concentrations and their constant dilution in the columns (Horton, Harding and Mitchell, 1991).

4.2.6 Differential scanning calorimetry

The thermal properties of QPI were determined by differential scanning calorimetry (DSC; μDSC3evo run, Setaram Instrumentation®, France). QPI (10%, w/w) was suspended in distilled water and kept under magnetic stirring for 1 h at 22 °C, without pH adjustment. Hermetically sealed pans were filled with around 0.5 g of QPI suspensions. A hermetically sealed pan with a matching mass of distilled water was used as reference. Samples were heated at a rate of 2 °C/min from 20 to 120 °C, kept at this temperature for 5 min and then cooled at the same rate to 20 °C. The denaturation temperature (T_d), defined as the temperature where the maximum transition peak occurred, and the denaturation enthalpy (ΔH), defined as the area below the transition peak, were calculated using the CALISTO software (Seteram Instrumentation®, France). Enthalpy was then converted to J/g QPI by considering the sample concentration (10%, w/w).

4.2.7 Effect of heat pre-treatment and absence of salt on phase behaviour

The effect of protein heat pre-treatment and absence of salt on the phase behaviour were also investigated. Both factors can affect both protein structure and protein-polysaccharide interactions, thus influencing phase behaviour. For the study of heat pre-treatment, the QPI stock solution was incubated at 55 °C for 30 min and then cooled to room temperature (HTQPI). For the investigation of the effect of salt, both QPI and MD stock solutions were prepared as described in Section 4.2.3.1, except for the absence of NaCl. Phase diagrams were then acquired as outlined in Section 4.2.3.3.

4.3 Results and discussion

4.3.1 Composition and yield of QPI

The total protein content of the quinoa flour used here was of 15.2%, close to previous reports of 14.0% protein in quinoa seeds (Elsohaimy, Refaay and Zaytoun, 2015). QPI was extracted by an aqueous-based extraction protocol at pH 9.0 followed by precipitation at pH 4.5, resulting in a protein yield of 19.4% and a wet weight protein content (i.e., purity) of 59 ± 3%. Both values are within the wide range previously reported in literature for QPI extracted at pH 9.0: ~9.2 – 37% for protein yield (Nongonierma et al., 2015; Ruiz et al., 2016a) and ~41 – 96% for protein content (Nongonierma et al., 2015; Ruiz et al., 2016b, 2016a; Steffolani et al., 2016; Mir, Riar and Singh, 2019a). The differences between protein extraction yield and content arise from variations in extraction protocols and the use of different quinoa cultivars. For example, the protein content obtained for QPI extracted at pH 9.0 from six different quinoa varieties varied between ~85 – 96% (Steffolani et al., 2016). The QPI extracted here further contained

11 ± 3% fat, 3.0 ± 0.6% starch, 1.4 ± 0.8% moisture, 3.0 ± 0.5% ash and 25.6% carbohydrate calculated by difference. The fat content of QPI is usually not reported in literature, presumably because it is non-detectable. However, most studies apply a quinoa flour defatting step using hexane or petroleum ether prior to QPI extraction. Yang et al. (2022b) reported a 4.9% fat content for their QPI extracted from defatted quinoa flour. Here, aqueous fractionation was used without prior flour defatting to avoid the use of toxic organic solvents. Therefore, a fraction (8.2%) of the fat contained in the flour was carried over into the QPI extract.

4.3.2 QPI-MD phase separation behaviour

The key aim of this study was to elucidate the phase behaviour of QPI and maltodextrin of DE 7 and DE 2 in aqueous mixture, and thus phase diagrams were constructed. Molecular weight data and micrographs were additionally acquired as supportive evidence for the assumed type of phase behaviour displayed by the QPI-MD systems. Figure 4-1 shows the mathematical approximation of the phase behaviour assuming segregative phase separation into two aqueous phases, each enriched in one of the two biopolymers. The experimentally acquired phase diagrams are shown in Figure 4-2. The QPI concentration axis in the phase diagrams refers to UV-Vis spectrophotometer measurements reported in Section 4.2.3.3. Alternative representations of the phase diagrams based on total protein are included in Figure A.1 (Appendix A).

The mathematical approximation method (Figure 4-1) suggests that QPI is less compatible with MD of DE 7 than with MD of DE 2, evidenced by the lower phase separation threshold value of 2.5% for QPI-MD DE 7, as opposed to 4% for QPI-MD

DE 2. Since the phase separation threshold corresponds to the minimum overall biopolymer concentration in the mixture required for phase separation (Tolstoguzov, 2002), a lower threshold value indicates a smaller area of miscibility, i.e., lower compatibility. The critical and threshold points are very close together for both systems, as demonstrated in Figure 4-1, which indicates a good symmetry of the mathematical approximations.

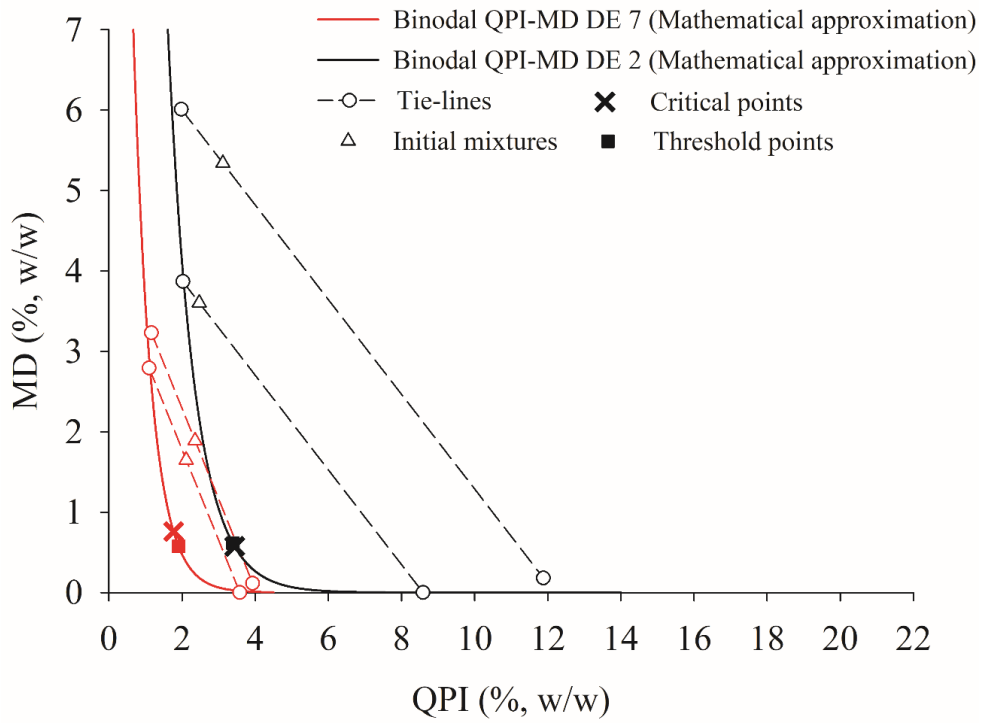

Figure 4-1. Mathematical approximations of the phase diagrams between QPI and MD of DE 7 or DE 2 at pH 7.0, 22 °C and 0.1 M NaCl.

The shape of both experimentally determined binodals is unusual (Figure 4-2), as it shows a shift away from both axes of the phase diagram, unlike the mathematically approximated binodals (Figure 4-1). The shift is congruent with an increase in concentration of MD and QPI, respectively, in the QPI- and MD-rich phases with increasing overall biopolymer concentration in the system. This unusual behaviour may

be due to molecular weight (M_w) fractionation of MD between the separated phases. Paselli SA2, the commercially available MD of DE 2 used here, has been reported to have a broad molecular weight distribution and to fractionate between the separated phases when mixed with agarose above the phase separation threshold (Loret et al., 2005). Molecular weight fractionation between separated phases was also observed for other biopolymer mixtures, e.g., dextran-locust bean gum (Garnier, Schorsch and Doublier, 1995), poly(ethylene oxide)-dextran (Edelman, van der Linden and Tromp, 2003) and gelatin-dextran systems (Edelman, Tromp and van der Linden, 2003). It is worth noting though that for all of the cited systems, including the agarose-Paselli SA2, classical segregative phase separation behaviour was reported.

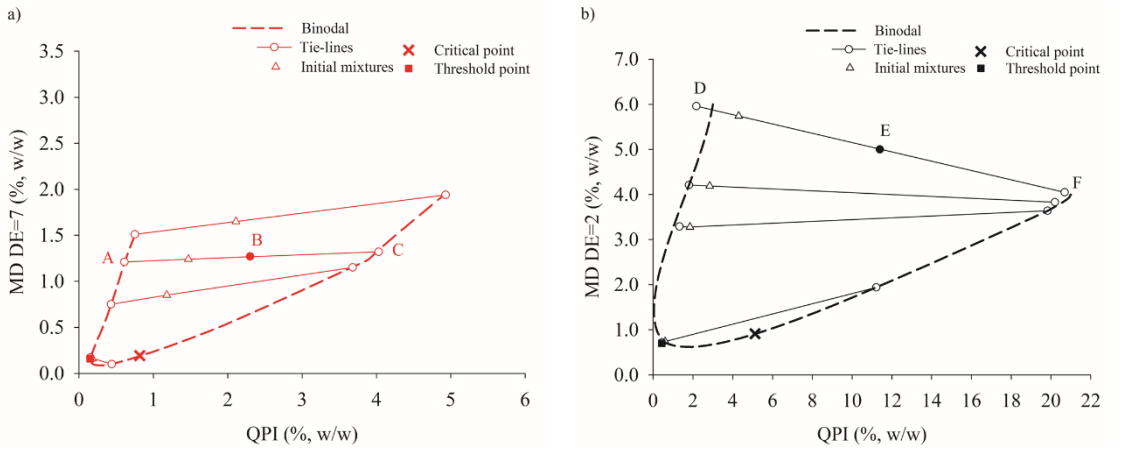

Figure 4-2. Experimental phase diagrams between QPI and MD DE 7 or DE 2 at pH 7.0, 22 °C and 0.1 M NaCl: a) QPI-MD DE 7 and b) QPI-MD DE 2. The letters identify samples that were imaged. The standard error (SE) for polymer concentrations in either phase of the QPI-MD DE 7 mixtures ranged between 0.1 – 1.0%, resulting in coefficients of variation (CV = SE/mean) of less than 20%. The SE for the QPI-MD DE 2 mixtures ranged between 0.05 – 1.8%, resulting in CVs of less than 10%, except for one outlier of 31% for MD concentration in one of the bottom phases.

To ascertain whether molecular weight fractionation caused the behaviour observed here, the M_w distribution of both MDs was assessed. The results of the SEC-MALS analysis of the maltodextrins and of the bottom phases of the QPI-MD mixtures are depicted in Figure 4-3. MD of DE 7 showed a single peak at 3.4×10^4 g/mol, with a shoulder at 8.6×10^4 g/mol (Figure 4-3a). In contrast, MD of DE 2 had a broad molecular weight distribution with two main peaks at ~1.2×10^4 g/mol and ~5×10^5 g/mol (Figure 4-3b), in agreement with Loret et al. (2005).

The SEC-MALS data suggests that both MDs fractionated between the phases, based on the chromatograms for the bottom phases of the mixtures (Figure 4-3c-d). The chromatogram for the bottom phase of the QPI-MD DE 7 mixture, which consisted of 4.9% QPI and 1.9% MD DE 7 shown in Figure 4-3c has two peaks: one at 4.1×10^4 g/mol, with a shoulder at 2.7×10^4 g/mol, and another one at 8.9×10^4 g/mol. Based on published literature (Abugoch et al., 2008; Mäkinen et al., 2016; Ruiz et al., 2016b; Kaspchak et al., 2017; Shen, Tang and Li, 2021; Yang et al., 2022b), the lower molecular weight peak and the shoulder can be assigned to the acidic and basic chains of globulin 11S, respectively. The higher molecular weight peak corresponds to the 8.6×10^4 g/mol fraction of MD of DE 7 that is present in the MD stock solution prior to phase separation (Figure 4-3a). The chromatogram for the bottom phase for QPI-MD DE 2 mixture (Figure 4-3d), which consisted of 20.7% QPI and 4% MD DE 2, shows a large peak at 2.6×10^5 g/mol followed by a shoulder at 5.5×10^5 g/mol. The peak corresponds to the main protein in QPI, globulin 11S, which is reported to have a molecular weight of $2.5 – 4.0\times10^5$ g/mol (300 – 390 kDa) (Ruiz et al., 2016b; Mir, Riar and Singh, 2018). The shoulder corresponds to the 5.0×10^5 g/mol fraction of MD DE 2 that is present in the MD stock solution prior to phase separation (Figure 4-3b). Hence, the peaks representing higher M_w in the chromatograms

for both MDs (Figure 4-3a-b) were also present in the data for each of the bottom phases (Figure 4-3c-d). The smaller M_w peaks, however, were absent, suggesting that the lower M_w fractions preferentially partitioned into the top phases (Loret et al., 2005).

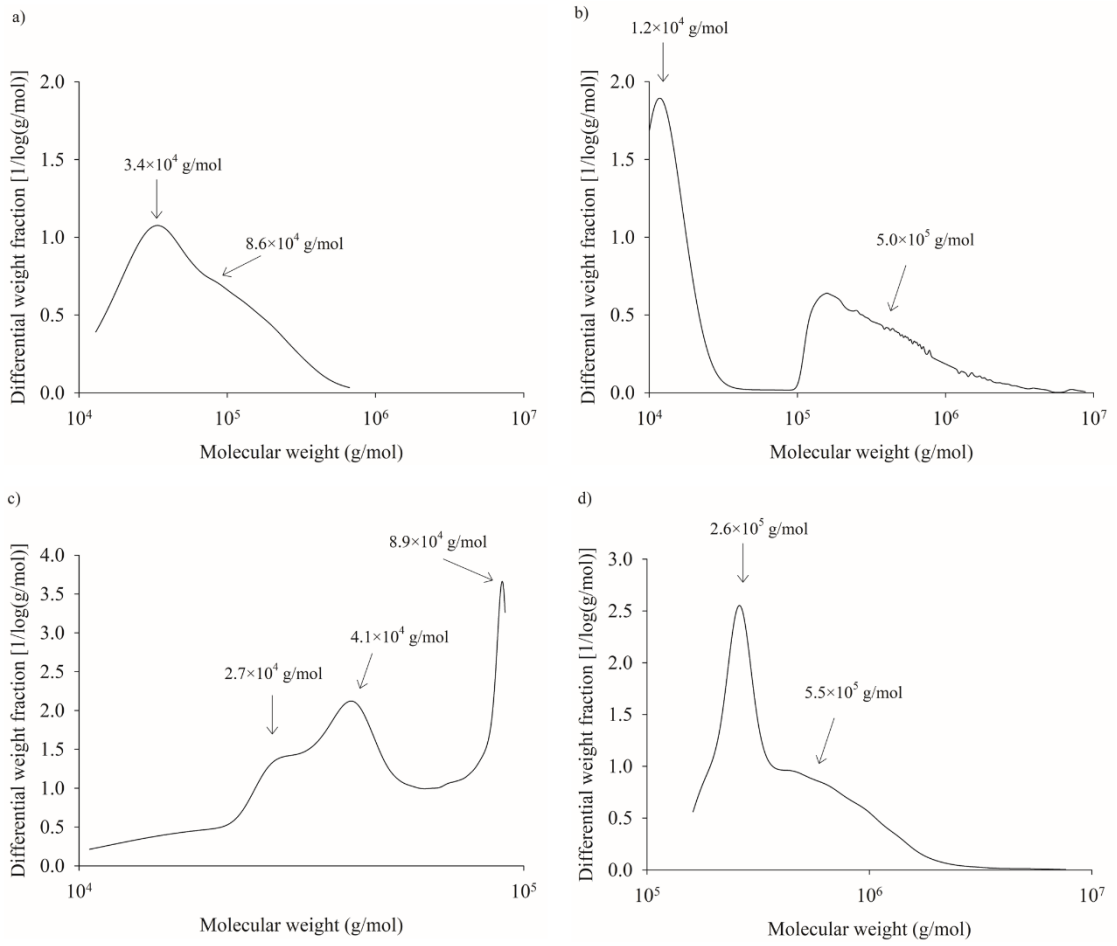

Figure 4-3. Molecular weight distribution of a) MD of DE 7 and b) MD of DE 2, and of the bottom phases of mixtures c) 4.9% QPI + 1.9% MD DE 7 and d) 20.7% QPI + 4% MD DE 2 in 0.1 M NaCl at 22 °C.

An atypical phase behaviour has previously been reported for mixtures of unrefined pea protein (PP) and sodium alginate (SA) (Mession et al., 2012a, 2012b). While the authors have manually fitted a binodal, the tie-lines of the PP-SA phase diagram indicate a shift of the binodal away from the axes. SA was reported to be entrapped in the highly viscous

protein-rich bottom phase at increasing biopolymer concentration and at increasing fraction of SA in the starting mixture. Other mixtures, such as κ-carrageenan-soy protein (Li et al., 2008b), amylopectin-milk protein (de Bont, van Kempen and Vreeker, 2002) and hydroxyethyl cellulose-latex colloids (Sperry, 1984) have displayed similar behaviour. Although latex particles and globular proteins are chemically and structurally different, they are both colloids and some of Sperry's (1984) elaborations are worth considering. Sperry (1984) observed that with increasing initial polysaccharide concentration and constant latex particle fraction in the system, the physical height of the latex particle-rich (bottom) phase increased. The height increase was proposed to be due to the formation of a volume-spanning network of latex particles with increasing interparticle void volume filled with dissolved polysaccharide. An increase in the bottom phase height with increasing initial polysaccharide concentration (at constant protein concentration), indicating the possible formation of a volume-spanning network such as the one proposed by Sperry (1984), was also noted here for both QPI-MD systems (Appendix A – Figure A.2), and has been reported for other biopolymer mixtures involving proteins (de Bont, van Kempen and Vreeker, 2002; Li et al., 2008b; Mession et al., 2012b). Moreover, the tie-lines in the experimentally determined phase diagrams (Figure 4-2) are not parallel, and the critical and threshold points do not coincide in either system, demonstrating asymmetry of the phase diagrams. According to Tolstoguzov (2000a), self-association of macromolecules can influence the excluded volume of the polymers and the affinity of the biopolymer molecules for the solvent, leading to a change in the slope of the tie-lines with an increase in the concentration of total biopolymer. Thus, the change in STL observed here could be explained by protein association and consequent entrapment of MD in the QPI-MD systems.

Before introducing micrographs acquired on the phase separated systems to elucidate their microstructure, it should be noted that the QPI stock solution contained protein aggregates (Appendix A – Figure A.3). Plant proteins are seldomly fully soluble in aqueous media, with a tendency to self-aggregation and high sedimentation rates, which is due to their complex quaternary structure and modifications in their physico-chemical properties, caused by extraction and drying processes (Amagliani and Schmitt, 2017; Sarkar and Dickinson, 2020). Imaging the MD stock solutions by optical microscopy (1 mm – 0.2 μm) revealed no structures, confirming complete dissolution of both MDs.

The microstructure of samples collected along a tie-line for each phase-separated QPI-MD system is depicted in Figure 4-4. The image labels correspond to the observed mixtures represented by the upper-case letters in Figure 4-2. The images are a true representation of the whole sample that was viewed under the microscope. The middle column relates to the initial mixtures, both of which were prepared to lie at the centre of the tie-line and imaged immediately after preparation. The left-hand side column shows the top phases and the right-hand side column the bottom phases. The bright structures represent clusters of protein (Chen et al., 2020), as confirmed by the micrograph under the same conditions of the QPI stock solution alone (Appendix A – Figure A.3), while the MD stock solution appear as a dark background.

The microstructure of the top phases of the segregated mixtures (Figure 4-4a and d) appear as protein aggregates varying in size from ~1 – 10 μm dispersed in a liquid continuous phase. The liquid phase is most likely pure MD, but the absence of soluble protein cannot be excluded. A similar microstructure was reported for the top/polysaccharide-rich phase of a sodium alginate-pea protein system (Mession et al., 2012b). Figure 4-4b and e show the initial mixtures but the typical bicontinuous structure

of phase separating biopolymer mixtures with equal phase volumes, usually at the centre point of a tie-line (Esquena, 2016), was not observed here in either system. Instead, the microstructure of the initial mixture is not unlike the microstructure of the top phases but denser in protein aggregates. The micrographs taken on the bottom phases of the segregated systems (Figure 4-4c and f) show a percolated protein network structure with an entrapped liquid phase, which is likely close to pure MD but could also contain soluble protein. Considering the molecular weight data, it is reasonable to postulate that fractions of either MD are entrapped within this network, as suggested by Sperry (1984).

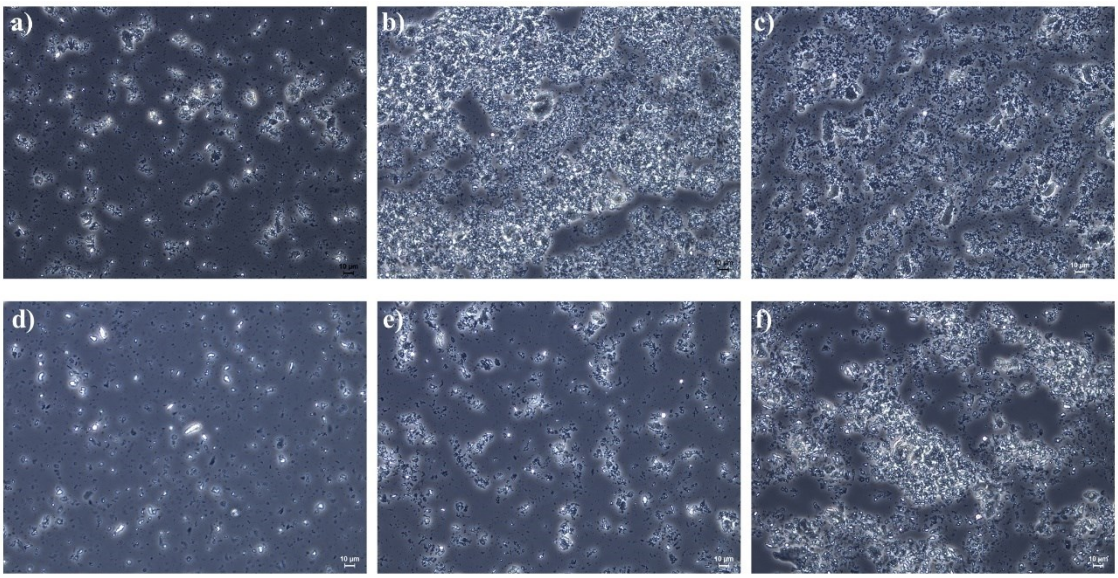

Figure 4-4. Light microscopy images of QPI-MD mixtures. The top row relates to QPI-MD DE 7 and the tie-line indicated in Figure 4-2a. The bottom row relates to the tie-line marked up in Figure 4-2b for QPI-MD DE 2. From left to right, the columns relate to the top phase, initial mixture and bottom phase. The image labels a-f concur with the upper-case letters A-F in Figure 4-2. The bright structures identify protein and the scale bars represent 10 µm.

Collectively, the phase diagrams, the M_w distribution of both MDs and the micrographs show that the QPI-MD systems display segregative phase behaviour, where the

segregation mechanism is depletion flocculation. This mechanism has been reported to occur in mixtures involving globular proteins and polysaccharides (Kim, Decker and McClements, 2006; Ercelebi and Ibanoğlu, 2007; Li et al., 2008a, 2008b; Gaaloul, Turgeon and Corredig, 2009) with a phase separation threshold of less than 1.0% (Doublier et al., 2000). Polysaccharide molecules lose conformational entropy when confined between two neighbouring globular molecules, giving rise to a region depleted of polymers. In the depleted region, the concentration of polymer is lower than in the bulk solution and a difference in osmotic pressure is created, which favours the displacement of solvent from the depleted region to the bulk. The difference in osmotic pressure induces attraction interactions between globular molecules (McClements, 2000; Tuinier, Dhont and de Kruif, 2000). The phase separation threshold values determined from the experimental phase diagrams were 0.3% and 1.2% for MD of DE 7 and DE 2, respectively (Figure 4-2), which is the first indication of depletion flocculation as the mechanism of phase separation (Doublier et al., 2000). Moreover, the shift of the binodals away from the axes and the increase in the bottom phase height with increasing MD concentration (Appendix A – Figure A.2) indicate that the self-association of QPI protein molecules during assumed depletion flocculation behaviour led to the formation of a volume-spanning protein network, depicted in Figure 4-4c and f, where the void volume was probably occupied by dissolved MD. The combination of depletion flocculation and the polysaccharide entrapment effect was also reported for κ-carrageenan-soy protein (Li et al., 2008b) and amylopectin-milk protein (de Bont, van Kempen and Vreeker, 2002) systems.

4.3.3 Effect of heat treatment and absence of salt on phase behaviour

The phase separation behaviour of biopolymer mixtures with a protein component is affected by protein conformation. Pre-heating a protein solution before mixing with a phase separating polysaccharide was previously reported to result in classical segregative phase separation behaviour (Kim, Decker and McClements, 2006; Chun et al., 2014). Since the native QPI-MD mixtures displayed an atypical phase behaviour, the influence of protein heat pre-treatment on one of the phase diagrams was examined.

The denaturation temperature of QPI was assessed by DSC (Figure 4-5). A single endothermic peak with an onset temperature of 84.5 °C and peak temperature of 90.1 °C was obtained. The peak temperature is usually taken as the denaturation temperature (T_d) and the value found for the QPI extracted here is consistent for globulin 11S (chenopodin), the main protein in quinoa seeds (Vera et al., 2019). The presence of a single endothermic peak indicates either the predominance of globulin 11S or the presence of several proteins of similar thermostability (Ruiz et al., 2016b). Similar T_d values have been reported for other plant globulins, such as pea protein (T_d = 87.4 °C) (Mession et al., 2012a) and red bean protein (T_d = 86 °C) (Meng and Ma, 2001).

Previously, the response of almond proteins to thermal incubation has been used to select temperatures that induce limited protein denaturation, preventing gelation that can occur with a greater extent of unfolding. Hydrophobicity, circular dichroism and SDS-PAGE analyses were used to show that heat treatment of almond protein at moderate temperature (55 – 75 °C) induced partial protein denaturation and aggregation, while the use of high temperature (85 – 95 °C) led to gelation (Devnani et al., 2020). Additionally, a thermogram revealed a denaturation temperature of 81 °C for almond protein isolate, while no change in heat flow was observed at temperatures lower than the onset of 70 °C

(Devnani et al., 2021). Based on these reports and the thermogram of QPI (Figure 4-5), a temperature of 55 °C was selected for the pre-heating of QPI stock solution (10%, w/w) to avoid extensive protein denaturation and gelation, producing heat treated QPI (HTQPI) (Section 4.2.7). Mixtures between HTQPI and MD DE 2 were then prepared as described in Section 4.2.3.2 and the phase diagrams determined as described in Section 4.2.3.3. Only mixtures with MD of DE 2 have been evaluated, as this molecule has been reported to show segregative phase behaviour with other proteins (Manoj, Kasapis and Chronakis, 1996; Beldengrün et al., 2018), thus making further comparison with the literature possible.

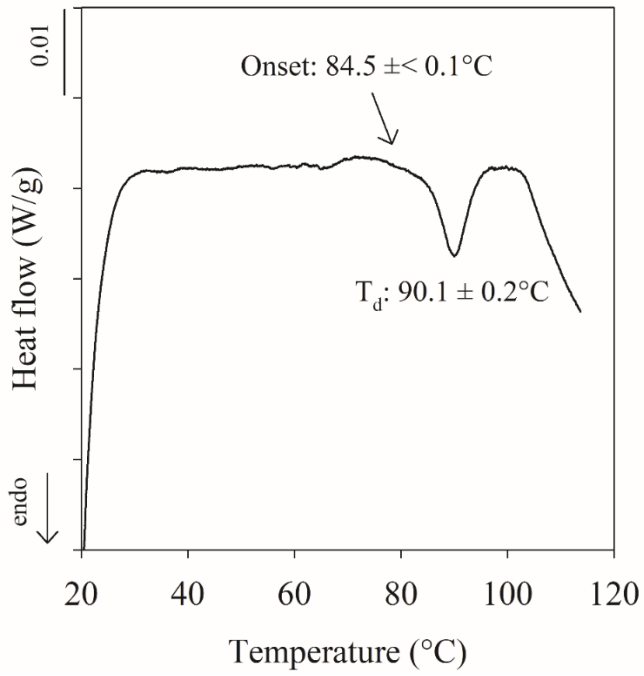

Figure 4-5. Thermogram of QPI (10%, w/w), showing only the heating step at a rate of 2 °C/min.

The resulting phase diagram, acquired with MD DE 2, is shown in Figure 4-6a. The data is compared with the binodal for the original QPI-MD of DE 2 system. Consistent with

Tolstoguzov (2002) reporting on biopolymer mixtures in general and Li et al. (2008b) discussing κ-carrageenan-soy protein mixtures, the thermal treatment of QPI decreased the phase separation threshold from 1.2%, observed for the QPI-MD of DE 2 system, to 0.6%. Nevertheless, the two-phase region was smaller in comparison to the original QPI-MD DE 2 system (black dashed line in Figure 4-6a), evidencing that the heat treatment of QPI shifted the binodals further away from the axes as each biopolymer concentration is increased. On the other hand, the symmetry of the phase diagram increased for the heat-treated system, as demonstrated by the proximity of the critical and threshold points (Zaslavsky, 1995).

Micrographs taken of samples from the tie-line indicated in Figure 4-6a and reproduced in Figure 4-6b-d reveal similar microstructures, i.e., protein aggregation, as observed for the original QPI-MD system (Figure 4-4). Evidently, the pre-heating of QPI did not yield the effect observed for whey protein isolate (WPI)-polysaccharide systems (Kim, Decker and McClements, 2006; Chun et al., 2014), i.e. a classical segregative phase separation. A major reason might be that in both studies, WPI was pre-heated at > 80 °C, i.e., above its thermal denaturation temperature and in the absence of salt.

As above-mentioned, another factor that can influence phase separation in aqueous media is the presence or absence of salt. At high concentrations, salt can partially shield the electrostatic repulsion between protein molecules, favouring hydrophobic interaction leading to increased association of protein molecules in biopolymer mixtures and greater incompatibility between proteins and polysaccharides (Grinberg and Tolstoguzov, 1997). Conversely, greater biopolymer compatibility may be expected at low salt concentrations, although salt can also influence solubility, making interactions complex.

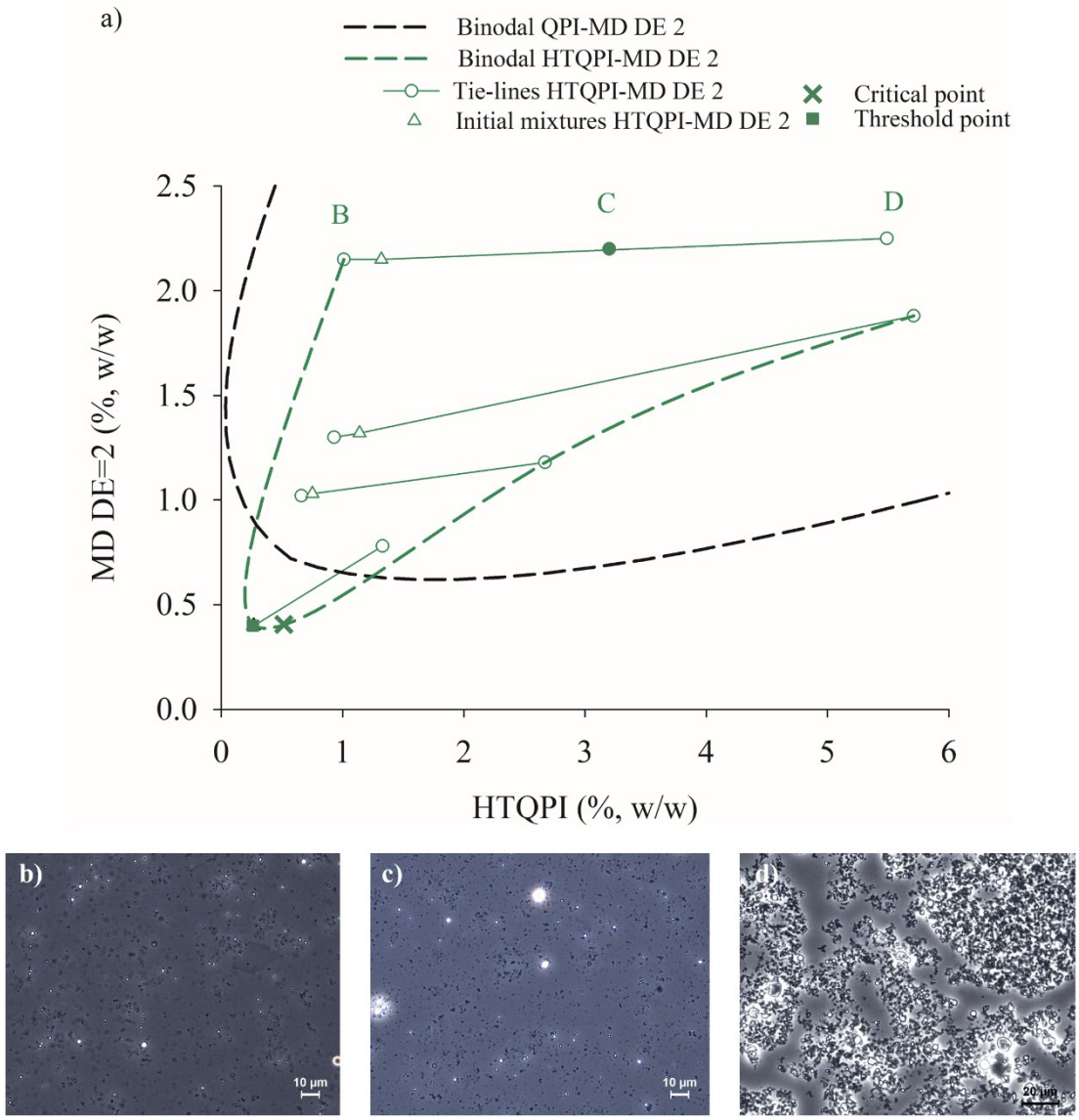

Figure 4-6. Effect of heat pre-treatment on the phase behaviour of QPI-MD DE 2: a) experimental phase diagram between HTQPI and MD of DE 2 at pH 7.0, 22 °C and 0.1 M NaCl, the letters (B-D) identify the samples for which the microstructure was also analysed; b) top phase, c) initial mixture and d) bottom phase. The bright structures are protein and the scale bars represent 10 µm and 20 µm.

Salt had a noticeable influence on the phase behaviour of the QPI-MD mixtures. Light micrographs of QPI-MD initial mixtures in the absence of salt (Appendix A – Figure A.4), captured immediately after mixture preparation, show a lower level of initial protein aggregation (Figures A.4a-b, bright structures) than the observed in the original mixtures

in the presence of NaCl (Figure 4-4b and e). This observation is consistent with the literature for the influence of salt on protein molecules (Li et al., 2009). In contrast, the initial mixture of heat pre-treated QPI-MD DE 2 showed similar initial protein self-association when mixed in either the absence (Figure A.4c) or presence of salt (Figure 4-6c).

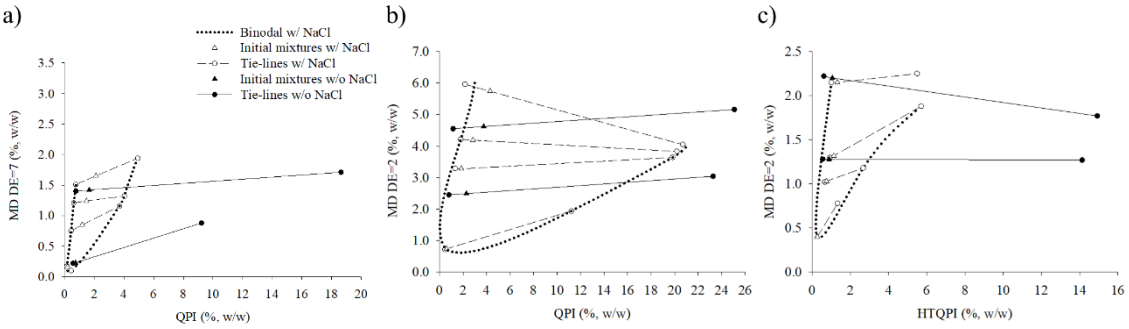

Figure 4-7. Effect of the absence of NaCl on the phase behaviour of mixtures between a) QPI-MD MD 7; b) QPI-MD DE 2; and C) HTQPI-MD DE 2 at pH 7.0 and 22 °C.

In the absence of salt, phase separation resulted in bottom phases of lower volume fractions than in the presence 0.1 M NaCl, indicating that QPI formed more compact bottom phases (Figure 4-7). This suggests that the absence of salt had a larger impact on the QPI-rich phase, which is expected since QPI is the charged biopolymer in the systems. Still, the composition of the equilibrium phases points to a similar binodal shape to that displayed by QPI-MD mixtures in 0.1 M NaCl. In both cases the concentration of MD in the QPI-rich phase and of QPI in the MD-rich phase increased with overall biopolymer concentration. Similar phase behaviour in the absence of salt was observed for WPI in mixture with either κ-carrageenan or pectin (Chun et al., 2014) and for konjac glucomannan-milk mixtures (Dai et al., 2017). The data also indicate that MD fractionated between the phases in the mixtures without NaCl, illustrating that many

aspects of segregative separation behaviour were common between samples with and without salt.

4.4 Conclusions

Systems involving quinoa protein isolate and maltodextrin of DE 7 and 2 are concluded to phase separate by depletion flocculation. The comparison between mathematically approximated and experimentally determined phase diagrams showed that QPI-MD mixtures followed a segregative separation behaviour but the shape of the binodals was atypical. As the initial biopolymer concentration increased, the polysaccharide and protein concentrations also increased in the QPI- and MD-rich phases, respectively, resulting in binodals that were shifted away from the axes. SEC-MALS and microstructure analyses suggested that the phase compositions were affected by the fractionation of MD between the phases and consequent entrapment of MD fractions within the aggregated network of the protein-rich phase. Similar atypical phase diagrams were observed when the systems were prepared in the absence of salt or when QPI was pre-heated before mixture with MD. Considering the great effects of solution pH on protein structure, which in turn will affect the phase behaviour of the protein-polysaccharide system, future work should consider the effect of the mixture's pH on QPI-MD phase diagrams. The results of this study are further evidence of the complicated phase behaviour of *plant* proteins and polysaccharide mixtures. Thus, the formulation of products with predictable properties, that meet the current consumer demand for plant-based foods, may be challenging.

Chapter 5. Modulation of physico-chemical and technofunctional properties of quinoa protein isolate: Effect of precipitation acid

Published article in Food Chemistry.

Amarante, M.C.A., Ong, L., Spyropoulos, F., Gras, S. and Wolf, B. (2024) 'Modulation of physico-chemical and technofunctional properties of quinoa protein isolate: Effect of precipitation acid', *Food Chemistry*, 457, pp. 140399. doi:10.1016/j.foodchem.2024.140399

Author contribution statement:

Marina Campos Assumpcao de Amarante: Conceptualisation, Formal analysis, Investigation, Methodology, Software, Validation, Visualisation, Writing - original draft, Writing - review & editing. **Lydia Ong**: Supervision, Writing - review & editing. **Fotis Spyropoulos**: Supervision, Writing - review & editing. **Sally Gras**: Conceptualisation, Funding acquisition, Project administration, Resources, Supervision, Writing - review & editing. **Bettina Wolf**: Conceptualisation, Funding acquisition, Project administration, Resources, Supervision, Writing - review & editing.

Acknowledgements: The authors would like to thank the Priestley Joint PhD Scholarship from the University of Birmingham (UK) and The University of Melbourne (Australia). This work was performed in part (FTIR measurements) at the Materials Characterisation and Fabrication Platform (MCFP) at the University of Melbourne and the Victorian Node of the Australian National Fabrication Facility (ANFF). The authors also thank the

Biological Optical Microscopy Platform (BOMP) at The Bio21 Molecular Science and Biotechnology Institute at The University of Melbourne for access to equipment, as well as the School of Chemistry of the University of Birmingham for the total nitrogen content analyses. Lydia Ong and Sally Gras are both supported by the Australian Research Council Centre of Excellence in Plants for Space, grant number CE230100015.

Abstract

The typically low solubility and gelation capacity of plant proteins can impose challenges in the design of high-quality plant-based foods. The acid used during the precipitation step of plant protein isolate extraction can influence protein functionality. Here, acetic acid and citric acid were used to extract quinoa protein isolate (QPI) from quinoa flour, as these acids are more kosmotropic than the commonly used HCl, thus promoting the stabilisation of the native protein structure. While proximate analysis showed that total protein was similar for the three isolates, precipitation with kosmotropic acids increased soluble protein, which correlated positively with gel strength. Microstructure analysis revealed that these gels contained a less porous protein network with lipid droplet inclusions. This study shows that the choice of precipitation acid offers an opportunity to tailor the properties of quinoa protein isolate for application, a strategy that is likely applicable to other plant protein isolates.

Keywords: plant protein; gelation; thermal properties; acid precipitation; kosmotropes; functionality.

5.1 Introduction

Quinoa (*Chenopodium quinoa* Willd.) is a pseudocereal cultivated in large scale mainly in the Andes mountains region of South America by Peru, Bolivia, Ecuador and Chile (Murphy et al., 2019). Quinoa seeds contain, on a dry weight basis, around 13 – 14% (w/w) protein, 6.5% (w/w) lipid, 69 – 72% (w/w) carbohydrate (of which, 60% is starch), 2.3% (w/w) ash and 9% (w/w) moisture (Elsohaimy, Refaay and Zaytoun, 2015; Alonso-Miravalles and O'Mahony, 2018). The protein is considered high quality as is presents a complete essential amino acid profile, which meets the amino acid requirements for adults suggested by the World Health Organization (WHO) and other organisations (WHO/FAO/UNU, 2007; Vilcacundo and Hernández-Ledesma, 2017). Consequently, quinoa protein is regarded as an attractive alternative to animal proteins in protein-rich foods (Föste et al., 2015).

The main proteins in quinoa seeds are globulin 11S and albumin 2S, corresponding to around 37% (w/w) and 35% (w/w) of the total protein content, respectively (Brinegar, Sine and Nwokocha, 1996). Globulin 11S, also known as chenopodin, is composed of subunits of 45 – 60 kDa in size, which are associated in hexameric units (300 – 360 kDa) (Brinegar and Goundan, 1993; Mäkinen, Zannini and Arendt, 2015; Liu et al., 2023). Each subunit contains an acidic α-chain (30 – 39 kDa) and a basic β-chain (20 – 25 kDa) linked by disulfide bonds (Brinegar and Goundan, 1993; Abugoch et al., 2008; Yang et al., 2022b). Albumin 2S is a small globular protein with a molecular weight of around 8 – 16 kDa (Brinegar, Sine and Nwokocha, 1996; Shen et al., 2022). Recently, the legumin-like globulin 13S and the vicilin-like globulin 7S have also been identified in quinoa seeds proteomics (Burrieza et al., 2019; Shen et al., 2022). While neither globulin 13S nor globulin 7S from quinoa have been further characterised, similar proteins have

been described in the literature for other pseudocereals. Globulin 13S is described as very similar to globulin 11S in terms of structure and size in buckwheat (*Fagopyrum* spp.) (Maksimovic et al., 1996; Janssen et al., 2017), while globulin 7S is reported to occur as tetrameric units of ~200 kDa, with subunits of 16 kDa, 38 kDa, 52 kDa and 66 kDa in size in amaranth (*Amaranthus hypochondriacus*) (Quiroga et al., 2010).

Quinoa protein can be obtained from quinoa seeds or quinoa flour by either dry or wet fractionation. In dry fractionation, quinoa seeds are coarsely milled and then sieved, allowing several size fractions to be collected. This method usually results in quinoa protein concentrates (QPC) with a low protein content in the range of 28 – 33% (w/w) (Opazo-Navarrete et al., 2018b, 2018a). In wet fractionation, quinoa seeds are finely milled into a flour, which is then defatted using organic solvents such as hexane or petroleum ether. The flour is then suspended in water, the pH of the suspension adjusted with sodium hydroxide to between 8 and 12 (Ruiz et al., 2016b; Mir, Riar and Singh, 2019a) and the solution agitated for 1 – 16 h to extract the protein (Ruiz et al., 2016a, 2016b). The soluble protein fraction is then recovered by centrifugation and, if not further purified, dried usually by freeze-drying (Valenzuela et al., 2013; Guerreo-Ochoa, Pedreschi and Chirinos, 2015; Vera et al., 2019).

Further purification of the soluble protein fraction by acid precipitation at pH 4 – 5 is typically applied to remove other water-extractable components, such as starch and fibres. This is then followed by solid-liquid separation by centrifugation and the precipitate is rinsed with water to remove remaining salts or contaminants, neutralised with sodium hydroxide and dried, most often by freeze-drying, to obtain quinoa protein isolate (QPI) (Abugoch et al., 2008; Ruiz et al., 2016b). Wet fractionation uses large quantities of water and energy, and some of the protein functionality, such as solubility and water holding

capacity, can be impaired due to the harsh solvent conditions (Schutyser and van der Goot, 2011; Alonso-Miravalles and O'Mahony, 2018; Opazo-Navarrete et al., 2018a). Despite these disadvantages, wet fractionation is well established not only at laboratory-scale but also in industry (Sim et al., 2021). It offers good process control and high extraction efficiency with final protein contents in QPI reported to be > 70% (w/w) (Ruiz et al., 2016b; Steffolani et al., 2016; Mir, Riar and Singh, 2019a).

The conditions applied during wet fractionation strongly influence the physico-chemical and technofunctional properties of QPI, as well as its suitable applications (Abugoch et al., 2008; Ruiz et al., 2016b; Mir, Riar and Singh, 2019a). Alkalinisation at pH 8 – 9 followed by HCl precipitation has been shown to provide QPI with improved protein solubility, thermal properties and heat-set gelation capacity, which could then be applied as an ingredient in high protein beverages and in semi-solid gelled foods. Alkalinisation at pH 10 – 11 followed by HCl precipitation has been reported to result in QPI that was more denatured, less soluble and of impaired gelation properties. Suggested applications include in liquid foods such as sauces and soups (Abugoch et al., 2008; Ruiz et al., 2016b).

The conditions applied during the acid precipitation step have been demonstrated to affect the functional properties of okara protein isolate (Cai et al., 2020). While acid precipitation of any kind of protein is typically conducted using hydrochloric acid (HCl), Cai et al. (2020) explored the use of alternative acids including citric acid and malic acid. They report that precipitation with HCl resulted in the highest solubility, water holding capacity and foaming capacity among the extracts. Precipitation with citric acid increased the oil holding capacity and emulsifying properties while precipitation with malic acid resulted in a higher surface hydrophobicity (Cai et al., 2020). The results are promising in view to obtaining tailored isolate properties. However, to the best of the authors'

knowledge, the effects of precipitation with acids other than HCl on the isolate properties and functionality have not yet been reported for other plant proteins.

The Hofmeister series describes the effect of ions during the salting in or salting out of proteins, providing a range of ions that could be considered for protein precipitation studies. The series further classifies anions and cations into kosmotropes or chaotropes (Hofmeister, 1888). Currently, the anionic Hofmeister series follows the order (from more kosmotropic to more chaotropic): SO_4^{2-} > HPO_4^{2-} > $Acetate^-$ > $Citrate^-$ > Cl^- > NO_3^- > ClO_3^- > I^- > ClO_4^- > SCN^- (Okur et al., 2017), with Cl^- generally considered as the dividing line between the kosmotropic and chaotropic effects (Kumar and Venkatesu, 2014; Okur et al., 2017). Anions follow the series for the salting out of proteins only when the effect of the protein backbone is stronger than that of the positively charged side chains, i.e., at pH values at or above their isoelectric point where their net charge is negative, as weakly hydrated anions (chaotropes) are attracted to the backbone, leading to salting in and consequent destabilisation and unfolding of the protein structure. In contrast, strongly hydrated anions (kosmotropes) are excluded from the protein backbone and promote the salting out effect, stabilising and protecting the protein structure (Okur et al., 2017).

In this study it was hypothesised that the physico-chemical and technofunctional properties of QPI could be modulated by the choice of acid used for protein precipitation, with reference to the Hofmeister series. Wet fractionation from quinoa flour was selected as the protein extraction method, with alkalinisation at pH 9.0 to maximise the preservation of the native structure of the protein (Abugoch et al., 2008; Ruiz et al., 2016b). Acetic acid and citric acid were chosen for the acid precipitation step and the properties of aqueous dispersions of QPI extracted with these more kosmotropic acids

were compared to QPI extracted with HCl. Proximate composition, soluble protein content, protein profile, thermal properties and gel microstructure were assessed.

5.2 Materials and methods

5.2.1 Materials

Quinoa flour produced from white quinoa seeds was purchased from The British Quinoa Company® (UK). The white quinoa seeds were grown on Shropshire farm (Ellesmere, UK), harvested in 2015, cleaned, selected, sorted and stored in 2016 – 2017. The seeds were then flaked and milled into flour in the first trimester of 2019. According to the manufacturer, the flour contained 14.3% (w/w) protein, 65.7% (w/w) carbohydrate (of which 2.6% were sugars), 6.8% (w/w) lipid and 6.8% (w/w) fibre on a dry weight basis. NaOH pellets (≥ 97%) and NaCl (≥ 99.5%) were purchased from Fisher Scientific® (UK). HCl (≥ 32%) and acetic acid (≥ 99.8%) were purchased from Honeywell® (UK). Citric acid (≥ 99.5%), a starch (Hexokinase) assay kit, dimethyl sulfoxide, Nile Red, Fast Green FCF and low viscosity mineral oil were all purchased from Sigma-Aldrich® (UK). The bicinchoninic acid (BCA) assay kit was purchased from G-Biosciences® (USA). All electrophoresis materials were acquired from Bio-Rad Laboratories® (USA). Double distilled water with a resistivity of 15.0 MW.cm (Millipore®, UK) was used in all experiments.

5.2.2 Protein extraction and characterisation

5.2.2.1 Extraction from quinoa flour

Quinoa protein isolate (QPI) was extracted from quinoa flour following the method described by Ruiz et al. (2016b), with modifications in centrifugal speed and in the acid precipitation step. Briefly, quinoa flour was sieved through a 250 μm aperture sieve to remove large particles and suspended in distilled water (10%, w/w). The pH was adjusted to 9.0 using 1.0 M NaOH and the suspensions were agitated for 4 h at 22 °C, then stored for 16 h at 4 °C to allow time for protein solubilisation. Thereafter, the flour suspensions were centrifuged for 30 min at 3220 × g and 10 °C. Three layers were obtained: a top layer of creamed lipid droplets, a middle layer containing the protein-rich supernatant and a bottom layer comprising residual flour. The combined cream and middle layer were poured through a cheesecloth to remove the cream layer. The residue was discarded alongside the flour sediment. The pH of the filtrate was adjusted to 4.5 using either HCl, acetic acid or citric acid, at a concentration of 1.0 M to precipitate the proteins. The supernatant was centrifuged as described above to recover the precipitate, which was then rinsed by re-suspending in distilled water and centrifuging once more. Finally, the precipitate was re-suspended in distilled water, neutralised using 1.0 M NaOH and freeze-dried for 72 h (Scanvac Coolsafe, Labogene®, Denmark). The freeze-dried isolates were labelled QPI-H, QPI-A and QPI-C depending on the acid used for extraction acid (HCl, acetic acid and citric acid, respectively) and kept at 4 °C until use.

Extraction yields were calculated as the weight ratio between freeze-dried QPI and the flour used for extraction (Equation 5-1).

$$\text{Extraction yield (\%, w/w)} = \frac{\text{weight of freeze-dried QPI (g)}}{\text{weight of flour used for extraction (g)}} \times 100\% \quad (5\text{-}1)$$

5.2.2.2 Determination of proximate composition and protein yield

The total protein content of the quinoa flour and extracted QPI was determined as total nitrogen content, via elemental analysis (Thermo Flash EA 1112, ThermoFisher Scientific®, UK), and converted to total protein using a conversion factor of 5.85 (Abugoch et al., 2008; Ruiz et al., 2016b). Protein yield was calculated from extraction yield, considering the total protein content of QPI and of quinoa flour (Equation 5-2).

$$\text{Protein yield (\%, w/w)} = \frac{\text{total protein in QPI (\%, w/w)} \times \text{extraction yield (\%, w/w)}}{\text{total protein in quinoa flour (\%, w/w)}} \quad (5\text{-}2)$$

Moisture, ash and lipid content of QPI were assayed through methods published by the Association of Official Analytical Chemists (AOAC, 2002), i.e., method numbers 934.01, 923.03 and 920.39 (using hexane as solvent), respectively. The carbohydrate content was determined by difference. The starch content of QPI was determined using a starch assay kit (Hexokinase, Sigma-Aldrich®, UK), where the starch in the sample is hydrolysed to glucose by amyloglucosidase and glucose concentration is then measured as the absorbance increase at 340 nm, a consequence of nicotinamide adenine dinucleotide (NAD) and hydrogen (H) formation. All results are reported as % (w/w).

5.2.2.3 Determination of soluble protein content

The soluble protein content of the obtained QPI powders was determined at different pH values and different concentrations. For the determination at different pH, QPI was resuspended in distilled water at 1% (w/w) and the pH adjusted to values ranging from 6.0 to 9.0 using 1.0 M NaCl or 1.0 M HCl. For the measurement of soluble protein at different concentrations, QPI was resuspended in distilled water at the concentrations of 5% (w/w), 10% (w/w), 15 % (w/w) and 20% (w/w) without pH adjustment (pH 6.8 ± 0.2). In either case, the suspensions were stirred for 1 h at 22 °C followed by centrifugation for 30 min at 2400 × g and 10 °C. The supernatants were recovered, weighed and their soluble protein content determined by the bicinchoninic acid (BCA) kit (G-Biosciences®, USA). The absorbance was recorded at 562 nm and protein content was determined by a calibration curve constructed using known concentrations of bovine serum albumin (BSA, provided with the kit). Finally, soluble protein content was calculated by Equation 5-3.

$$\text{Soluble protein (\%, w/w)} = \frac{\text{protein concentration in supernatant (mg/mL)} \times \text{volume of supernatant (mL)}}{\text{weight of freeze-dried QPI (mg)}} \times 100\% \quad (5\text{-}3)$$

5.2.3 Physico-chemical and technofunctional properties

5.2.3.1 Analysis of protein profile

Native- and SDS-PAGE under reducing and non-reducing conditions were applied to acquire the protein profile of the extracted QPI. The samples consisted of the supernatants

of 10 mg/mL QPI-H, QPI-A and QPI-C aqueous suspensions without pH adjustment (pH 6.8 ± 0.2) after centrifugation for 30 min at 2400 × g and 10 °C. The samples were mixed with native sample buffer or Laemmli sample buffer with or without 2-mercaptoethanol in a 1:1 ratio. When SDS-PAGE was performed, samples mixed with Laemmli buffer were also heated for 5 min at 100 °C. 10 µL of each sample and 10 µL of protein standards with molecular weights between 10 – 250 kDa were then loaded into Mini-PROTEAN® 4 – 20% polyacrylamide gels. Electrophoretic runs were performed at a constant voltage of 200 V, using running buffers containing 25 mM Tris, 192 mM glycine and, for SDS-PAGE only, 0.1% SDS at pH 8.3. After the runs, the protein bands in the gels were stained with Coomassie Brilliant Blue for 1 h and destained with destain solution composed of 30% (w/w) methanol and 7% (w/w) acetic acid.

5.2.3.2 ζ-potential and particle size measurements

A Zetasizer Nano ZS (Malvern Panalytical®, UK) was used to acquire ζ-potential and particle size data at 22 °C. QPI was suspended in distilled water at a concentration of 1% (w/w), without pH adjustment (pH 6.8 ± 0.2), stirred for 1 h at 22 °C and immediately used for analysis. All samples were appropriately diluted to prevent multiple scattering phenomena. The refractive indices used were 1.45 for QPI and 1.33 for water, with a backscattering measurement angle of 173° used for particle size determination (Ruiz et al., 2016b).

5.2.3.3 Differential scanning calorimetry

Differential scanning calorimetry (μDSC3evo run, Setaram Instrumentation®, France) was applied to determine the thermal properties of the QPI extracted. QPI was suspended in distilled water at a concentration of 10% (w/w), without pH adjustment (pH 6.8 ± 0.2), stirred for 1 h at 22 °C and immediately used for analysis. DSC pans were filled with around 0.5 g of QPI suspension and hermetically sealed. A pan with a matching mass of distilled water was used as reference. Samples were heated at a rate of 1.2 °C/min from 20 °C to 100 °C, kept at this temperature for 5 min and then cooled at the same rate to 20 °C. The denaturation temperature (T_d), defined as the temperature where the maximum transition peak occurred, as well as the denaturation enthalpy (ΔH), defined as the area below the transition peak, were calculated using the equipment software. Enthalpy was then converted to J/g protein by considering the sample concentration (10%, w/w) and the total protein content of each QPI.

5.2.3.4 Confocal laser scanning microscopy

Confocal laser scanning microscopy (CLSM) was used to visualise the microstructure of 10% (w/w) and 20% (w/w) gelled QPI samples using a published method for imaging (Ong et al., 2011). Briefly, an aliquot of 10 μL of 0.1% Fast Green FCF dye solution (1 mg/mL in MilliQ water) was added to 480 μL of a QPI suspension at a concentration of 10% (w/w) or 20% (w/w), followed by the addition of 10 μL of 0.1% Nile Red solution (1 mg/mL in dimethyl sulfoxide). The stained suspensions were transferred to glass vials and the lids were sealed with parafilm. The glass vials were incubated in a dry block heater and subjected to a temperature profile akin to the gelation profile applied in the

rheometer (see Section 5.2.3.6) except that the heating rate was of 1.2 °C/min due instrument limitation. The temperature of the samples was recorded using a datalogger thermometer (TC Direct, Australia) and the data collected by the TestLink SE521 software used to calculate the experimental heating rate. A piece of each gel (~ 5 mm x 5 mm x 2 mm) was then transferred to a microscope slide (ProSciTech, Australia) with a 2 mm thick spacer and covered with a cover slip (ProSciTech, Australia). The images were acquired on a confocal laser scanning microscope (Leica Sp8, Leica Microsystems, Germany) equipped with a 63× oil immersion objective. Z-stacks of gel microstructures were obtained using 638 nm and 488 nm laser excitation for Fast Green FCF and Nile Red, respectively. Imaris 10 Microscopy Image Analysis Software (Oxford Instruments, UK) was used to process the CLSM images. At least three z-stacks of different regions of each sample were taken and analysed. Quantification of the size of oil bodies/droplets in the gels as well as gel porosity was performed using the surface creation function of Imaris (Ong et al., 2020), analysing at least 5,000 surfaces in each image. Unstained areas were assumed to be pores. This area was quantified by subtracting the area occupied by protein and oil bodies/droplets, identified using the surface creation function of the software, from the total area of the image.

5.2.3.5 Fourier transform infrared spectroscopy

Fourier transform infrared spectroscopy (FTIR) spectra of 10% (w/w) or 20% (w/w) QPI gels were obtained with a Lumos II FTIR microscope (Bruker, USA), equipped with an attenuated total reflectance unit. The absorbance of the samples was recorded at wavelengths 400 – 4000 cm^{-1} with 4 cm^{-1} of resolution. Quantitative analysis of the FTIR spectra was carried out by applying the second derivative of the Amide I region

(1600 – 1700 cm^{-1}), followed by baseline subtraction and Gaussian deconvolution with the OriginLab® (version 2019) software (OriginLab Corporation, USA). The contribution of each peak to the Amide I region was obtained as the ratio of the individual peak area and the total area of the deconvoluted peaks.

5.2.3.6 Rheological methods

A dynamic shear rheometer (MCR 300 Anton Paar®, Anton Paar, Austria) fitted with a smooth parallel plate geometry (50 mm diameter, 1 mm gap) was used throughout. QPI was suspended in distilled water at a concentration of 10% (w/w) or 20% (w/w) without pH adjustment (pH 6.8 ± 0.2), stirred for 1 h at 22 °C and immediately used for analysis. To avoid water evaporation during all measurements, low viscosity mineral oil was carefully pipetted around the outer rim of the sample and the samples also covered with a solvent trap and the equipment's Peltier hood.

The gelation properties were investigated by temperature sweeps recording the storage (G') and loss (G'') moduli. Samples were heated from 20 °C to 90 °C at a heating rate of 1 °C/min, held for 5 min at 90 °C, followed by cooling to 20 °C at 1 °C/min, using 1% strain and an angular frequency of 10 rad/s. Immediately afterwards, without removing the sample from the gap, a time sweep (1% strain and 10 rad/s frequency) of 5 min at 20 °C was performed, followed by a frequency sweep (0.1 – 100 rad/s at 1% strain, 10 points per decade) and an amplitude sweep (0.1 – 1000% at 10 rad/s, 10 points per decade). The angular frequency (ω) dependence of the G' data was fitted with Equation 5-4.

$$\log(G') = n \times \log(\omega) + K \quad (5\text{-}4)$$

In this equation, the slope (n) indicates the type of gel network, where n = 0 characterises an elastic network, while a higher value identifies a more viscous network. The K value is the intercept of the linear regression and provides an indication of the strength of the gel network (Creusot et al., 2011; Tanger et al., 2022). Additionally, the yield stress (τ_y) of the gels was determined from amplitude sweep data as the maximum of the elastic stress (G' × strain) as a function of the strain (Yang, Scriven and Macosko, 1986; Walls et al., 2003).

5.2.3.7 Water holding capacity

To determine water holding capacity (WHC, %) QPI was suspended in distilled water at a concentration of 10% (w/w) or 20% (w/w) without pH adjustment (pH 6.8 ± 0.2) and stirred for 1 h at 22 °C. The suspensions were transferred to centrifuge tubes and incubated for 30 min at 90 °C in a water bath. The samples were then allowed to cool for 30 min at room temperature (22°C) before centrifugation for 5 min at 2400 × g and 10 °C. Following published method (Devnani et al., 2020), the supernatant was drained, the weight of the gels recorded and WHC (%) calculated using Equation 5-5.

$$\text{WHC (\%, w/w)} = \frac{\text{weight of the gel after centrifugation (g)}}{\text{weight of the gel before centrifugation (g)}} \times 100\% \quad (5\text{-}5)$$

5.2.4 Statistical analyses

All measurements were performed in triplicate and the results expressed as the mean ± the standard deviation (SD). Results were analysed by analysis of variance (ANOVA) followed by Tukey's post-test to verify significant differences among the means, considering a confidence level of 95% ($p < 0.05$) using the SigmaPlot® (14.5) software (Grafiti LLC, USA).

Principal components analysis (PCA) was applied to the data obtained for total protein and soluble protein content, thermal properties, gelation properties and WHC and used to explore and visualise the correlation between the properties and the different concentrations of QPI samples using the OriginLab® (version 2019) software (OriginLab Corporation, USA).

5.3 Results and discussion

5.3.1 Composition, extraction yield and protein yield

QPI was extracted from quinoa flour by wet extraction under alkaline conditions followed by acid precipitation with one of three different acids: hydrochloric acid (QPI-H), acetic acid (QPI-A) or citric acid (QPI-C) at 1.0 M. This acid concentration allows a direct comparison between the acids applied when all other factors are standardised. The extraction yield was similar ($p > 0.05$) between the three experimental conditions, with values of ~5% (w/w) (Table 5-1). The protein content was statistically significantly lower for QPI-H samples ($p < 0.05$) compared to QPI precipitated with either of the two more kosmotropic acids (QPI-A and QPI-C); ~56% (w/w) vs ~60% (w/w) and ~59% (w/w), respectively. However, considering the small difference in protein content, there was no

statistically significant difference in protein yield between the three extracts, with values of ~18% (w/w).

Table 5-1. Chemical composition (%, w/w) on wet basis, extraction yield (%, w/w) and protein yield (%, w/w) of QPI precipitated with HCl (QPI-H), acetic acid (QPI-A) and citric acid (QPI-C).

	Protein isolates		
	QPI-H	QPI-A	QPI-C
Protein (%)	56.0 ± 0.5^{b}	59.9 ± 0.2^{a}	58.7 ± 0.7^{a}
Lipid (%)	11.3 ± 3.4^{b}	22.3 ± 3.5^{a}	27.4 ± 0.8^{a}
Carbohydrate (%)*	29.0 ± 3.4	9.7 ± 3.5	10.3 ± 1.1
of which starch (%)	2.2 ± 0.2^{a}	0.3 ± 0.2^{c}	1.4 ± 0.4^{b}
Moisture (%)	$0.6 \pm < 0.1^{b}$	4.9 ± 0.3^{a}	0.5 ± 0.2^{b}
Ash (%)	3.1 ± 0.3^{a}	3.2 ± 0.2^{a}	3.1 ± 0.1^{a}
Extraction yield (%)	4.8 ± 0.3^{a}	4.8 ± 0.3^{a}	$4.8 \pm < 0.1^{a}$
Protein yield (%)	17.5 ± 1.3^{a}	18.7 ± 1.0^{a}	18.4 ± 0.4^{a}

*Carbohydrate calculated by difference, the SD presented was obtained by calculation of the standard error using the SD of the individual means used to obtain the carbohydrate content. Equal lowercase letters in the same row indicate that there is no significant difference among the means (Tukey's test, $p > 0.05$).

The values for protein yield and protein content determined here are within the range reported in literature for QPI extracted at pH 9 using HCl for precipitation: 9.2 – 46% (w/w) for protein yield (Nongonierma et al., 2015; Ruiz et al., 2016a, 2016b; Sánchez-Reséndiz et al., 2019) and 41 – 96% (w/w) for protein content (Nongonierma et al., 2015; Ruiz et al., 2016a, 2016b; Steffolani et al., 2016; Mir, Riar and Singh, 2019a). The extraction yields (Table 5-1), though, were slightly lower than the range of 8.1 – 13.4% (w/w) reported in literature for equivalent extraction conditions (Mir, Riar and Singh, 2019a; Sánchez-Reséndiz et al., 2019). Several factors may be responsible for the lower extraction yield, such as the flour storage conditions and the quinoa

variety/cultivar used, as well as slight differences in extraction times and strength of the base and acid used for extraction across different studies (Sánchez-Reséndiz et al., 2019; Kumar et al., 2021).

The lipid content (Table 5-1) of the extracted QPI was higher by a factor of 2 – 4 than that reported previously for QPI extracted from solvent-based defatted quinoa flour (Yang et al., 2022b). In most studies, a flour defatting step using hexane or petroleum ether is applied prior to QPI extraction. Here, the flour defatting step using organic solvents was omitted to limit the materials used for extraction to green solvents. Instead, the creamed lipid layer formed during the centrifugation of the alkalinised flour was removed by simple filtration with the help of a cheesecloth (Geerts et al., 2018). However, it appears that the filtrate still contained oil droplets. These would either be native quinoa oil bodies or broken up and re-emulsified oil bodies. The stabilisation of oil bodies is complex and involves a mixture of amphiphilic lipids and proteins (Tzen et al., 1993; White, Fisk and Gray, 2006). In either case, the presence of protein at the droplet surface leads to the precipitation of the droplets during the acidification step, resulting in an increase in lipid content of the QPI. Considering the fact that acids with a higher kosmotropic effect than HCl suppress protein unfolding during extraction (Zhang and Cremer, 2010), it is possible that the use of acetic acid and citric acid also protected the structure of oil body-associated proteins in QPI, which partially suppressed oil bodies aggregation and creaming, and resulted in extracts with a higher lipid content than when HCl was used for precipitation. However, further studies are necessary to ascertain this hypothesis.

The starch and carbohydrate contents were also different between the samples. QPI-H had the highest ($p < 0.05$) starch content among the samples, which is consistent with the also highest concentration of carbohydrate (2.2% and 29.0%, w/w, respectively). While

QPI-A and QPI-C contained similar carbohydrate contents (~10%, w/w), QPI-A contained a statistically lower concentration of starch (0.3% vs 1.4%, w/w). This suggests that the two kosmotropic acids have distinct effects on starch recovery during wet fractionation for quinoa protein extraction; however, further research is needed to determine the extent of this influence. Moisture content was not significantly different between QPI-H and QPI-C, ranging 0.5 – 0.6% (w/w), which is comparable to prior reports (Yang et al., 2022b), although the moisture content of QPI-A was significant higher (4.9%, w/w). Finally, the ash content of all three QPI extracts was similar at ~3% (w/w), comparable with the past literature (Mir, Riar and Singh, 2019a; Yang et al., 2022b).

5.3.2 Soluble protein content

The soluble protein content of the extracted QPI samples was assessed at a fixed concentration of 1% (w/w) in the pH value range of 6 – 9 (Figure 5-1a) and at a range of protein concentrations (1 – 20%, w/w) at natural pH (6.8 ± 0.2) (Figure 5-1b). The pH range of 6 – 9 was chosen because the natural pH of the isolates is between 6 – 7 while pH 9 was the pH used during the alkalinisation step. The protein concentration range of 1 – 20% (w/w) was selected anticipating the investigation of the gelation properties of the isolates at 10% and 20% (w/w) concentration.

The soluble protein content of QPI-H increased steadily with pH (Figure 5-1a), reaching its maximum value of ~56% (w/w) at pH 9. The soluble protein content of QPI precipitated with the kosmotropic acids was significantly higher than that of QPI-H at all pH values applied ($p < 0.05$, Appendix B – Table B.1). Further, at pH values above 6, the

soluble protein content of QPI-A or QPI-C did not significantly change ($p > 0.05$) as a function of pH, remaining at around 70% (w/w), indicating that, within the pH range of 7 – 9, the protein in these samples had maximum solubility. The higher soluble protein content shown by QPI-A and QPI-C was expected, considering that kosmotropic acids protect native protein structures (Zhang and Cremer, 2010). When dispersed in water in the absence of added salts, electrostatic repulsion between charged regions of native protein molecules promotes interactions between proteins and the solvent, enhancing protein solubility (Bryant and McClements, 1998). For QPI-H, it is expected that the protein molecules are more unfolded, leading to more pronounced protein-protein interactions, such as disulfide bridges, hydrogen bonds and hydrophobic interactions, which consequently reduce protein solubility (Nicolai, 2019).

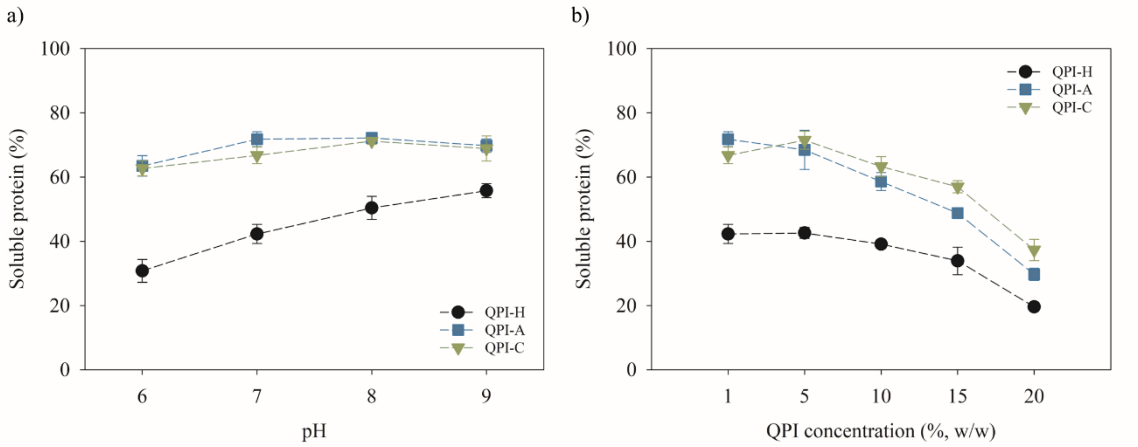

Figure 5-1. Solubility (%, w/w) of QPI precipitated with HCl (QPI-H, ● black), acetic acid (QPI-A, ■ blue) and citric acid (QPI-C, ▼ green) at a) 1% (w/w) concentration at pH 6.0 – 9.0 and 22 °C and at b) 1, 5, 10, 15 and 20% (w/w) concentration at pH 6.8 ± 0.2 and 22 °C.

With increasing concentration of QPI, the soluble protein content of all three samples showed an initial plateau before progressively decreasing (Figure 5-1b). The observed

decrease at concentrations above 5% (w/w) is possibly due to self-assembly of native proteins occurring at higher concentrations, as previously reported for soy protein (Chen et al., 2016). Again, the solubility of QPI-A and QPI-C was significantly higher than that of QPI-H, at all concentrations ($p < 0.05$, Appendix B – Table B.2).

5.3.3 Particle size and ζ-potential

The particle size distributions of QPI precipitated with the different acids were multimodal (Figure 5-2), with at least three peaks occurring for each sample. All three samples showed a large peak at around 1000 nm and a smaller peak at around 8000 nm, likely related to small and large protein aggregates, respectively. In fact, the peak for QPI-H at 8000 nm was slightly higher than that for QPI-A or QPI-C which is consistent with the lower solubility of QPI-H (Figure 5-1a-b). QPI-H and QPI-A also showed a small peak at around 100 nm, while both QPI-A and QPI-C displayed a peak at ~400 nm. The smaller peak at ~100 nm was absent in QPI-C samples. In general, the peak sizes are higher than those reported for pea protein extracted using similar conditions (Tanger, Engel and Kulozik, 2020). It should be noted though that, in the cited report, the pea protein was filtered through a 0.2 μm size filter before analysis to remove aggregates. Here, on the other hand, the QPI samples were simply diluted, which may explain the larger sizes. Nonetheless, the pea protein samples also showed a multimodal particle size distribution, with at least two peaks at low ionic strength (Tanger, Engel and Kulozik, 2020).

The ζ-potential values were −43.4 ± 1.0 mV for QPI-H, −40.9 ± 0.7 mV for QPI-A and −38.6 ± 0.6 mV for QPI-C. The net negative charges were expected as the samples were

analysed at pH ~6.8 ± 0.2 which is above the isoelectric point of pH~4.5 reported for QPI (Mir, Riar and Singh, 2019a). These values themselves compare well with ζ-potential data reported for okara proteins precipitated with HCl, citric acid and malic acid (Cai et al., 2020).

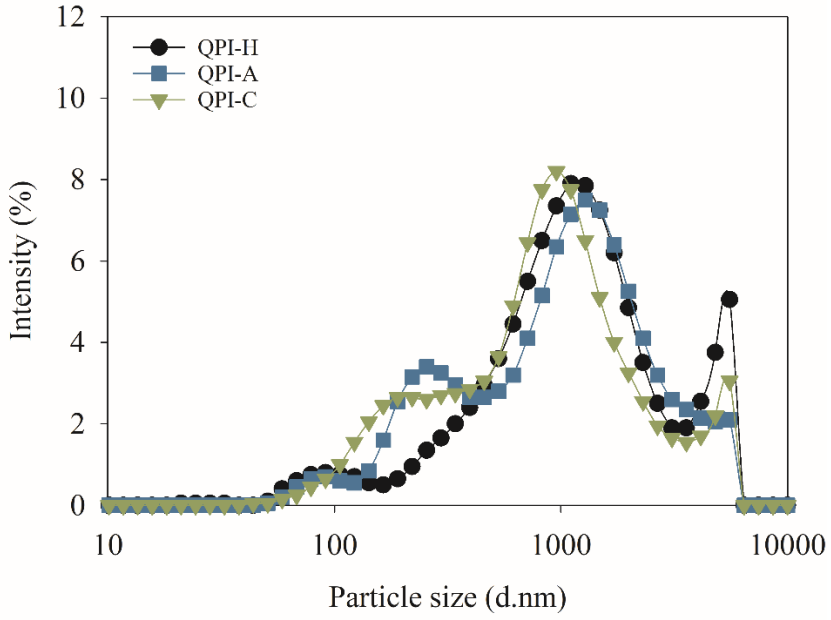

Figure 5-2. Particle size distribution of 1% (w/w) samples of QPI precipitated with HCl (QPI-H, ● black), acetic acid (QPI-A, ■ blue) and citric acid (QPI-C, ▼ green) (mean of 3 measurements).

5.3.4 Protein profile

The protein profile of QPI samples was analysed by Native-PAGE and by SDS-PAGE under non-reducing and reducing conditions (Figure 5-3). Overall, the protein profile in the QPI samples was similar, irrespective of the type of acid used to precipitate the protein. The protein isolates were mainly composed of globulins and albumins, consistent with their aqueous extraction under basic conditions at pH 9 as reported previously (Abugoch et al., 2008; Ruiz et al., 2016b).

No major differences between the samples were identified by Native-PAGE (Figure 5-3a), where the protein structure remains intact due to the absence of reducing agents. Four main bands were detected, likely corresponding, from top to bottom, to the hexamer form of globulin 11S (~360 kDa), the tetramer form of globulin 7S (~200 kDa) and the subunit form of globulin 11S (45 – 55 kDa, two bands), as it has been shown that globulin 11S may also occur as monomers (subunits) under non-denaturing conditions (van de Vondel, Lambrecht and Delcour, 2020; van de Vondel et al., 2021).

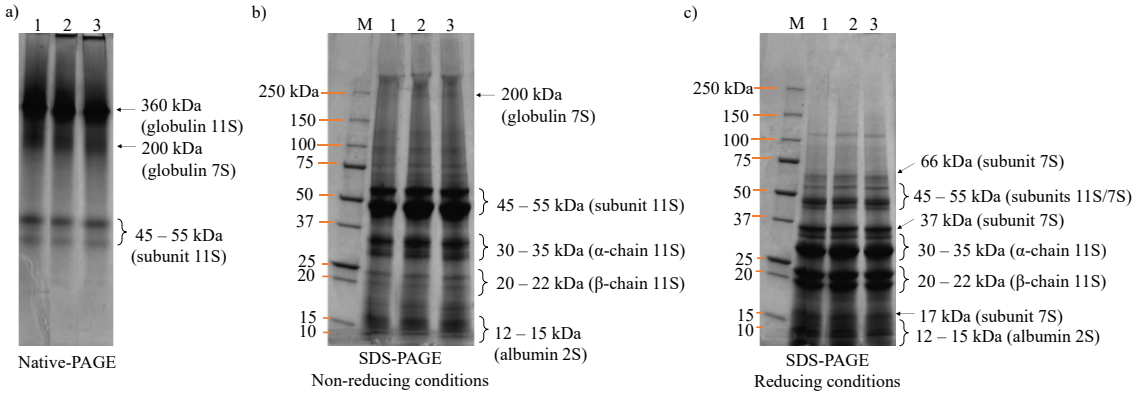

Figure 5-3. Gel electrophoresis of QPI precipitated with HCl (QPI-H), acetic acid (QPI-A) and citric acid (QPI-C): a) Native-PAGE; b) SDS-PAGE under non-reducing conditions; c) SDS-PAGE under reducing conditions. Legend: M- protein standards; 1- QPI-H; 2- QPI-A; 3- QPI-C.

The profiles obtained for the three samples by SDS-PAGE under non-reducing and reducing conditions were also highly similar. In SDS-PAGE under non-reducing conditions, i.e., in the absence of 2-mercaptoethanol, the subunit of globulin 11S is expected to remain intact, although it has been reported to also occur as the dissociated α- and β-chains under these conditions with corresponding bands displaying lower intensities than the associated subunit (45 – 55 kDa) (Kaspchak et al., 2017; van de

Vondel, Lambrecht and Delcour, 2020). In addition to a band identifying albumin 2S (12 – 15 kDa) and to fainter bands identifying the α- and β-chains of globulin 11S (30 – 35 and 20 – 22 kDa, respectively), strong bands at 45 – 55 kDa characterising the intact subunit of globulin 11S were identified (Figure 5-3b). A faint band at ~200 kDa was also detected in all extracts, corresponding to the tetramer of globulin 7S.

Under reducing conditions, i.e., in the presence of 2-mercaptoethanol, the subunit of globulin 11S is expected to dissociate due to breakage of the disulfide bond that links the α- and β-chains (Kaspchak et al., 2017). In addition to the bands corresponding to albumin 2S and to fainter bands identifying the subunit of globulin 11S, intense bands corresponding to the α- and β-chains of globulin 11S were detected in the three QPI samples (Figure 5-3c). Additional bands at 17 kDa, 37 kDa, 50 kDa and 66 kDa were also detected in all extracts, corresponding to the completely disassociated tetramer of globulin 7S, as previously reported for the pseudocereal amaranth (*Amaranthus* spp.) (Quiroga et al., 2010). Overall, both SDS-PAGE profiles were consistent with the literature for QPI (Abugoch et al., 2008; Mäkinen et al., 2016; Ruiz et al., 2016b; Kaspchak et al., 2017; Shen, Tang and Li, 2021; Yang et al., 2022b).

5.3.5 Thermal properties

The thermal properties of the extracted QPI samples were assessed by DSC (Figure 5-4). Independent of extraction acid applied, the samples showed a single endothermic transition. The denaturation temperature (T_d) of ~89 °C, the onset temperature (T_o) of ~83 °C and the endset temperature (T_e) of ~93 °C were not statistically different between the samples (Table 5-2). The T_d values were in line with values reported in literature for

globulin 11S, the main protein in QPI (Vera et al., 2019), and for other plant globulins, such as pea protein (T_d = 87 °C) (Mession et al., 2012a), almond protein (T_d = 81 °C) (Devnani et al., 2021) and red bean protein (T_d = 86 °C) (Meng and Ma, 2001). It should be acknowledged that higher T_d values have also been reported for QPI (~97 – 98 °C) (Abugoch et al., 2008; Ruiz et al., 2016b). However, denaturation temperatures can vary due to differences in primary processing conditions and extraction protocols (Devnani et al., 2021), as well as heating rates used during thermal analysis (Mession et al., 2013).

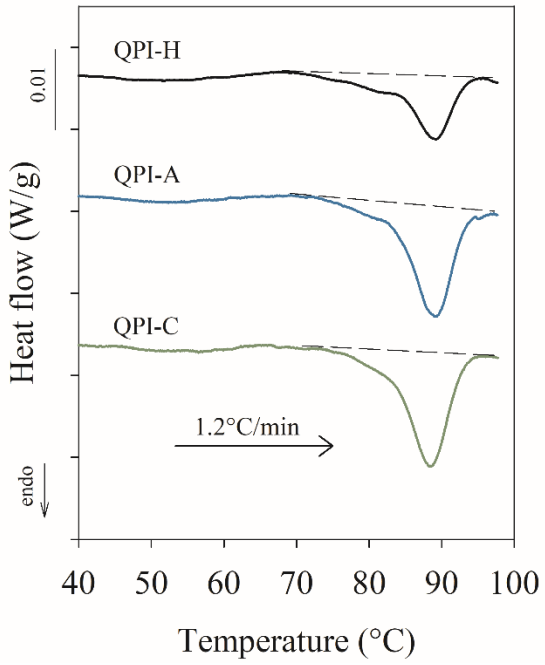

Figure 5-4. DSC thermograms (mean of 3 measurements) of 10% (w/w) samples of QPI precipitated with HCl (QPI-H, black), acetic acid (QPI-A, blue) and citric acid (QPI-C, green) during heating from 20 to 100 °C at a rate of 1.2 °C/min. The dashed lines limit the area below the peaks which was integrated to give the denaturation enthalpy.

The order of magnitude for the denaturation enthalpy (ΔH) values reported in Table 5-2 is in agreement with literature (Steffolani et al., 2016; Tanger et al., 2022). The ΔH for

QPI-C was significantly higher than for QPI-H ($p < 0.05$), consistent with the soluble protein content being higher for this extract (Figure 5-1a-b). QPI-A showed a very similar ΔH to QPI-C, although the difference with QPI-H was not statistically significant ($p > 0.05$), due to this sample's higher standard deviation compared to QPI-C. The higher ΔH value for QPI-A and QPI-C contributes to the evidence presented so far that precipitation with kosmotropic acids results in extracts containing less unfolded protein compared to precipitation with HCl.

Table 5-2. Enthalpy (ΔH) and temperature of denaturation (T_d), as well as onset (T_o) and endset (T_e) temperatures of QPI precipitated with HCl (QPI-H), acetic acid (QPI-A) and citric acid (QPI-C).

	Protein isolates		
	QPI-H	QPI-A	QPI-C
T_o (°C)	83.8 ± 1.0[a]	83.4 ± 0.4[a]	83.0 ± 0.5[a]
T_d (°C)	88.8 ± 0.5[a]	89.1 ± 0.1[a]	88.5 ± 0.3[a]
T_e (°C)	92.8 ± 0.4[a]	92.6 ± 0.2[a]	92.6 ± 0.3[a]
ΔH (J/g protein)	3.0 ± 0.3[b]	4.4 ± 0.8[ab]	4.5 ± 0.6[a]

Equal lowercase letters in the same row indicate that there is no significant difference among the means (Tukey's test, $p > 0.05$).

5.3.6 Microstructure of QPI gels

The microstructure of heat-induced gels containing 10% (w/w) or 20% (w/w) of QPI consisted of a protein network with small integrated oil droplets, see Figure 5-5. Figures B.1 and B.2 (Appendix B) show the microstructure of each gel stained solely for either the protein or lipid to allow separate visualisation and analysis. Oil droplets ranged in size between 0.2 μm and 10 μm. Since native quinoa oil bodies, which arise from the embryo fraction of the quinoa seed, are around ~0.2 – 0.5 μm in size (Prego, Maldonado and

Otegui, 1998) it is possible that native oil bodies were carried over to QPI during extraction. Larger droplets, though, are expected to correspond to re-emulsified oil. Under gelation, the included oil droplets can act as active or inactive fillers in soft solid systems. Active fillers show strong interaction with the gel matrix and thus reinforce the gel structure, while inactive fillers have poor affinity with the matrix and consequently weaken the gel network. The active or inactive nature of the filler depends on surface composition and properties, where protein-stabilised oil droplets usually behave as active fillers within protein gels while surfactant-covered oil droplets act as inactive fillers (Dickinson and Chen, 1999; Ben-Harb et al., 2018; Klost and Drusch, 2019). Here, the oil droplets appear to be integrated in the protein network, as shown in the cross-sectional projections of each gel (Figure 5-5), indicating that these might have acted as active fillers within the protein network, likely contributing to gel strength. While the present work focused on the impact of the different acid treatments on the protein component, future research should focus on the interactions between protein and oil droplets and the effects of this interaction on the functionality of QPI.

Significant differences were observed between the microstructure of the three 10% (w/w) gels, with QPI-H gels showing significantly higher porosity (72.6 ± 1.6%, $p < 0.05$) than QPI-A and QPI-C gels (59.3 ± 2.7% and 63.1 ± 1.5%, respectively) when assessed by image analysis. This difference can be visualised in the cross-sectional images of each gel, where the 10% (w/w) QPI-H gels contained unstained areas visible in the cross-sectional projections (Figure 5-5a), potentially corresponding to aqueous pores, whereas the 10% (w/w) QPI-A and QPI-C gels showed a less porous gel network with almost no void spaces. In a mixed protein suspension, it is the soluble or native protein present in suspension that unfolds upon heating and triggers protein aggregation

and network formation resulting in heat-induced protein gels (Brodkorb et al., 2016; Nicolai, 2019). Thus, the structure of the gel can provide an indication of the initial concentration of soluble or native protein in a sample. The lower porosity of 10% (w/w) QPI-A and QPI-C gels suggests a stronger gel network formation compared to QPI-H gels and this observation is consistent with the higher soluble protein content and ΔH of these samples (Figure 5-1, Table 5-2). Together these observations provide further evidence that a higher concentration of native protein structure was preserved during extraction with the kosmotropic acids.

The microstructure of the three gel samples formed from 20% (w/w) QPI consisted of a more coarsely aggregated gel network compared to the structure observed for the 10% (w/w) QPI samples (Figures 5-5b vs 5-5a); void spaces were also visible in some areas. However, there were fewer differences between the microstructure of the three gels at this concentration and the porosities were similar ($p > 0.05$), ranging from 52.2 ± 3.0% to 58.4 ± 0.1%.

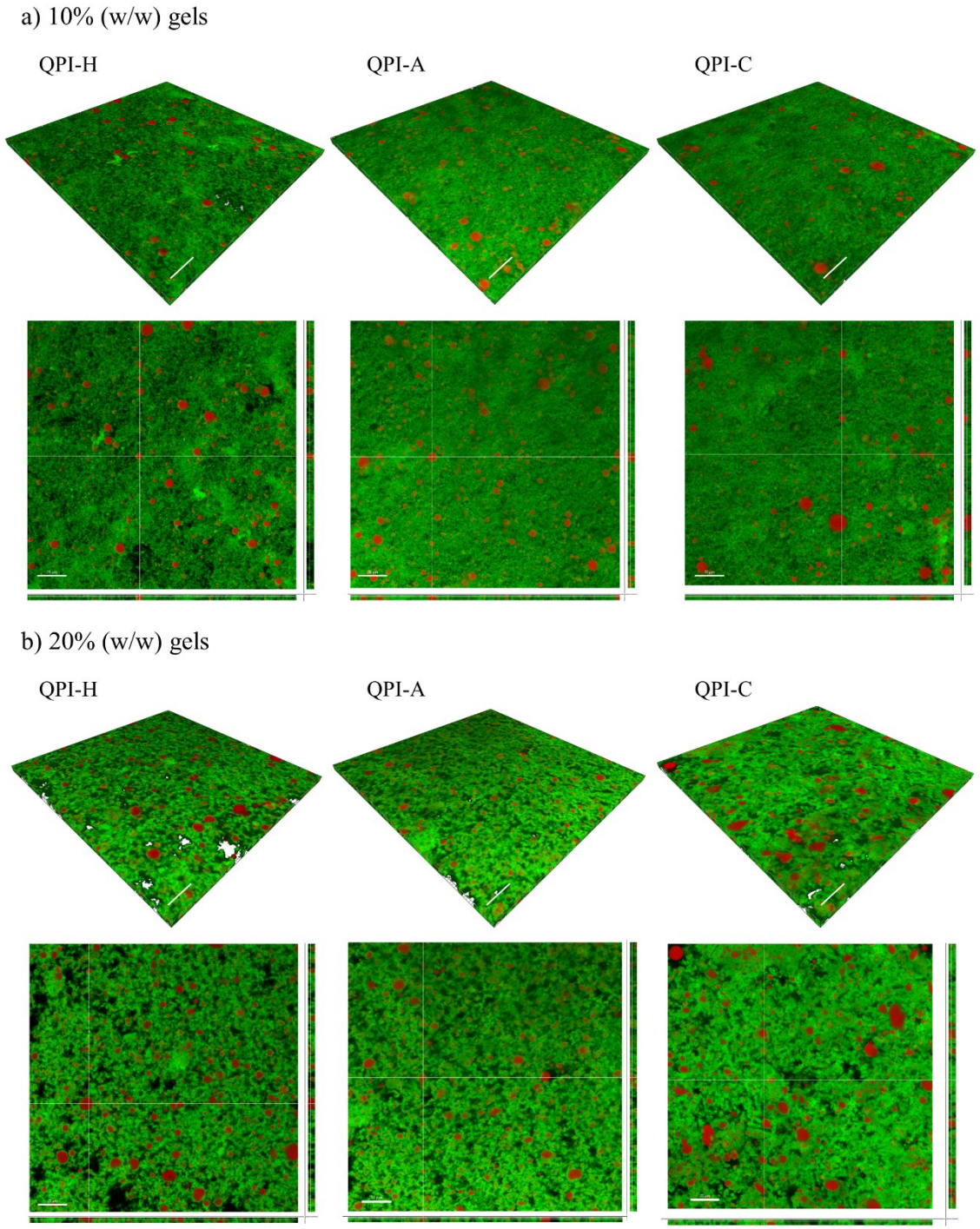

Figure 5-5. Confocal laser scanning microscopy images of heat-induced gels composed of a) 10% (w/w) QPI or b) 20% (w/w) QPI, where the protein had been prepared by precipitation with HCl (QPI-H), acetic acid (QPI-A) or citric acid (QPI-C). The protein network is stained green and lipid droplets are stained red. The scale bars represent 20 µm. The samples are shown in projected view (top of a or b), as well as in cross section (bottom of a or b), where the projection in the x-z and y-z direction is shown adjacent to the x-y image.

5.3.7 Fourier transform infrared spectroscopy of QPI gels

The FTIR spectra measured for the 10% (w/w) and 20% (w/w) QPI protein gels were similar between the samples regardless of precipitation acid and contained a large number of peaks (Figure 5-6a). The broad peak at 3300 cm^{-1} (2960 – 3700 cm^{-1} range) is related to free hydroxyl groups (-OH) and the interactions of protein molecules with water, including the Amide A region, while the small peak at ~2900 cm^{-1} is likely linked to the Amide B region (Goormaghtigh, Ruysschaert and Raussens, 2006; Mir, Riar and Singh, 2020; Figueroa-González et al., 2022). Amide A and B vibrational modes arise from C=O and N-H stretching of protein bonds (Goormaghtigh, Ruysschaert and Raussens, 2006; Mir, Riar and Singh, 2021b). The following small peak at ~2850 cm^{-1} is likely corresponding to the stretching of CH_2 and CH_3 groups of fatty acids present in the samples (Andrade et al., 2019; Figueroa-González et al., 2022). Also related to the presence of lipids is the small peak found between 1700 cm^{-1} and 1800 cm^{-1}, which can be associated to C=O stretch of esters or carboxyl groups (Andrade et al., 2019). The peak at 1600 – 1700 cm^{-1} corresponds to the Amide I region, characterised by the presence of C=O and C-N bonds, while the peak at 1500 – 1600 cm^{-1} corresponds to the Amide II region, characterised by C-N and N-H bonds (Goormaghtigh, Ruysschaert and Raussens, 2006; Mir, Riar and Singh, 2020). Finally, the region 1400 – 1450 cm^{-1} is associated with lipids, identifying stretching of C=O bonds in COO^- and COOH groups (Andrade et al., 2019), while the peaks below 1400 cm^{-1} identify the Amide III region, associated with the α-helix content of proteins (Goormaghtigh, Ruysschaert and Raussens, 2006; Mir, Riar and Singh, 2020).

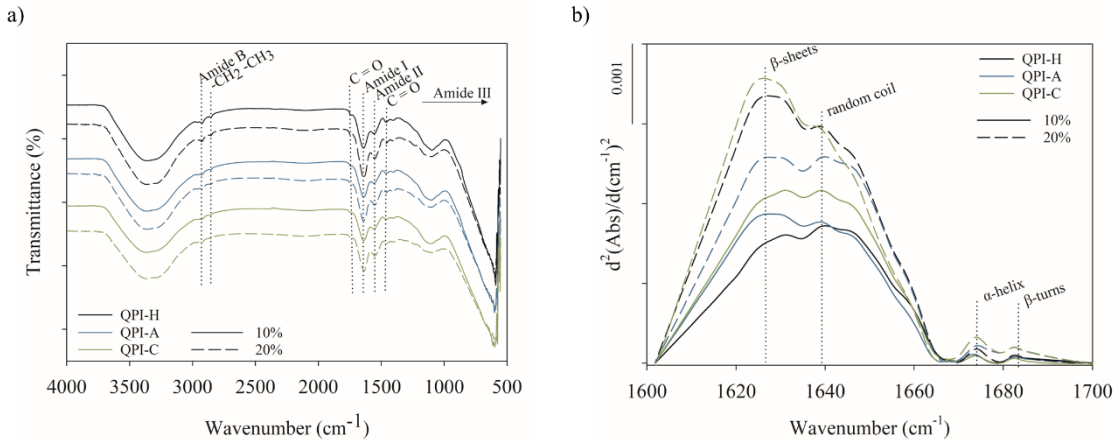

Figure 5-6. Secondary structure of gels of 10% (w/w) and 20% (w/w) QPI precipitated with HCl (QPI-H, black), acetic acid (QPI-A, blue) and citric acid (QPI-C, green) (mean of two measurements): a) FTIR spectra; b) second derivative of the Amide I region of FTIR spectra.

Table 5-3. Contribution of secondary structure conformations to the overall protein structure of gels of 10% (w/w) and 20% (w/w) QPI precipitated with HCl (QPI-H), acetic acid (QPI-A) and citric acid (QPI-C).

		Secondary structure conformation (%)			
Concentration	Sample	β-sheet	Random coil	α-helix	β-turn
10% (w/w)	QPI-H	$45.2 \pm 4.1^{a,A}$	$50.1 \pm 2.9^{a,A}$	$2.7 \pm 0.8^{a,A}$	$2.1 \pm 0.3^{a,A}$
	QPI-A	$50.9 \pm < 0.1^{a,A}$	$44.1 \pm 2.0^{a,A}$	$2.9 \pm 0.4^{a,A}$	$2.1 \pm 1.7^{a,A}$
	QPI-C	$50.2 \pm 1.2^{a,A}$	$46.4 \pm 0.6^{a,A}$	$2.1 \pm 1.2^{a,A}$	$1.3 \pm 0.7^{a,A}$
20% (w/w)	QPI-H	$50.6 \pm 0.3^{a,A}$	$43.4 \pm 1.1^{ab,B}$	$3.5 \pm 1.0^{a,A}$	$2.5 \pm 0.4^{a,A}$
	QPI-A	$46.5 \pm 3.3^{a,A}$	$46.4 \pm 0.3^{a,A}$	$3.8 \pm 1.3^{a,A}$	$3.2 \pm 1.7^{a,A}$
	QPI-C	$50.4 \pm 1.8^{a,A}$	$42.2 \pm 0.7^{b,B}$	$4.7 \pm 0.3^{a,A}$	$2.7 \pm 0.7^{a,A}$

Equal lowercase letters in the same column indicate that there is no significant difference between the means of samples at the same concentration (Tukey's test, $p > 0.05$). Equal uppercase letters in the same column indicate that there is no significant difference between the means of samples at different concentrations (Tukey's test, $p > 0.05$).

The second derivative of the Amide I region of the spectra was obtained to give the contribution of each secondary structure conformation to the overall protein structure after gel formation (Table 5-3, Figure 5-6b). Peaks at ~1625 cm^{-1} are related to β-sheets,

while the peaks at ~1640 cm^{-1} correspond to random coil structures, at ~1675 cm^{-1} to α-helix structures and at ~1685 cm^{-1} to β-turns (Figueroa-González et al., 2022). The 20% (w/w) gels showed slightly higher intensity peaks than the 10% (w/w) gels in the Amide I region due to the higher protein concentration of these samples; however, there was no obvious shift in the position of the peak maxima among the samples as a result of the different treatments. The secondary structure content was found to be statistically similar ($p > 0.05$) between all 10% (w/w) samples. The 20% (w/w) QPI-C and QPI-H gels showed a significant reduction ($p < 0.05$) in random coil content compared to the 10% (w/w) gels (Table 5-3), which can also be identified by the decrease in peak intensity at the random coil region relative to the peak identifying the β-sheet structures in Figure 5-6b; while 20% (w/w) QPI-A did not show significantly different random coil content compared to the remaining samples. A reduction in the content of unordered random coil structures is associated with an increased structural stability in the samples (Carbonaro, Maselli and Nucara, 2012; Singh, Siddiqi and Sogi, 2021; Figueroa-González et al., 2022). Apart from this small difference though, the FTIR results indicate that the different acid treatments did not induce great changes in the secondary structure of QPI proteins. The differences found in soluble protein content, thermal properties and microstructure between different acid treated samples likely arise from changes in tertiary and quaternary structures during protein extraction. Similar to this observation, it has been previously reported that high-pressure homogenisation induced significant changes in QPI solubility, emulsifying and foaming capacity and gel strength, however, no changes in secondary structure were found by FTIR analysis of the samples before and after treatment (Luo et al., 2022a). Further, other studies reported alterations in the functional properties of QPI

after enzymatic hydrolysis (Fan et al., 2023) or sonication (Qin et al., 2018), while FTIR analysis detected only subtle changes in secondary structure.

5.3.8 Rheological properties

The heat-induced gelation of 10% (w/w) and 20% (w/w) suspensions of QPI precipitated with HCl (QPI-H), acetic acid (QPI-A) and citric acid (QPI-C) was studied rheologically by applying a temperature sweep. The samples were heated from 20 °C to 90 °C at 1 °C/min, held at 90 °C for 5 min and cooled from 90 °C to 20 °C at 1 °C/min while recording the storage (G') and loss (G") moduli (Figure 5-7).

The gelation temperature (T_{gel}), defined as the temperature at the intercept between a linear extrapolation of the rapidly increasing G' (indicated by arrows in Figure 5-7a-b) and the temperature axis (Sun and Arntfield, 2010; Ruiz et al., 2016b), was not statistically different ($p > 0.05$) among the 10% (w/w) QPI samples, ranging between 79.8 °C and 81.8 °C (Table 5-4). This temperature range was only slightly lower than the onset temperature range of thermal transition determined by DSC (T_o, Table 5-2), ~86 °C to ~89 °C. Initial G' values were higher for the 20% (w/w) samples than those observed for the 10% (w/w) samples. In general, G' increases with concentration because there are more protein crosslinking opportunities (Sun and Arntfield, 2010), which also explains the lower gelation temperature range (36.2 – 44.3 °C, $p > 0.05$) for the 20% (w/w) QPI gels compared to 10% (w/w) samples.

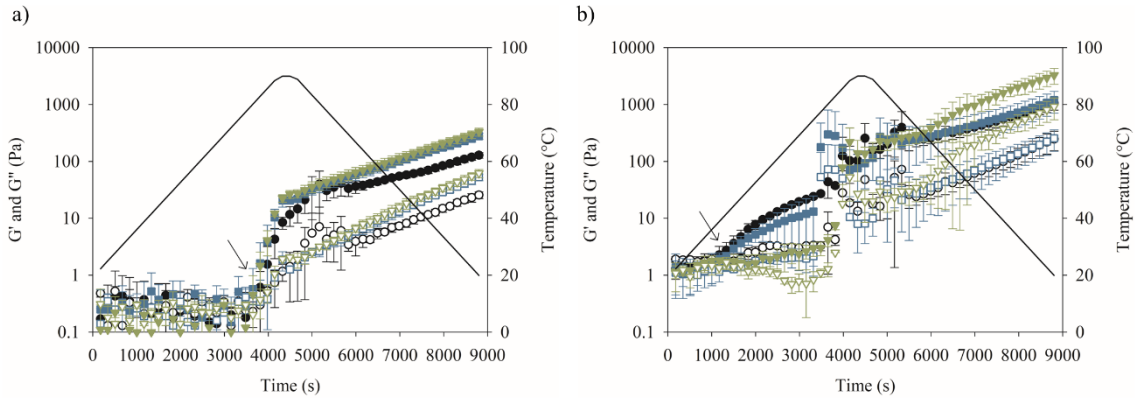

Figure 5-7. Gelation of QPI precipitated with HCl (QPI-H, ● black), acetic acid (QPI-A, ■ blue) and citric acid (QPI-C, ▼green) at concentration of a) 10% (w/w) or b) 20% (w/w) QPI. Closed symbols represent the storage modulus (G'), open symbols represent the loss (G'') modulus, the solid line represents the temperature profile and arrows indicate the gelation temperature (T_{gel}).

Table 5-4. Gelation temperatures (T_{gel}), final storage modulus (G'_{20}), frequency dependency (n) and yield stress (τ_y) obtained for 10% (w/w) and 20% (w/w) gels of QPI precipitated with HCl (QPI-H), acetic acid (QPI-A) or citric acid (QPI-C).

	Concentration (%, w/w)	T_{gel} (°C)	G'_{20} (Pa)*	n	τ_y (Pa)
QPI-H	10	81.8 ± 4.0^{a}	128.5 ± 14.6^{b}	0.10 ±< 0.10^{a}	14.8 ± 2.0^{b}
QPI-A		81.1 ± 3.0^{a}	278.7 ± 34.2^{a}	0.11 ±< 0.10^{a}	60.5 ± 17.5^{a}
QPI-C		79.8 ± 2.3^{a}	330.9 ± 52.7^{a}	0.10 ±< 0.10^{a}	70.5 ± 9.1^{a}
QPI-H	20	36.2 ± 5.4^{a}	1061.5 ± 263.4^{b}	0.11 ±< 0.10^{ab}	71.7 ± 20.7^{a}
QPI-A		36.8 ± 1.1^{a}	1205.2 ± 496.3^{b}	0.11 ±< 0.10^{b}	101.6 ± 44.5^{a}
QPI-C		44.3 ± 11.2^{a}	3289.9 ± 1018.3^{a}	0.15±< 0.10^{a}	101.6 ± 10.3^{a}

*Final values at the end of the temperature sweep, when the temperature returned to 20 °C. Equal lowercase letters in the same column indicate that there is no significant difference among the means at the same concentration (Tukey's test, $p > 0.05$).

G' and G'' moduli continued to increase during the holding and cooling periods for all gel samples (Figure 5-7). This behaviour was previously reported for gels of QPI (Ruiz et al.,

2016b; Patole, Cheng and Yang, 2022; Yang et al., 2022b) as well as pea (Tanger et al., 2022) and almond protein (Devnani et al., 2021). The aggregation and gelation rates are determined by the rate at which proteins denature and become able to form reactive bonds; in the case of heat-induced gelation this process is faster with an increase in temperature. Not all native proteins denature and participate in the network formation at the same time. However, due to different denaturation temperatures these are progressively incorporated into the network as the temperature increases. G' therefore starts to increase at the gelation temperature and continues to increase until all proteins are structurally perturbed and incorporated into the gel. A period of network restructuring and reinforcement may also follow, with G' continuing to increase slowly during cooling (Nicolai, 2019). Here, G' did not reach a plateau while holding at the highest temperature nor during cooling, indicating that the gel microstructure continued to develop as the temperature was lowered to 20 °C (Figure 5-7). However, the samples appeared to have reached a steady state at the final temperature as the G' values remained constant during the 5 min time sweep (1% strain, 10 rad/s) that was applied at 20 °C, immediately after the temperature sweep (Appendix B – Figure B.3).

The final gel strength recorded at 20 °C (G'_{20}) differed between 10% (w/w) samples (Figure 5-7a, Table 5-4), consistent with the different microstructures observed for these samples (Figure 5-5a). The 10% (w/w) QPI-A and QPI-C gels showed a significantly higher gel strength than the 10% (w/w) QPI-H gel ($p < 0.05$). Further, the G'_{20} values of the samples correlated positively to soluble protein content ($R^2 = 0.99$) (Appendix B – Figure B.4), illustrating the contribution of native soluble proteins to gel network formation as previously reported for globular proteins (Nicolai, 2019).

The final gel strength (G'_{20}) of the 20% (w/w) gels was 4- to 10-fold higher than for the 10% (w/w) gels (Table 5-4, Figure 5-7b), which was expected due to the more coarsely aggregated protein network formed by these samples (Figure 5-5b) containing greater protein and solids content. The higher final gel strength likely arises from a greater number of protein cross-links and greater extent of macromolecule entanglement, which reinforce the gel network (Sun and Arntfield, 2010; Felix et al., 2021; Quintero et al., 2022). This increase in interactions between proteins was evidenced in the reduced soluble protein content of all samples at 20% (w/w) concentration (Figure 5-1b). Previously, an increase in QPI concentration from 10% (w/w) to 15% (w/w) gave a ~7-fold increase in final gel strength for heat-induced gels formed at pH 7.0 without salt addition (Kaspchak et al., 2017); these 15% (w/w) gels were also reported to be more self-supporting than 10% (w/w) QPI gels. Quinoa flour gels also became ~4-fold stronger, as the flour concentration increased from 15% to 30% (w/w) (Felix et al., 2021). The same trend was observed for heat-induced pea protein isolate (PPI) gels at a concentration range of 4 – 18% (w/w), where the final gel strength increased with PPI concentration following a power law relationship (Sun and Arntfield, 2010).

While both acetic acid and citric acid are reported to be kosmotropic acids, with some studies even describing acetate as being more kosmotropic than citrate (Ries-Kautt and Ducruix, 1989; Okur et al., 2017), QPI-C showed a significantly higher ($p < 0.05$) final gel strength than both QPI-H and QPI-A at 20% (w/w) concentration. This effect can be explained in terms of the difference in the kosmotropic capacity of the acids and their influence on protein solubility. Kosmotropic anions are highly hydrated and do not interact strongly with the protein backbone when in solution, consequently promoting salting out of the protein, i.e., protein precipitation with reduced structural unfolding.

Polyprotic acids, such as citric acid, have greater kosmotropic capacity than monoprotic acids, such as acetic acid and HCl, as the dissociation products from these acids also act as kosmotropes contributing further to the salting out effect and further preventing protein unfolding during extraction (Hofmeister, 1888; Kunz, Henle and Ninham, 2004). At 10% (w/w) concentration, the protein content within the samples was not sufficiently high for any difference between the kosmotropic effects of acetic acid and citric acid to be observed. As a result, the solubility and final gel strengths of 10% (w/w) QPI-A and QPI-C were not significantly different ($p > 0.05$, Figure 5-1b and Table 5-4). As the solids concentration was increased to 20% (w/w), this difference in kosmotropic capacity became more evident due to an increase in protein concentration in the samples and QPI-C showed significantly higher ($p < 0.05$) solubility and final gel strength than QPI-A. A correlation also existed between solubility, which is considered an indirect measure of native protein content, with final gel strength ($R^2 = 0.73$), as observed for 10% (w/w) QPI samples (Appendix B – Figure B.4).

Frequency sweeps (0.1 – 100 rad/s) at 1% strain were performed on all QPI gels following the time sweep at 20 °C. All samples displayed a gel-like behaviour (Appendix B – Figure B.5) and showed similar and low frequency dependency (n = 0.1 – 0.2, Table 5-4), regardless of concentration and extraction acid.

Finally, amplitude sweeps (0.1 – 1000%) at 10 rad/s were carried out (Appendix B – Figure B.6). All samples displayed a linear viscoelastic (LVE) region at the lower strain range applied. However, there were differences among the samples and between the two concentrations. For 10% (w/w) gels, the LVE region was slightly less extended for QPI-H compared to QPI-A and QPI-C. At the same time, the yield stress (τ_y, Table 5-4) for QPI-A and QPI-C gels was statistically significantly higher than for QPI-H, consistent

with the contribution of the kosmotropic acids to the formation of stronger QPI gel structures. In case of the 20% (w/w) gels, the LVE region was shorter than for the 10% (w/w) gels and shortest for QPI-C, but comparable for QPI-H and QPI-A. However, the τ_y values of these samples were not statistically significantly different (Table 5-4) and indicate a similar microstructure breakpoint.

5.3.9 Water holding capacity of the QPI gels

The water holding capacity (WHC) of QPI gels at both concentrations was determined to assess whether this property may explain observed differences in gel strength and gelation, especially for the 20% (w/w) gels (Figure 5-8). The WHC is a measure of the ability of a gel to retain water against gravity and is related to functional properties of the gelling polymer, such as swelling, solubility and syneresis (Zayas, 1997).

The WHC capacity of the 10% (w/w) QPI-A and QPI-C gels was significantly greater than for 10% (w/w) QPI-H gel (Figure 5-8), consistent with the final gel strength of these samples (Table 5-4). On the other hand, the WHC of the 20% (w/w) gels was not significantly different among the samples. In fact, except for the 10% (w/w) QPI-H gel, all other samples showed equal ($p > 0.05$) WHC values of > 91%, independent of QPI concentration. This result, bearing in mind the τ_y values (Table 5-4), the gel microstructures (Figure 5-5) and the secondary protein structure results (Table 5-3), strengthens the hypothesis that the 20% (w/w) gels had similar structural properties, in spite of the statistically higher final gel strength displayed by QPI-C.

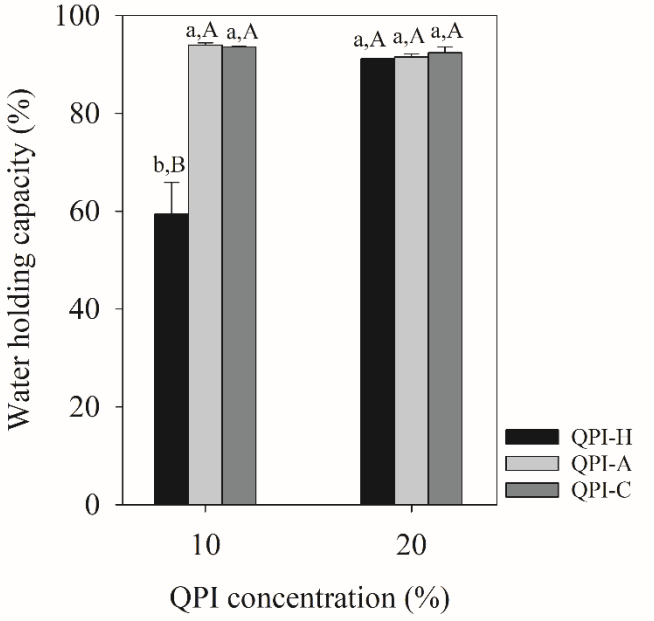

Figure 5-8. Water holding capacity of 10% (w/w) and 20% (w/w) QPI gels. Equal lowercase letters and equal uppercase letters indicate that there is no significant difference among the means at a same concentration and at both concentrations, respectively (Tukey's test, $p > 0.05$).

5.3.10 Principal components analysis

Principal components analysis (PCA) was applied to the dataset to visualise the correlation between the properties and the QPI samples at both concentrations. The two principal components (PCs) accounted for 77.4% of the total variation of the dataset (Figure 5-9). The length of the auto vectors indicates the contribution of each property to the variance explained by each PC, where the angle between the vectors shows the correlation between the properties. An angle of ≥ 90° suggests no correlation between the properties; while angles of < 90° indicate a positive correlation and angles around 180° indicate a negative correlation (Gower, Lubbe and le Roux, 2011).

Four groups of strongly positively correlated properties could be identified within the PCA graph (Figure 5-9). These were: (i) gelation temperature (T_{gel}), denaturation

temperature (T_d) and soluble protein content at pH 7 (top left quarter), (ii) protein content and denaturation enthalpy (ΔH) (top right quarter), (iii) G' and G" (bottom right quarter) and (vi) WHC and yield stress (close to the PC1 axis).

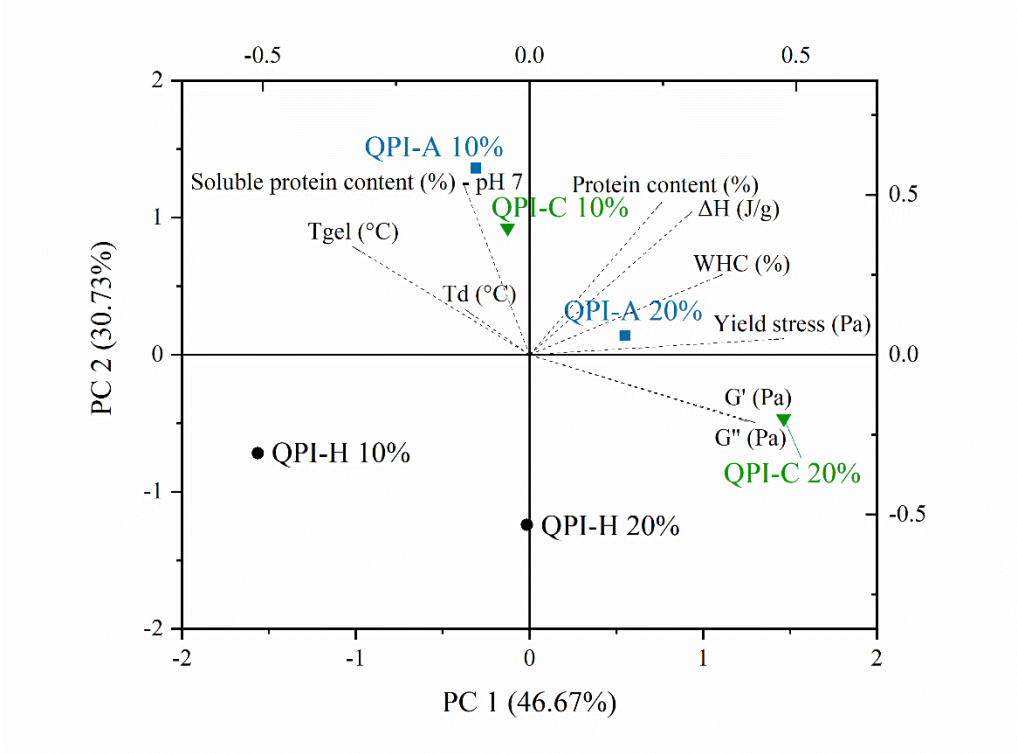

Figure 5-9. Principal components analysis of the total protein and soluble protein contents, thermal properties, gelation properties and WHC data.

In addition to the four groups of properties, the sample treatments are also grouped in the PCA graph according to their similarity. Results for QPI-A and QPI-C at 10% (w/w) concentration were similar, due to the significantly higher soluble protein content, denaturation temperature, as well as higher final gel strength in comparison to QPI-H. In contrast, the 20% (w/w) samples varied in soluble protein content (Figure 5-1b and Table B.2), while the final gel strength of QPI-C was statistically higher than that of QPI-H and QPI-A at this concentration (G'_{20}, Table 5-4). Thus the 20% (w/w) samples appear as spaced apart on the PCA graph.

5.4. Conclusions

A microstructure model is proposed (Figure 5-10) to explain the role of the choice of precipitation acid on the functional properties of quinoa protein isolate (QPI) at both concentrations studied. As the Cl^- ion is more weakly hydrated, it becomes attracted to the protein backbone when in solution, leading to a higher extent of protein unfolding than acetic acid and citric acid, which instead are excluded from the protein backbone, preventing unfolding (Okur et al., 2017). Precipitation with HCl (QPI-H) therefore resulted in a higher initial unfolded protein content, i.e., lower soluble protein content and denaturation enthalpy, and more extensive protein-protein interactions than precipitation with acetic acid (QPI-A) and citric acid (QPI-C). Upon dispersion in water at 10% (w/w) concentration and heat-induced gelation, native proteins in the quinoa protein isolate samples denatured and triggered gel formation, which, in the case of QPI-H, was hindered by the initial aggregation in the sample, resulting in weaker gels than QPI-A and QPI-C at 10% (w/w) protein concentration (Figure 5-10).

At the higher QPI concentration of 20% (w/w), a fraction of the native protein present in the suspensions was likely involved in self-assembly, as evidenced by the lower soluble protein content at this concentration. Upon heat-induced gelation, the native self-assembled proteins participated in network formation along with the soluble protein, reinforcing the gel structure. Ultimately, QPI-C showed a higher final gel strength than QPI-A and QPI-H, probably due to its higher soluble protein content at these higher concentrations.

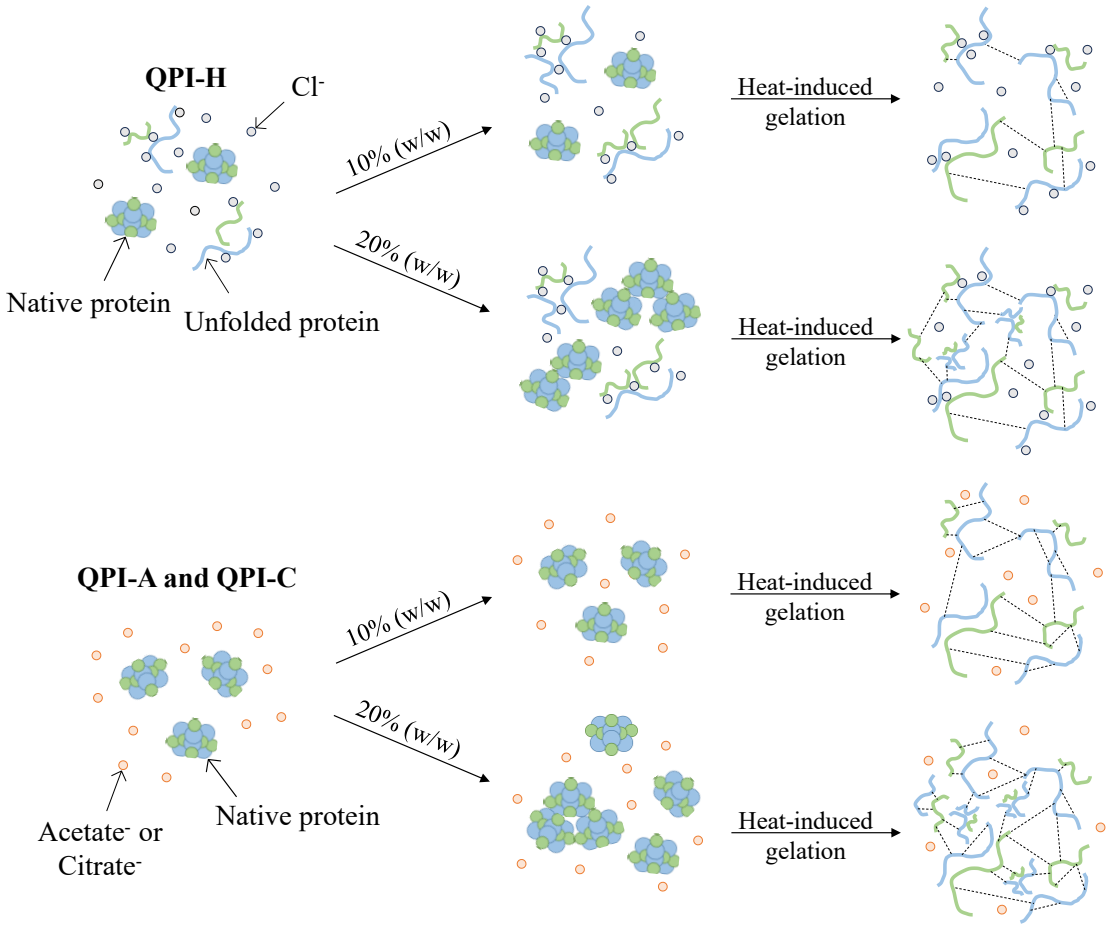

Figure 5-10. The role of the different ions from the choice of precipitation acid, HCl (QPI-H), acetic acid (QPI-A) or citric acid (QPI-C) on the structure of extracted QPI proteins and during heat-induced gelation at 10% (w/w) and 20% (w/w) concentration. Green and blue structures represent the acidic and the basic chains of globulin 11S, respectively.

This study shows for the first time that the physico-chemical and technofunctional properties of quinoa protein isolate can be modulated by the choice of precipitation acid. This approach enables the control of protein structure even in the absence of a flour defatting step and offers an opportunity to expand the application range of these protein isolates. Further, this approach is expected to be applicable to other plant protein isolates, aiding in the design of novel vegan or vegetarian products with tuneable properties.

Chapter 6. Modulation of physico-chemical and technofunctional properties of quinoa protein isolate: Effect of dispersion conditions on isolates precipitated with different acids

Unpublished material not submitted for publication at the time of submission of this thesis.

Author contribution statement:

Marina Campos Assumpcao de Amarante: Conceptualisation, Formal analysis, Investigation, Methodology, Software, Validation, Visualisation, Writing - original draft, Writing - review & editing. **Lydia Ong**: Supervision, Writing - review & editing. **Fotis Spyropoulos**: Supervision, Writing - review & editing. **Sally Gras**: Conceptualisation, Funding acquisition, Project administration, Resources, Supervision, Writing - review & editing. **Bettina Wolf**: Conceptualisation, Funding acquisition, Project administration, Resources, Supervision, Writing - review & editing.

Acknowledgements: The authors would like to thank the Priestley Joint PhD Scholarship from the University of Birmingham (UK) and The University of Melbourne (Australia). This work was performed in part (FTIR measurements) at the Materials Characterisation and Fabrication Platform (MCFP) at the University of Melbourne and the Victorian Node of the Australian National Fabrication Facility (ANFF). The authors also thank the Biological Optical Microscopy Platform (BOMP) at The Bio21 Molecular Science and Biotechnology Institute at The University of Melbourne for access to equipment, as well as the School of Chemistry of the University of Birmingham for the total nitrogen content

analyses. Lydia Ong and Sally Gras are both supported by the Australian Research Council Centre of Excellence in Plants for Space, grant number CE230100015.

Abstract

This study was designed to assess whether the functionality of quinoa protein isolate (QPI) precipitated with acetic acid (QPI-A), citric acid (QPI-C) or HCl (QPI-H) could be further improved or modulated through choice of dispersion conditions. The soluble protein content, protein profile, secondary structure, thermal properties, gelation behaviour and microstructure of the isolates were evaluated. Dispersing in water for 24 h promoted the solubilisation of QPI-H and improved gel strength. Dispersion in 0.1 M NaCl for 1 h resulted in extensive protein aggregation and hindered gel formation in QPI-A and QPI-C. Dialysis before dispersion impaired the gelation properties for all three types of isolates. The demonstrated ability to improve or modulate the functional properties of QPI not only by choice of precipitation acid but also by dispersion conditions provides a handle for product formulators to broaden the application spectrum for QPI across a range of food textures.

Keywords: plant protein; gelation; thermal properties; acid precipitation; kosmotropes; functionality.

6.1 Introduction

Plant proteins are regarded as attractive alternatives to animal proteins in healthier and more sustainable diets. Compared to animal proteins, plant protein production is cheaper (Asgar et al., 2010), requires a fraction of the water and land space (Mattice and Marangoni, 2019) and emits lower levels of greenhouse gases (Scarborough et al., 2014). The lower functionality of plant proteins compared to animal proteins, however, can impose challenges in the design of high quality plant-based foods (McClements and Grossmann, 2021; Day, Cakebread and Loveday, 2022).

Newly emerging plant proteins may provide attractive properties for food formulation and design, such as greater solubility, as well as improved heat-set gelation and thermal properties. While soy has been extensively explored as a plant protein source (Grabowska et al., 2016; Chiang et al., 2019; Chantanuson et al., 2022), it still presents a few limitations, such as a beany flavour and the presence of antinutritional compounds that may lead to allergenicity (Martínez-Villaluenga et al., 2008). Pea protein recently emerged as an interesting plant protein source, mainly because it has a similar protein profile to soy and shows low allergenicity (Lam et al., 2018; Liu et al., 2022). However, there is a need for diversification of plant protein sources, as less conventional plant species might be key to ensure worldwide food security in the near future (Granado-Rodríguez et al., 2022; Bogueva and McClements, 2023; Chaudhary, Walia and Kumar, 2023).

Quinoa (*Chenopodium quinoa* Willd.) is a pseudocereal cultivated in several regions across the world but mainly in the Andes mountains region of South America (Murphy et al., 2019). Quinoa seeds contain 13 – 14% (w/w) protein (Elsohaimy, Refaay and Zaytoun, 2015; Alonso-Miravalles and O'Mahony, 2018), which is of high quality due to

its complete essential amino acid composition, meeting the recommended daily amino acid intake for adults (WHO/FAO/UNU, 2007; Vilcacundo and Hernández-Ledesma, 2017). A better understanding of quinoa protein and the application of this ingredient in protein-rich foods is therefore of broad scientific and commercial interest.

Quinoa protein isolate (QPI) is usually extracted from quinoa flour by wet fractionation, consisting of alkalinisation at pH 8 – 11, followed by acid precipitation at pH 4 – 5 with hydrochloric acid (HCl) (Abugoch et al., 2008; Nongonierma et al., 2015; Ruiz et al., 2016b; Toapanta et al., 2016; Mir, Riar and Singh, 2019a). This method typically leads to a purity of > 70% (w/w) of good quality protein (Ruiz et al., 2016b; Steffolani et al., 2016; Mir, Riar and Singh, 2019a) and it is well established at commercial scale (Sim et al., 2021), although there is still room for optimisation of these processes through a better understanding of the effect of process parameters and their impact on protein yield and quality.

While it is well reported that the physico-chemical and technofunctional properties of QPI are affected by the pH of the alkalinisation step (Abugoch et al., 2008; Ruiz et al., 2016b; Mir, Riar and Singh, 2019a), the results reported in Chapter 5 show that these properties are also affected by the acid used during the precipitation step. In this previous study, QPI was extracted by alkalinisation at pH 9, followed by precipitation with the commonly used HCl as well as acetic acid and citric acid, which are more kosmotropic than HCl. Kosmotropic anions are strongly hydrated ions that become excluded from the protein backbone when in solution, promoting the precipitation of proteins while suppressing unfolding. Whereas chaotropic anions are weakly hydrated and become attracted to the protein backbone when in solution, promoting structure destabilisation and unfolding (Okur et al., 2017). Cl^- generally represents the dividing line between the

kosmotropic and chaotropic behaviours (Kumar and Venkatesu, 2014). In Chapter 5, each protein isolate, i.e., QPI precipitated with HCl (QPI-H), with acetic acid (QPI-A) or with citric acid (QPI-C), was dispersed by agitating in water for 1 h at 22 °C. It was demonstrated that acetic acid and citric acid protected the native protein structure, resulting in a > 60% increase in soluble protein content at pH 7 and ~50% increase in denaturation enthalpy compared to precipitation with HCl. During heat-induced gelation, gels formed from 10% (w/w) QPI-H showed a lower final gel strength (128.5 ± 14.6 Pa) and a more open gel network than 10% (w/w) QPI-A and QPI-C gels (gel strengths of 278.7 ± 34.2 Pa and 330.9 ± 52.7 Pa, respectively).

The conditions used to disperse protein isolates have previously been found to impact their functional properties. It was recently reported that dispersion of pea protein isolate overnight (~16 h) resulted in an increase of ~20% in protein solubility compared to dispersion for 40 min, which improved the performance of these protein isolates across a range of potential applications (Chen, Hall and Moraru, 2023). Further, dispersion overnight or for 24 h has been used to promote complete dispersion of whey, pea and quinoa protein isolates, although the solubility of the isolates before dispersion for this longer time is rarely reported (de Vries et al., 2017; Qin et al., 2018; Lan et al., 2020b, 2020a; He et al., 2022; Luo et al., 2022b; Tanger et al., 2022).

The study of the effect of salt during dispersion is also relevant, as zero salt conditions are unlikely to occur in industry as part of food formulation strategies (Dickinson, 2014). NaCl addition up to a concentration of 0.5 M has been shown to increase the denaturation enthalpy of soy and pea protein isolates at pH 5.6 – 8.0 by 1.1 to 1.4-fold (Damodaran, 1988; Sun and Arntfield, 2010, 2011, 2012); however, there is no consensus in the literature regarding the effect of NaCl on the heat-induced gelation properties of these

proteins at pH 7.0 (Sun and Arntfield, 2010, 2011, 2012; Tanger et al., 2022). There is little information on the effect of NaCl on the functional properties of QPI, although one study has shown that increasing NaCl concentration from 0 M to 0.2 M at pH 7.0 decreased solubility and promoted protein aggregation during heating due to charge screening and reduction of electrostatic repulsion between the protein molecules. Consequently, final gels were stronger but of more heterogenous microstructure (Yang et al., 2022b). Here, the aim was to better understand the effect of NaCl dispersion on the functional properties of QPI precipitated with acetic acid and citric acid.

Building on the knowledge reported in Chapter 5, the effect of dispersion conditions on the physico-chemical and technofunctional properties of QPI-H, QPI-A and QPI-C was examined. It was hypothesised that these conditions can be used to further improve or modulate the functional properties of QPI. Dispersion in water for 24 h was expected to improve the soluble protein content of all three QPI extracts and positively impact on thermal properties and heat-induced gelation properties. Dispersion in 0.1 M NaCl solution was expected to enhance protein aggregation during heat-induced gelation thus resulting in a stronger gel, especially for QPI-H as it was the most denatured QPI of the three isolates. Furthermore, a dialysis step prior to freeze-drying of the extracts precipitated with the three different acids was applied to test the hypothesis that the effect of the different precipitation acids on protein structure would not persist after the removal of the associated ions.

6.2 Materials and methods

6.2.1 Materials

Quinoa flour from white quinoa seeds was purchased from The British Quinoa Company® (Ellesmere, UK). The white quinoa seeds were grown on Shropshire farm (Ellesmere, UK), harvested in 2015, cleaned, selected, sorted and stored in 2016 – 2017. The seeds were then flaked and milled into flour in the first trimester of 2019. According to the manufacturer, the flour contained 14.3% (w/w) protein, 65.7% (w/w) carbohydrate (of which 2.6% (w/w) were sugars), 6.8% (w/w) lipid and 6.8% (w/w) fibre. NaOH pellets (≥ 97%), NaCl (≥ 99.5%) and Spectrum Spectra/Por 1 RC dialysis membranes (6 – 8 kDa molecular weight cut-off) were purchased from Fisher Scientific® (UK). HCl (≥ 32%) and acetic acid (≥ 99.8%) were purchased from Honeywell® (UK). Citric acid (≥ 99.5%), dimethyl sulfoxide, Nile Red, Fast green FCF and low viscosity mineral oil were purchased from Sigma-Aldrich® (UK). A bicinchoninic acid (BCA) assay kit was purchased from G-Biosciences® (USA). All electrophoresis materials were acquired from Bio-Rad Laboratories® (USA). Double distilled water with a resistivity of 15.0 MΩ.cm (Millipore®, UK) was used throughout.

6.2.2 Quinoa protein isolate extraction and characterisation

6.2.2.1 Extraction and precipitation with different acids

Quinoa protein isolate (QPI) was extracted from quinoa flour as described previously following the method developed by Ruiz et al. (2016b) with modifications in centrifugal speed and the acid precipitation step (Chapter 5, Section 5.2.2.1). Briefly, quinoa flour was sieved through a 250 μm aperture sieve and then suspended in water (10%, w/w),

followed by pH adjustment to 9.0 using 1 M NaOH. Flour suspensions were agitated for 4 h at 22 °C, then stored for 16 h at 4 °C. After centrifugation for 30 min at 3220 × g and 10 °C, three layers were formed: a top layer of creamed lipid droplets, a middle layer of protein-rich supernatant and a bottom layer of residual flour. The creamed lipid layer was discarded together with the residual flour by filtration of the supernatant with the aid of a cheesecloth. The pH of the supernatant was then adjusted to 4.5 to precipitate the proteins using either 1 M HCl, acetic acid or citric acid. The precipitate was separated by centrifugation as described above, rinsed by re-suspension in water and centrifuged once more. Finally, the precipitate was re-suspended in water, neutralised using 1 M NaOH and either freeze-dried for 72 h (Labogene®, Scanvac Coolsafe, Denmark) or dialysed against water for 72 h, where the water was changed twice a day before freeze-drying (Tanger, Engel and Kulozik, 2020). The freeze-dried isolates were kept at 4 °C until use. The extraction yield was calculated as the weight ratio between freeze-dried QPI and the flour used for extraction (Equation 6-1). The total protein content of the quinoa flour and extracted QPI was determined as total nitrogen content, via elemental analysis (Thermo Flash EA 1112, ThermoFisher Scientific®, UK) and converted to total protein (%) using the conversion factor of 5.85 (Abugoch et al., 2008; Ruiz et al., 2016b). Protein yield was calculated from the extraction yield, considering the total protein content of the QPI and of quinoa flour (Equation 6-2).

$$\text{Extraction yield (\%, w/w)} = \frac{\text{weight of freeze-dried QPI (g)}}{\text{weight of flour used for extraction (g)}} \times 100\% \qquad (6\text{-}1)$$

$$\text{Protein yield (\%, w/w)} = \frac{\text{total protein in QPI (\%)} \times \text{extraction yield (\%)}}{\text{total protein in quinoa flour (\%)}} \quad (6\text{-}2)$$

6.2.2.2 Dispersion conditions

QPI samples were dispersed in either water for 1 h or 24 h or in a solution of 0.1 M NaCl for 1 h at 22 °C using a magnetic stirrer. Dialysed QPI samples were similarly dispersed in water or a solution of 0.1 M NaCl for 1 h at 22 °C using a magnetic stirrer.

6.2.2.3 Determination of soluble protein content

1% (w/w) QPI samples were prepared following the various dispersion protocols, without pH adjustment, as the natural pH of the suspensions was 6.8 ± 0.2. The suspensions were centrifuged for 30 min at 2400 × g and 10 °C. The supernatants were then weighed and their soluble protein concentration determined by the bicinchoninic acid (BCA) method (G-Biosciences®, USA). The absorbance was recorded at 562 nm and the protein concentration determined using a calibration curve constructed using known concentrations of bovine serum albumin. The soluble protein concentration was calculated using Equation 6-3:

$$\text{Soluble protein (\%, w/w)} = \frac{\text{protein concentration in supernatant (mg/mL)} \times \text{volume of supernatant (mL)}}{\text{weight of freeze-dried QPI (mg)}} \times 100\% \quad (6\text{-}3)$$

6.2.3 Physico-chemical and technofunctional properties of QPI extracts

6.2.3.1 Analysis of protein profile

Native- and SDS-PAGE under non-reducing and reducing conditions were performed to acquire the protein profile of the QPI dispersions. Aqueous suspensions of 10 mg/mL QPI-H, QPI-A and QPI-C without pH adjustment (pH 6.8 ± 0.2) were centrifuged for 30 min at 2400 × g and 10 °C and the supernatants used for analysis. The supernatants were mixed (1:1 ratio) with native sample buffer or Laemmli sample buffer with or without 2-mercaptoethanol. For SDS-PAGE, samples mixed with Laemmli buffer were also heated for 5 min at 100 °C. Then, 10 µL of each sample and of protein molecular weight standards (10 – 250 kDa) were loaded into Mini-PROTEAN® 4 – 20% polyacrylamide gels. Electrophoretic runs were performed at a constant voltage of 200 V, with running buffers containing 25 mM Tris, 192 mM glycine and, for SDS-PAGE only, 0.1% SDS at pH 8.3. At the end of the runs, the gels were stained with Coomassie Brilliant Blue for 1 h and destained with destain solution containing 30% (w/w) methanol and 7% (w/w) acetic acid.

6.2.3.2 Differential scanning calorimetry

Differential scanning calorimetry (µDSC3evo run, Setaram Instrumentation®, France) was used to determine the thermal properties of QPI dispersed under the different conditions at a concentration of 10% (w/w). DSC pans were filled with ~0.5 g of QPI dispersion and hermetically sealed, while a pan with a matching mass of water was used as reference. Samples were heated at a rate of 1.2 °C/min from 20 °C to 100 °C, kept at this temperature for 5 min and then cooled at the same rate to 20 °C. The denaturation

temperature (T_d), defined as the temperature where the maximum endothermic transition peak occurred, as well as the denaturation enthalpy (ΔH), defined as the area below the transition peak, were calculated using the equipment software. Enthalpy was then converted to J/g protein using the sample concentration (10%, w/w) and the total protein content of each QPI extract.

6.2.3.3 Confocal laser scanning microscopy

Confocal laser scanning microscopy (CLSM) was used to observe the microstructure of the initial QPI dispersions before gelation and then following heat-induced gelation using a published protocol (Ong et al., 2011). An aliquot of 10 µL of 0.1% Fast Green FCF dye solution (1 mg/mL in MilliQ water) was added to 480 µL of 10% (w/w) QPI dispersion, followed by the addition of 10 µL of 0.1% Nile Red solution (1 mg/mL in dimethyl sulfoxide). For image collection of QPI dispersions before gelation, 50 µL samples of stained dispersions were mixed with 200 µL of 0.5% agarose (prepared at ~100 °C and allowed to cool to ~40 °C). A further sample of 6 – 7 µL of this mixture was then pipetted into a cavity slide and covered with a cover slip. For image collection of heat-induced QPI gels, the stained suspensions were transferred to glass vials and the lids were sealed with parafilm. The glass vials were incubated in a dry block heater and subjected to a temperature profile similar to that applied in the rheometer (see Section 6.2.3.5) except that the heating rate was of 1.2 °C/min, due to instrument limitation. A piece of each gel (~ 5 mm x 5 mm x 2 mm) was then transferred to a microscope slide (ProSciTech, Australia) with a 2 mm thick spacer and covered with a cover slip (ProSciTech, Australia). All images were acquired on a confocal laser scanning microscope (Leica Sp8, Leica Microsystems, Germany) equipped with a 63× oil immersion objective using 638 nm and

488 nm laser excitation for Fast Green FCF and Nile Red, respectively. Imaris 10 Microscopy Image Analysis Software (Oxford Instruments, UK) was used to process the CLSM images. At least three z-stacks of different regions of each sample were taken and analysed. Quantification of the size of oil bodies/droplets in the gels was performed using the surface creation function of Imaris (Ong et al., 2020), where at least 2,300 surfaces were analysed in each image. Unstained areas were assumed to be pores. This area was quantified by subtracting the area occupied by protein and oil bodies/droplets, identified using the surface creation function of the software, from the total area of the image.

6.2.3.4 Fourier transform infrared spectroscopy

Fourier transform infrared spectroscopy (FTIR) spectra of 10% (w/w) QPI gels were obtained with a Lumos II FTIR microscope (Bruker, USA), equipped with an attenuated total reflectance unit. The spectra were recorded at wavelengths 400 – 4000 cm^{-1} with 4 cm^{-1} of resolution. Quantitative analysis of the spectra was carried out by applying the second derivative of the Amide I region (1600 – 1700 cm^{-1}), followed by baseline subtraction and Gaussian deconvolution with the OriginLab® (version 2019) software (OriginLab Corporation, USA). The contribution of each peak to the Amide I region was obtained as the ratio of the individual peak area and the total area of the deconvoluted peaks.

6.2.3.5 Rheological methods

A dynamic shear rheometer (MCR 300 Anton Paar®, Austria) fitted with a smooth parallel plate geometry (50 mm diameter, 1 mm gap) was used to study the gelation properties of

the 10% (w/w) QPI dispersions. During all measurements, low viscosity mineral oil was carefully pipetted around the outer rim of the samples, which were also covered with a solvent trap and the equipment's Peltier hood, to avoid water evaporation.

The gelation properties were assessed by temperature sweeps recording the storage (G') and loss (G'') moduli. Samples were heated from 20 °C to 90 °C at a heating rate of 1 °C/min, held for 5 min at 90 °C, followed by cooling to 20 °C at 1 °C/min, using 1% strain and an angular frequency of 10 rad/s. Without removing the sample from the gap, a time sweep of 5 min at 20 °C was performed using 1% strain and 10 rad/s frequency, followed by a frequency sweep (0.1 – 100 rad/s, 10 points per decade) at 1% strain and an amplitude sweep (0.1 – 1000%, 10 points per decade) at 10 rad/s. The angular frequency (ω) dependence of the G' data was fitted with Equation 6-4.

$$\log\left(G^{'}\right) = n \times \log(\omega) + K \tag{6-4}$$

Where the slope (n) indicates the type of gel network, with values close to zero characterising an elastic network and higher values characterising a viscous network. The intercept (K) indicates the strength of the gel network (Creusot et al., 2011; Tanger et al., 2022). Additionally, the yield stress (τ_y) of the gels was determined from the amplitude sweep data as the maximum value of a plot of elastic stress (G' × strain) vs strain (Yang, Scriven and Macosko, 1986; Walls et al., 2003).

6.2.4 Statistical analyses

All measurements were performed in duplicate and results expressed as mean ± standard deviation (SD). Results were analysed by analysis of variance (ANOVA) followed by

Tukey's post-test to verify significant differences between the means, considering a confidence level of 95% ($p < 0.05$) using the SigmaPlot® (14.5) software (Grafiti LLC, USA).

Principal components analysis (PCA) was applied to the soluble protein content, thermal properties and gelation properties data and used to explore and visualise the correlation between the properties using the OriginLab® (version 2019) software (OriginLab Corporation, USA).

6.3 Results and discussion

6.3.1 Extraction and protein yield

The addition of a dialysis step after acid precipitation was not found to significantly affect the protein yield, which was otherwise similar for samples extracted with each of the three different acids hydrochloric acid (QPI-H), acetic acid (QPI-A) and citric acid (QPI-C) (Table 6-1). However, dialysis did increase the total protein content ($p < 0.05$) of the extracts, due to a slight concentration of the protein as a result of salt removal (Scopes, 1994).

6.3.2 Soluble protein content

Dispersion in either water or 0.1 M NaCl for 1 h led to a lower soluble protein content for QPI-H compared to QPI-A and QPI-C (Figure 6-1, data values reported in Appendix C – Table C.1). This is in agreement with the higher kosmotropic effect of acetic acid and citric acid compared to HCl (Okur et al., 2017), and shows that QPI-H was initially more aggregated than QPI-A and QPI-C. Upon dispersion in water for 24 h, all non-dialysed

samples showed similar soluble protein contents ($p > 0.05$, Figure 6-1), indicating that QPI-H required a longer time for complete dissolution than QPI-A and QPI-C. This is likely a consequence of disassembly of protein aggregates in QPI-H over a longer dispersion time, as previously shown for soy globulins (Chen et al., 2016). Dispersion overnight or for 24 h has been previously used to promote complete dissolution of QPI extracted by the same wet fractionation method used here (using HCl as the precipitation acid), although soluble protein content before and after dispersion were not reported (He et al., 2022; Luo et al., 2022b).

Table 6-1. Extraction yield, total protein content and protein yield of QPI samples precipitated with HCl (QPI-H), acetic acid (QPI-A) or citric acid (QPI-C) without or with dialysis.

		Extraction yield (%, w/w)	Total protein content (%, w/w)	Protein yield (%, w/w)
Non-dialysed	QPI-H	$4.7 \pm 0.5^{a,A}$	$56.2 \pm 0.3^{c,D}$	$17.3 \pm 1.8^{a,A}$
	QPI-A	$4.8 \pm 0.4^{a,A}$	$59.8 \pm 0.3^{a,CD}$	$18.6 \pm 1.4^{a,A}$
	QPI-C	$4.7 \pm 0.1^{a,A}$	$58.3 \pm 0.4^{b,D}$	$18.2 \pm 0.2^{a,A}$
Dialysed	QPI-H	$4.6 \pm 0.8^{a,A}$	$65.7 \pm 0.8^{ab,AB}$	$19.6 \pm 3.5^{a,A}$
	QPI-A	$4.8 \pm 0.7^{a,A}$	$68.7 \pm 0.6^{a,A}$	$21.5 \pm 3.1^{a,A}$
	QPI-C	$5.1 \pm 0.7^{a,A}$	$62.5 \pm 2.0^{b,BC}$	$20.8 \pm 2.7^{a,A}$

Equal lowercase letters in the same column indicate that there is no significant difference between the means of different QPI samples in the same condition, i.e., non-dialysed or dialysed (Tukey's test, $p > 0.05$). Equal uppercase letters in the same column indicate that there is no significant difference between the means of all samples, regardless of condition (Tukey's test, $p > 0.05$).

All dialysed QPI samples dispersed in either water or 0.1 M NaCl for 1 h contained significantly less ($p < 0.05$) soluble protein (12 – 16%, w/w) than the non-dialysed samples (Figure 6-1). The values were lower than literature reports of 45 – 75% (w/w) soluble protein for QPI extracted by wet fractionation followed by 24 h of dialysis

(Steffolani et al., 2016; Wang et al., 2021a). Here, dialysis was progressed for 72 h, suggesting that the removal of stabilising salts was more complete which induced denaturation and the formation insoluble aggregates. While pea protein dialysed for 72 h has been reported to remain stable, this might have been a consequence of the higher salt content of those extracts after extraction with Na_3PO_4 solution containing KCl (Tanger, Engel and Kulozik, 2020).

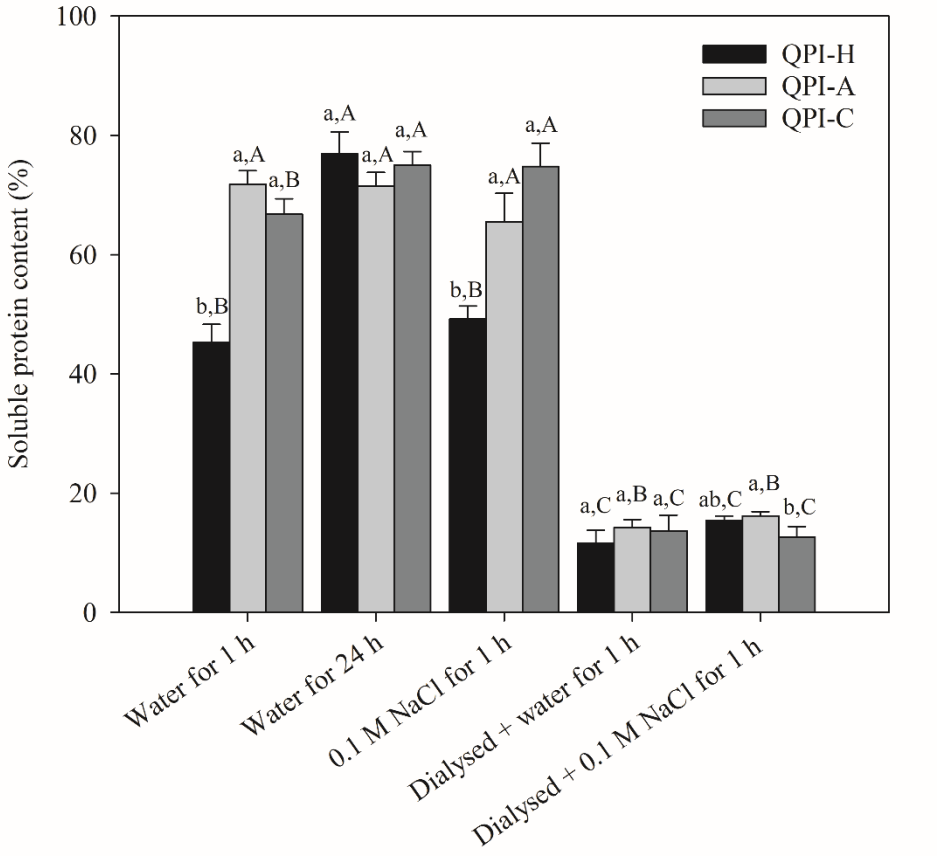

Figure 6-1. Soluble protein content (%, w/w) measured in QPI samples precipitated with HCl (QPI-H), acetic acid (QPI-A) or citric acid (QPI-C) and dispersed under different conditions. Equal lowercase letters for different QPI samples under the same dispersion condition and equal uppercase letters for same QPI sample under different dispersion conditions indicate that there is no significant difference between the means (Tukey's test, $p > 0.05$).

6.3.3 Protein profile

The protein profile of QPI samples under different dispersion conditions was analysed by Native-PAGE and SDS-PAGE under reducing and non-reducing conditions (Figure 6-2). Figure 6-2a shows a schematic of the main proteins in QPI and their relative size. Globulin 11S is composed of subunits of 45 – 55 kDa in size which associate to form hexameric units (300 – 360 kDa) (Brinegar and Goundan, 1993; Mäkinen, Zannini and Arendt, 2015). Each subunit contains an acidic α-chain (30 – 39 kDa) and a basic β-chain (20 – 25 kDa), which are linked by disulfide bonds (Abugoch et al., 2008; Yang et al., 2022b). Albumin 2S is a small globular protein with a molecular weight of around 12 – 15kDa (Brinegar, Sine and Nwokocha, 1996; Shen et al., 2022). Recently, the vicilin-like globulin 7S has also been identified in quinoa seeds (Burrieza et al., 2019; Shen et al., 2022). Literature on the pseudocereal amaranth (*Amaranthus hypochondriacus*) has reported globulin 7S to occur as a tetrameric unit of ~200 kDa, with subunits of 16 kDa, 38 kDa, 52 kDa and 66 kDa in size (Quiroga et al., 2010).

In Native-PAGE, the protein structure remains intact due to the absence of any denaturing and reducing agents. In SDS-PAGE under non-reducing conditions, proteins are expected to dissociate into subunits due to denaturation, while subunits containing chains linked by disulfide bonds are expected to remain intact due to the absence of reducing agents. In contrast, when 2-mercaptoethanol is added to generate reducing conditions in SDS-PAGE, subunits containing chains linked by disulfide bonds are expected to dissociate (Kaspchak et al., 2017).

The protein profile of the QPI samples was not impacted by the precipitation acid, but rather by the dispersion conditions. The protein profiles of all non-dialysed QPI samples dispersed in water for either 1 h or 24 h and all dialysed QPI samples dispersed in either

water or 0.1 M NaCl were highly similar. Thus, for simplicity, Figure 6-2 shows only the non-dialysed and dialysed samples dispersed in water for 1 h (Figures 6-2b and d). The protein profiles of all non-dialysed QPI samples dispersed in 0.1 M NaCl were slightly different from that of samples dispersed in water, and thus are shown in Figure 6-2c. All protein profiles under native, non-reducing and reducing conditions are shown in Appendix C – Figure C.1.

Four bands were identified in Native-PAGE for each non-dialysed sample under the different dispersion conditions (Figures 6-2b-c, Appendix C – Figure C.1a-c), most likely corresponding to the hexameric form of globulin 11S (~360 kDa), the tetrameric form of globulin 7S (~200 kDa) and the subunit of globulin 11S (45 – 55 kDa, 2 bands), as it has been previously reported that globulin 11S can occur as monomers (subunits) under non-denaturing conditions (van de Vondel, Lambrecht and Delcour, 2020; van de Vondel et al., 2021). Only one band was clearly visible in the Native-PAGE of the dialysed samples. This band corresponded to globulin 11S as later confirmed by the SDS-PAGE bands under non-reducing and reducing conditions (Figure 6-2d). Fewer bands were expected in these samples, as the soluble protein was lower (Figure 6-1).

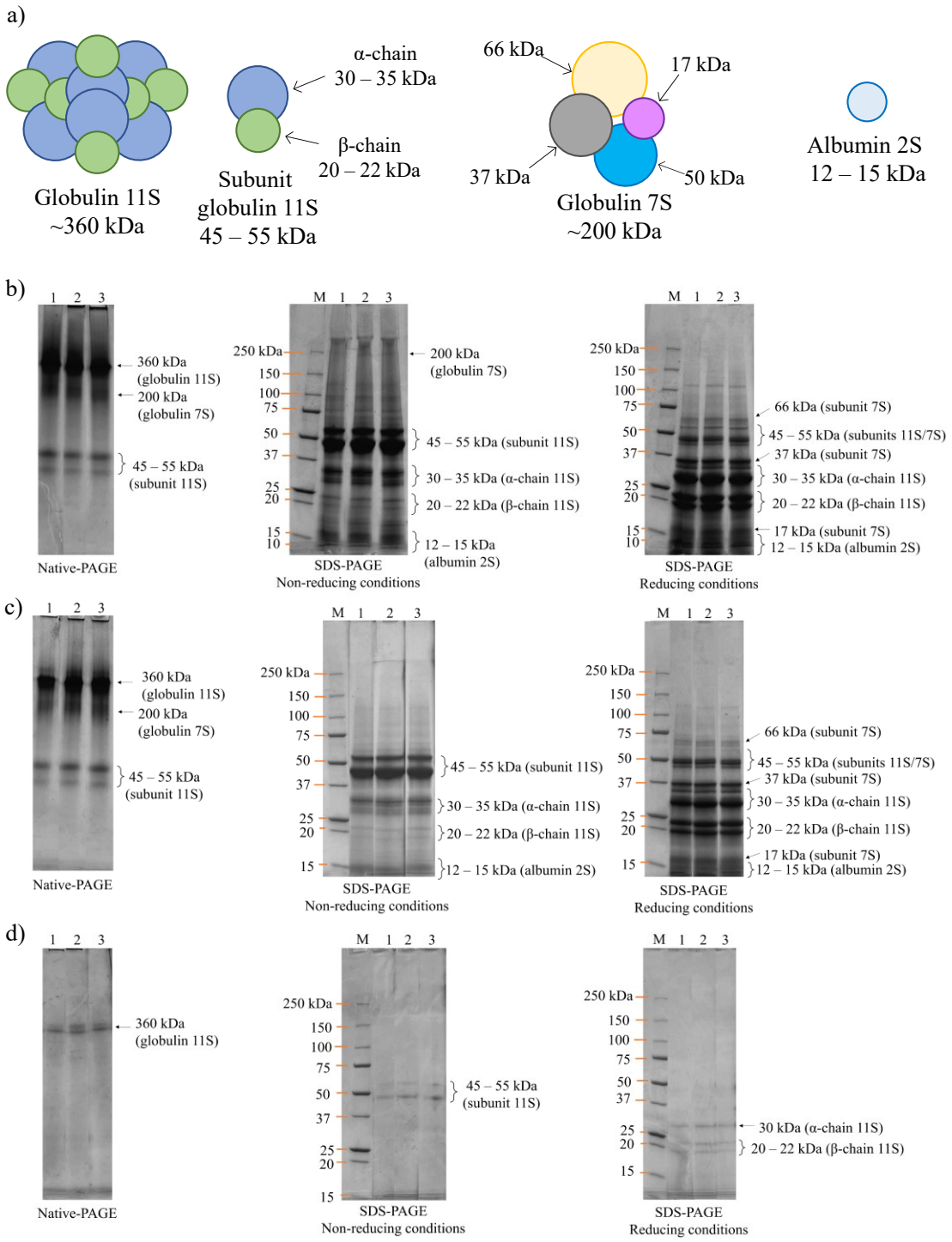

Figure 6-2. Protein profile of QPI samples: a) size schematics of the main proteins in QPI: globulin 11S, globulin 7S and albumin 2S; gel electrophoresis of QPI samples under different dispersion conditions: b) dispersed in water for 1 h; c) dispersed in 0.1 M NaCl for 1 h; d) dialysed and dispersed in water for 1 h. M- protein markers; 1- QPI-H; 2- QPI-A; 3- QPI-C.

In the non-reducing SDS-PAGE of the non-dialysed QPI samples, bands were identified at 12 – 15 kDa corresponding to albumin 2S, at 30 – 35 kDa and 20 – 22 kDa corresponding to the α- and β-chains of globulin 11S, respectively, as well as at 45 – 55 kDa, characteristic of the intact subunit of globulin 11S (Figure 6-2b-c). The bands for the dissociated α- and β-chains are fainter than for the associated subunit as previously reported in literature (Kaspchak et al., 2017; van de Vondel, Lambrecht and Delcour, 2020). For samples dispersed in water for 1 h or 24 h, an additional faint band at 200 kDa was identified corresponding to the tetramer of globulin 7S, which was more noticeable for QPI-A and QPI-C. This band was absent in the samples dispersed in 0.1 M NaCl (Figure 6-2c) but the reducing SDS-PAGE later confirmed that globulin 7S was indeed present under this dispersion condition. The dialysed QPI samples dispersed in water or 0.1 M NaCl solution for 1 h showed only one band corresponding to the subunit of globulin 11S (45 – 55 kDa) under non-reducing conditions (Figure 6-2d), confirming the identification of the band in Native-PAGE. Again, the lack of other bands is consistent with the low solubility of the dialysed samples (Figure 6-1) and it further indicates that in these samples globulin 7S and albumin 2S were completely denatured.

In reducing SDS-PAGE of the non-dialysed samples dispersed in water or NaCl, intense bands corresponding to the α- and β-chains of globulin 11S were identified (30 – 35 kDa and 20 – 22 kDa). Bands corresponding to the assembled subunit (45 – 55 kDa) were also still present but, as expected, at lower intensity compared to non-reducing SDS-PAGE (Figure 6-2b-c). Additionally, the globulin 7S tetramer observed by non-reducing SDS-PAGE at 200 kDa was completely disassembled into subunits of 17 kDa, 37 kDa, 50 kDa and 66 kDa, as previously reported for the pseudocereal amaranth (*Amaranthus* spp.) (Quiroga et al., 2010). These bands confirm that globulin 7S was present in the

samples dispersed in NaCl, despite the band at 200 kDa being absent under non-reducing conditions for these samples. For the dialysed samples, under reducing conditions, only faint bands corresponding to the α- and β-chains of globulin 11S (Figure 6-2d) were identified, consistent with the identification of only globulin 11S under native and non-reducing conditions.

Overall, all non-dialysed samples dispersed in water for 1 h or 24 h and in 0.1 M NaCl showed intense protein bands as expected due to the high soluble protein content in these samples (Figure 6-1). The dialysed samples, however, showed only faint bands corresponding to globulin 11S, indicating that globulin 7S and albumin 2S were completely denatured during dialysis and only a fraction of globulin 11S remained, consistent with the low soluble protein content of these samples.

6.3.4 Thermal properties

According to the results of DSC analysis, all non-dialysed samples had similar thermal properties (Figure 6-3a, Table 6-2). 10% (w/w) QPI suspensions showed a single peak at protein denaturation temperatures (T_d) between 86 °C and 93 °C, within the range reported in literature for globulins from QPI (T_d = 81.6 – 98.0 °C) (Abugoch et al., 2008; Ruiz et al., 2016b; Vera et al., 2019). In contrast, all dialysed samples showed relatively small thermal transitions, with dialysed QPI-H and QPI-C dispersed in water for 1 h not showing any peaks at all (Figure 6-3b and Table 6-2), indicating extensive denaturation prior to the DSC thermal event (Abugoch et al., 2008; Ruiz et al., 2016b; Tanger et al., 2022) as expected from the low soluble protein of these sample.

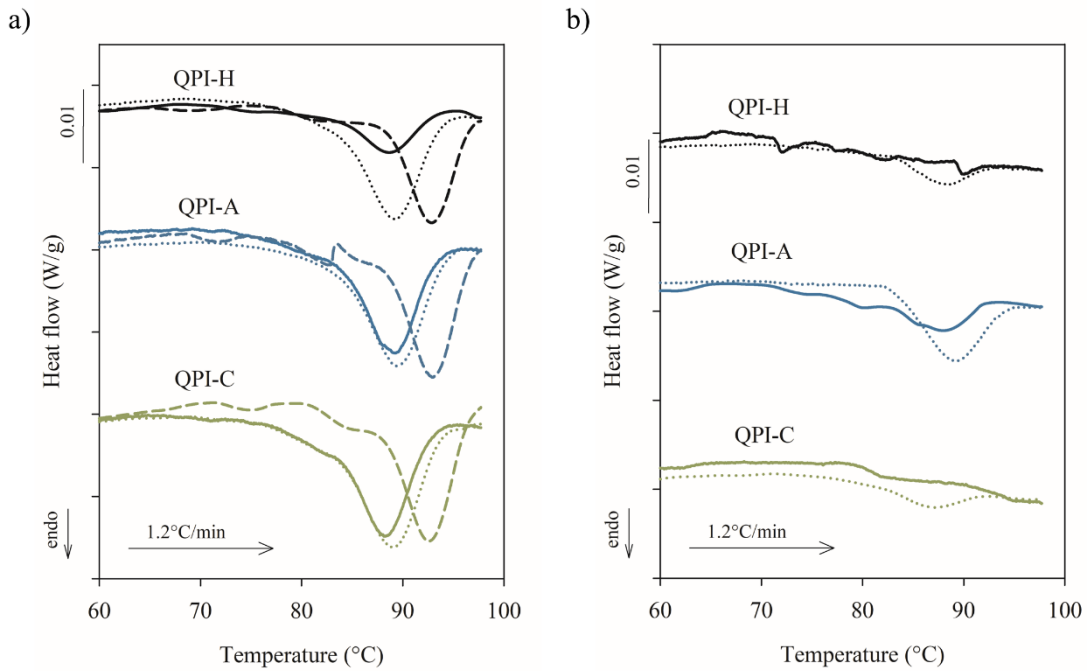

Figure 6-3. DSC thermograms (mean of three measurements) showing the heating of 10% (w/w) QPI samples precipitated with different acids: a) non-dialysed dispersed in water for 1 h (solid), dispersed in water for 24 h (dotted) and dispersed in 0.1 M NaCl for 1 h (dashed); b) dialysed and dispersed in water for 1 h (solid) and dialysed and dispersed in 0.1 M NaCl for 1 h (dotted). Suspensions were heated at a rate of 1.2 °C/min from 20 °C to 100 °C.

The T_d values for non-dialysed samples dispersed in 0.1 M NaCl for 1 h were higher ($p < 0.05$) than for QPI dispersed in water for 1 h or 24 h (Figure 6-3a and Table 6-2). A shift to higher peak denaturation temperatures in the presence of NaCl was also previously reported for pea protein (Sun and Arntfield, 2010, 2012; Tanger et al., 2022) and soy protein (Damodaran, 1988). This effect is a result of the neutralisation of the charged side chains of the proteins in the presence of NaCl, which leads to a reduction of inter- and intrachain repulsion and increase in the stability of the tertiary and quaternary protein structures (Damodaran, 1988).

Table 6-2. Enthalpy (ΔH) and temperature of denaturation (T_d), as well as onset (T_o) and endset (T_e) temperatures of QPI samples precipitated with HCl (QPI-H), acetic acid (QPI-A) or citric acid (QPI-C) and dispersed using a range of different conditions.

	Dispersion conditions	T_o (°C)	T_d (°C)	T_e (°C)	ΔH (J/g protein)
QPI-H	Water 1 h	$83.1 \pm 0.2^{a,B}$	$88.6 \pm 0.1^{b,C}$	$93.0 \pm 0.3^{a,B}$	$3.2 \pm 0.1^{b,AB}$
	Water 24 h	$83.2 \pm 0.1^{a,B}$	$89.1 \pm < 0.1^{a,B}$	$93.2 \pm 0.7^{a,B}$	$4.6 \pm 1.3^{a,A}$
	0.1 M NaCl 1 h	$88.6 \pm 0.5^{a,A}$	$92.8 \pm < 0.1^{a,A}$	$96.5 \pm < 0.1^{a,A}$	$3.7 \pm < 0.1^{b,A}$
	Dialysed + water 1 h	-	-	-	-
	Dialysed + 0.1 M NaCl 1 h	$84.2 \pm 0.7^{a,B}$	$87.9 \pm 0.2^{b,D}$	$90.6 \pm 0.8^{b,C}$	$0.7 \pm < 0.1^{b,B}$
QPI-A	Water 1 h	$83.4 \pm 0.6^{a,B}$	$89.1 \pm 0.1^{a,B}$	$92.5 \pm 0.1^{a,B}$	$4.8 \pm 0.4^{a,A}$
	Water 24 h	$83.1 \pm 0.5^{a,B}$	$89.5 \pm 0.2^{a,B}$	$93.5 \pm 1.0^{a,B}$	$5.2 \pm 0.1^{a,A}$
	0.1 M NaCl 1 h	$87.7 \pm 0.5^{a,A}$	$92.9 \pm 0.1^{a,A}$	$96.5 \pm 0.2^{a,A}$	$5.3 \pm < 0.1^{a,A}$
	Dialysed + water 1 h	82.0 ± 0.5^{B}	87.4 ± 1.4^{B}	91.7 ± 0.2^{B}	1.9 ± 1.1^{B}
	Dialysed + 0.1 M NaCl 1 h	$83.5 \pm 0.6^{ab,B}$	$89.1 \pm 0.2^{a,B}$	$93.3 \pm 0.2^{a,B}$	$2.3 \pm 0.1^{a,B}$
QPI-C	Water 1 h	$82.8 \pm 0.5^{a,B}$	$88.3 \pm 0.1^{b,C}$	$92.4 \pm 0.1^{a,BC}$	$4.9 \pm 0.4^{a,A}$
	Water 24 h	$82.7 \pm 0.2^{a,B}$	$89.0 \pm < 0.1^{a,B}$	$93.6 \pm 0.2^{a,B}$	$5.5 \pm < 0.1^{a,A}$
	0.1 M NaCl 1 h	$87.6 \pm < 0.1^{a,A}$	$92.6 \pm < 0.1^{b,A}$	$96.5 \pm < 0.1^{a,A}$	$5.2 \pm 0.1^{a,A}$
	Dialysed + water 1 h	-	-	-	-
	Dialysed + 0.1 M NaCl 1 h	$81.0 \pm 0.3^{b,C}$	$86.8 \pm 0.1^{c,D}$	$91.4 \pm 0.7^{ab,C}$	$0.6 \pm 0.2^{b,B}$

QPI-H, QPI-A and QPI-C refer to QPI precipitated with HCl, acetic acid and citric acid, respectively. Equal lowercase letters in the same column indicate that there is no significant difference between the means of different QPI samples in the same dispersion condition (Tukey's test, $p > 0.05$). Equal uppercase letters in the same column indicate that there is no significant difference between the means of a same QPI sample in different dispersion conditions (Tukey's test, $p > 0.05$).

Non-dialysed QPI-A and QPI-C dispersed in either water or 0.1 M NaCl for 1 h showed statistically significant higher denaturation enthalpies (ΔH) than QPI-H under the same conditions, while when dispersed in water for 24 h no statistically significant difference in ΔH was observed between the samples (Table 6-2). These results are consistent with

the soluble protein data (Figure 6-1), as QPI-H required a longer dispersion time than QPI-A and QPI-C to produce the same results. Table 6-2 also shows that even though dispersion in 0.1 M NaCl increased the T_d of the QPI samples, the denaturation enthalpies were not significantly different ($p < 0.05$) in relation to dispersion in water for 1 h. As pointed out by Damodaran (1988), it is expected for the denaturation enthalpy to be higher at higher T_d. The tertiary and quaternary conformations of the proteins dispersed in NaCl, however, might not be the same as when dispersed in water, therefore resulting in improved thermal stability (higher T_d) but an unchanged or even smaller ΔH (Damodaran, 1988; Sun and Arntfield, 2012). As for the dialysed QPI dispersed in water or 0.1 M NaCl for 1 h, all samples had substantially lower denaturation enthalpy values than the non-dialysed samples ($p < 0.05$); the absence of an endothermic peak for QPI-H and QPI-C dialysed and dispersed in water for 1 h also prevented the determination of ΔH for these samples (Table 6-2).

6.3.5 Secondary protein structure of QPI under different dispersion conditions

Heat-induced gels of QPI samples showing differences in soluble protein content, protein profile and thermal properties were additionally characterised by FTIR. These samples were all three types of QPI dispersed in water for 1 h and in 0.1 M NaCl for 1 h and dialysed before dispersion in water for 1 h. All FTIR spectra were highly similar regardless of precipitation acid and dispersion conditions (Figure 6-4a). The peak at 3300 cm^{-1} (2960 – 3700 cm^{-1} range) corresponds to free hydroxyl groups (-OH) and the Amide A region, which, together with the Amide B region (small peak at ~2900 cm^{-1}), is associated with C=O and N-H stretching of protein bonds and their interaction with water (Goormaghtigh, Ruysschaert and Raussens, 2006; Mir, Riar and Singh, 2020, 2021b;

Figueroa-González et al., 2022). Small peaks related to the presence of lipids in the sample include the one at ~2850 cm^{-1}, corresponding to the stretching of CH_2 and CH_3 in fatty acids, and the one between 1700 and 1800 cm^{-1}, associated to the C=O stretch of esters or carboxyl groups (Andrade et al., 2019; Figueroa-González et al., 2022). The Amide I region, characterised by the peak at 1600 – 1700 cm^{-1}, is related to the presence of C=O and C-N bonds of proteins, while the Amide II region is identified by the peak at 1500 – 1600 cm^{-1}, characterised by C-N and N-H bonds (Goormaghtigh, Ruysschaert and Raussens, 2006; Mir, Riar and Singh, 2020). Peaks below 1400 cm^{-1} identify the Amide III region which is related to the content of α-helix structures in protein samples (Goormaghtigh, Ruysschaert and Raussens, 2006; Mir, Riar and Singh, 2020).

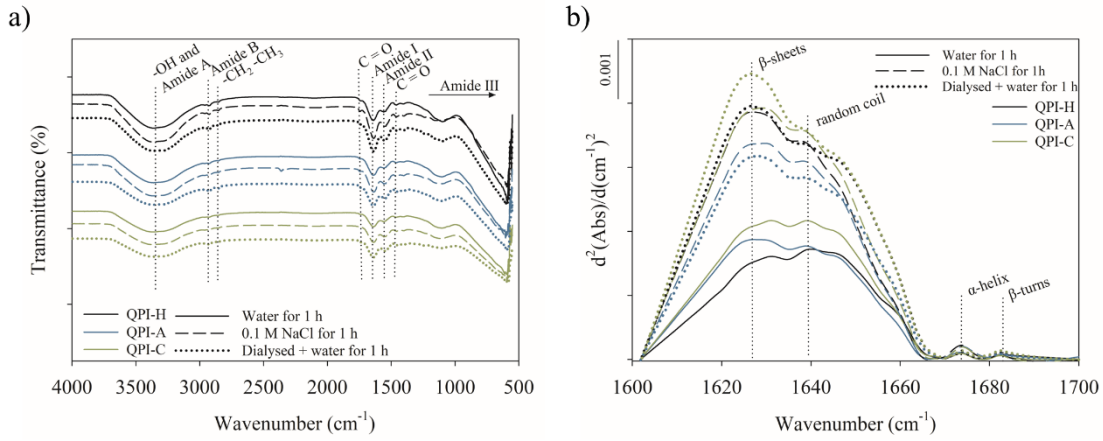

Figure 6-4. Secondary structure of gels of QPI samples under different dispersion conditions (mean of two measurements): a) FTIR spectra; b) second derivative of Amide I region.

Table 6-3. Contribution of the different secondary structure conformation to the overall protein structure of gels of QPI precipitated with HCl (QPI-H), acetic acid (QPI-A) and citric acid (QPI-C) dispersed under different conditions.

Dispersion conditions	Sample	Secondary structure conformation (%)			
		β-sheet	Random coil	α-helix	β-turn
Water for 1 h	QPI-H	45.2 ± 4.1^{a,A}	50.1 ± 2.9^{a,A}	2.7 ± 0.8^{a,A}	2.1 ± 0.3^{a,A}
	QPI-A	50.9 ±< 0.1^{a,A}	44.1 ± 2.0^{a,A}	2.9 ± 0.4^{a,A}	2.1 ± 1.7^{a,A}
	QPI-C	50.2 ± 1.2^{a,A}	46.4 ± 0.6^{a,A}	2.1 ± 1.2^{a,A}	1.3 ± 0.7^{a,A}
0.1 M NaCl for 1 h	QPI-H	50.6 ± 0.3^{a,A}	44.6 ± 0.9^{a,A}	3.3 ±< 0.1^{a,A}	1.4 ± 0.5^{a,A}
	QPI-A	51.3 ± 3.9^{a,A}	43.0 ± 2.1^{a,A}	3.8 ± 1.0^{a,A}	1.8 ± 0.7^{a,A}
	QPI-C	53.5 ± 2.0^{a,A}	42.5 ± 2.3^{a,A}	2.9 ± 0.1^{a,A}	1.1 ± 0.1^{a,A}
Dialysed + water for 1 h	QPI-H	53.0 ± 4.3^{a,A}	43.2 ± 4.1^{a,A}	2.1 ± 0.3^{a,A}	1.6 ±< 0.1^{a,A}
	QPI-A	52.6 ± 1.5^{a,A}	43.6 ± 1.6^{a,A}	2.3 ± 0.2^{a,A}	1.5 ± 0.2^{a,A}
	QPI-C	55.5 ±< 0.1^{a,A}	40.9 ± 0.9^{a,A}	1.9 ± 0.1^{a,A}	1.7 ± 0.8^{a,A}

QPI-H, QPI-A and QPI-C refer to QPI precipitated with HCl, acetic acid and citric acid, respectively. Equal lowercase letters in the same column indicate that there is no significant difference between the means of different QPI samples in the same dispersion condition (Tukey's test, $p > 0.05$). Equal uppercase letters in the same column indicate that there is no significant difference between the means of a same QPI sample in different dispersion conditions (Tukey's test, $p > 0.05$).

The second derivative of the Amide I region in the FTIR spectra was applied to give information on the secondary structure of QPI samples (Figure 6-4b, Table 6-3). β-sheets and random coil structures were the major secondary structure elements contributing to the overall protein structure in all QPI gels under the three different dispersion conditions. This indicates a balance between ordered and disordered conformations in all gel samples under different dispersion conditions (Carbonaro, Maselli and Nucara, 2012; Singh, Siddiqi and Sogi, 2021), likely arising from the unfolding of protein structure and re-organisation for network formation during heat-induced gelation. The gels of non-dialysed QPI dispersed in 0.1 M NaCl or dialysed QPI dispersed in water for 1 h showed slightly higher intensities in the second derivative of the Amide I region compared to QPI dispersed in water for 1 h (note scale of 0.001 $d^2(Abs)/d(cm^{-1})^2$ in Figure 6-4b). However,

there was no obvious shift in peak maxima position among the samples and the structural content of gel samples formed under different dispersion conditions was not significantly different ($p > 0.05$) (Table 6-3), indicating that the change in intensity was probably too small to result in a statistically significant difference in secondary structure after gel formation.

6.3.6 Microstructure of QPI samples before and after gelation

Confocal laser scanning micrographs of all QPI-H, QPI-A and QPI-C suspensions, i.e., before heat-induced gelation, showed clear evidence of suspended protein and lipid droplets (Figure 6-5), stained by Fast Green FCF (green structures) and Nile Red (red structures), respectively. In Chapter 5 (Sections 5.3.1 and 5.3.6), a lipid content of 11.3 – 27.4% (w/w) was found for these samples, present as natural oil bodies of around 0.2 – 0.5 μm in size (Prego, Maldonado and Otegui, 1998) and re-emulsified oil droplets of up to 10 μm in size (Figure 6-5). Regarding the protein, suspensions of non-dialysed QPI dispersed in water for 1 h or 24 h showed a low extent of protein aggregation, while clumping and aggregation of protein was visible in samples that were dispersed in 0.1 M NaCl for 1 h. This observation is congruent with NaCl screening protein surfaces charges (Bryant and McClements, 1998). Extensive aggregation also occurred in suspensions of dialysed samples that were then dispersed in either water or 0.1 M NaCl for 1 h, as expected from the high denaturation of these samples shown by the low soluble protein content and denaturation enthalpy results (Figure 6-1 and Table 6-2).

Dispersion of the QPI samples for 24 h in water resulted in a similar gelled protein network microstructure among the three samples, whereas there were some subtle

differences between the microstructure of the protein network for gels formed from QPI-A and QPI-C compared to QPI-H after dispersion in water for 1 h (Figure 6-5). This observation is consistent with the soluble protein content and thermal properties being more comparable between these samples after the longer period of protein dispersion.

The gels formed after dispersion in 0.1 M NaCl were more aggregated and heterogeneous for all three types of QPI (Figure 6-5). The protein network in these gels was irregular and open, with many void regions. NaCl appeared to have caused protein contraction and therefore a reduction in the ability of QPI proteins to form networks, in agreement with the altered tertiary and quaternary protein conformations indicated by the higher denaturation temperatures in DSC analysis (Figure 6-3 and Table 6-2). Consistent with the observations made here, it has previously been reported that QPI gels formed without salt addition showed a finer and more homogeneous microstructure by CLSM, while an increasingly heterogenous gel microstructure with large aggregates was formed at increasing NaCl concentrations (0.02 M – 0.2 M NaCl) (Yang et al., 2022b).

The removal of stabilising salts during dialysis also affected the microstructure of the gels formed by heat-induced gelation, as the already denatured (Table 6-2) and aggregated structures (Figure 6-1) present in the water and the 0.1 M NaCl dispersions impaired the formation of a continuous gel network (Figure 6-5). Instead, large protein clumps were still observed after the heat treatment and the lipid phase appeared to be loosely associated with these protein structures.

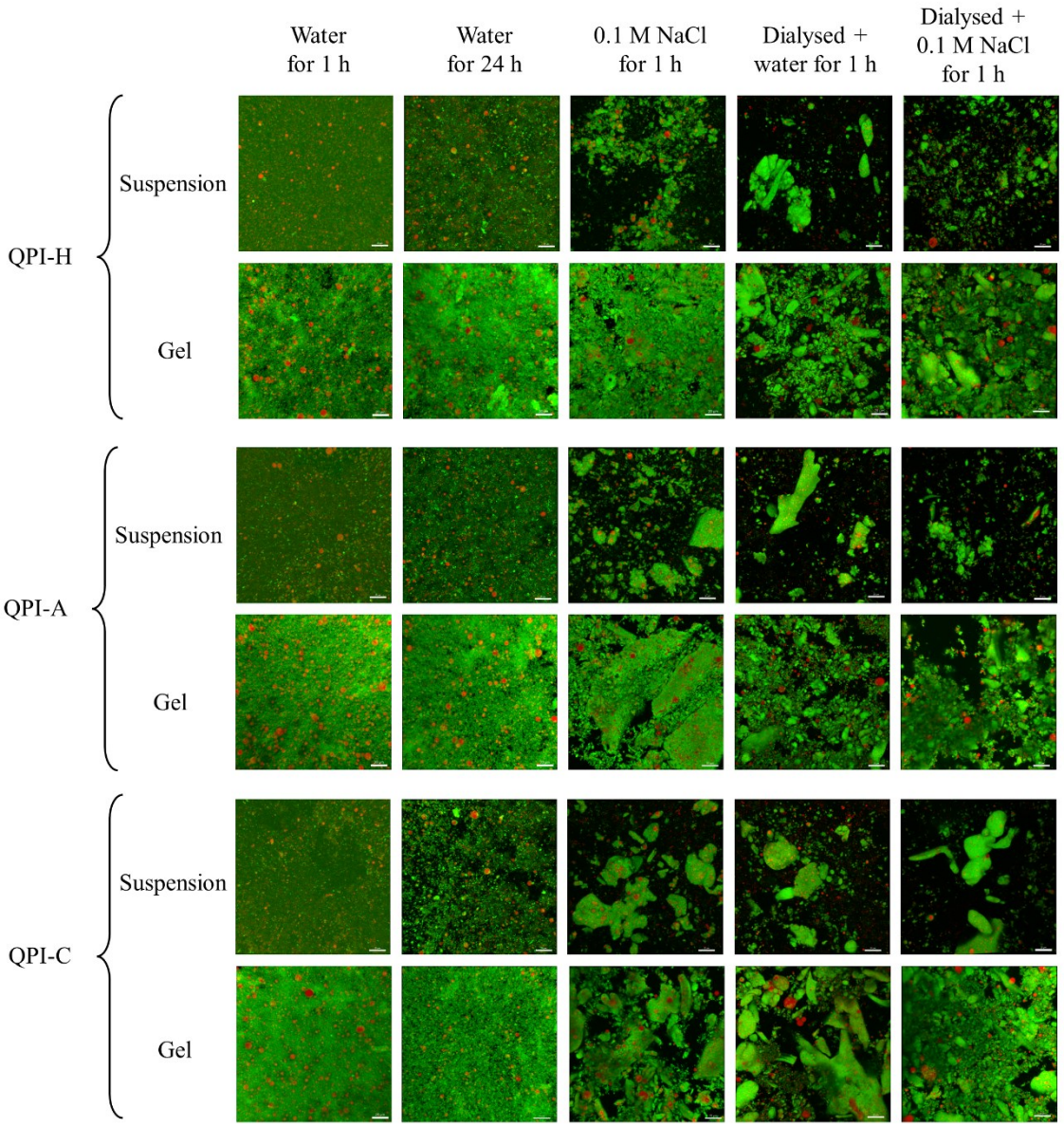

Figure 6-5. Confocal laser scanning microscopy of suspensions and heat-induced gels formed by 10% (w/w) QPI samples precipitated with HCl (QPI-H), acetic acid (QPI-A) or citric acid (QPI-C) and dispersed using different conditions. Protein structures are stained green and lipid droplets are stained red. The scale bars represent 20 µm.

6.3.7 Rheological properties

The heat-induced gelation of 10% (w/w) QPI suspensions was studied by applying temperature sweeps in a shear rheometer (Figure 6-6). Samples were heated from 20 °C to 90 °C at 1 °C/min, held at 90 °C for 5 min and cooled from 90 °C to 20 °C at 1 °C/min,

while recording the storage (G') and loss (G") moduli. Immediately after the temperature sweep, a time sweep (1% strain and 10 rad/s frequency) of 5 min at 20 °C was performed, followed by a frequency sweep (0.1 – 100 rad/s at 1% strain, 10 points per decade) and an amplitude sweep (0.1 – 1000% at 10 rad/s, 10 points per decade) (Appendix C – Figures C.2 – C.4). Table 6-4 shows the gelation temperature (T_{gel}), determined as the temperature of the intercept between a linear extrapolation of the rapidly rising G' (indicated by arrows in Figure 6-6) and the temperature axis (Sun and Arntfield, 2010; Ruiz et al., 2016b), the G' value recorded at the end of the temperature sweep (20 °C, denoted as final gel strength G'_{20}), the slope of the frequency dependence of G' (n) and the yield stress analysed from amplitude sweeps (τ_y).

The gelation behaviours of all samples were as expected based on protein solubility, denaturation enthalpy and gel network microstructure discussed earlier. G' and G" of all dialysed samples did not develop during temperature sweeps (Figure 6-6d-e), whereas the non-dialysed samples showed G' profiles that where characteristic of globular proteins, i.e., G' starts to increase at T_{gel} during heating and continues to increase during cooling due to network reinforcement (Nicolai, 2019). The T_{gel} values of all non-dialysed samples (77 – 85 °C) were comparable with the onset denaturation temperature observed during DSC analysis (T_o, Table 6-2). While the G' values of all non-dialysed samples continued to increase throughout the cooling stage (Figure 6-6a-c), time sweeps at the final temperature (20 °C) showed that both moduli remained constant, finally reaching the end of network formation (Appendix C – Figure C.2).

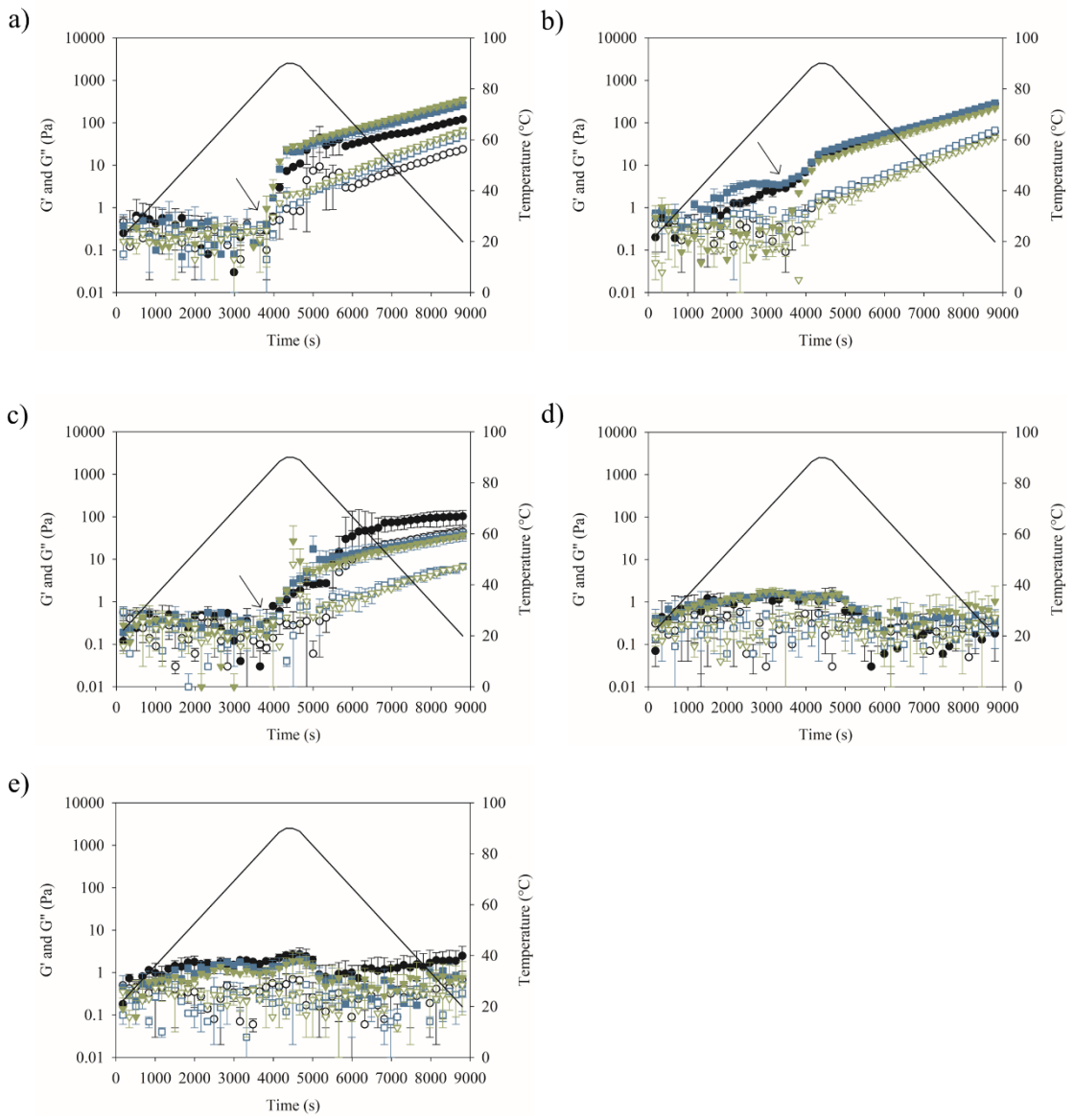

Figure 6-6. Gelation of 10% (w/w) QPI precipitated with HCl (QPI-H, ● black), acetic acid (QPI-A, ■ blue) and citric acid (QPI-C, ▼ green): a) dispersed in water for 1 h; b) dispersed in water for 24 h; c) dispersed in 0.1 M NaCl for 1 h; d) dialysed and dispersed in water for 1 h; e) dialysed and dispersed in 0.1 M NaCl for 1 h. Closed symbols represent the storage modulus (G'), open symbols represent the loss (G") modulus, the solid line represents the temperature profile and arrows indicate the gelation temperature (T_{gel}).

Table 6-4. Gelation temperatures (T_{gel}), final gel strength (G'_{20}), frequency dependency (n) and yield stress (τ_y) obtained for gels produced from 10% (w/w) QPI precipitated with HCl (QPI-H), acetic acid (QPI-A) or citric acid (QPI-C) and dispersed under different conditions.

	Dispersion conditions	T_{gel} (°C)	Storage modulus (G'_{20}, Pa)*	n	τ_y
QPI-H	Water 1 h	$84.0 \pm 1.6^{a,A}$	$120.7 \pm 7.5^{b,B}$	$0.1 \pm < 0.1^{a,B}$	$15.7 \pm 1.7^{b,B}$
	Water 24 h	$81.0 \pm 1.9^{a,A}$	$279.1 \pm 29.9^{a,A}$	$0.1 \pm < 0.1^{a,AB}$	$62.6 \pm 0.8^{a,A}$
	0.1 M NaCl 1 h	$84.8 \pm 0.4^{a,A}$	$102.8 \pm 38.7^{a,B}$	$0.2 \pm < 0.1^{a,A}$	$1.4 \pm 0.8^{a,C}$
	Dialysed + water 1 h	-	$0.3 \pm < 0.1^{a,C}$	-	-
	Dialysed + 0.1 M NaCl 1 h	-	$2.5 \pm 1.6^{a,C}$	-	-
QPI-A	Water 1 h	$82.9 \pm 2.3^{a,A}$	$264.3 \pm 33.2^{a,A}$	$0.1 \pm < 0.1^{a,A}$	$50.7 \pm 5.8^{a,A}$
	Water 24 h	$82.3 \pm 0.8^{a,A}$	$292.5 \pm 48.0^{a,A}$	$0.1 \pm < 0.1^{a,A}$	$51.3 \pm 16.4^{a,A}$
	0.1 M NaCl 1 h	$85.4 \pm 1.9^{a,A}$	$38.6 \pm 11.7^{a,B}$	$0.1 \pm < 0.1^{b,A}$	$2.5 \pm 0.3^{a,B}$
	Dialysed + water 1 h	-	$0.4 \pm 0.3^{a,B}$	-	-
	Dialysed + 0.1 M NaCl 1 h	-	$0.5 \pm 0.3^{a,B}$	-	-
QPI-C	Water 1 h	$81.0 \pm 4.3^{a,A}$	$348.7 \pm 60.4^{a,A}$	$0.1 \pm < 0.1^{a,A}$	$68.0 \pm 11.3^{a,A}$
	Water 24 h	$76.3 \pm 2.3^{a,A}$	$219.2 \pm 5.7^{a,B}$	$0.1 \pm < 0.1^{a,A}$	$54.6 \pm 8.5^{a,A}$
	0.1 M NaCl 1 h	$85.4 \pm 1.2^{a,A}$	$37.1 \pm 4.8^{a,C}$	$0.1 \pm < 0.1^{b,B}$	$3.5 \pm 0.3^{a,B}$
	Dialysed + water 1 h	-	$1.0 \pm 1.3^{a,C}$	-	-
	Dialysed + 0.1 M NaCl 1 h	-	$0.9 \pm 0.8^{a,C}$	-	-

*Final storage modulus at the end of the temperature sweep, when the temperature returned to 20 °C. QPI-H, QPI-A and QPI-C refer to QPI precipitated with HCl, acetic acid and citric acid, respectively. Equal lowercase letters in the same column indicate that there is no significant difference between the means of different QPI samples in the same dispersion condition (Tukey's test, $p > 0.05$). Equal uppercase letters in the same column indicate that there is no significant difference between the means of a same QPI sample in different dispersion conditions (Tukey's test, $p > 0.05$).

When dispersed in water for 1 h, the final gel strength (G'_{20}, Table 3) of non-dialysed QPI-A and QPI-C were statistically higher than that of QPI-H, whereas there was no statistically significant difference ($p > 0.05$) among the samples when dispersed in water for 24 h. There was also no statistically significant difference among the G'_{20} values of the non-dialysed samples dispersed in 0.1 M NaCl for 1 h, despite the soluble protein content and ΔH values of QPI-H being statistically significantly lower than the values recorded for QPI precipitated with the more kosmotropic acids. Further, there was no difference ($p > 0.05$) in the final gel strength of non-dialysed QPI-H dispersed in 0.1 NaCl or water for 1 h; while for QPI-A and QPI-C, G'_{20} was statistically significantly lower when dispersed in 0.1 NaCl than when dispersed in water for 1h (Table 3). These results indicate that NaCl addition did not affect gel network formation of QPI-H, which had lower solubility, but potentially had negative effects on QPI-A and QPI-C gelation, preparations with higher protein solubility. It has been reported that at neutral pH the addition of salt increases the gel strength of heat-induced quinoa protein gels formed by suspensions of low solubility, while it reduced the strength of gels formed by suspensions of high solubility (Kaspchak et al., 2017). Thus, it is possible that the screening of charges by NaCl benefits the formation of a protein network in samples that show higher initial aggregation, such as QPI-H, while it hinders gel network formation of highly soluble samples, such as QPI-A and QPI-C. Future studies should explore the relationship between increasing salt concentration at different pH values on the solubility, thermal properties and gelation capacity of QPI.

As for the dialysed samples, the final gel strength recorded was very low and varied little from the initial G' measured at the start of the temperature sweeps (Figure 6-6d-e, Table 6-4). This result was expected from the microstructures observed, the significantly lower

($p < 0.05$) soluble protein and denaturation enthalpies and the absence of most protein bands shown in the protein profile of these samples. This result confirms the extensive protein denaturation triggered by the removal of all salt molecules from QPI samples and shows the importance of the ions intrinsically present in the samples, originating both from the minerals of the plant matrix and from the addition of base and acid during wet fractionation. The significance of this finding is that ions need to be retained during extraction in order to preserve functionality and unit operations involving dialysis or other forms of ion removal need to be avoided or carefully managed to ensure ion retention or substitution.

Frequency sweeps confirmed gel formation in all non-dialysed samples, where G' and G'' were parallel to each other throughout the frequency range applied with the slope (n) of G' close to zero (Table 6-4, Appendix C – Figure C.3). The frequency sweeps on the dialysed samples returned low values for both moduli, associated with large standard deviations, as would be expected based on the knowledge already established for this sample set.

Finally, amplitude sweeps (Appendix C – Figure C.4) for the non-dialysed samples dispersed in water for either 1 h or 24 h showed linear viscoelastic regions (LVR) at the lower strain range applied and G' and G'' dropped off at similar strain values. As expected though, the yield stress (τ_y, Table 6-4) for QPI-H dispersed in water for 1 h was statistically lower than that of the other non-dialysed samples dispersed in water. When dispersed in 0.1 M NaCl solution, QPI-H gels presented a smaller LVR than QPI-A and QPI-C, although the τ_y did not significantly differ between samples under the same condition. For dialysed samples, LVR or yield stress were not determined, as expected from the lack of gel formation.

6.3.8 Principal components analysis

Principal components analysis (PCA) was applied to the dataset to determine correlations between the properties and the samples dispersed using different conditions. The two principal components (PCs) accounted for 87.2% of the total variation within the dataset, as shown in Figure 6-7. The length of the variable vectors in this Figure correspond to their contribution to the variance explained by each PC, while the angle between the vectors indicates the correlation between properties. Angles smaller than 90° indicate that properties are positively correlated, while angles around 180° indicate that properties are negatively correlated (Gower, Lubbe and le Roux, 2011).

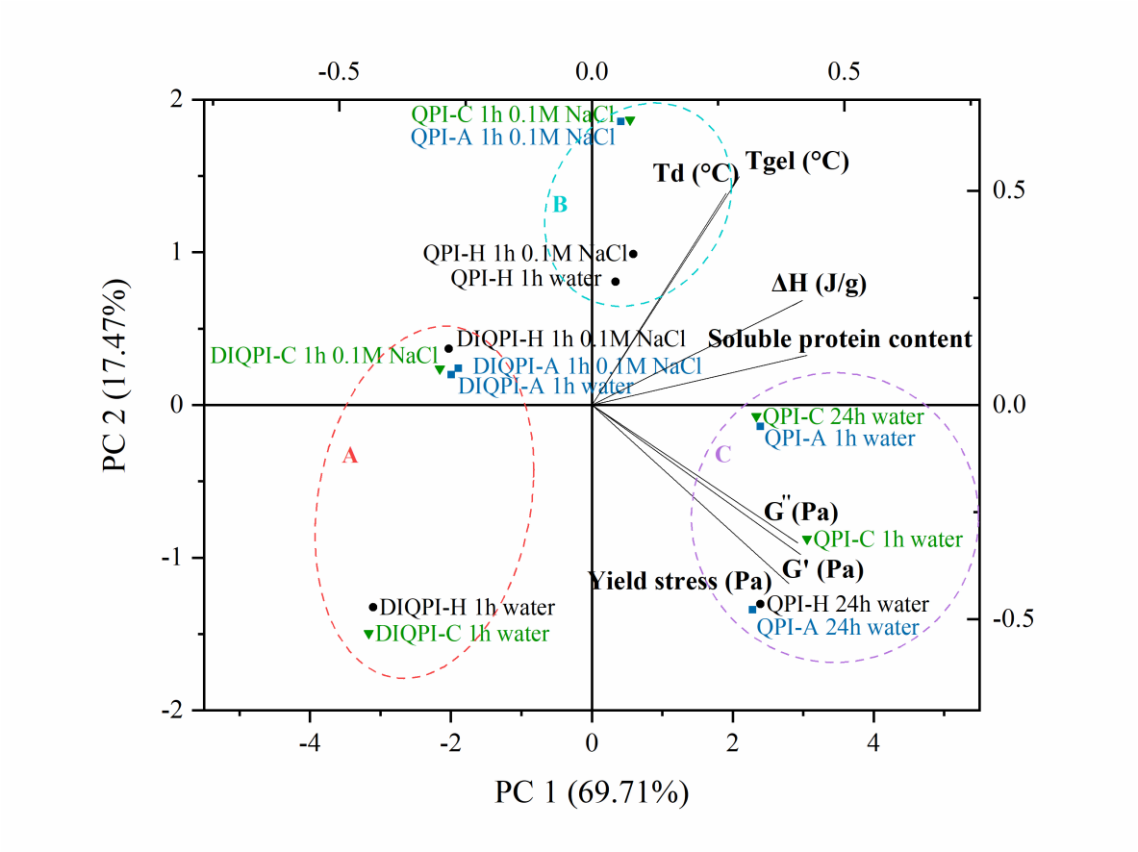

Figure 6-7. Principal components analysis of soluble protein content, thermal properties and gelation properties data.

Three groups of strongly positively correlated properties were recognized, i.e., (i) denaturation temperature (T_d) and gelation temperature (T_{gel}), (ii) denaturation enthalpy (ΔH) and soluble protein content and (iii) G', G" and yield stress. These three groups were expected, based on the results shown so far and the relationship identified between the properties discussed above.

Further, PCA allows for the samples under different dispersion conditions to be organised into clusters, according to their similarity. Three clusters could be identified taking into consideration the position of the samples along PC1, which accounts for 69.7% of the total variation of the dataset and these are marked by coloured ellipses in Figure 6-7. All dialysed samples are organised into cluster A in the negative quadrant of PC1, showing strong negative correlation with the properties analysed, which are all located in the positive quadrant of PC1. All dialysed samples showed low soluble protein content and low denaturation enthalpies and did not demonstrate an ability to form heat-induced gels. All non-dialysed QPI samples dispersed in 0.1 M NaCl, as well as QPI-H dispersed in water for 1 h, are organised into cluster B located near the origin of the PC1 axis. Network formation in QPI-A and QPI-C was negatively affected by dispersion in 0.1 M NaCl, leading to highly aggregated protein structures (Figure 6-5); whereas the final gel strength of QPI-H was similar under dispersion in water or 0.1 M NaCl for 1 h. All the remaining non-dialysed samples dispersed in water for 1 h, or 24 h, are organised in cluster C in the positive quadrant of PC1, showing positive correlation with the properties studied (Figure 6-7). Dispersion in water for 24 h improved the soluble protein content, denaturation enthalpy and gelation properties of QPI-H, increasing its similarity to QPI-A and QPI-C, resulting in stronger heat-induced gels. In general, the different dispersion conditions had pronounced effects on the technofunctional properties of QPI precipitated with the three

different acids, with dispersion in 0.1 M NaCl leading to the formation of protein aggregates and dialysis negatively affecting gelation properties.

6.4 Conclusions

The dispersion conditions applied to quinoa protein isolate (QPI) after precipitation with three different acids, either HCl or the more kosmotropic acids acetic acid and citric acid, were found to impact on protein functional properties. The effects induced by the dispersion conditions differed to those induced by precipitation acid type alone, resulting in a range of different protein structures and heat-induced gel networks. Based on these new results, the microstructure model proposed earlier (Chapter 5, Section 5.4) can be expanded (Figure 6-8). As previously reported, the use of HCl as the precipitation acid during quinoa protein isolate (QPI-H) extraction leads to a higher extent of protein unfolding, because Cl^- is weakly hydrated and becomes attracted to the protein backbone when in solution, promoting structure destabilisation and unfolding (Figure 6-8a). The heat-induced gelation of QPI-H after dispersion in water for 1 h is hindered by the initial aggregation in this sample, resulting in weak gel networks (Figure 6-8a upper images). In contrast, kosmotropic anions such as acetate (QPI-A) and citrate (QPI-C) are strongly hydrated and are excluded from the protein backbone when in solution, stabilising the structure and preventing unfolding. This results in a higher initial native protein content in QPI-A and QPI-C. Stronger gel networks are then formed during the heat-induced gelation of QPI-A or QPI-C dispersed in water for 1 h (Figure 6-8a lower images). Upon dispersion in water for 24 h, the solubility of QPI-H is improved, probably due to disassembly of aggregates over time, which led to improved gel network formation

(Figure 6-8a middle images), while less difference is observed for samples of QPI-A or QPI-C after 24 h of dispersion (Figure 6-8a lower images).

Dispersion in 0.1 M NaCl likely promoted the screening of charges on protein surfaces in all three non-dialysed QPI samples (Figure 6-8b), leading to protein aggregation in the suspensions prior to gelation. Upon heat-induced gelation, native proteins in these samples denatured and triggered gel formation, which in QPI-A and QPI-C was hindered by the initial aggregation in the suspensions, resulting in highly aggregated gel microstructures and low gel strengths.

The removal of all salt molecules during dialysis (Figure 6-8c central image) resulted in a low soluble protein content in all QPI samples, including QPI precipitated with HCl. This suggests that Cl^- still exerted some level of stabilisation to protein structure, although lower than acetate and citrate. Dialysis therefore led to a low native protein content in QPI samples, which was not sufficient to trigger gel network formation upon heat-induced gelation (Figure 6-8c upper and lower images).

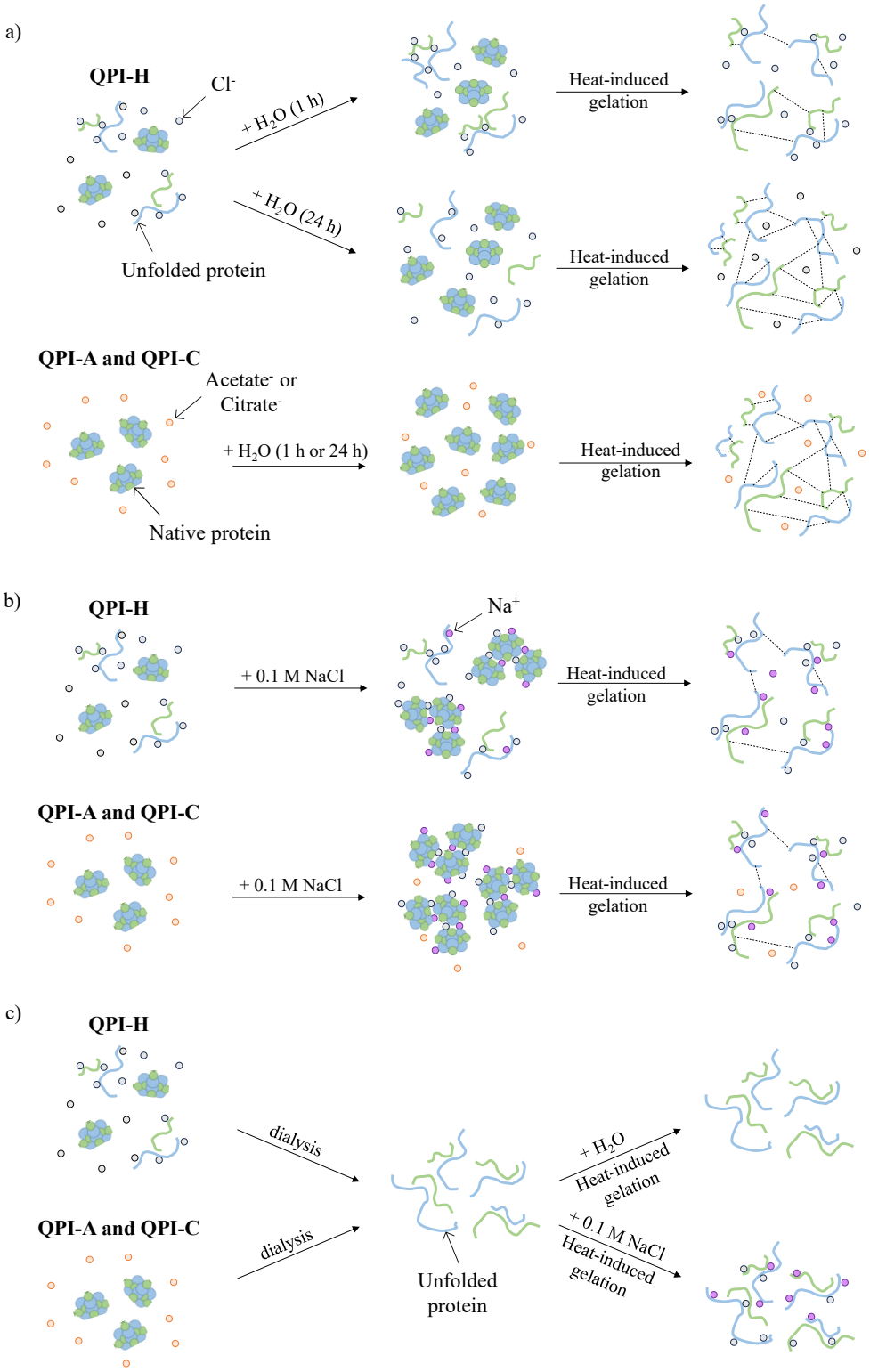

Figure 6-8. Role of different ions on the structure of proteins in QPI precipitated with HCl (QPI-H), acetic acid (QPI-A) and citric acid (QPI-C): a) dispersion in water for 1 h or 24 h; b) dispersion in 0.1 M NaCl for 1 h; and c) dialysis before freeze-drying and dispersion in water or 0.1 M NaCl for 1 h. Green and blue structures represent the acidic and the basic chains of globulin 11S, respectively.

Overall, this study shows for the first time that the functional properties of QPI can be modulated by both precipitation acid and dispersion conditions, with the most promising conditions for heat-induced gel formation involving dispersion in water for at least 1 h or up to 24 h for sample precipitated in HCl. The approaches reported here offer a handle at the product development stage by allowing the manipulation of protein structure and subsequent performance, expanding the possible applications for quinoa protein isolates across different textures ranging from liquid foods, such as protein shakes and yogurt, to semi-solid foods, such as plant-based meats and cheeses. Moreover, it is conceivable that the strategies developed here can be applied to other plant proteins, contributing to the much-needed diversification of highly functional plant protein sources in the food industry.

Chapter 7. Characterisation of oil bodies and protein isolates extracted from cryo-milled quinoa seeds

Unpublished material not submitted for publication at the time of submission of this thesis.

Author contribution statement:

Marina Campos Assumpcao de Amarante: Conceptualisation, Formal analysis, Investigation, Methodology, Software, Validation, Visualisation, Writing - original draft, Writing - review & editing. **Thomas Holt:** Methodology, Formal analysis (fatty acid composition); **Lydia Ong:** Supervision, Writing - review & editing; **Fotis Spyropoulos:** Supervision, Writing - review & editing. **Bettina Wolf:** Conceptualisation, Funding acquisition, Project administration, Resources, Supervision, Writing - review & editing. **Sally Gras:** Conceptualisation, Funding acquisition, Project administration, Resources, Supervision, Writing - review & editing.

Acknowledgements: The authors would like to thank the Priestley Joint PhD Scholarship from the University of Birmingham (UK) and The University of Melbourne (Australia). This work was performed in part (FTIR measurements) at the Materials Characterisation and Fabrication Platform (MCFP) at the University of Melbourne and the Victorian Node of the Australian National Fabrication Facility (ANFF). The authors also thank the Biological Optical Microscopy Platform (BOMP) at The Bio21 Molecular Science and Biotechnology Institute at The University of Melbourne for access to equipment. Lydia

Ong and Sally Gras are both supported by the Australian Research Council Centre of Excellence in Plants for Space, grant number CE230100015.

Abstract

Quinoa has recently emerged as a healthier alternative to rice, due to its higher protein content and complete essential amino acid composition. Despite quinoa proteins gaining considerable attention, there is still a gap in our understanding of the properties and stability of quinoa oil bodies (OB), which show great potential for use as an ingredient in emulsified products. This study characterised quinoa OB recovered by aqueous extraction from cryo-milled quinoa seeds. The remaining flour suspension was used to extract quinoa protein isolate by alkalinisation followed by precipitation with HCl, acetic acid or citric acid. Microscopy, ζ-potential and droplet size distribution indicated good OB stability, which was retained after acid treatment. Cryo-milling followed by precipitation with citric acid led to a fine stranded gel microstructure in heat-induced protein gels with high final gel strength. This study improves our knowledge of quinoa OB properties and illustrates the potential of cryo-milling as a method for extracting two highly functional plant-based ingredients.

Keywords: plant protein; gelation; oil bodies; cryo-milling; microstructure; oleosome.

7.1 Introduction

In recent years, the food industry has developed food formulations using more sustainable ingredients, catalysed by the increase in world population, climate change and consumer demands for ethical and healthier foods (Bogueva and McClements, 2023). Plant proteins are consequently receiving increased scientific attention. Many plant-based food products are designed to have similar appearance, texture and flavour to their animal-based counterparts, to aid the transition from animal-based to plant-based foods. The functional and sensory properties of the protein and lipid fractions are key determinants of the final product attributes and so are critical to the commercial success of such products (Kyriakopoulou et al., 2021; Kyriakopoulou, Keppler and van der Goot, 2021).

The technofunctional properties of plant proteins, including their solubility, thermal properties and gelation capacity, have been studied extensively (O'Kane et al., 2004; Sun and Arntfield, 2010; Ruiz et al., 2016b; Tanger et al., 2022). In terms of structuring of plant-based food products, soy and pea proteins have gained especial attention, due to their capacity to form strong heat-induced protein gels and/or their complete essential amino acid profile (Gorissen et al., 2018; Schreuders et al., 2019). It is important to explore alternative protein sources, however, as these may possess different texturising properties and offer a similar nutritional benefit whilst enabling a broader spectrum of end-product textures for consumers.

Fat is also an essential component of plant-based food products, conferring the desired texture and functionality and improving the overall organoleptic properties of the products (Kyriakopoulou, Keppler and van der Goot, 2021). The use of naturally occurring oil bodies (or oleosomes) from plant sources in food formulation is promising, as these oil bodies may be directly applied as a base for emulsified products, without the

need for prior homogenisation to form oil droplets (Tzen et al., 1993; White, Fisk and Gray, 2006). Thanks to their unique structure of triacylglycerol droplets stabilised by a monolayer of phospholipids, anchored at the interface with the hydrophobic region of specialised proteins, called oleosins or oil body-associated proteins, plant oil bodies are stable against fatty acid oxidation (Fisk et al., 2008; Gray et al., 2010) and can also act as carriers for flavour molecules (Fisk et al., 2011) and bioactives (White et al., 2009; Zheng et al., 2019). Several sources of oil bodies have been well studied, including sunflower, peanut, soy, almond and rapeseed (Iwanaga et al., 2008; Gray et al., 2010; Fisk et al., 2011; Grundy et al., 2016; Zhang et al., 2017; de Chirico et al., 2018, 2020; Romero-Guzmán et al., 2020b), with several informative reviews published (Tzen, 2012; Huang, 2018; Nikiforidis, 2019; Hao et al., 2022; Şen et al., 2024), illustrating the potential of these ingredients.

Quinoa (*Chenopodium quinoa* Willd.) is a pseudocereal containing all essential amino acids, which recently has seen a rise in popularity as a healthier alternative to rice (Vilcacundo and Hernández-Ledesma, 2017). Quinoa seeds contain around 13 – 14% (w/w) protein, 6.5 – 6.9% (w/w) lipid, 69 – 72% (w/w) carbohydrate (of which 60% is starch), 9 – 10% (w/w) moisture and 2.3 – 3.0% (w/w) ash (Alonso-Miravalles and O'Mahony, 2018), as well as vitamins B, C and E (Vilcacundo and Hernández-Ledesma, 2017) and minerals such as Ca, P, Fe, Mg, Zn and K (Konishi et al., 2004) when examined by compositional analysis. The seeds are small and roughly spherical, with a diameter of 1.0 – 2.5 mm (Figure 7-1). The bran fraction, composed of the seed coat and embryo, surrounds the starch-rich perisperm (Alvarez-Jubete, Arendt and Gallagher, 2010; Alonso-Miravalles and O'Mahony, 2018). The embryo contains two cotyledons, or embryonic leaf structures and is composed of oblong-shaped cells containing spherical

protein bodies (~0.5 – 3 µm in diameter) and oil bodies (~0.2 – 0.5 µm in diameter) (Figure 7-1). In contrast, the perisperm is composed of uniform thin-walled cells, containing compound starch granules ~20 – 25 µm in diameter, which consist of oval aggregates of starch granules (Prego, Maldonado and Otegui, 1998) (Figure 7-1).

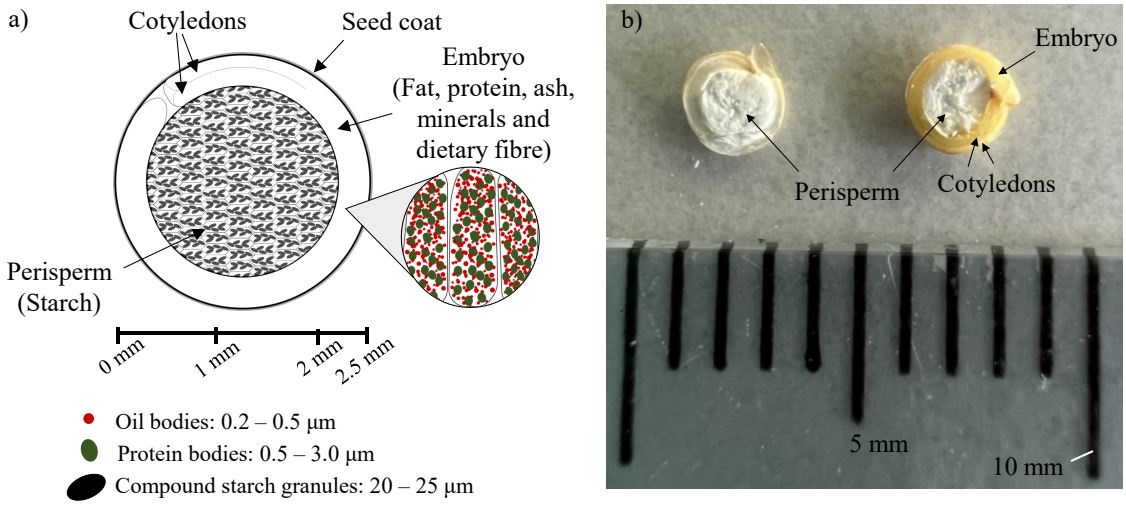

Figure 7-1. Structure of the quinoa seed in cross section: a) schematic indicating the key macrostructual domains and microstructural components, constructed based on prior work (Prego, Maldonado and Otegui, 1998; Alonso-Miravalles and O'Mahony, 2018); and b) a picture of the cross-section of a white quinoa seed that has been cut in half, with the two sides of the same seed showing the macrostructural domains corresponding to the schematic in a). The scale at the bottom indicates a length of 10 mm.

Our knowledge of the extraction and properties of globular quinoa storage proteins has increased dramatically in the last few years (Abugoch et al., 2008; Ruiz et al., 2016b; Kaspchak et al., 2017; van de Vondel, Lambrecht and Delcour, 2020, 2022). Globulins and albumins are known to make up to 77% (w/w) of the total protein in quinoa seeds (Koziol, 1992), with globulin 11S and albumin 2S being the most abundant (Brinegar, Sine and Nwokocha, 1996; Abugoch et al., 2009). The legumin-like globulin 13S and

vicilin-like globulin 7S, as well as proteins associated with oil bodies, have recently been identified in quinoa seeds but more information on their structure is needed (Burrieza et al., 2019; van de Vondel, Lambrecht and Delcour, 2020; Shen et al., 2022). Chapters 5 and 6 of this work report on wet extraction methods to manipulate the physico-chemical and technofunctional properties of quinoa protein isolate (QPI) extracted from quinoa flour. In the previous chapters, heat-induced gels of QPI obtained by precipitation with HCl, acetic acid or citric acid varied not only in gel strength but also in lipid content, which ranged from 11.3 ± 3.4% to 27.4 ± 0.8% (w/w) lipid integrated in the protein gel as a mixture of native oil bodies and re-emulsified oil droplets.

While the composition of quinoa oil is known, there are no studies on the extraction and characterisation of quinoa oil bodies. Quinoa oil is mainly composed of unsaturated fatty acids, where linoleic acid (C18:2, Ω6), oleic acid (C18:1), palmitic acid (C16:0) and α-linolenic (C18:3, Ω3) correspond to about 50%, 25%, 10% and 5% (w/w) of the total fatty acids, respectively (Koziol, 1992; Ruales and Nair, 1993; Alvarez-Jubete, Arendt and Gallagher, 2009, 2010). As for plant oil bodies in general, the most common approach for their recovery from seeds involves soaking the seeds in an aqueous solution followed by mechanical disruption, typically with a blender. The oil bodies are then collected in the form of an emulsion cream layer after centrifugation (Tzen et al., 1997; Grundy et al., 2016; Qi et al., 2017; de Chirico et al., 2018, 2020; Romero-Guzmán et al., 2020b; Yang et al., 2022a). This method can negatively affect the stabilising membrane of the oil bodies, leading to aggregation and coalescence (Karefyllakis, van der Goot and Nikiforidis, 2019). Thus, it is essential to develop oil body extraction methods that do not affect their membrane and consequent stability (Nikiforidis, 2019).

Cryo-milling is a good alternative to conventional seed milling methods, such as jet, pin or ball milling, as it solidifies the oil and increases the brittleness of seed particles, allowing an easier break up into smaller fragments (Schutyser and van der Goot, 2011; Sharma et al., 2016; de Bondt et al., 2020). This method has been mainly applied for the grinding of spices to protect essential oils against heat damage by maintaining a low temperature while absorbing the heat generated during grinding (Singh and Goswami, 1999; Mékaoui et al., 2016; Sharma et al., 2016; Katiyar, Biswas and Tiwary, 2021). More recently it has been shown to protect the protein content of ground pepper (Liu et al., 2018) and it was used as a pre-treatment to extract oils from pumpkin seeds (Balbino et al., 2019) and fennel seeds (Marčac et al., 2023) resulting in improved oil extraction yield. There is one report on the recovery of intact oil bodies from rapeseeds by cryo-milling with liquid nitrogen (di Bari et al., 2018); to the best of the author's knowledge though, this technique has not yet been applied to quinoa seeds.

This study set out to characterise the properties and stability of quinoa oil bodies (OB) and determine whether cryo-milling could be an effective method for extraction. It was hypothesised that cryo-milling of quinoa seeds would protect the lipid and protein fractions against heat damage and solidify the oil bodies during grinding. This would consequently allow the aqueous extraction of oil bodies using creaming and solid-liquid separation while protecting the oil body membrane during extraction and improving OB stability. It was also hypothesised that the protein fraction would be protected against heat-induced denaturation during grinding, resulting in improved protein functional properties. Thus, the protein-rich flour remaining after OB recovery was used for the extraction of QPI by wet fractionation consisting of alkalinisation at pH 9 followed by acid precipitation at pH 4.5 with HCl, acetic acid and citric acid. The physico-chemical

and technofunctional properties of the extracted QPI, including soluble protein content, protein profile, secondary structure, thermal and rheological properties, were then also studied. Further, extracted oil bodies were also treated with the same acids used during protein extraction to understand the effect of these acids on oil body stability.

7.2 Materials and methods

7.2.1 Materials

Organic white quinoa seeds produced by Wellness Road were purchased from Coles supermarket in Melbourne, Australia. According to the product label, the seeds contained, on a dry weight basis, 12.7% (w/w) protein, 60.4% (w/w) carbohydrate (of which 2.1% was sugars), 6.1% (w/w) lipid and 8.4% (w/w) fibre. HPLC grade 95% (w/v) n-hexane was purchased from Honeywell (UK), 14% (w/v) boron trifluoride in methanol and 32.5% (w/v) saturated NaCl were purchased from Thermo Fisher Scientific (USA) and 0.5 N KOH in methanol was purchased from Alfa Aesar (USA). An electrophoresis cell (Mini-Sub Cell GT), protein standards (Precision Plus Protein Kaleidoscope) and a Bradford protein assay kit were acquired from Bio-Rad Laboratories (USA). All remaining electrophoresis materials were purchased from Thermo Fisher Scientific (USA). Nile Red and Fast Green FCF were purchased from Sigma-Aldrich (UK). Purified water (resistivity > 18.2 M Ω.cm at 25 °C) produced with a Milli-Q Direct-Q (Type 3) water purifier (Merck Millipore Corporation, USA) was used for all experiments.

7.2.2 Study of quinoa oil bodies

7.2.2.1 Extraction of quinoa oil bodies

Figure 7-2 shows a flow diagram of the extraction processes involved in this study, including the extraction of quinoa oil bodies. Quinoa seeds were washed in running tap water to clean the seeds and left to air dry on a tray overnight (16 h). The seeds were placed in a ceramic mortar and liquid nitrogen was carefully poured over the seeds. After ~2 min, the frozen seeds were transferred to a coffee grinder and milled in 5 cycles of 10 s grinding with a 10 s pause. The flour was still cold to the touch at the end of the milling process, indicating that there was no excessive increase in temperature during milling. Flour suspensions were prepared in purified water using a ratio of 1:4 (flour:water) and vigorously agitated on a magnetic stirrer for 10 min at 22 °C before centrifuging for 30 min at 18000 × g at a temperature of 4 °C. At the end of the centrifugation process, three sample layers were identified: a top layer containing creamed oil bodies, a liquid middle layer containing soluble protein and a bottom layer containing flour particles. The creamed oil bodies were recovered with a spatula, the remaining suspension was then vortexed to remix the liquid middle layer and the flour before centrifuging again. A new layer of creamed oil bodies was then formed, also recovered with a spatula and combined with the oil bodies separated in the previous step. The combined oil body volume was centrifuged twice to further separate any small flour particles; the product of this process was considered the isolated oil bodies, as indicated in Figure 7-2.

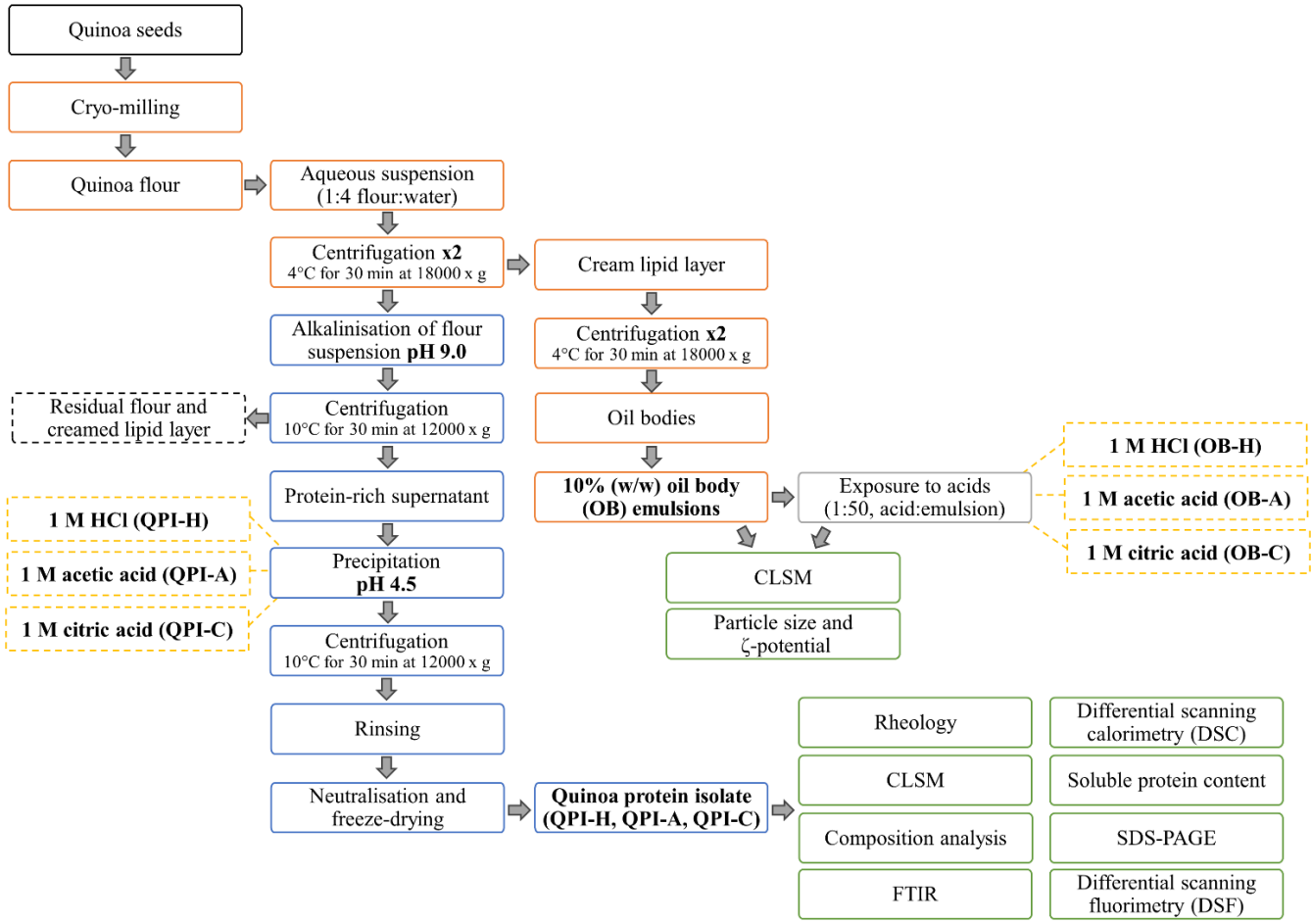

Figure 7-2. Schematic flow diagram illustrating the process of quinoa oil body (OB) extraction (shown in orange), including the exposure to HCl (-H), acetic acid (-A) and citric acid (-C), and of quinoa protein isolate (QPI) extraction (shown in blue) from cryo-milled quinoa seeds, followed by treatment with either HCl (-H), acetic acid (-A) and citric acid (-C). The largest by product stream contains the residual flour and creamed lipid layer generated after the centrifugation of the alkalinised flour suspension during QPI extraction, shown in a box with dashed outline to the left. Analyses performed to characterise the resulting OB and QPI in this study are shown in green on the right.

7.2.2.2 Estimation of creaming diameter of quinoa oil bodies

Stokes' law can explain the behaviour of particles in a fluid following the assumptions of laminar flow, spherical and homogenous particles of smooth surface and lack of interaction between particles. The creaming velocity (v, m/s) of oil droplets is determined by Equation 7-1, where r (m) is the droplet radius, g (m/s^2) the acceleration due to gravity, ρ_1 and ρ_2 (kg/m^3) the density of the dispersed and the continuous phase, respectively and η_c (Pa.s) the viscosity of the continuous phase (Stokes, 1850).

$$v = \frac{2gr^2(\rho_2 - \rho_1)}{9\eta_c} \quad (7\text{-}1)$$

This relationship allows for the calculation of the smallest oil droplet size that phase separates for accelerated creaming in the centrifugal field (g) of 18000 × g (1.7×10^6 m/s^2) applied in the extraction process. Assuming a continuous phase density of 1000 kg/m^3 (i.e. approximately that of water), oil phase density of 929 kg/m^3 (soybean oil at 4 °C) (Esteban et al., 2012), continuous phase viscosity of 0.001 Pa.s (~water), height of the centrifugation tubes of 0.12 m and a centrifugation time of 30 min, the droplet size can be calculated. It follows that oil droplets > 0.31 µm in diameter in the quinoa flour suspension will cream. The oil body size expected from the literature is ~0.2 – 0.5 µm (Prego, Maldonado and Otegui, 1998) and based on the calculation of the "creaming" diameter, the majority of the oil bodies were expected to be recovered in the cream phase, unless tightly bound to embryo fragments in the sedimented phase.

7.2.2.3 Preparation of quinoa oil body emulsions

10% (w/w) quinoa oil body emulsions were prepared by dispersing the recovered oil bodies in Milli-Q water without pH adjustment, using a magnetic stirrer. The natural pH of the emulsions was 6.8 ± 0.2. The emulsions were then exposed to 1 M HCl, acetic acid or citric acid to understand the effect of these acids on oil body stability. OB emulsions were mixed with each acid at a ratio of 1:50 (suspension:acid) (pH 4.5 ± 0.2) and vortexed before assessment for particle size distribution, ζ-potential and microstructure.

7.2.2.4 Droplet size distribution and ζ-potential of quinoa oil body emulsions

The droplet size distribution and ζ-potential of the emulsions were evaluated using a Zetasizer Nano ZS (Malvern Instruments, UK). All samples were appropriately diluted to prevent multiple scattering phenomena. The refractive indices used were 1.47 for oil (dispersed phase) and 1.33 for water (continuous phase) (Repo-Carrasco, Espinoza and Jacobsen, 2003; Mufari et al., 2020).

7.2.3 Study of quinoa protein isolate

7.2.3.1 Extraction of quinoa protein isolate

Quinoa protein isolate (QPI) was extracted from the quinoa flour suspension that remained after oil body extraction (blue unit operations in Figure 7-2), following the method described by Ruiz et al. (2016b) although modifications in centrifugal speed and in the acid precipitation step were applied (Chapter 5, Section 5.2.2.1). The pH of the 10% (w/w) flour suspension was adjusted to 9.0 using 1.0 M NaOH to solubilise the proteins in the flour, followed by agitation for 4 h at 22 °C and storage for 16 h at 4 °C.

The flour suspensions were then centrifuged for 30 min at 12000 × g at a temperature of 10 °C. Three sample layers formed: a top layer containing creamed oil bodies, a protein-rich low viscosity middle layer and a bottom layer containing residual flour (Valenzuela et al., 2013; Ruiz et al., 2016b; van de Vondel, Lambrecht and Delcour, 2020). The observation of a cream layer revealed that the flour suspensions still contained some lipid, likely remaining from the oil body extraction process due to the difficulty of completely removing the creamed oil bodies from the remaining supernatant. The cream layer was removed with a spatula and discarded with the residual flour. The pH of the protein-rich phase was then adjusted to 4.5 using either 1.0 M HCl, acetic acid or citric acid followed by centrifugation as above to obtain three protein precipitates. These were rinsed by re-suspension in purified water and centrifugation. Finally, the precipitates were re-suspended in purified water, neutralised using 1.0 M NaOH and freeze-dried for 72 h (Alpha 3-4 LSCbasic, Martin Christ, Germany). The freeze-dried products were called quinoa protein isolates (QPI) and labelled as QPI-H, QPI-A and QPI-C depending on the extraction acid applied (HCl, acetic acid and citric acid, respectively); these samples were then stored at 4 °C until use. Extraction yields were calculated as the weight ratio between freeze-dried QPI and the flour used for extraction according to Equation 7-2.

$$\text{Extraction yield (\%, w/w)} = \frac{\text{weight of freeze-dried QPI (g)}}{\text{weight of flour used for extraction (g)}} \times 100\% \qquad (7\text{-}2)$$

7.2.3.2 Determination of proximate composition

The total protein content of the quinoa flour and extracted QPI was determined via elemental analysis (Leco TruMac CN analyser, Leco Corporation, USA) for total nitrogen

and converted to total protein by applying a factor of 5.85 (Abugoch et al., 2008; Ruiz et al., 2016b). Protein yield was calculated from the extraction yield, considering the total protein content of QPI and quinoa flour using Equation 7-3.

$$\text{Protein yield (\%, w/w)} = \frac{\text{total protein in QPI (\%, w/w)} \times \text{extraction yield (\%, w/w)}}{\text{total protein in quinoa flour (\%, w/w)}} \quad (7\text{-}3)$$

The moisture content of QPI was assayed through method 934.01 published by the Association of Official Analytical Chemists (AOAC, 2002) and lipid content was assayed using the Vanillin assay following a published protocol (Williams et al., 2011).

7.2.3.3 Soluble protein content

Soluble protein was determined by dispersing 1% (w/w) QPI without pH adjustment in water (pH 6.8 ± 0.2) and agitating for 1 h at 22 °C followed by centrifugation for 1 h at 2400 × g at a temperature of 10 °C. The supernatants were weighed and their soluble protein content determined by the Bradford method using the Bio-Rad protein assay kit. The absorbance was recorded at 595 nm and the protein concentration determined using a calibration curve constructed using known concentrations of the protein bovine serum albumin provided with the kit. Finally, the soluble protein content was calculated using Equation 7-4.

$$\text{Soluble protein (\%, w/w)} = \frac{\text{protein concentration in supernatant (mg/mL)} \times \text{volume of supernatant (mL)}}{\text{weight of freeze-dried QPI (mg)}} \times 100\% \quad (7\text{-}4)$$

7.2.3.4 Protein structure of QPI

7.2.3.4.1 Protein profile of QPI

SDS-PAGE was conducted under reducing and non-reducing conditions to acquire the protein profile of the soluble fraction of extracted QPI. Samples were prepared from the supernatants obtained when 10 mg/mL QPI-H, QPI-A and QPI-C suspensions were centrifuged for 1 h at 2400 × g at a temperature of 10 °C. Samples of 20 µl of the supernatants were mixed with 10 µl of Bolt™ LDS sample buffer either with or without 4 µl of dithiothreitol (DTT) and then heated for 10 min at 70 °C prior to loading 10 µl of the mixture onto 12% Bis-Tris Plus Bolt™ Mini Gels. An aliquot of 10 µL of protein standards of molecular weights between 10 – 250 kDa were also loaded onto the gels. Electrophoretic runs were performed at the constant voltage of 200 V, using Bolt™ MES SDS running buffer. After the runs, the protein bands in the gels were stained with Coomassie Brilliant Blue for 15 min and destained with destain solution composed of 30% (w/v) methanol and 7% (w/v) acetic acid. In SDS-PAGE under non-reducing conditions, i.e., in the absence of DTT, subunits containing chains linked by disulfide bonds are expected to remain intact. As for SDS-PAGE under reducing conditions, the presence of DTT creates reducing conditions resulting in the dissociation of protein subunits containing chains linked by disulfide bonds (Kaspchak et al., 2017).

7.2.3.4.2 Fourier Transform Infrared Spectroscopy

Fourier-transform infrared spectroscopy (FTIR) was used to characterise freeze-dried QPI and 10% (w/w) QPI gels using an FTIR microscope (Lumos II, Bruker, USA) equipped with an attenuated total reflectance unit. The absorbance of the samples was recorded at wavelengths between 400 – 4000 cm^{-1} with a resolution of 4 cm^{-1}. Quantitative analysis of the FTIR spectra was carried out by applying the second derivative of the Amide I region (1600 – 1700 cm^{-1}) followed by baseline subtraction and Gaussian deconvolution with the OriginLab® (version 2019) software (OriginLab Corporation, USA). The contribution of each peak to the Amide I region was determined by calculating the ratio of the individual peak area and the total area of the deconvoluted peaks.

7.2.3.4.3 Thermal properties of QPI

Differential scanning calorimetry (Nano DSC, TA Instruments, USA) was applied to determine the thermal properties of extracted QPI. Samples of QPI (1%, w/w) were suspended in purified water without pH adjustment (pH 6.8 ± 0.2), stirred for 1 h at 22 °C and immediately used for analysis. A volume of 600 µL of purified water or sample was then loaded into the reference and sample capillary cell, respectively. The system was then pressurized to 3 atm and the cells were hermetically sealed. Samples were heated at a rate of 1 °C/min from 20 °C to 100 °C, kept at this temperature for 5 min and then cooled at 1 °C/min to 20 °C. The denaturation temperature (T_d), defined as the temperature where the maximum transition peak occurred, and the denaturation enthalpy (ΔH), defined as the integrated area below the transition peak, were calculated using the

equipment software. Enthalpy was then converted to J/g protein by considering the concentration (1%, w/w) and the total protein content of the samples.

The thermal properties of QPI were also analysed by nano differential scanning fluorimetry (Tycho NT.6, NanoTemper, Germany) by measuring the fluorescence signal of tryptophan residues at 350 nm and of tyrosine residues at 330 nm over a range of temperatures. The fluorescence of tryptophan or tyrosine residues is sensitive to protein folding/unfolding, allowing the change in ratio of 350 nm/330 nm with temperature to be used as a measure of the unfolding profile of proteins, providing complimentary information to DSC analysis (Davis et al., 2018). QPI (10%, w/w) was suspended in purified water without pH adjustment (pH 6.8 ± 0.2), stirred for 1 h at 22 °C and immediately used for analysis. Samples were loaded into 10 µL capillaries and loaded into the equipment where they were heated from 35 °C to 95 °C at a heating rate of 30 °C/min. Fluorescence signals at 300 nm and 350 nm were recorded and results are reported as the change in the ratio between the fluorescence for these two wavelengths with temperature. The first derivative of the 350 nm/330 nm ratio is used to determine the inflection temperature of the unfolding transition, i.e., a peak corresponding to the T_d measured by DSC. The Δ_{ratio}, defined as the difference between the 350 nm/330 nm ratio at the beginning and at the end of the unfolding profile was also determined, where a reduction in Δ_{ratio} indicates a lower content of folded, or native, protein.

7.2.3.5 Rheological assessment of QPI gelation properties

A shear rheometer (Discovery HR-2, TA Instruments, USA) fitted with a smooth parallel plate geometry (40 mm diameter, 1 mm gap) was used throughout. QPI (10%, w/w) was

suspended in purified water without pH adjustment (pH 6.8 ± 0.2), stirred for 1 h at 22 °C and the suspensions used immediately for determination of gelation properties. To avoid water evaporation during all measurements, vegetable oil was carefully pipetted around the outer rim of the sample and the samples also covered with a solvent trap.

Heat-induced gelation was investigated by applying an oscillatory shear temperature sweep recording the storage (G') and loss (G") modulus. Samples were heated from 20 °C to 90 °C at a heating rate of 1 °C/min, held at 90 °C for 5 min, followed by cooling to 20 °C at 1 °C/min, using 1% strain and an angular frequency of 10 rad/s. Immediately afterwards, without removing the sample from the gap when the sample was at 20 °C, a time sweep (1% strain and 10 rad/s frequency) of 5 min was performed followed by a frequency sweep (0.1 – 100 rad/s at 1% strain, 10 points per decade) and finally an amplitude sweep (0.1 – 1000% at 10 rad/s, 10 points per decade). The G' data obtained in the frequency sweeps were fitted to Equation 7-5.

$$\log\left(G^{'}\right) = n \times \log(\omega) + K \tag{7-5}$$

In this equation, the slope (n) corresponds to the type of gel network with n = 0 for ideal elastic networks and n > 1 for viscoelastic networks, while the intercept of the linear regression (K) provides an indication of the strength of the gel network (Creusot et al., 2011; Tanger et al., 2022). Further, the elastic stress (G' × strain) of each sample during amplitude sweeps was plotted as a function of shear strain, identifying a clear maximum, defined as the yield stress (τ_y) of the gels (Yang, Scriven and Macosko, 1986; Walls et al., 2003).

7.2.4 Microstructure assessment

7.2.4.1 Confocal laser scanning microscopy

Confocal laser scanning microscopy (CLSM) was used to visualise the microstructure of the quinoa seeds, oil body emulsions and QPI gels using a published method (Ong et al., 2011). The stains 0.1% Fast Green FCF and 0.1% Nile Red (NR) were prepared in purified water and in dimethyl sulfoxide, respectively, and applied at this concentration throughout. Seeds were split in the middle with a scalpel and stained with 10 µL of FCF solution followed by 10 µL of NR solution. The stained seeds were placed on a glass slide (ProSciTech, Australia) equipped with a spacer and covered with a cover slip (ProSciTech, Australia). Oil body emulsions were prepared for imagining by adding 10 µL of FCF solution to 480 µL of 10% (w/w) oil body emulsion followed by the addition of 10 µL of NR solution. Stained emulsion samples 50 µL in volume were mixed with 200 µL of 0.5% (w/w) agarose, which had been prepared at ~100 °C and allowed to cool to ~40 °C, and 6 – 7 µL of this mixture was then pipetted onto a cavity slide and covered with a cover slip. To inspect the microstructure of QPI gels, 10% (w/w) QPI suspensions were stained with FCF solution and NR solution in the same proportions stated above. The samples were then subjected to temperature sweeps in the rheometer, as described in Section 7.2.3.5. Following rheological analysis and gel formation, a piece of of each gel (~ 5 mm x 5 mm x 2 mm) was cut with a scalpel, transferred onto a glass slide containing a spacer and covered with a cover slip for further imaging.

All images were acquired on a confocal laser scanning microscope (Leica Sp8, Leica Microsystems, Germany) equipped with a 63× oil immersion objective. Images were obtained using 638 nm and 488 nm laser excitation for Fast Green FCF and Nile Red, respectively. At least three z-stacks of different regions of each sample were taken and

analysed. Imaris 10 Microscopy Image Analysis Software (Oxford Instruments, UK) was used to process the CLSM images. Quantification of oil body size in quinoa seeds, OB emulsions and QPI gels, as well as the quantitative determination of QPI gel porosity, were performed using the surface creation function of Imaris (Ong et al., 2020), where ~1,300 surfaces were analysed in the quinoa seeds, at least 200 surfaces were analysed in the OB emulsion images and at least 5,000 surfaces were analysed in the QPI gels images. Unstained areas were assumed to be pores. This area was quantified by subtracting the area occupied by protein and oil bodies/droplets, identified using the surface creation function of the software, from the total area of the image.

7.2.4.2 Digital microscopy of quinoa seeds

To complement the CLSM images, the structure of quinoa seeds was also visualised using a digital microscope (Dino-Lite Edge, Dino-Lite, USA). Seeds were split in the middle using a scalpel before observation under the microscope. Images were captured using the DinoCapture 2.0 software (Dino-Lite, USA).

7.2.5 Determination of fatty acid composition

The layer of creamed oil bodies before acid treatment, as well as the lipid extracted from QPI, were analysed for fatty acid composition. Lipids were extracted from QPI samples using method number 920.39 published by the Association of Official Analytical Chemists (AOAC, 2002) using hexane as a solvent. Samples of 6 mg of extracted lipids were subjected to saponification by the addition of 300 μL of 0.5 N KOH in methanol at 60 °C, which was allowed to react for 5 min. The fatty acids were then converted to

methyl esters (FAME) by the addition of 300 µL of 14% (w/v) boron trifluoride (BF_3) in methanol 60 °C, which was allowed to react for 5 min (Torres et al., 2011). Finally, 200 µL of 32.5% (w/v) saturated NaCl was added to the mixture followed by 200 µL of hexane before centrifugation for 2 min at 3000 × g and 22 °C. An aliquot of the organic layer was diluted 1:10 in hexane for analysis by gas chromatography-mass spectrophotometry (GC-MS) (GC-2010, Shimadzu, Japan), using a Omegawax100 column (Supelco Analytical, Sigma Aldrich, USA). A volume of 1 µL of sample was injected at 250 °C using helium as the mobile phase at a linear velocity of 35 cm/s. The column was kept for 2 min at 180 °C, then heated to 280 °C at a rate of 30 °C/min and kept at this temperature for 5 min. The column was operated in split mode with a ratio of 1/100. Quadrupole mass spectrometry settings were: electrical ionisation at 70 meV with ion source at 200 °C and interface at 280 °C, solvent cut of 1.8 min and scan mode of 40 – 400 m/z. Peak area was standardized using an internal standard of pentadecanoic acid (C15:0), which was continuously added at a concentration of 0.5 mg/mL and measured as pentadecanoic acid methyl ester. The identification of the compounds was carried out by matching with mass spectra from the NIST1 library provided by the equipment, as well as manual comparison (Mufari et al., 2020).

7.2.6 Statistical analyses

All measurements were performed in triplicate, except for thermal analysis measurements, which were performed in duplicate. All results are expressed as the mean ± the standard deviation (SD). All results were analysed by analysis of variance (ANOVA) followed by Tukey's post-test to verify significant differences between the means, considering a confidence level of 95% ($p < 0.05$).

7.3 Results and discussion

7.3.1 Microstructure of quinoa seeds

The location of the oil bodies *in situ* within the cross section of the quinoa seed was first examined by digital and confocal laser scanning microscopy, as shown in Figure 7-3. The lipid and protein are predominantly located in the embryo (Opazo-Navarrete et al., 2018a), one of the three successive layers shown in the unstained digital micrograph image, which includes the outer seed coat, embryo and perisperm (Figure 7-3a). The yellow layer of the embryo was 300 – 350 μm thick, making it easily distinguishable from the white inner starch-rich perisperm layer.

The Nile Red stained oil bodies appear as spherical droplets near Fast Green FCF stained oblong-shaped embryonic cells (Figure 7-3b) when the embryo is examined in cross section by CLSM. Fast Green FCF stained spherical protein bodies also appear within the embryonic cells (identified by white arrows). While the 0.5 – 3 μm diameter of the protein bodies was consistent with previous reports in the literature (Prego, Maldonado and Otegui, 1998), the oil bodies ranged in diameter from 0.5 – 8.0 μm, with the majority (~99% of the analysed oil bodies) ranging from 0.5 – 5.5 μm. This size is much larger than previous reports of 0.2 – 0.5 μm oil bodies, when quinoa seeds were assessed at a smaller scale by Transmission Electron Microscopy and Scanning Electron Microscopy (Prego, Maldonado and Otegui, 1998), which could reflect different quinoa varieties or cultivars. Approximately 1300 Nile Red stained spherical oil bodies could be observed in each ~153 μm^2 image (magnification 20x and 4x digital zoom), illustrating the broad potential for extraction of this lipid fraction.

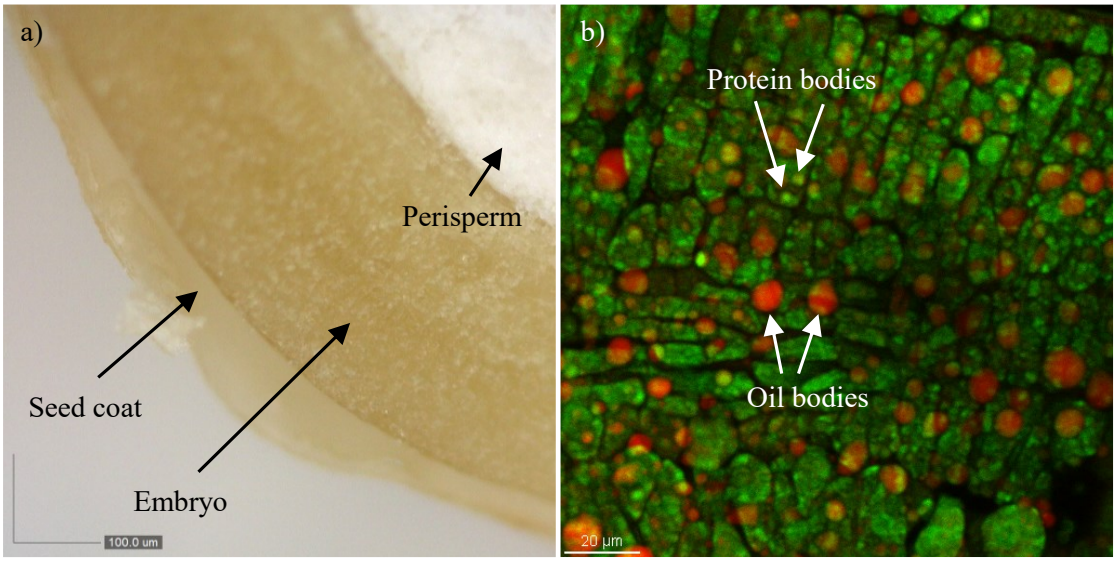

Figure 7-3. Microstructure of the quinoa seed in cross section and location of oil bodies as shown by light microscopy using: a) a digital microscope to show three key macrostructural domains from the outer layer of the seed coat to the inner perisperm, which differ in opacity (scale bar represents 100 µm); and b) confocal scanning laser microscopy of the embryo, where the protein bodies can be identified as Fast Green FCF stained structures and the oil bodies as Nile Red stained structures, both indicated by the white arrows, while unstained areas appear black (scale bar represents 20 µm).

7.3.2 Oil body emulsions

7.3.2.1 Microstructure of quinoa oil body emulsions

The 10% (w/w) oil body emulsions prepared by re-dispersing the cream layer of the centrifuged aqueous flour extract (Figure 7-4) showed Nile Red stained oil bodies of a similar size (0.5 – 5.0 µm) and appearance to the droplets observed *in situ* within the embryo of the quinoa seeds (0.5 – 5.5 µm; Figure 7-3b). A protein coating could be observed at the surface of some of the oil droplets (see inset in Figure 7-4a), which could indicate oil body-associated proteins at their surface, as expected from literature reports for soy, rapeseed and almond oil bodies (Grundy et al., 2016; Qi et al., 2017; de Chirico et al., 2020; Zhou et al., 2022); alternatively this protein could have associated with the oil bodies during extraction to form a recombined protein layer. The images also show

assemblies of oil bodies, indicated by white arrows, which may arise from protein-protein interaction.

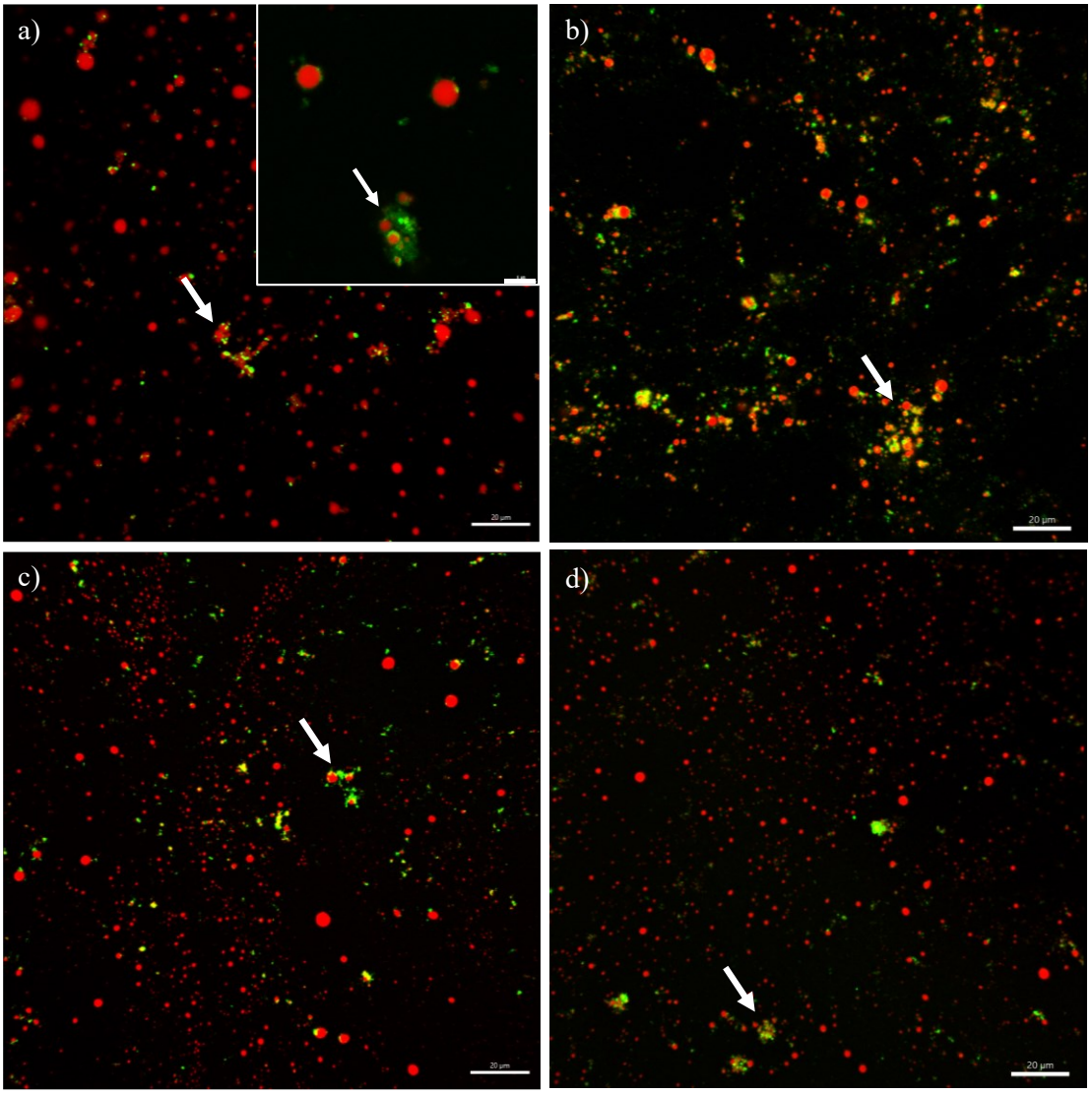

Figure 7-4. Microstructure of OB emulsions a) before and after treatment with b) HCl (OB-H), c) acetic acid (OB-A) or d) citric acid (OB-C) as determined by CLSM imaging. The protein can be identified as green structures stained by Fast Green FCF and the oil bodies as Nile Red stained structures, while unstained areas appear black. Assemblies of oil bodies and protein are indicated by white arrows in images a-d and the inset in a) shows the surface of an assembly in higher resolution. The scale bar represents 20 µm in images a-d, while the inset is a 4x digital zoom where the scale bar represents 5 µm.

The quinoa oil body emulsion was not significantly affected by changing the pH to 4.5 with either HCl (OB-H, Figure 7-4b), acetic acid (OB-A, Figure 7-4c) or citric acid (OB-C, Figure 7-4d), which were previously used to extract quinoa protein isolates in Chapters 5 and 6 of this work. The microstructure of the individual and clustered oil bodies after acid treatment resembled the untreated samples (Figure 7-4a). This behaviour differs considerably to soy oil bodies recovered by wet milling of soybeans, which are significantly affected by acid treatment with aggregation and coalescence occurring at pH 4 – 5, due to a reduction in the electrostatic repulsion between oil bodies as a result of oil body-associated proteins at their surface reaching their isoelectric point (Iwanaga et al., 2008; Qi et al., 2017). This discrepancy may be due to the different milling processes applied for oil body recovery. The soy oil bodies in the referenced studies were extracted by wet milling of soybeans with blenders or homogenisers and the shear or increase in temperature during grinding may have affected the stability of the oil bodies, rendering their surface more susceptible to acid treatment. In contrast, cryo-milling is reported to solidify oils and protect oil bodies against heat damage during grinding (Schutyser and van der Goot, 2011; Sharma et al., 2016) and, thus, likely protected the surface of oil bodies during their extraction from quinoa seeds.

7.3.2.2 Droplet size distribution

The successful recovery of quinoa oil bodies predominantly in their native size after cryo-milling was confirmed by dynamic light scattering. The size distribution ranged from 0.2 – 5.5 µm (Figure 7-5a), only slightly different from that observed by CLSM *in situ* for the oil bodies in quinoa seeds or within emulsions (0.5 – 5.5 µm; Figure 7-3b and Figure 7-4). Within this range there was a large intensity peak at 2.3 – 3.1 µm and a

smaller intensity peak at ~0.35 µm. The latter was expected from the calculation of the "creaming" diameter by Stokes' law, which indicated that droplets larger than ~0.31 µm in diameter would cream during separation from quinoa flour (Section 7.2.2.2).

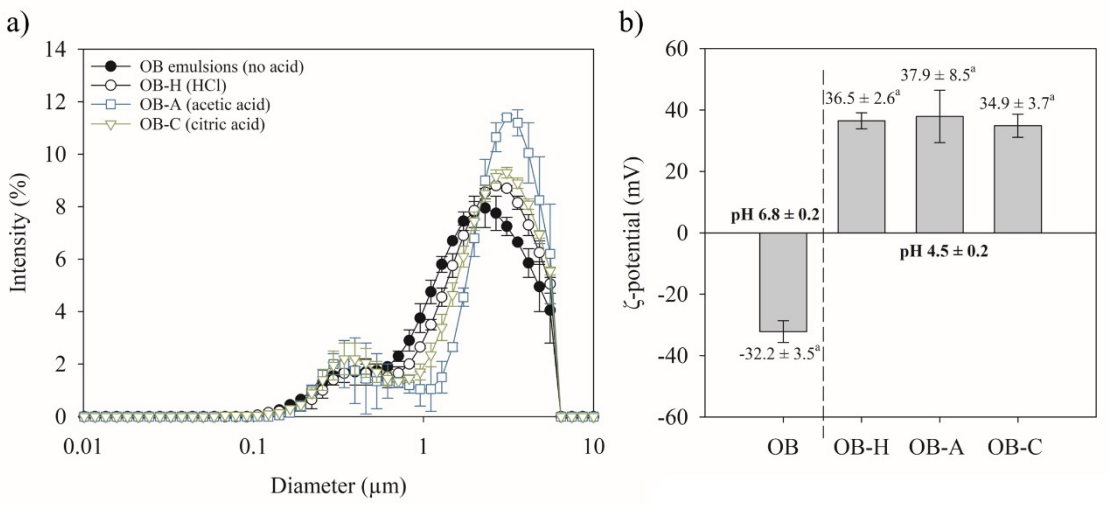

Figure 7-5. Physico-chemical properties of OB emulsions extracted from quinoa seeds: a) droplet size distribution determined by dynamic light scattering; where data are the mean with standard deviation and b) ζ-potential of OB emulsions before and after treatment with HCl (OB-H), acetic acid (OB-A) or citric acid (OB-C), where the initial and final pH are shown together with the ζ-potential values.

In general, quinoa OB extracted by cryo-milling showed good stability against acid treatment, with very little change in size observed at pH 4.5. Only a small level of disruption to OB membrane and droplet coalescence was observed during acid treatment, as the large droplet fraction increased slightly from 2.3 µm to 2.6 – 3.1 µm, as shown in Figure 7-5a. This result represents an advantage over soy oil bodies recovered by wet milling of soybeans, which showed poor stability at pH 4 – 5, with a change in droplet size from 2.8 µm to 8.4 µm when the pH was shifted from 7.0 to 5.0 (Qi et al., 2017). This further supports the hypothesis that cryo-milling protects the surface of oil bodies

during extraction and suggests that quinoa OB may be used as an ingredient in foods processed under acidic conditions, such as yoghurt and kefir (Ghazani et al., 2023).

7.3.2.3 ζ-potential

The surface charge of oil body emulsions was collected as an indicator of OB stability, as electrostatic repulsion between the proteins at the surface of the oil body can protect against coalescence and/or flocculation. In this measure, the higher the absolute ζ-potential value, the greater the emulsion stability (Iwanaga et al., 2008; Qi et al., 2017).

The ζ-potential value of quinoa oil body emulsion was −32.2 ± 3.5 mV, indicating high stability at the pH used for extraction (pH 6.8 ± 0.2; Figure 7-5b). This ζ-potential is higher than previously reported for soy (−10 mV to −15 mV) (Iwanaga et al., 2008; Qi et al., 2017) but comparable to that of peanut (−35 mV) (Gao et al., 2022), almond (−34 mV) (Grundy et al., 2016) and rapeseed oil body emulsions (~ −38 mV) (de Chirico et al., 2018) measured at a similar pH of 6.8 – 7.0.

Further, the absolute ζ-potential was unaltered by acid treatment when the pH was reduced to 4.5 ± 0.2 with any of the three acids ($p > 0.05$). Similar absolute ζ-potential values at pH ~4 and ~7 have also been observed for peanut and sunflower oil bodies (Zhou et al., 2019; Ghazani et al., 2023), while oil body emulsions from rapeseed and soy have displayed absolute ζ-potential values close to zero at pH 4 – 5, as the protein associated with these oil bodies was near the isoelectric point (Iwanaga et al., 2008; Qi et al., 2017; de Chirico et al., 2018). This result indicates that quinoa oil body emulsions had a high level of stability even after acid treatment and this effect was independent of the type of acid used.

Based on the ζ-potential values observed here (Figure 7-5b), the isoelectric point of quinoa oil body-associated proteins is likely close to pH 5.0. The ζ-potential values shifted from negative before acid treatment at pH 6.8 ± 0.2 (i.e., −32.2 ± 3.5 mV), where oil body-associated proteins are above their isoelectric point and deprotonated, to positive after acid treatment at pH 4.5 ± 0.2 (i.e. +34.9 ± 3.7 mV to +37.9 ± 8.5 mV), where the oil body-associated proteins are below their isoelectric point and protonated. This potential isoelectric point is within the range reported for OB extracted from soy, peanut and sunflower (pH 4.3 – 6.2) (Qi et al., 2017; Wang et al., 2019a; Ghazani et al., 2023). To the best of the author's knowledge, this is the first report of these properties for quinoa oil bodies, which indicate potential applications for this ingredient as a result of high stability at acidic pH.

7.3.3 Quinoa protein isolates

7.3.3.1 Composition of QPI extracted from cryo-milled quinoa seeds and precipitated with different acids

The cryo-milling applied in this study improved most composition and yield measures determined for QPI, except for soluble protein content (Table 7-1). In contrast, the choice of acid used for precipitation during extraction did not alter many measures except for soluble protein content.

Cryo-milling significantly increased the protein content obtained from the flour suspension after oil body extraction from 56 – 60% (w/w) in Chapter 5 (Section 5.3.1) to ~70% (w/w) (Table 7-1). The three acids used for precipitation, hydrochloric acid (QPI-H), acetic acid (QPI-A) or citric acid (QPI-C), resulted in similar protein contents

ranging from 72.8 ±< 0.1% to 74.4 ± 0.5% (w/w). This protein content is also within the range of 41 – 96% (w/w) reported by other authors for wet extraction of QPI from quinoa flour produced by conventional milling methods, such as ball or blade milling (Nongonierma et al., 2015; Ruiz et al., 2016a, 2016b; Steffolani et al., 2016; Mir, Riar and Singh, 2019a).

Similarly, the protein recovered measured by the protein yield was high after cryo-milling, with yields exceeding 40% (w/w); this value is higher than the ~20% (w/w) reported in Chapter 5 (Section 5.3.1) and is at the higher end of the range of 9.2 – 46% (w/w) reported by other authors using wet fractionation from conventionally-milled quinoa seeds (Nongonierma et al., 2015; Ruiz et al., 2016a, 2016b; Sánchez-Reséndiz et al., 2019). The high protein yield was also independent of the precipitation acid used (Table 7-1).

Table 7-1. Composition (%, w/w) on wet basis, extraction yield (%, w/w), protein yield (%, w/w) and soluble protein content (%, w/w) measured at pH 6.8 ± 0.2 of QPI extracted from cryo-milled quinoa seeds after precipitation with HCl (QPI-H), acetic acid (QPI-A) and citric acid (QPI-C).

	Protein isolates		
	QPI-H	QPI-A	QPI-C
Protein (%)	73.2 ± 0.3^{b}	74.4 ± 0.5^{a}	72.8 ±< 0.1^{b}
Lipid (%)	13.0 ± 0.9^{a}	13.7 ± 1.6^{a}	15.6 ± 2.0^{a}
Carbohydrate (%)*	13.8 ± 1.0	11.9 ± 1.7	11.6 ± 2.0
Moisture (%)	1.7 ± 0.3^{ab}	1.4 ± 0.3^{b}	2.3 ± 0.4^{a}
Extraction yield (%)	6.2 ±< 0.1^{a}	6.2 ± 0.3^{a}	6.7 ± 0.4^{a}
Protein yield (%)	42.2 ± 0.2^{a}	43.1 ± 2.3^{a}	45.5 ± 3.0^{a}
Soluble protein content (%)	13.6 ± 3.3^{b}	23.3 ± 2.4^{a}	26.9 ± 2.5^{a}

*Carbohydrate calculated by difference, so the SD presented was obtained by calculation of the standard error using the SD of the individual means used to obtain the carbohydrate content. Equal lowercase letters in the same row indicate that there is no significant difference among the means (Tukey's test, $p > 0.05$).

The large increase in protein content and yield of QPI obtained from cryo-milled quinoa seeds relative to the obtained from commercially-sourced quinoa flour (Chapter 5) indicates that cryo-milling protected the protein content of quinoa during extraction, as it was previously reported for ground pepper (Liu et al., 2018). Further, the additional step of oil body removal applied here prior to protein extraction decreased the concentration of lipids in the final protein extracts and thus contributed to the increase in protein yield relative to the previous study.

Cryo-milling also resulted in a slightly higher extraction yield of 6% (w/w) compared to ~5% (w/w) in Chapter 5 (Section 5.3.1), although this is still below the range of 8.1 – 13.4% (w/w) reported in literature (Mir, Riar and Singh, 2019a; Sánchez-Reséndiz et al., 2019; Olivera-Montenegro et al., 2022). This difference relative to literature reports could be due to the removal of the proteins associated with the oil bodies during the OB extraction procedure, as well as other minor differences in extraction conditions (Sánchez-Reséndiz et al., 2019; Kumar et al., 2021), or the use of different quinoa varieties or cultivars.

The lipid content in the QPI produced here with cryo-milling was 13.0 – 15.6% (w/w) (Table 7-1), within the range obtained without cryo-milling (~11 – 27%; Chapter 5, Section 5.3.1). Here, the lipid content was unaffected by choice of acid, whereas previously, in the absence of cryo-milling, the acid used for precipitation altered the lipid content of the extracts (~22% (w/w) for QPI-A, ~27% (w/w) for QPI-C and ~11% (w/w) for QPI-H). As noted previously, the lipid content is 2.5 to 3.0-fold higher than reported in other studies where a flour defatting step using hexane or petroleum ether was applied prior to protein extraction (Patole, Cheng and Yang, 2022; Yang et al., 2022b). Further, the carbohydrate and moisture contents of the extracted QPI were similar between the

different acid treatments and within the range expected from the literature of 1.6 – 18.8% (w/w) carbohydrate and 0.7 – 6.8% (w/w) moisture (Abugoch et al., 2008; Steffolani et al., 2016; Kaspchak et al., 2017; Yang et al., 2022b).

The fatty acid composition of the OB emulsion obtained by cryo-milling and before acid treatment (Appendix D – Table D.1) was in accordance with literature for quinoa seeds and flour obtained by conventional milling (Koziol, 1992; Ruales and Nair, 1993; Alvarez-Jubete, Arendt and Gallagher, 2009). The fatty acid profile also remained unchanged ($p > 0.05$) after acid treatment (Appendix D – Table D.1), consistent with previous reports where no difference in fatty acid composition was found for peanut oil bodies exposed to different pH (Gao et al., 2022).

The soluble protein content of the QPI assessed here at pH 6.8 ± 0.2 (13.6 ± 3.3% – 26.9 ± 2.5% (w/w); Table 7-1) was lower than the range of 42.3 ± 3.0% – 71.8 ± 2.3% (w/w) reported in Chapter 5 (Section 5.3.2). This suggests that QPI obtained by cryo-milling shows a higher initial aggregation than QPI obtained from commercially-sourced flour. This result may be a consequence of the use of different quinoa varieties between the two studies, as this data was not available from the manufacturer of the seeds used here, or it could be a consequence of cryo-milling. Plant proteins physiologically occur under various association states in the raw material, i.e., a mixture of monomers and oligomers, and different raw material varieties/cultivars, conditions of raw material harvesting and storage, as well as protein extraction and purification conditions affect protein organisation (Schmitt et al., 2021). Thus, it is possible that the proteins in the quinoa seeds used here inherently exist in the raw material predominantly under an aggregated colloidal state, or that the rapid freezing by liquid nitrogen followed by shear during cryo-milling induced changes in the aggregation state of quinoa proteins. In either

case, these protein aggregates may have sedimented during solubility assessment, resulting in the lower soluble protein content of these samples. Further studies are necessary to determine if cryo-milling results in the aggregation of quinoa proteins during extraction.

While the total protein content of the three protein isolates was similar with QPI-H and QPI-C showing only slightly lower values than QPI-A, the soluble protein of the isolate precipitated with HCl was significantly lower ($p < 0.05$) than for QPI-A and QPI-C. This result was expected, since kosmotropic anions, such as acetate and citrate, facilitate the precipitation of proteins through salting out, preventing unfolding. In contrast, the chloride anion shows a more chaotropic effect, promoting hydration, protein unfolding and denaturation (Metrick and MacDonald, 2015; Okur et al., 2017). Precipitation with acetic acid and citric acid therefore protected the native protein structure against unfolding during extraction, resulting in protein isolates of enhanced soluble protein content compared to precipitation with HCl, consistent with the observations in Chapter 5 (Section 5.3.2).

7.3.3.2 Molecular protein properties

7.3.3.2.1 Protein profile

The protein profile of QPI obtained from cryo-milled quinoa seeds evaluated by SDS-PAGE under non-reducing and reducing conditions (Figure 7-6) was similar to that reported in the literature for QPI samples (Abugoch et al., 2008; Mäkinen et al., 2016; Ruiz et al., 2016b; Kaspchak et al., 2017; Shen, Tang and Li, 2021; Yang et al., 2022b). Some protein bands were slightly fainter for QPI-H than QPI-A and QPI-C in both

reducing and non-reducing conditions, which again was expected due to the lower soluble protein content of QPI-H (Table 7-1).

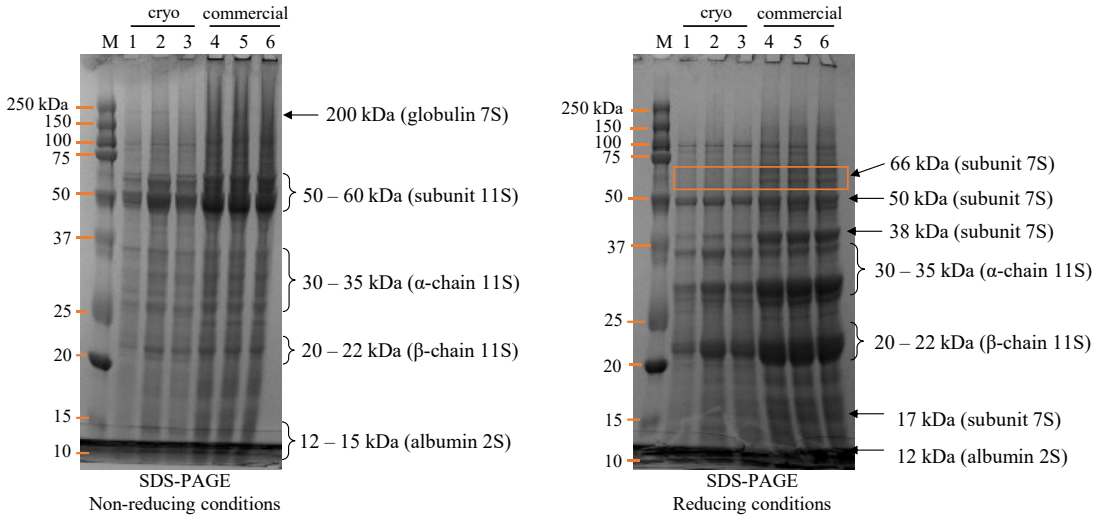

Figure 7-6. SDS-PAGE under non-reducing and reducing conditions of QPI precipitated with HCl (QPI-H), acetic acid (QPI-A) or citric acid (QPI-C): 1 – 3) extracted from cryo-milled quinoa seeds and 4 – 6) extracted from commercially-sourced quinoa flour. M indicates the protein molecular weight markers and the numbers 1-6 refer to: 1- QPI-H; 2- QPI-A; 3- QPI-C; 4- QPI-H; 5- QPI-A; 6- QPI-C.

The bands observed in non-reducing SDS-PAGE (Figure 7-6) largely correspond to the expected protein units found in Chapters 5 and 6, with bands identified at 12 – 16 kDa corresponding to albumin 2S, at 30 – 35 kDa and 20 – 22 kDa corresponding to the α- and β-chains of globulin 11S, respectively and at 50 – 60 kDa corresponding to the intact subunit of globulin 11S (Brinegar and Goundan, 1993; Abugoch et al., 2008; Shen et al., 2022; Yang et al., 2022b; Liu et al., 2023). A faint band at 200 kDa was also identified in all samples, corresponding to the tetramer of globulin 7S, as previously reported in the pseudocereal amaranth (*Amaranthus* spp.) (Quiroga et al., 2010).

The bands observed in reducing SDS-PAGE (Figure 7-6) were also largely as expected from observations in Chapters 5 and 6; the globulin 7S tetramer was disassembled into subunits of 16 kDa, 38 kDa and 50 kDa, as reported earlier in amaranth (Quiroga et al., 2010). Intense bands at 20 – 35 kDa and 20 – 22 kDa corresponding to the dissociated α- and β-chains of globulin 11S were also identified under reducing conditions, as expected from the reduction of disulfide bonds by DTT under these conditions.

A direct comparison was also made between the protein profile obtained here for QPI extracted with the three different acids from cryo-milled seeds and the QPI extracted with the three different acids from commercially-sourced quinoa flour used in Chapters 5 and 6 (Figure 7-6). The protein profiles were largely comparable, except for the differences above noted in soluble protein content (Table 7-1) and for the band at 66 kDa observed using SDS-PAGE under reducing conditions, which corresponds to one of the subunits of globulin 7S; this band was present in samples from commercially-sourced quinoa flour and absent in the samples from cryo-milled seeds. This vicilin-like globulin 7S is little characterised in quinoa and the molecular weight is inferred from the equivalent protein in the pseudocereal amaranth (Quiroga et al., 2010; van de Vondel, Lambrecht and Delcour, 2020; Shen et al., 2022). While this observation indicates that the molecular weights of globulin 7S subunits could differ across different quinoa varieties or cultivars, the protein could also be affected by the different milling conditions and further investigation is required to confirm whether this globulin contributes significantly to QPI properties.

7.3.3.2.2 Secondary protein structure of QPI

FTIR spectra were acquired for the freeze-dried QPI and of heat-induced gel samples prepared from 10% (w/w) QPI suspensions (Figure 7-7a) to identify any changes in sample profile due to cryo-milling and heat-induced gelation. The spectra obtained here for all QPI gels were similar to the obtained in Chapter 5 for samples extracted from commercially-sourced quinoa flour, showing peaks at similar wavelengths. Freeze-dried and gel samples obtained from cryo-milled seeds also displayed peaks at similar wavelengths. The peak at 3300 cm^{-1} associated with the presence of hydroxyl groups (-OH) in the Amide A region became broader upon gelation in water, spanning a range of 3700 – 2960 cm^{-1}, as expected due to the presence of a greater number of hydroxyl groups (Figure 7-7a).

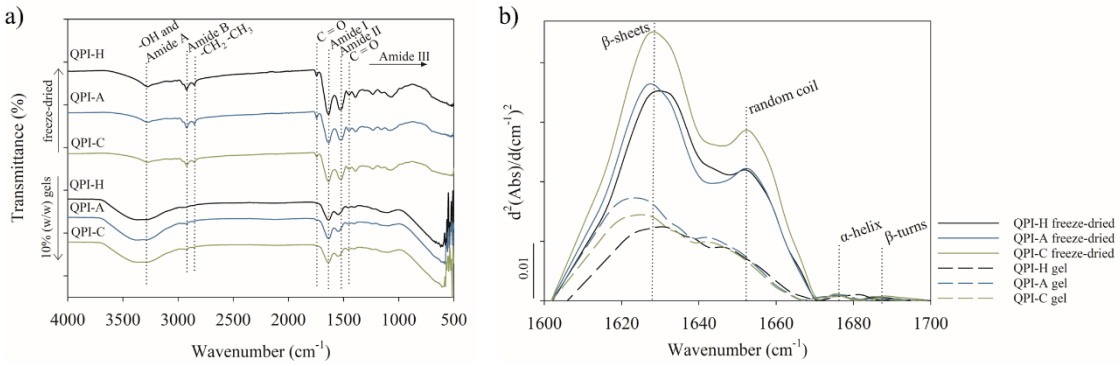

Figure 7-7. Secondary structure of QPI proteins (mean of two measurements): a) FTIR spectra of freeze-dried QPI or gels of 10% (w/w) QPI precipitated with HCl (QPI-H), acetic acid (QPI-A) or citric acid (QPI-C); b) second derivative of the Amide I region of the FTIR spectra in a).

The secondary protein structure was also assessed using the second derivative of the Amide I region (1600 – 1700 cm^{-1}) (Table 7-2). In Figure 7-7b, peaks at ~1625 cm^{-1} (range

1580 – 1680 cm^{-1}) correspond to β-sheets, peaks at ~1650 cm^{-1} (1640 – 1660 cm^{-1}) correspond to random coil structures, peaks at ~1670 cm^{-1} (1645 – 1690 cm^{-1}) correspond to α-helical structures and peaks at ~1690 cm^{-1} (1670 – 1700 cm^{-1}) correspond to β-turns (Figueroa-González et al., 2022).

Table 7-2. Contribution of secondary structure conformation to the overall protein structure of freeze-dried QPI or 10% (w/w) gels of QPI precipitated with HCl (QPI-H), acetic acid (QPI-A) or citric acid (QPI-C).

		Secondary structure conformation (%)			
	Sample	β-sheet	Random coil	α-helix	β-turn
Freeze-dried QPI	QPI-H	$59.4 \pm 0.2^{a,AB}$	$37.9 \pm 0.7^{a,A}$	$1.9 \pm 0.9^{a,A}$	$0.8 \pm < 0.1^{a,A}$
	QPI-A	$60.1 \pm 0.2^{a,A}$	$37.2 \pm 0.3^{a,A}$	$1.8 \pm 0.1^{a,A}$	$0.9 \pm 0.6^{a,A}$
	QPI-C	$59.2 \pm 1.5^{a,AB}$	$38.5 \pm 1.7^{a,A}$	$1.5 \pm 0.7^{a,A}$	$0.9 \pm 0.5^{a,A}$
10% (w/w) QPI gels	QPI-H	$54.3 \pm 0.2^{a,AB}$	$40.1 \pm 0.3^{a,A}$	$4.5 \pm 0.2^{a,A}$	$1.0 \pm 0.3^{a,A}$
	QPI-A	$58.2 \pm 1.7^{a,AB}$	$37.9 \pm 2.0^{a,A}$	$2.6 \pm 0.4^{a,A}$	$1.3 \pm 0.2^{a,A}$
	QPI-C	$51.0 \pm 4.9^{a,B}$	$43.1 \pm 3.7^{a,A}$	$4.4 \pm 1.9^{a,A}$	$1.6 \pm 0.8^{a,A}$

Equal lowercase letters in the same column indicate that there is no significant difference between the means of QPI samples at the same condition, i.e., freeze-dried or gel (Tukey's test, $p > 0.05$). Equal uppercase letters in the same column indicate that there is no significant difference between the means of freeze-dried and gel samples (Tukey's test, $p > 0.05$).

The secondary protein structure predominantly consisted of β-sheets and random coil structures, consistent with the observed in Chapters 5 and 6 of this work (Sections 5.3.7 and 6.3.5), with very little significant difference observed between treatments. Cryo-milling did not appear to cause negative disturbances in the secondary structure of the extracted QPI but instead may have promoted a protective effect, as 10% (w/w) QPI-H gels here had a lower random coil content ($p < 0.05$) but an otherwise similar secondary structure composition to that obtained in Chapter 5 for the same sample (Section 5.3.7).

This observation is in line with the hypothesis that cryo-milling would protect the protein fraction of quinoa seeds against heat-induced denaturation during grinding.

Among the cryo-milled samples, freeze-dried QPI-C showed slightly more intense peaks in the Amide I region than QPI-A and QPI-H. Gel formation resulted in a slight shift to lower wavelengths compared to freeze-dried samples. The spectra for QPI-H gels was also shifted towards higher wavenumbers compared to the spectra for QPI-A and QPI-C gels (Figure 7-7b), which may be a result of some unfolding of the tertiary protein structure (Luo et al., 2022b) which is expected due to the significantly lower soluble protein of QPI-H samples compared to QPI-A and QPI-C samples ($p < 0.05$, Table 7-1) despite similar total protein content.

7.3.3.2.3 Thermal properties

The thermal properties of the three QPI samples were assessed via differential scanning calorimetry (DSC) and differential scanning fluorimetry (DSF). The DSC and DSF thermograms are shown in Figure 7-8 and key DSC parameters including the peak onset temperature (T_o), peak transition or denaturation temperature (T_d), peak endset temperature (T_e) and denaturation enthalpy (ΔH) are given in Table 7-3, together with the characteristic DSF parameters including the inflection temperature (T_i) and the Δ_{ratio} (difference between the 350 nm/330 nm ratio at the beginning and at the end of the unfolding profile).

Cryo-milling did not appear to significantly affect the denaturation temperature of QPI samples and a single endothermic transition peak was recorded at ~88.0 °C (T_d,

Table 7-3 and Figure 7-8a), coinciding with T_d values reported in the literature for globulin 11S from quinoa (Vera et al., 2019).

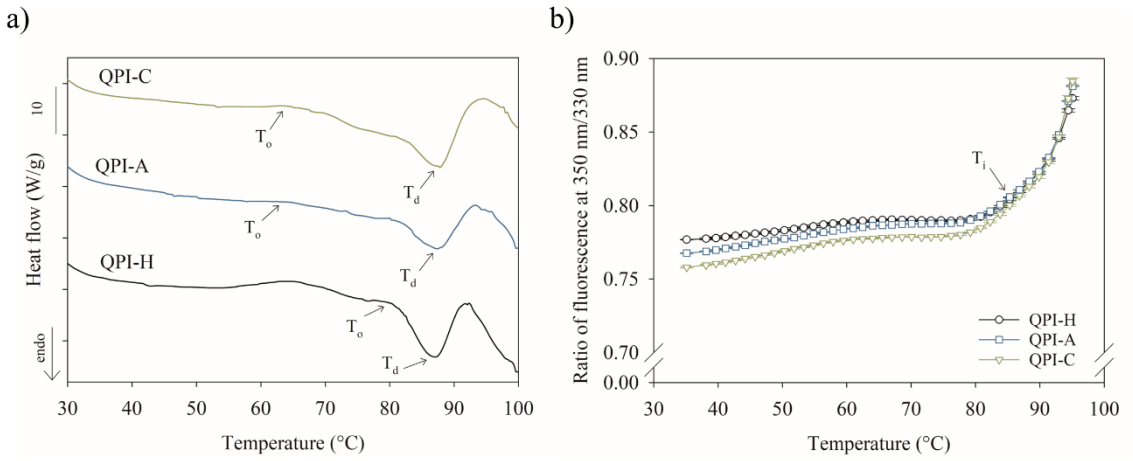

Figure 7-8. Thermal properties of QPI precipitated with HCl (QPI-H), acetic acid (QPI-A) or citric acid (QPI-C): a) DSC thermogram showing heat flow, peak onset temperature (T_o) and peak transition or denaturation temperature (T_d) for each sample, where data are the mean of two measurements and the variability is given in Table 7-3, 10 also indicates the scale of the y axis; and b) DSF thermogram showing the ratio of fluorescence at 350 nm/330 nm and the inflection temperature (T_i) for each sample, where the data are the mean of two measurements with standard deviation in the direction of the y-axis.

Table 7-3. The thermal properties of QPI precipitated with HCl (QPI-H), acetic acid (QPI-A) or citric acid (QPI-C), as obtained by the DSC and DSF analysis.

	Protein isolates		
	QPI-H	QPI-A	QPI-C
T_o (°C)	80.3 ± 0.1^b	$69.0 \pm 5.7^{a,b}$	64.5 ± 2.1^a
T_d (°C)	87.2 ± 0.8^a	88.2 ± 0.1^a	87.8 ± 0.2^a
T_e (°C)	91.8 ± 0.6^a	94.1 ± 1.5^a	95.0 ± 1.4^a
T_i (°C)	85.9 ± 0.3^a	84.5 ± 0.3^b	85.7 ± 0.3^a
ΔH (J/g protein)	1.7 ± 0.2^b	2.6 ± 0.2^b	4.4 ± 0.4^a
Δ_{ratio}	$0.10 \pm < 0.01^c$	$0.11 \pm < 0.01^b$	$0.13 \pm < 0.01^a$

Equal lowercase letters in the same row indicate that there is no significant difference among the means (Tukey's test, $p > 0.05$).

The choice of acid had a greater effect than cryo-milling and the thermal transition spanned a much wider temperature range for the two isolates precipitated with the kosmotropic acids, QPI-A and QPI-C, compared to the protein isolate precipitated with HCl (Figure 7-8a). Other differences between the three treatments included QPI-C having the greatest difference between endset and onset temperature and showing the highest ($p < 0.05$) denaturation enthalpy among the samples (Table 7-3; 4.4 ± 0.4 J/g), which was similar to the observed in Chapter 5 with commercially-sourced quinoa flour (4.5 ± 0.6 J/g; Section 5.6.5). Whereas QPI-H and QPI-A samples showed lower ΔH values (Table 7-2; 1.7 ± 0.2 J/g and 2.6 ± 0.2 J/g, respectively) than the reported in Chapter 5 with commercially-sourced quinoa flour (3.0 ± 0.3 J/g and 4.4 ± 0.8 J/g, respectively; Section 5.6.5). These observations suggest that the choice of citric acid as precipitation acid after cryo-milling had the least detrimental effect on the native protein structure followed by acetic acid and hydrochloric acid. Citric acid and acetic acid have been reported to show interchangeable kosmotropic effects, with some studies reporting acetate as being more kosmotropic than citrate (Ries-Kautt and Ducruix, 1989; Okur et al., 2017). The kosmotropic capacity of polyprotic acids, such as citric acid, is greater than monoprotic acids, such as acetic acid and HCl, however, as the dissociation products further contribute to the salting out of proteins, preventing unfolding (Kunz, Henle and Ninham, 2004).

The DSF assessment, reported as the ratio of the fluorescence signal at 350 nm to 330 nm (Figure 7-8b), was consistent with DSC measurements. All samples showed a gradual increase with temperature until ~80°C, where the slope increases sharply. The T_i of all three samples, corresponding to the peak in the first derivative of the DSF thermogram, was ~85°C, which is comparable to the T_d values obtained by DSC. The

trend in Δ_{ratio} between samples also corresponded to the trend observed for the denaturation enthalpy (ΔH, Table 7-3), as QPI-C had the highest Δ_{ratio} ($p < 0.05$), indicating a higher content of native, unfolded protein.

7.3.3.3 Gel properties

The gel properties of aqueous samples of 10% (w/w) QPI-H, QPI-A and QPI-C were assessed via small amplitude oscillatory rheometry, recording the storage (G') and loss (G") moduli while initially increasing temperature (20 – 90 °C at 1 °C/min), holding at a maximum temperature (90 °C for 5 min) and then cooling (90 – 20 °C at 1 °C/min). Immediately afterwards, a time sweep (1% strain and 10 rad/s frequency) of 5 min at 20 °C was performed, followed by a frequency sweep (0.1 – 100 rad/s at 1% strain, 10 points per decade) and finally an amplitude sweep (0.1 – 1000% at 10 rad/s, 10 points per decade) (Figure 7-9). Key parameters are given in Table 7-4, including the gelation temperature (T_{gel}), defined as the temperature given by the intercept between a linear extrapolation of the rapidly rising G' and the temperature axis (Sun and Arntfield, 2010; Ruiz et al., 2016b), the G' value and the loss factor (tan δ) recoded at the end of the holding step at minimum temperature (20 °C), denoted the final gel strength G'_{20} and tan δ_{20}, the slope of the frequency dependence of G' (n) defined in Equation 7-5 and the yield stress analysed from the amplitude sweeps (τ_y).

All 10% (w/w) QPI samples showed initial G' values of ~10 – 25 Pa. The G' and G" of both QPI-A and QPI-C initially decreased during heating then increased sharply at ~63 °C, denoted as the T_{gel} (Figure 7-9a-b), which was consistent with the thermal transition measured by DSC (T_o, Table 7-3). The G' and G" moduli then continued to

increase during holding at 90 °C and subsequent cooling to 20 °C. QPI-H differed to the other two samples, with an initial slight decrease in G' and G" but no marked increase in both moduli towards the end of the heating stage, so that a T_{gel} could not be determined.

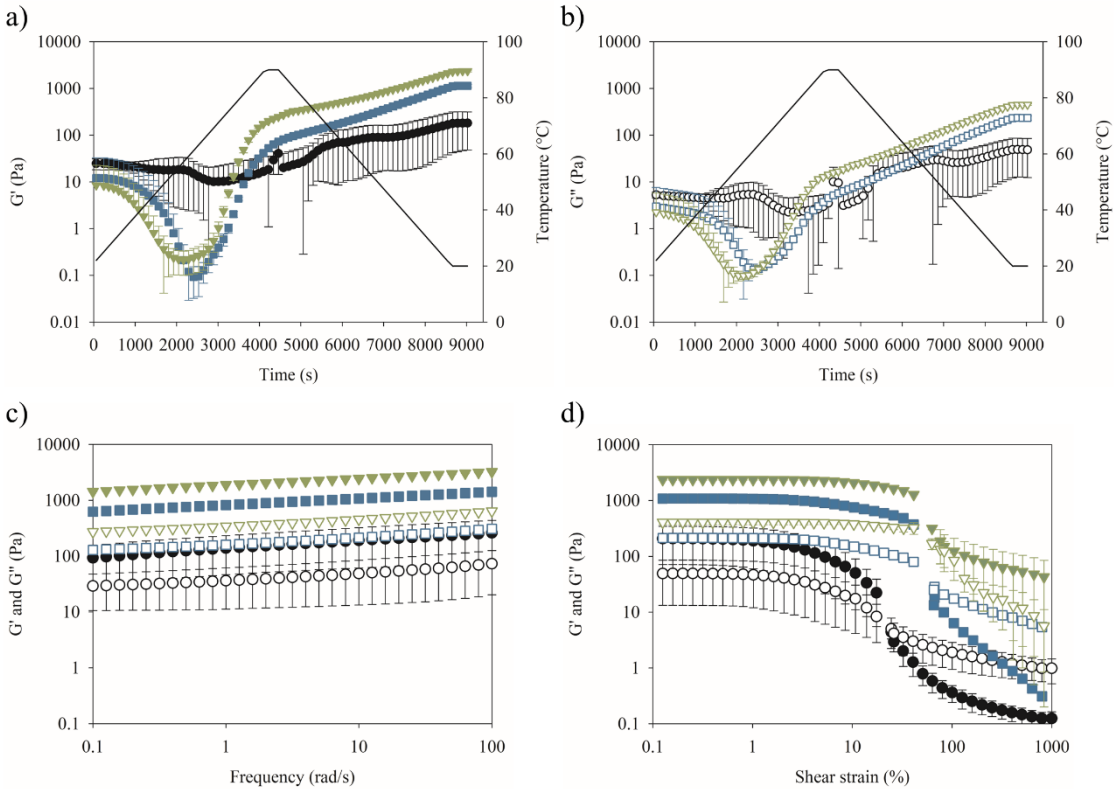

Figure 7-9. The rheological properties and gelation of 10% (w/w) QPI precipitated with HCl (QPI-H, ●), acetic acid (QPI-A, ■) or citric acid (QPI-C, ▼): a) storage modulus (G', closed symbols) and b) loss modulus (G", open symbols) as a function of temperature sweeps in rheometer, indicated by the solid black line; both storage modulus (G', closed symbols) and loss modulus (G", open symbols) as a function of c) angular frequency and d) shear strain.

These observations are in contrast to the reported in Chapter 5 (Section 5.3.8), where all 10% (w/w) QPI samples showed initial G' values of < 1 Pa and no significant change was observed up to the gelation temperature, which ranged between 79.8 °C and 81.8 °C; subsequently, the G' values of all samples continued to increase during the holding and

cooling stages. Ultimately, the final gel strengths (G'_{20}) of QPI-A and QPI-C achieved here were 4- and 7-fold higher than those found in Chapter 5, while the final gel strength of QPI-H remained statistically similar ($p > 0.05$) in the two studies. This is despite QPI samples extracted from cryo-milled seeds displaying lower soluble protein content (< 27%, w/w) than the reported in Chapter 5 (> 40%, w/w). This indicates that the protein aggregates present in the QPI samples obtained from cryo-milled seeds still participated in network formation during heat-induced gelation reinforcing the gel structures, as the whole isolate was used in the evaluation of the gelation properties (Section 7.2.3.5). The protein isolates extracted by cryo-milling also showed accentuated differences induced by the choice of precipitation acid. QPI-C formed the strongest heat-induced gel of all the samples (G'_{20} = 2371 ± 102 Pa; Table 7-4 and Figure 7-9a-b) likely due to its higher native protein content, as shown by the soluble protein results (Table 7-1) and consistently with the higher kosmotropic effect of citric acid (Hofmeister, 1888; Kunz, Henle and Ninham, 2004). On the other hand, the data for QPI-H were poorly reproducible compared to QPI-C and QPI-A (Figure 7-9a-b), suggesting that both the aqueous sample and final gel were more heterogeneous. Further, the G'_{20} value for QPI-H was significantly lower ($p < 0.05$) than for QPI-C and QPI-A (Table 7-4). This behaviour was unsurprising given the lower soluble protein content and poor denaturation enthalpy of QPI-H. This result indicates that cryo-milling of quinoa seeds acted synergistically with precipitation with the more kosmotropic acids, especially with citric acid, which helped to preserve the native functionality of quinoa proteins, as previously indicated by literature (Liu et al., 2018; Katiyar, Biswas and Tiwary, 2021), resulting in even stronger gels than the previously reported in Chapter 5.

Table 7-4. Rheological properties and gelation of QPI gels including the gelation temperature (T_{gel}), final storage modulus (G'_{20}), loss factor (tan δ_{20}), frequency dependence of G' (n) and yield stress (τ_y) obtained for 10% (w/w) gels form from QPI precipitated with HCl (QPI-H), acetic acid (QPI-A) or citric acid (QPI-C).

	T_{gel} (°C)	Storage modulus (G'_{20}, Pa)*	Loss factor (tan δ_{20})	n	τ_y (Pa)
QPI-H	-	182 ± 134^{c}	$0.28 \pm < 0.10^{a}$	$0.14 \pm < 0.10^{a}$	6 ± 4^{c}
QPI-A	63 ± 2^{a}	1141 ± 91^{b}	$0.21 \pm < 0.10^{b}$	$0.12 \pm < 0.10^{b}$	167 ± 28^{b}
QPI-C	63 ± 3^{a}	2371 ± 102^{a}	$0.19 \pm < 0.10^{c}$	$0.12 \pm < 0.10^{b}$	530 ± 14^{a}

*These values were recorded at the end of the temperature sweep, when the temperature returned to 20 °C. Equal lowercase letters in the same column indicate that there is no significant difference among the means (Tukey's test, $p > 0.05$).

QPI-A and QPI-C had statistically lower tan δ_{20} than QPI-H ($p < 0.05$; Table 7-4), suggesting a higher gel elasticity and stability of the gel network, as expected (Sun and Arntfield, 2010, 2011; Tanger et al., 2022). Further, gel formation by all three samples was confirmed by frequency sweeps (Figure 7-9c), where G' and G" were parallel and the slope of G' (n) was close to zero (Table 7-4). Amplitude sweeps (Figure 7-9d) showed a linear viscoelastic (LVE) region at lower strains for all samples; however, as expected from the earlier discussion, QPI-H showed the shortest LVE, quantified as the yield stress (Table 7-4), followed by QPI-A and QPI-C.

7.3.3.4 Gel microstructure

Since rheological properties are causally linked to microstructure, confocal laser scanning micrographs of heat-induced 10% (w/w) QPI gels were acquired (Figure 7-10a-c), where protein was stained with Fast Green FCF (green structures) and lipid was stained with Nile Red (red structures). The microstructure of the gels is shown both in cross section

and projected view and quantitative image analysis performed for further comparison (Figure 7-10d).

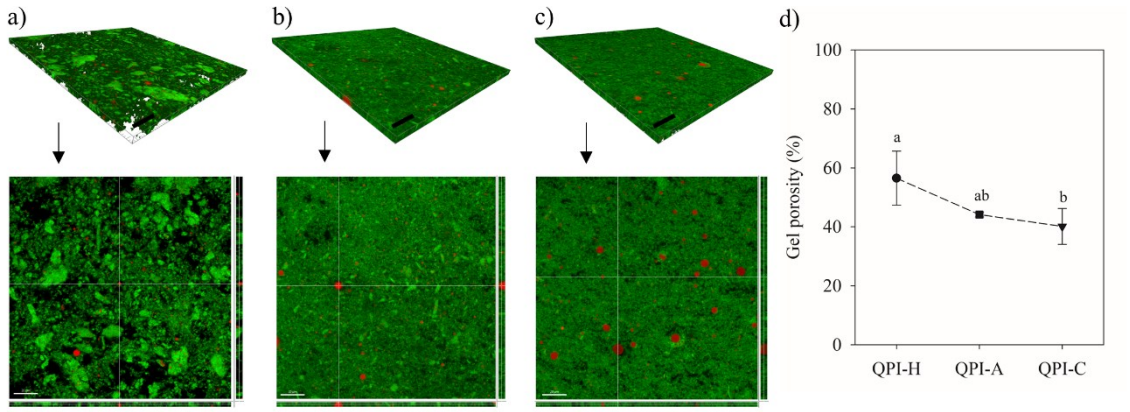

Figure 7-10. Microstructure and porosity of heat-induced gels formed by 10% (w/w) QPI samples precipitated with a) HCl (QPI-H), b) acetic acid (QPI-A) and c) citric acid (QPI-C). The gels were visualised by CLSM, and Fast green FCF stained protein appears green, while Nile red stained oil bodies appear red. The samples are shown in projected view (top images), as well as in cross section (bottom images), where the projection in the x-z and y-z direction is shown adjacent to the x-y image, scale bar represents 20 µm; d) gel porosity (%) determined by analysis of CLSM images of the three protein treatments. Equal lowercase letters indicate that there is no significant difference among the means (Tukey's test, $p > 0.05$).

Cryo-milling appeared to impact on both the microstructure of the extracted quinoa components and their arrangement within the gel network. The oil bodies integrated in the present QPI gels were 0.5 – 5.0 µm in diameter, smaller than in Chapter 5, where QPI was extracted from commercially-source quinoa flour (0.2 – 10 µm; Section 5.3.6) and likely contained a mixture of native oil bodies and re-emulsified oil droplets. This suggests a lower extent of re-emulsification of the oil bodies extracted together with QPI from cryo-milled quinoa seeds, resulting in the smaller droplets observed here.

Further, as for the gelation properties, it appears that cryo-milling accentuated the microstructural differences between the QPI gels reported here compared to the previously observed in Chapter 5 (Section 5.3.6). Although the 10% (w/w) QPI-H gels were slightly more porous than 10% (w/w) QPI-A and QPI-C gels, the microstructures were largely similar in this previous study. In contrast, protein aggregates are easily visible within the gel microstructures of 10% (w/w) QPI-H and QPI-A extracted from cryo-milled seeds (Figure 7-10a-b), likely a consequence of the lower soluble protein content of the present samples (13.6 – 23.3% vs 42.3 – 71.8% in Chapter 5). Further, the gel microstructures here appear to transition from highly heterogeneous structures, consisting of large aggregated protein structures that were loosely associated with oil droplets for QPI-H samples (Figure 7-10a) to a fine stranded protein network with fewer void spaces for QPI-C (Figure 7-10c); while QPI-A gels appear to contain a mixture of the two microstructures, with some protein aggregates embedded within the protein network (Figure 7-10b). This observation is somewhat confirmed by the gel porosity results (Figure 7-10d), which show that QPI-H gels were significantly ($p < 0.05$) more porous than QPI-C, as a result of the particulate microstructure; whereas the porosity of QPI-A gels did not significantly differ from that of the other two samples, representing a mixed microstructure.

Under heat-induced gelation, the structure of native globular proteins unfolds with the increase in temperature and allows protein aggregation through hydrophobic interactions (Kharlamova et al., 2016). If the electrostatic repulsion between protein molecules is weak, protein-protein interactions form at any point in the protein surface, leading to the formation of spherical aggregates, i.e., microgels; whereas if the electrostatic repulsion between the protein aggregates is strong, protein-protein interactions form at only a few

points and the aggregates tend to organise in strands (Bryant and McClements, 1998; Nicolai, 2019). As more protein is incorporated to the gel network, both types of aggregates are strengthened by inter- and intramolecular disulfide bonds resulting from sulfhydryl-disulfide interchange or sulfhydryl oxidation (McSwiney, Singh and Campanella, 1994), forming a volume-spanning particulate or filamentous gel, respectively. During cooling, the protein gel network continues to develop and this gel is reinforced by short-range interactions, such as hydrogen bonds (Bryant and McClements, 1998; O'Kane et al., 2004). Cl^- is weakly hydrated and is attracted to the protein backbone when in solution, which not only leads to unfolding of the protein structure but also to screening of protein surface charges (Okur et al., 2017), which likely led to the formation of microgels and a particulate gel for QPI-H (Figure 7-10a). More kosmotropic anions are strongly hydrated and become excluded from the protein backbone when in solution, protecting the protein structure (Okur et al., 2017). QPI-C showed higher denaturation enthalpy (Table 7-3) and final gel strength (Table 7-4) than QPI-A, indicative of a higher kosmotropic effect of citric acid and consequently a higher protection of native protein structure. It is then expected that the native protein molecules retained their surface charges and the stronger electrostatic repulsion led to the formation of strands and filamentous gels in QPI-C (Figure 7-10c). QPI-A generally showed results for soluble protein content, thermal properties, gelation properties and gel porosity that were either similar to those of QPI-H or QPI-C or exactly midway. It is therefore not surprising that the gel microstructure of this sample (Figure 7-10b) appears to be a mixture of particulates and filamentous structures.

7.4 Conclusions

Cryo-milling of quinoa seeds allowed oil bodies to be recovered largely in their native state. The extracted oil bodies had high absolute ζ-potential, indicating good stability against coalescence, and were stable after acid treatment, illustrating their potential use as ingredients in acidic food products or processes. Cryo-milling further resulted in high protein recovery. While soluble protein content was reduced, the native protein structure also appeared protected during extraction using a kosmotropic acid and the gelation properties of QPI were improved compared to previous studies. Citric acid appeared most promising for precipitating QPI from quinoa flour suspensions following OB extraction, as it led to more native, soluble protein and a significantly higher denaturation enthalpy. Heat-induced gels formed from citric acid-treated QPI formed a fine-stranded microstructure with few pores, which had high gel strength, elasticity and stability. In contrast, QPI precipitation with HCl led to heterogenous, porous and weak gels. Cryo-milling of seeds followed by protein precipitation with citric acid is an interesting combined strategy for the extraction of oil bodies and protein isolates for the formulation of plant-based foods, which may have broader applicability to a range of plant protein sources.

Chapter 8. General conclusions and future work

This thesis provides insights on the phase behaviour of quinoa protein isolate (QPI), as well as processing options for the modulation of its properties. It also presents a strategy to recover quinoa oil bodies (OB) along with QPI, two highly functional ingredients for the design of new plant-based food products (Figure 8-1). This chapter describes the main findings of this work and how it helped advance the knowledge on extraction strategies to allow the utilisation of quinoa protein and oil bodies in microstructure engineering of food products. Recommendations for future work are also presented.

8.1 General conclusions

Approaches to explore the use of QPI in the microstructure engineering of plant-based food products were investigated in this research. In the first approach (Chapter 4), segregative phase diagrams of QPI and MD mixtures were created, aiming at the understanding of their phase behaviour to facilitate the creation of tailored microstructures in plant-based foods. QPI-MD mixtures phase separated by depletion flocculation, where fractions of MD were entrapped within the aggregated network of the QPI-rich phase (Figure 8-1). This finding led to the conclusion that the formation of microstructures such as gel particles or fibres, which require a phase separation mechanism of thermodynamic incompatibility forming droplets dispersed in a continuous phase, is not possible with QPI-MD mixtures. This study was further evidence of the previously reported complex segregative phase behaviour of plant proteins and showed that the formulation of plant-based food microstructures of predictable properties using this approach is more challenging than first expected.

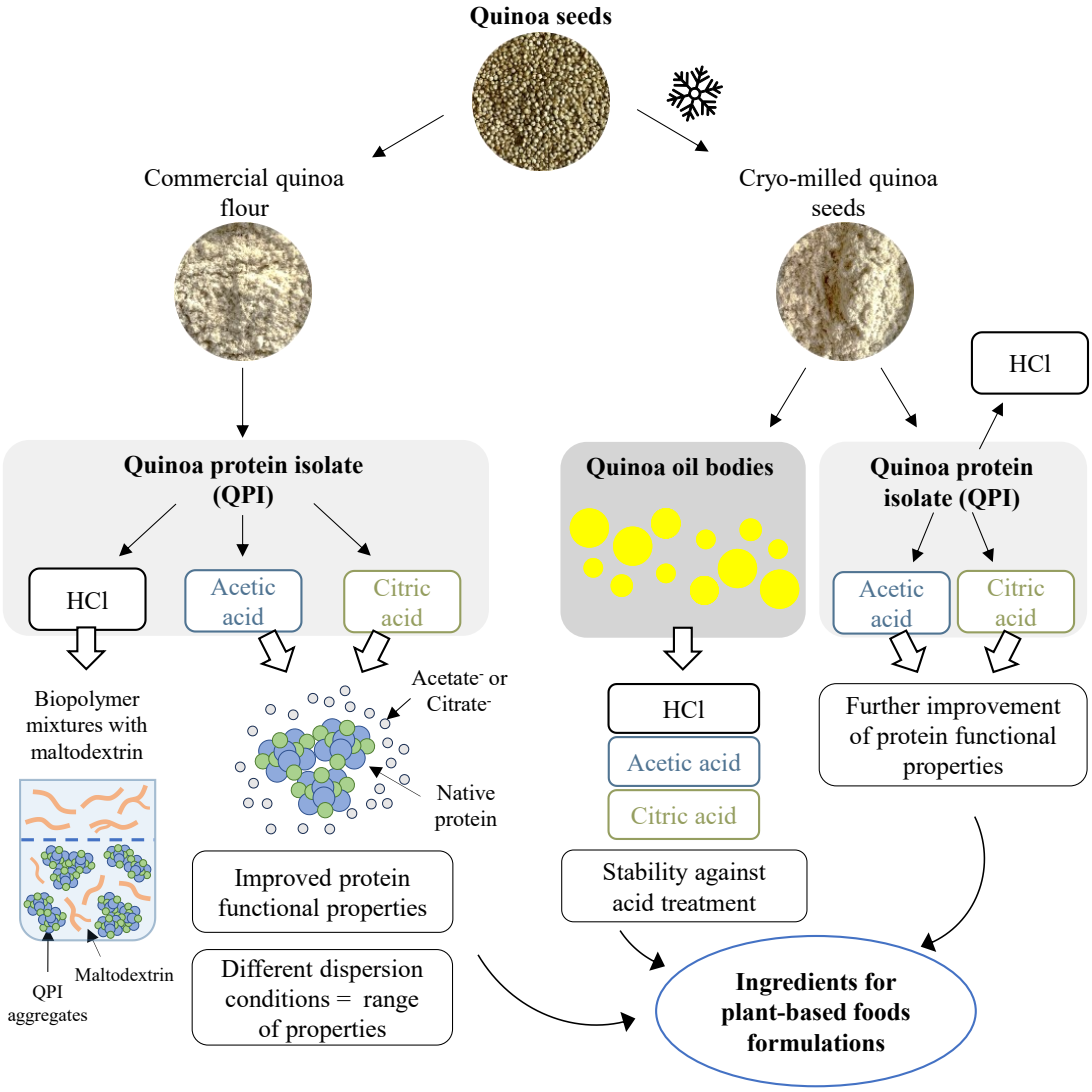

Figure 8-1. Schematic diagram that illustrates the conclusions of this thesis. Strategies to recover quinoa protein isolates and oil bodies as highly functional ingredients for food formulations were developed.

Secondly (Chapter 5), the effect of the acid used during the precipitation step of QPI extraction on the physico-chemical and technofunctional properties of the protein isolate was examined (Figure 8-1). This was investigated as a strategy to modulate or improve protein functionality, as the typically low solubility and gelation capacity of plant proteins can impose challenges in the microstructure design of plant-based foods that aim to substitute animal-based products. Improved soluble protein content, thermal properties

and heat-induced gel strength were achieved simply by substituting the commonly used HCl for a more kosmotropic acid, either acetic acid or citric acid, classified by the Hofmeister series as acids that confer a protection to the native structure of proteins during precipitation. While one previous work investigated the effect of precipitation with HCl, citric acid and malic acid on some structural and functional properties of okara protein isolate (Cai et al., 2020), there are no other reports on the impact of precipitation with different acids on the thermal properties and gelation behaviour of plant proteins. As these properties are determining factors in the use of these proteins in the structuring of food products, the findings of the present research offer an opportunity to better understand and to expand the application range of plant protein isolates. Further, as wet fractionation is the most commonly applied method to extract plant proteins at industry-scale, the strategy developed here can be easily employed to extract other plant proteins with similar results expected based on the kosmotropic effect of the precipitation acids. These findings could help prevent, at least in part, the well-documented loss of functionality of some commercial plant protein isolates that undergo extensive denaturation during extraction and processing, e.g., commercial pea protein isolate.

The effect of the dispersion conditions on functional properties were also evaluated (Chapter 6). It was found that QPI precipitated with HCl requires a longer dispersion time to achieve the same functionality as the samples precipitated with the more kosmotropic acids, while dispersion in 0.1 M NaCl and dialysis before dispersion led to extensive protein aggregation and hindered gel formation. These findings showed for the first time that the functional properties of QPI can be modulated by both precipitation acid and dispersion conditions. A range of different protein structures and heat-induced gel

networks were obtained, broadening the application spectrum for QPI across different textures.

The modulation of its extraction conditions also revealed that QPI can be extracted with a significant content of lipids, ~10 – 30% (w/w), see Section 5.3.1. However, there was a gap in literature pertaining the properties of the lipid fraction of quinoa, with no studies evaluating the extraction and characterisation of quinoa oil bodies, which also show interesting potential application in the formulation of plant-based foods, especially of emulsion-based products. Thus, a strategy was developed to recover oil bodies (OB) from cryo-milled quinoa seeds, based on the knowledge that freezing with liquid nitrogen solidifies oils in the plant matrix. This allowed the recovery of oil bodies of good structural stability before and after acid treatment through creaming and successive centrifugations (Chapter 7, Figure 8-1). These findings demonstrate that quinoa oil bodies can potentially be applied in the formulation of acidic food products, such as yoghurt and kefir. Further, a mass balance showed that cryo-milling of quinoa seeds before wet fractionation resulted in a 2.5-fold increase in OB recovery compared to direct application of wet fractionation using the commercially-sourced flour used in Chapters 5 and 6. Although further studies are necessary, cryo-milling appears to be a promising approach to achieve high OB recoveries, while preserving their structure.

The cryo-milled quinoa seeds were also used for QPI extraction (Chapter 7, Figure 8-1), in which precipitation with the more kosmotropic acids, acetic acid and citric acid, resulted in further improvement of heat-induced gelation properties compared to when the samples were extracted from commercially-sourced quinoa flour. In this approach, the use of citric acid led to even higher soluble protein content, denaturation enthalpy and final gel strength than acetic acid. Results showed that cryo-milling of quinoa seeds can

be used to recover oil bodies and, coupled with the use of citric acid instead of HCl during protein extraction, it can be a preferable strategy to extract QPI of improved functionality.

Overall, the approaches explored in this research contributed to our understanding of the challenges involved in the extraction and use of plant proteins as food ingredients, namely the lack of information on the phase behaviour of these proteins and the loss of functionality during extraction by wet fractionation of some commercial plant protein isolates. The investigation of the phase behaviour of QPI in mixture with maltodextrin provided information on the possibilities for structuring quinoa proteins and uncovered other areas of investigation. The simple change of the acid used during extraction altered QPI material properties, resulting in protein isolates of improved solubility, thermal properties and gelation properties; while the different dispersion conditions provided alternatives to enable the application of QPI in different types of plant-based products to deliver desired textural properties. These findings will likely impact the plant protein field both in terms of research and application at industry-scale, as these insights offer opportunities to: (1) preserve the native structure of plant proteins during large scale extraction, which is key to ensuring the functionally and, consequently, application of these ingredients; and (2) further expand the application of plant proteins to a range of different product textures. Finally, the combined strategy to recover quinoa protein isolate and oil bodies by cryo-milling of quinoa seeds developed in this thesis shows great potential to achieve high recoveries of two highly functional ingredients for food formulations and it is expected to be transferable to other plant protein sources.

8.2 Future work

This thesis has identified areas for future exploration, which include further investigation of the phase behaviour of QPI-polysaccharide mixtures, further characterisation of quinoa oil bodies and their associated proteins, the evaluation of the transferability of the findings of this research to other plant sources and the translation of research findings to industry-scale.

- **Purification of QPI and investigation of its phase behaviour with negatively charged polysaccharides.** As discussed throughout this thesis (see Sections 4.3.1, 5.3.1 and 7.3.3.1), the extraction method used resulted in quinoa protein isolates of relatively high carbohydrate and lipid contents. There is evidence in the literature that indicates that the protein purity of plant protein isolates influences their phase behaviour and microstructure when in mixture with polysaccharides. For example, pea protein isolate purified by ion exchange chromatography to recover the legumin fraction (purity of 80%) showed a segregative phase behaviour in mixture with sodium alginate, showing a water-in-water emulsion microstructure, that is, droplets of soluble protein dispersed in a sodium alginate continuous phase (Mession et al., 2012a). Therefore, it would be interesting to perform the purification of QPI by appropriate methods, such as ultrafiltration and ion-exchange chromatography, to achieve a higher protein content than obtained here (> 80%). The highly pure protein isolate could then be used to create phase diagrams with polysaccharides, where the effect of protein-polysaccharides interactions could be evaluated without the possible interference of other components. Further, maltodextrin is a neutral polysaccharide and, although it is a widely used biopolymer for the

creation of water-in-water emulsions in systems containing highly pure protein solutions, its charge neutrality may have hindered its phase separation when in mixture with QPI. As the proteins in QPI present negative charges at pH 7, it would be interesting to evaluate the phase behaviour of QPI in mixture with negatively charged polysaccharides, as repulsion forces are likely to be more pronounced (Tolstoguzov, 2000b). Possible negatively charged polysaccharides to be investigated include sodium alginate, carrageenan and pectin. It is then likely that water-in-water emulsion microstructures would be formed, which could be further processed to create kinetically trapped microstructures, such as gel particles and fibres, by droplet deformation and gelation of the protein phase under shear (Section 2.2.3).

- **Evaluation of the impact of other dispersion conditions on the functionality of quinoa protein isolates.**

  Chapter 6 explored the effects of several dispersion conditions on the functional properties of QPI. At pH 6.8 ± 0.2, dispersion in 0.1 M NaCl solution seemed to negatively affect the gelation properties of non-dialysed QPI extracted with acetic and citric acid, while it positively contributed to the final gel strength of QPI precipitated with HCl. As the relationship between salt concentration and pH has been shown to impact solubility, thermal properties and gelation capacity of plant proteins (Sun and Arntfield, 2011; Kaspchak et al., 2017; Tanger et al., 2022), future research should further investigate the combination of pH and salt concentration on the functional properties of QPI. A NaCl range of 0.1 – 1.0 M would allow the study of the complete impact of industry-relevant salt

concentrations, while a pH range of 3 – 9 would provide information on the impact of salt concentration at the isoelectric point (~4.5) of QPI proteins, where the charges at the proteins' surface are neutralised and the solubility is at its lowest, as well as bellow it, where the proteins are positively charged, and above it, where the proteins are negatively charged and show increasing solubility with increase in pH value (Ruiz et al., 2016b). A range of results may be expected, as there is little consensus in literature on the impact of pH and salt concentration of the functional properties of plant proteins. For example, one study reported that the increase in salt concentration increased the gel strength of heat-induced quinoa protein gels formed at a pH 3.5, where the protein had low solubility, while it reduced the gel strength of gels formed at pH 7.0 where the protein had high solubility (Kaspchak et al., 2017). Whereas another study showed that increasing NaCl concentration from 0 M to 0.2 M at pH 7.0 decreased solubility but increased final gel strength of quinoa protein gels (Yang et al., 2022b). Thus, a study evaluating the relationship between salt concentration and pH, spanning wide ranges of investigation, would help elucidate the behaviour of these proteins under different conditions, better directing QPI application in product development. Further, wide concentration ranges of other salts should be investigated. For example, $CaCl_2$ is another widely used salt in many food processes but its effect on QPI gelation has been studied only at very low concentrations (< 0.05 M) (Kaspchak et al., 2017; Yang et al., 2022b).

- **Extraction and characterisation of quinoa oil body-associated proteins.** hapter 7 presented a fundamental study on the extraction and characterisation of

quinoa oil bodies. The results provided insights on the role of quinoa oil body-associated proteins, however, in-dept knowledge of their structure-function relationship is still lacking. Oil body-associated proteins are amphiphilic proteins found at the surface of oil bodies and are responsible for their structural stability (Tzen and Huang, 1992; White, Fisk and Gray, 2006; Deleu et al., 2010; Maurer et al., 2013; Cao et al., 2015; Qi et al., 2017). Understanding the physico-chemical properties and structure of these proteins is essential to enable the future application of oil bodies. Thus, future work should focus on their extraction and characterisation from quinoa oil bodies, including evaluation of protein profile by SDS-PAGE (Qi et al., 2017; de Chirico et al., 2018) and assessment of structural changes with pH by surface hydrophobicity, FTIR and/or circular dichroism analyses (Purkrtova et al., 2007; Qi et al., 2017; Gao et al., 2022).

- **Evaluation of the transferability of the combined strategy for oil bodies and protein isolate extraction from cryo-milled seeds to other plant sources, as well as to industry-scale.** While cryo-milling has been recently used as a pre-treatment in the extraction of oils from pumpkin seeds (Balbino et al., 2019) and fennel seeds (Marčac et al., 2023), as well as in the recovery of oil bodies from rapeseeds (di Bari et al., 2018), this thesis is the first report on the combined extraction of both oil bodies and protein isolates from cryo-milled seeds. While it is expected that this strategy is transferrable to other plant sources, it would be interesting for future work to test this hypothesis. Potential targets should have a balanced protein and lipid content, to ensure a good recovery of both ingredients. For example, pea and lentil are increasingly studied sources of plant protein,

however, their lipid content is very low (< 3%, w/w) (Chung et al., 2008). Thus, although the oil bodies extraction developed in this research could still be applied to these plant materials, the oil bodies recovery is expected to be very low. Alternative plant protein sources that have higher a lipid content include soy, chickpea, hemp seed, almond and peanut (Table 8-1); these are therefore interesting candidates for the combined extraction strategy. Further, future work should also focus on the transferability of the combined strategy to industry-scale. The present thesis has shown that cryo-milling has promise as a cost-effective technique, due to its potential to achieve high oil bodies and protein isolates recoveries, while preserving their structure and functionality at laboratory-scale (Chapter 7). However, while there are cryo-mills/cryo-grinders available commercially, mainly for use at laboratory-scale, efforts for the design and development of equipment to enable cryo-milling of plant materials at industry-scale are still lacking, due to the reduced cooling efficiency of large-scale mills (Katiyar, Biswas and Tiwary, 2021). Thus, further investigation on the applicability of this technique for the obtainment of highly functional ingredients for food formulations is needed.

Table 8-1. Protein and lipid contents (%, w/w) of potential targets for the combined strategy for oil bodies and protein isolate extraction.

Plant protein source	Protein content (%, w/w)	Lipid content (%, w/w)	Reference
Soy	34.0 – 43.6	13.8 – 18.9	(Gorissen et al., 2018; Aulia et al., 2023)
Chickpea	21.0 – 25.0	6.5 – 7.1	(Chung et al., 2008; Boye et al., 2010)
Hemp seed	50.0 – 51.0	10.0 – 29.3	(Mihoc et al., 2012; Gorissen et al., 2018; Plati et al., 2021)
Almond	19.5 – 20.0	43.4 – 55.2	(Venkatachalan and Sathe, 2006; Gallier, Gordon and Singh, 2012)
Peanut	21.1 – 26.5	41.3 – 48.7	(Venkatachalan and Sathe, 2006; Hao et al., 2016)

References

Abugoch, L.E., Castro, E., Tapia, C., Añón, M.C., Gajardo, P. and Villarroel, A. (2009) 'Stability of quinoa flour proteins (*Chenopodium quinoa* Willd.) during storage', *International Journal of Food Science and Technology*, 44 (10), pp. 2013–2020. doi:10.1111/j.1365-2621.2009.02023.x.

Abugoch, L.E., Romero, N., Tapia, C.A., Silva, J. and Rivera, M. (2008) 'Study of some physicochemical and functional properties of quinoa (*Chenopodium Quinoa* Willd) protein isolates', *Journal of Agricultural and Food Chemistry*, 56 (12), pp. 4745–4750. doi:10.1021/jf703689u.

Abugoch, L.E., Tapia, C., Villamán, M.C., Yazdani-Pedram, M. and Díaz-Dosque, M. (2011) 'Characterization of quinoa protein-chitosan blend edible films', *Food Hydrocolloids*, 25 (5), pp. 879–886. doi:10.1016/j.foodhyd.2010.08.008.

Agarwal, D., Kim, E.H.J., Feng, L., Wade, C., Moggré, G.-J., Morgenstern, M.P. and Hedderley, D.I. (2023) 'Microstructure, rheological and water mobility behaviour of plant-based protein isolates (pea and quinoa) and locust bean gum mixtures', *Food Research International*, 164, pp. 112311. doi:10.1016/j.foodres.2022.112311.

Aguilera, J.M. (2005) 'Why food micro structure?', *Journal of Food Engineering*, 67 (1–2), pp. 3–11. doi:10.1016/j.jfoodeng.2004.05.050.

Akdogan, H. (1999) 'High moisture food extrusion', *International Journal of Food Science and Technology*, 34 (3), pp. 195–207. doi:10.1046/j.1365-2621.1999.00256.x.

Akharume, F.U., Aluko, R.E. and Adedeji, A.A. (2021) 'Modification of plant proteins for improved functionality: a review', *Comprehensive Reviews in Food Science and Food Safety*, 20 (1), pp. 198–224. doi:10.1111/1541-4337.12688.

Albalasmeh, A.A., Berhe, A.A. and Ghezzehei, T.A. (2013) 'A new method for rapid determination of carbohydrate and total carbon concentrations using UV spectrophotometry', *Carbohydrate Polymers*, 97 (2), pp. 253–261. doi:10.1016/j.carbpol.2013.04.072.

Albertsson, P.-A. and Tjerneld, F. (1994) "Phase diagrams." In Walter, H. and Johansson, G. (eds.) *Methods in enzymology*. Academic Press. pp. pp. 3–13.

Alonso-Miravalles, L. and O'Mahony, J.A. (2018) 'Composition, protein profile and rheological properties of pseudocereal-based protein-rich ingredients', *Foods*, 7 (5). doi:10.3390/foods7050073.

Alrosan, M., Tan, T.-C., Mat Easa, A., Gammoh, S., Alu'datt, M.H., Tranchant, C.C., Almajwal, A.M., Maghaydah, S., Dheyab, M.A., Jameel, M.S., Al-Qaisi, A. and Al Qudsi, F.R. (2023) 'Preparation of lentil and quinoa protein complexes through protein–protein interactions and water kefir–assisted fermentation to improve protein quality and functionality', *Frontiers in Sustainable Food Systems*, 7, pp. 1–12. doi:10.3389/fsufs.2023.1174597.

Alrosan, M., Tan, T., Easa, A.M., Gammoh, S., Kubow, S. and Alu'datt, M.H. (2022) 'Mechanisms of molecular and structural interactions between lentil and quinoa proteins in aqueous solutions induced by pH recycling', *International Journal of Food Science & Technology*, 57 (4), pp. 2039–2050. doi:10.1111/ijfs.15422.

Alvarez-Jubete, L., Arendt, E.K. and Gallagher, E. (2009) 'Nutritive value and chemical composition of pseudocereals as gluten-free ingredients', *International Journal of Food Sciences and Nutrition*, 60 (4), pp. 240–257. doi:10.1080/09637480902950597.

Alvarez-Jubete, L., Arendt, E.K.K. and Gallagher, E. (2010) 'Nutritive value of pseudocereals and their increasing use as functional gluten-free ingredients', *Trends in Food Science and Technology*, 21 (2), pp. 106–113. doi:10.1016/j.tifs.2009.10.014.

Amagliani, L. and Schmitt, C. (2017) 'Globular plant protein aggregates for stabilization of food foams and emulsions', *Trends in Food Science and Technology*, 67, pp. 248–259. doi:10.1016/j.tifs.2017.07.013.

Ando, H., Chen, Y.C., Tang, H., Shimizu, M., Watanabe, K. and Mitsunaga, T. (2002) 'Food components in fractions of quinoa seed', *Food Science and Technology Research*, 8 (1), pp. 80–84. doi:10.3136/fstr.8.80.

Andrade, J., Pereira, C.G., Almeida Junior, J.C. de, Viana, C.C.R., Neves, L.N. de O., Silva, P.H.F. da, Bell, M.J.V. and Anjos, V. de C. dos (2019) 'FTIR-ATR determination of protein content to evaluate whey protein concentrate adulteration', *LWT - Food Science and Technology*, 99, pp. 166–172. doi:10.1016/j.lwt.2018.09.079.

Anton Paar (n.d.) *Basics of rheology*. Available at: https://wiki.anton-paar.com/en/basics-of-rheology/ (Accessed: 13 January 2024).

Antonov, Y.A., Dmitrochenko, A.P. and Leontiev, A.L. (2006) 'Interactions and compatibility of 11 S globulin from *Vicia Faba* seeds and sodium salt of carboxymethylcellulose in an aqueous medium', *International Journal of Biological Macromolecules*, 38 (1), pp. 18–24. doi:10.1016/j.ijbiomac.2005.12.011.

Antonov, Y.A., Grinberg, V.Y., Zhuravskaya, N.A. and Tolstoguzov, V.B. (1980) 'Liquid two-phase water-protein-polysaccharide systems and their processing into textured protein products', *Journal of Texture Studies*, 11, pp. 199–215.

Antonov, Y.A., Lashko, N.P., Glotova, Y.K., Malovikova, A. and Markovich, O. (1996) 'Effect of the structural features of pectins and alginates on their thermodynamic compatibility with gelatin in aqueous media', *Food Hydrocolloids*, 10 (1), pp. 1–9. doi:10.1016/S0268-005X(96)80047-6.

Antonov, Y.A., Losinskaya, N. V., Grinberg, V.Y., Dianova, V.T. and Tolstoguzov, V.B. (1979) 'Phase equilibria in water-protein-polysaccharide systems. III. Water-soy bean globulins-polysaccharide systems', *Colloid and Polymer Science*, 257 (11), pp. 1159–1171. doi:10.1007/BF01517240.

Antonov, Y.A. and Soshinsky, A.A. (2000) 'Interactions and compatibility of ribuloso-1,5-bisphosphate carboxylase/oxygenase from alfalfa with pectin in aqueous medium', *International Journal of Biological Macromolecules*, 27 (4), pp. 279–285. doi:10.1016/S0141-8130(00)00129-X.

Antonov, Y.A. and Wolf, B.A. (2006) 'Phase behavior of aqueous solutions of bovine serum albumin in the presence of dextran, at rest, and under shear', *Biomacromolecules*, 7 (5), pp. 1562–1567. doi:10.1021/bm050899i.

AOAC (2002) *Official methods of analysis*. 17th ed. Horwitz, W. (ed.). Association of Official Analytical Chemists.

Arndt, C., Koristka, S., Feldmann, A. and Bachmann, M. (2019) “Native

polyacrylamide gels.” In Kurien, B.T. and Scofield, R.H. (eds.) *Electrophoretic separation of proteins*. Humana Press. pp. pp. 87–91.

Asgar, M.A., Fazilah, A., Huda, N., Bhat, R. and Karim, A.A. (2010) 'Nonmeat protein alternatives as meat extenders and meat analogs', *Comprehensive Reviews in Food Science and Food Safety*, 9, pp. 513–529. doi:10.1111/j.1541-4337.2010.00124.x.

Atefi, E., Fyffe, D., Kaylan, K.B. and Tavana, H. (2016) 'Characterization of aqueous two phase systems from volume and density measurements', *Journal of Chemical and Engineering Data*, 61 (4), pp. 1531–1539. doi:10.1021/acs.jced.5b00901.

Augustin, M.A. and Cole, M.B. (2022) 'Towards a sustainable food system by design using faba bean protein as an example', *Trends in Food Science and Technology*, 125, pp. 1–11. doi:10.1016/j.tifs.2022.04.029.

Aulia, R., Amanah, H.Z., Lee, H., Kim, M.S., Baek, I., Qin, J. and Cho, B.K. (2023) 'Protein and lipid content estimation in soybeans using Raman hyperspectral imaging', *Frontiers in Plant Science*, 14, pp. 1–12. doi:10.3389/fpls.2023.1167139.

Balbino, S., Dorić, M., Vidaković, S., Kraljić, K., Škevin, D., Drakula, S., Voučko, B., Čukelj, N., Obranović, M. and Ćurić, D. (2019) 'Application of cryogenic grinding pretreatment to enhance extractability of bioactive molecules from pumpkin seed cake', *Journal of Food Process Engineering*, 42 (8), pp. 1–13. doi:10.1111/jfpe.13300.

di Bari, V., de Chirico, S., Bramante, F. and Gray, D.A. (2018) “Cryo-milling as novel processing approach for oil body recovery.” In *1st International Oil Body Conference*. Wageningen, The Netherlands, 2018. p. pp. 19.

Bartashus, J. and Srinivasan, G. (2021) *Plant-based foods poised for explosive growth*. Bloomberg Intelligence: Data-Driven Research report.

Beldengrün, Y., Aragon, J., Prazeres, S.F., Montalvo, G., Miras, J. and Esquena, J. (2018) 'Gelatin/maltodextrin water-in-water (W/W) emulsions for the preparation of cross-linked enzyme-loaded microgels', *Langmuir*, 34 (33), pp. 9731–9743. doi:10.1021/acs.langmuir.8b01599.

Beldengrün, Y., Dallaris, V., Jaén, C., Protat, R., Miras, J., Calvo, M., García-Celma, M.J. and Esquena, J. (2020) 'Formation and stabilization of multiple water-in-water-in-water (W/W/W) emulsions', *Food Hydrocolloids*, 102, pp. 105588. doi:10.1016/j.foodhyd.2019.105588.

Ben-Harb, S., Panouillé, M., Huc-Mathis, D., Moulin, G., Saint-Eve, A., Irlinger, F., Bonnarme, P., Michon, C. and Souchon, I. (2018) 'The rheological and microstructural properties of pea, milk, mixed pea/milk gels and gelled emulsions designed by thermal, acid, and enzyme treatments', *Food Hydrocolloids*, 77, pp. 75–84. doi:10.1016/j.foodhyd.2017.09.022.

Berrazaga, I., Micard, V., Gueugneau, M. and Walrand, S. (2019) 'The role of the anabolic properties of plant-versus animal-based protein sources in supporting muscle mass maintenance: a critical review', *Nutrients*, 11 (8), pp. 1825. doi:10.3390/nu11081825.

de Bock, P., van Bockstaele, F., Muylle, H., Quataert, P., Vermeir, P., Eeckhout, M. and Cnops, G. (2021) 'Yield and nutritional characterization of thirteen quinoa (*Chenopodium quinoa* Willd.) varieties grown in North-West Europe—Part I', *Plants*,

10 (12), pp. 2689. doi:10.3390/plants10122689.

Bogueva, D. and McClements, D.J. (2023) 'Safety and nutritional risks associated with plant-based meat alternatives', *Sustainability*, 15 (19), pp. 14336. doi:10.3390/su151914336.

de Bondt, Y., Liberloo, I., Roye, C., Windhab, E.J., Lamothe, L., King, R. and Courtin, C.M. (2020) 'The effect of wet milling and cryogenic milling on the structure and physicochemical properties of wheat bran', *Foods*, 9 (12), pp. 1–16. doi:10.3390/foods9121755.

de Bont, P.W., van Kempen, G.M.P. and Vreeker, R. (2002) 'Phase separation in milk protein and amylopectin mixtures', *Food Hydrocolloids*, 16 (2), pp. 127–138. doi:10.1016/S0268-005X(01)00070-4.

Bowland, E.L., Allen Foegeding, E. and Hamann, D.D. (1995) 'Rheological analysis of anion-induced matrix transformations in thermally induced whey protein isolate gels', *Food Hydrocolloids*, 9 (1), pp. 57–64. doi:10.1016/S0268-005X(09)80194-X.

Boye, J.I., Aksay, S., Roufik, S., Ribéreau, S., Mondor, M., Farnworth, E. and Rajamohamed, S.H. (2010) 'Comparison of the functional properties of pea, chickpea and lentil protein concentrates processed using ultrafiltration and isoelectric precipitation techniques', *Food Research International*, 43 (2), pp. 537–546. doi:10.1016/j.foodres.2009.07.021.

Brinegar, C. and Goundan, S. (1993) 'Isolation and characterization of chenopodin, the 11S seed storage protein of quinoa (*Chenopodium quinoa*)', *Journal of Agricultural and Food Chemistry*, 41 (2), pp. 182–185. doi:10.1021/jf00026a006.

Brinegar, C., Sine, B. and Nwokocha, L. (1996) 'High-cysteine 2S seed storage proteins from quinoa (*Chenopodium quinoa*)', *Journal of Agricultural and Food Chemistry*, 44 (7), pp. 1621–1623. doi:10.1021/jf950830+.

Brodkorb, A., Croguennec, T., Bouhallab, S. and Kehoe, J.J. (2016) “Heat-induced denaturation, aggregation and gelation of whey proteins.” In *Advanced Dairy Chemistry*. pp. pp. 155–178.

Brown, C.R.T., Foster, T.J., Norton, I.T. and Underdown, J. (1995) “Influence of shear on the microstructure of mixed biopolymer systems.” In Harding, S.E., Hill, S.E. and Mitchell, J.R. (eds.) *Biopolymer mixtures*. Nottingham, UK: Nottingham University Press.

Bryant, C.M. and McClements, D.J. (1998) 'Molecular basis of protein functionality with special consideration of cold-set gels derived from heat-denatured whey', *Trends in Food Science and Technology*, 9 (4), pp. 143–151. doi:10.1016/S0924-2244(98)00031-4.

Burrieza, H.P., López-Fernández, M.P. and Maldonado, S. (2014) 'Analogous reserve distribution and tissue characteristics in quinoa and grass seeds suggest convergent evolution', *Frontiers in Plant Science*, 5, pp. 1–11. doi:10.3389/fpls.2014.00546.

Burrieza, H.P., Rizzo, A.J., Moura Vale, E., Silveira, V. and Maldonado, S. (2019) 'Shotgun proteomic analysis of quinoa seeds reveals novel lysine-rich seed storage globulins', *Food Chemistry*, 293, pp. 299–306. doi:10.1016/j.foodchem.2019.04.098.

Cai, Y., Huang, L., Tao, X., Su, J., Chen, B., Zhao, M., Zhao, Q. and van der Meeren, P.

(2020) 'Adjustment of the structural and functional properties of okara protein by acid precipitation', *Food Bioscience*, 37, pp. 100677. doi:10.1016/j.fbio.2020.100677.

Cao, H., Huang, Q., Wang, C., Guan, X., Huang, K. and Zhang, Y. (2022) 'Effect of compositional interaction on in vitro digestion of starch during the milling process of quinoa', *Food Chemistry*, 403, pp. 134372. doi:10.1016/j.foodchem.2022.134372.

Cao, Y., Zhao, L., Ying, Y., Kong, X., Hua, Y. and Chen, Y. (2015) 'The characterization of soybean oil body integral oleosin isoforms and the effects of alkaline pH on them', *Food Chemistry*, 177, pp. 288–294. doi:10.1016/j.foodchem.2015.01.052.

Carbonaro, M., Maselli, P. and Nucara, A. (2012) 'Relationship between digestibility and secondary structure of raw and thermally treated legume proteins: a Fourier transform infrared (FT-IR) spectroscopic study', *Amino Acids*, 43 (2), pp. 911–921. doi:10.1007/s00726-011-1151-4.

Caro, N., Medina, E., Díaz-Dosque, M., López, L., Abugoch, L. and Tapia, C. (2016) 'Novel active packaging based on films of chitosan and chitosan/quinoa protein printed with chitosan-tripolyphosphate-thymol nanoparticles via thermal ink-jet printing', *Food Hydrocolloids*, 52, pp. 520–532. doi:10.1016/j.foodhyd.2015.07.028.

Cerdán-Leal, M.A., López-Alarcón, C.A., Ortiz-Basurto, R.I., Luna-Solano, G. and Jiménez-Fernández, M. (2020) 'Influence of heat denaturation and freezing–lyophilization on physicochemical and functional properties of quinoa protein isolate', *Cereal Chemistry*, 97 (2), pp. 373–381. doi:10.1002/cche.10253.

Chantanuson, R., Nagamine, S., Kobayashi, T. and Nakagawa, K. (2022) 'Preparation of soy protein-based food gels and control of fibrous structure and rheological property by freezing', *Food Structure*, 32, pp. 100258. doi:10.1016/j.foostr.2022.100258.

Chaudhary, N., Walia, S. and Kumar, R. (2023) 'Functional composition, physiological effect and agronomy of future food quinoa (*Chenopodium quinoa* Willd.): a review', *Journal of Food Composition and Analysis*, 118, pp. 105192. doi:10.1016/j.jfca.2023.105192.

Che Man, Y.B., Syahariza, Z.A. and Rohman, A. (2010) "Fourier transform infrared (FTIR) spectroscopy: development, techniques, and application in the analyses of fats and oils." In Rees, O.J. (ed.) *Fourier transform infrared spectroscopy: developments, techniques and applications*. Nova Science Publishers.

Chen, D., Fang, F., Federici, E., Campanella, O. and Jones, O.G. (2020) 'Rheology, microstructure and phase behavior of potato starch-protein fibril mixed gel', *Carbohydrate Polymers*, 239, pp. 116247. doi:10.1016/j.carbpol.2020.116247.

Chen, F.L., Wei, Y.M., Zhang, B. and Ojokoh, A.O. (2010) 'System parameters and product properties response of soybean protein extruded at wide moisture range', *Journal of Food Engineering*, 96 (2), pp. 208–213. doi:10.1016/j.jfoodeng.2009.07.014.

Chen, J. and Dickinson, E. (1999) 'Effect of surface character of filler particles on rheology of heat-set whey protein emulsion gels', *Colloids and Surfaces B: Biointerfaces*, 12 (3–6), pp. 373–381. doi:10.1016/S0927-7765(98)00091-5.

Chen, N., Zhao, M., Chassenieux, C. and Nicolai, T. (2016) 'Structure of self-assembled native soy globulin in aqueous solution as a function of the concentration and the pH', *Food Hydrocolloids*, 56, pp. 417–424.

doi:https://doi.org/10.1016/j.foodhyd.2015.12.028.

Chen, S., Hall, A.E. and Moraru, C.I. (2023) 'Functionality of pea protein isolate solutions is affected by reconstitution conditions', *Journal of Food Science*, 88 (11), pp. 4630–4638. doi:10.1111/1750-3841.16788.

Chen, X., He, X., Sun, J. and Wang, Z. (2022) 'Phytochemical composition, antioxidant activity, α-glucosidase and acetylcholinesterase inhibitory activity of quinoa extract and its fractions', *Molecules*, 27 (8), pp. 2420. doi:10.3390/molecules27082420.

Chiang, J.H., Loveday, S.M., Hardacre, A.K. and Parker, M.E. (2019) 'Effects of soy protein to wheat gluten ratio on the physicochemical properties of extruded meat analogues', *Food Structure*, 19, pp. 100102. doi:10.1016/j.foostr.2018.11.002.

de Chirico, S., di Bari, V., Foster, T. and Gray, D.A. (2018) 'Enhancing the recovery of oilseed rape seed oil bodies (oleosomes) using bicarbonate-based soaking and grinding media', *Food Chemistry*, 241, pp. 419–426. doi:10.1016/j.foodchem.2017.09.008.

de Chirico, S., di Bari, V., Romero Guzmán, M.J., Nikiforidis, C. V., Foster, T. and Gray, D.A. (2020) 'Assessment of rapeseed oil body (oleosome) lipolytic activity as an effective predictor of emulsion purity and stability', *Food Chemistry*, 316, pp. 126355. doi:10.1016/j.foodchem.2020.126355.

Chronakis, I.S. (1998) 'On the molecular characteristics, compositional properties, and structural-functional mechanisms of maltodextrins: a review', *Critical Reviews in Food Science and Nutrition*, 38 (7), pp. 599–637. doi:10.1080/10408699891274327.

Chronakis, I.S. and Kasapis, S. (1995) 'Preparation and analysis of water continuous very low fat spreads', *LWT - Food Science and Technology*, 28 (5), pp. 488–494. doi:10.1006/fstl.1995.0082.

Chun, J.Y., Hong, G.P., Surassmo, S., Weiss, J., Min, S.G. and Choi, M.J. (2014) 'Study of the phase separation behaviour of native or preheated WPI with polysaccharides', *Polymer*, 55 (16), pp. 4379–4384. doi:10.1016/j.polymer.2014.06.082.

Chung, H.J., Liu, Q., Hoover, R., Warkentin, T.D. and Vandenberg, B. (2008) 'In vitro starch digestibility, expected glycemic index, and thermal and pasting properties of flours from pea, lentil and chickpea cultivars', *Food Chemistry*, 111 (2), pp. 316–321. doi:10.1016/j.foodchem.2008.03.062.

Contreras-Jiménez, B., Torres-Vargas, O.L. and Rodríguez-García, M.E. (2019) 'Physicochemical characterization of quinoa (*Chenopodium quinoa*) flour and isolated starch', *Food Chemistry*, 298, pp. 124982. doi:10.1016/j.foodchem.2019.124982.

Corgneau, M., Gaiani, C., Petit, J., Nikolova, Y., Banon, S., Ritié-Pertusa, L., Le, D.T.L. and Scher, J. (2019) 'Nutritional quality evaluation of commercial protein supplements', *International Journal of Food Science & Technology*, 54 (8), pp. 2586–2594. doi:10.1111/ijfs.14170.

Creusot, N., Wierenga, P.A., Laus, M.C., Giuseppin, M.L.F. and Gruppen, H. (2011) 'Rheological properties of patatin gels compared with β-lactoglobulin, ovalbumin, and glycinin', *Journal of the Science of Food and Agriculture*, 91 (2), pp. 253–261. doi:10.1002/jsfa.4178.

Croll, T., Munro, P.D., Winzor, D.J., Trau, M. and Nielsen, L.K. (2003) 'Quantitative prediction of phase diagrams for polymer partitioning in aqueous two-phase systems',

Journal of Polymer Science Part B: Polymer Physics, 41 (5), pp. 437–443. doi:10.1002/polb.10402.

Dai, S., Jiang, F., Shah, N.P. and Corke, H. (2017) 'Stability and phase behavior of konjac glucomannan-milk systems', *Food Hydrocolloids*, 73, pp. 30–40. doi:10.1016/j.foodhyd.2017.06.025.

Damodaran, S. (1988) 'Refolding of thermally unfolded soy proteins during the cooling regime of the gelation process: effect on gelation', *Journal of Agricultural and Food Chemistry*, 36, pp. 262–269.

Damodaran, S., Parkin, K.L. and Fennema, O.R. (2008) *Fennema's Food Chemistry*. 4th ed. CRC Press.

Davis, K.B., Zhang, Z., Karpova, E.A. and Zhang, J. (2018) 'Application of tyrosine-tryptophan fluorescence resonance energy transfer in monitoring protein size changes', *Analytical Biochemistry*, 557, pp. 142–150. doi:10.1016/j.ab.2018.07.022.

Day, L., Cakebread, J.A. and Loveday, S.M. (2022) 'Food proteins from animals and plants: differences in the nutritional and functional properties', *Trends in Food Science and Technology*, 119, pp. 428–442. doi:10.1016/j.tifs.2021.12.020.

Dekkers, B.L., Nikiforidis, C. V. and van der Goot, A.J. (2016) 'Shear-induced fibrous structure formation from a pectin/SPI blend', *Innovative Food Science and Emerging Technologies*, 36, pp. 193–200. doi:10.1016/j.ifset.2016.07.003.

Deleu, M., Vaca-Medina, G., Fabre, J.F., Roïz, J., Valentin, R. and Mouloungui, Z. (2010) 'Interfacial properties of oleosins and phospholipids from rapeseed for the stability of oil bodies in aqueous medium', *Colloids and Surfaces B: Biointerfaces*, 80 (2), pp. 125–132. doi:10.1016/j.colsurfb.2010.05.036.

Devnani, B., Ong, L., Kentish, S. and Gras, S. (2020) 'Heat induced denaturation, aggregation and gelation of almond proteins in skim and full fat almond milk', *Food Chemistry*, 325, pp. 126901. doi:10.1016/j.foodchem.2020.126901.

Devnani, B., Ong, L., Kentish, S. and Gras, S.L. (2021) 'Structure and functionality of almond proteins as a function of pH', *Food Structure*, 30, pp. 100229. doi:10.1016/j.foostr.2021.100229.

Dickinson, E. (2014) "Understanding food structures: the colloid science approach." In *Food structures, digestion and health*. Elsevier. pp. pp. 3–49. doi:10.1016/B978-0-12-404610-8.00001-3.

Dickinson, E. (2019) 'Particle-based stabilization of water-in-water emulsions containing mixed biopolymers', *Trends in Food Science and Technology*, 83, pp. 31–40. doi:10.1016/j.tifs.2018.11.004.

Dickinson, E. and Chen, J. (1999) 'Heat-set whey protein emulsion gels: Role of active and inactive filler particles', *Journal of Dispersion Science and Technology*, 20 (1–2), pp. 197–213. doi:10.1080/01932699908943787.

Ding, P., Wolf, B., Frith, W.J., Clark, A.H., Norton, I.T. and Pacek, A.W. (2002) 'Interfacial tension in phase-separated gelatin/dextran aqueous mixtures', *Journal of Colloid and Interface Science*, 253 (2), pp. 367–376. doi:10.1006/jcis.2002.8572.

Doublier, J.-L., Garnier, C., Renard, D. and Sanchez, C. (2000) 'Protein-polysaccharide

interactions', *Current Opinion in Colloid and Interface Science*, 5, pp. 171–198. doi:https://doi.org/10.1016/S1359-0294(00)00054-6.

Duran, N.M., Galante, M., Spelzini, D. and Boeris, V. (2018a) 'The effect of carrageenan on the acid-induced aggregation and gelation conditions of quinoa proteins', *Food Research International*, 107, pp. 683–690. doi:10.1016/j.foodres.2018.03.015.

Duran, N.M., Spelzini, D. and Boeris, V. (2019) 'Characterization of acid – induced gels of quinoa proteins and carrageenan', *LWT - Food Science and Technology*, 108, pp. 39–47. doi:10.1016/j.lwt.2019.03.052.

Duran, N.M., Spelzini, D., Wayllace, N., Boeris, V. and Barroso da Silva, F.L. (2018b) 'A combined experimental and molecular simulation study of factors influencing interaction of quinoa proteins–carrageenan', *International Journal of Biological Macromolecules*, 107, pp. 949–956. doi:10.1016/j.ijbiomac.2017.09.076.

Edelman, M.W., van der Linden, E. and Tromp, R.H. (2003) 'Phase separation of aqueous mixtures of poly(ethylene oxide) and dextran', *Macromolecules*, 36 (20), pp. 7783–7790. doi:10.1021/ma0341622.

Edelman, M.W., Tromp, R.H. and van der Linden, E. (2003) 'Phase-separation-induced fractionation in molar mass in aqueous mixtures of gelatin and dextran', *Physical Review E*, 67 (2), pp. 021404. doi:10.1103/PhysRevE.67.021404.

Elliott, A.D. (2020) 'Confocal microscopy: principles and modern practices', *Current Protocols in Cytometry*, 92 (1), pp. 1–18. doi:10.1002/cpcy.68.

Elsohaimy, S.A., Refaay, T.M. and Zaytoun, M.A.M. (2015) 'Physicochemical and functional properties of quinoa protein isolate', *Annals of Agricultural Sciences*, 60 (2), pp. 297–305. doi:10.1016/j.aoas.2015.10.007.

Ercelebi, E.A. and Ibanoğlu, E. (2007) 'Influence of hydrocolloids on phase separation and emulsion properties of whey protein isolate', *Journal of Food Engineering*, 80 (2), pp. 454–459. doi:10.1016/j.jfoodeng.2006.05.027.

Esquena, J. (2016) 'Water-in-water (W/W) emulsions', *Current Opinion in Colloid and Interface Science*, 25, pp. 109–119. doi:10.1016/j.cocis.2016.09.010.

Esquena, J. (2023) 'Recent advances on water-in-water emulsions in segregative systems of two water-soluble polymers', *Current Opinion in Food Science*, 51, pp. 101010. doi:10.1016/j.cofs.2023.101010.

Esteban, B., Riba, J.R., Baquero, G., Rius, A. and Puig, R. (2012) 'Temperature dependence of density and viscosity of vegetable oils', *Biomass and Bioenergy*, 42, pp. 164–171. doi:10.1016/j.biombioe.2012.03.007.

Estivi, L., Pellegrino, L., Hogenboom, J.A., Brandolini, A. and Hidalgo, A. (2022) 'Antioxidants of amaranth, quinoa and buckwheat wholemeals and heat-damage development in pseudocereal-enriched einkorn water biscuits', *Molecules*, 27 (21). doi:10.3390/molecules27217541.

Eubel, H., Braun, H.P. and Millar, A.H. (2005) 'Blue-native PAGE in plants: a tool in analysis of protein-protein interactions', *Plant Methods*, 1 (1), pp. 1–13. doi:10.1186/1746-4811-1-11.

Fan, X., Guo, H., Richel, A., Zhang, L., Liu, C., Qin, P., Blecker, C. and Ren, G. (2023) 'Preparation, physicochemical properties, and formation mechanism of quinoa self-assembled peptide-based hydrogel', *Food Hydrocolloids*, 145, pp. 109139. doi:10.1016/j.foodhyd.2023.109139.

Fang, Y., Zhang, B. and Wei, Y. (2014) 'Effects of the specific mechanical energy on the physicochemical properties of texturized soy protein during high-moisture extrusion cooking', *Journal of Food Engineering*, 121 (1), pp. 32–38. doi:10.1016/j.jfoodeng.2013.08.002.

Felix, M., Camacho-Ocaña, Z., López-Castejón, M.L. and Ruiz-Domínguez, M. (2021) 'Rheological properties of quinoa-based gels. an alternative for vegan diets', *Food Hydrocolloids*, 120, pp. 106827. doi:10.1016/j.foodhyd.2021.106827.

Figueroa-González, J.J., Lobato-Calleros, C., Vernon-Carter, E.J., Aguirre-Mandujano, E., Alvarez-Ramirez, J. and Martínez-Velasco, A. (2022) 'Modifying the structure, physicochemical properties, and foaming ability of amaranth protein by dual pH-shifting and ultrasound treatments', *LWT - Food Science and Technology*, 153, pp. 112561. doi:10.1016/j.lwt.2021.112561.

Fisk, I.D., Linforth, R.S.T., Taylor, A.J. and Gray, D.A. (2011) 'Aroma encapsulation and aroma delivery by oil body suspensions derived from sunflower seeds (*Helianthus annus*)', *European Food Research and Technology*, 232 (5), pp. 905–910. doi:10.1007/s00217-011-1459-z.

Fisk, I.D., White, D.A., Lad, M. and Gray, D.A. (2008) 'Oxidative stability of sunflower oil bodies', *European Journal of Lipid Science and Technology*, 110 (10), pp. 962–968. doi:10.1002/ejlt.200800051.

Forciniti, D., Hall, C.K. and Kula, M.R. (1990) 'Interfacial tension of polyethyleneglycol-dextran-water systems: influence of temperature and polymer molecular weight', *Journal of Biotechnology*, 16 (3), pp. 279–296. doi:https://doi.org/10.1016/0168-1656(90)90042-A.

Föste, M., Elgeti, D., Brunner, A.K., Jekle, M. and Becker, T. (2015) 'Isolation of quinoa protein by milling fractionation and solvent extraction', *Food and Bioproducts Processing*, 96, pp. 20–26. doi:10.1016/j.fbp.2015.06.003.

Frith, W.J. (2010) 'Mixed biopolymer aqueous solutions - phase behaviour and rheology', *Advances in Colloid and Interface Science*, 161 (1–2), pp. 48–60. doi:10.1016/j.cis.2009.08.001.

Gaaloul, S., Turgeon, S.L. and Corredig, M. (2009) 'Influence of shearing on the physical characteristics and rheological behaviour of an aqueous whey protein isolate-κappa-carrageenan mixture', *Food Hydrocolloids*, 23 (5), pp. 1243–1252. doi:10.1016/j.foodhyd.2008.09.011.

Gallier, S., Gordon, K.C. and Singh, H. (2012) 'Chemical and structural characterisation of almond oil bodies and bovine milk fat globules', *Food Chemistry*, 132 (4), pp. 1996–2006. doi:10.1016/j.foodchem.2011.12.038.

Gao, Y., Zheng, Y., Yao, F. and Chen, F. (2022) 'Effects of pH and temperature on the stability of peanut oil bodies: new insights for embedding active ingredients', *Colloids and Surfaces A: Physicochemical and Engineering Aspects*, 654, pp. 130110.

doi:10.1016/j.colsurfa.2022.130110.

Garnier, C., Schorsch, C. and Doublier, J.L. (1995) 'Phase separation in dextran/locust bean gum mixtures', *Carbohydrate Polymers*, 28 (4), pp. 313–317. doi:10.1016/0144-8617(95)00090-9.

Geerts, M.E.J., Dekkers, B.L., van der Padt, A. and van der Goot, A.J. (2018) 'Aqueous fractionation processes of soy protein for fibrous structure formation', *Innovative Food Science and Emerging Technologies*, 45, pp. 313–319. doi:10.1016/j.ifset.2017.12.002.

Gharsallaoui, A., Yamauchi, K., Chambin, O., Cases, E. and Saurel, R. (2010) 'Effect of high methoxyl pectin on pea protein in aqueous solution and at oil/water interface', *Carbohydrate Polymers*, 80 (3), pp. 817–827. doi:10.1016/j.carbpol.2009.12.038.

Ghazani, S.M., Pensini, E., Hargreaves, J., Mata, A., Guldiken, B. and Marangoni, A.G. (2023) 'Oleosome interfacial engineering to enhance their functionality in foods', *Current Research in Food Science*, 6, pp. 100682. doi:10.1016/j.crfs.2023.100465.

Gómez, M.J.R., Prieto, J.M., Sobrado, V.C. and Magro, P.C. (2021) 'Nutritional characterization of six quinoa (*Chenopodium quinoa* Willd) varieties cultivated in Southern Europe', *Journal of Food Composition and Analysis*, 99, pp. 103876. doi:10.1016/j.jfca.2021.103876.

Goormaghtigh, E., Ruysschaert, J.-M. and Raussens, V. (2006) 'Evaluation of the information content in infrared spectra for protein secondary structure determination', *Biophysical Journal*, 90 (8), pp. 2946–2957. doi:10.1529/biophysj.105.072017.

Gorissen, S.H.M., Crombag, J.J.R., Senden, J.M.G., Waterval, W.A.H., Bierau, J., Verdijk, L.B. and van Loon, L.J.C. (2018) 'Protein content and amino acid composition of commercially available plant-based protein isolates', *Amino Acids*, 50 (12), pp. 1685–1695. doi:10.1007/s00726-018-2640-5.

Gower, J., Lubbe, S. and le Roux, N. (2011) *Understanding Biplots*. Wiley. doi:10.1002/9780470973196.

Grabowska, K.J., Zhu, S., Dekkers, B.L., de Ruijter, N.C.A., Gieteling, J. and van der Goot, A.J. (2016) 'Shear-induced structuring as a tool to make anisotropic materials using soy protein concentrate', *Journal of Food Engineering*, 188, pp. 77–86. doi:10.1016/j.jfoodeng.2016.05.010.

Grace, H.P. (1982) 'Dispersion phenomena in high viscosity immiscible fluid systems and application of static mixers as dispersion devices in such systems', *Chemical Engineering Communications*, 14 (3–6), pp. 225–277. doi:10.1080/00986448208911047.

Granado-Rodríguez, S., Maestro-Gaitán, I., Matías, J., Rodríguez, M.J., Calvo Magro, P., Hernandez, L.E., Bolaños, L. and Reguera, M. (2022) 'Changes in nutritional quality-related traits of quinoa seeds under different storage conditions', *Frontiers in Nutrition*, 9, pp. 995250. doi:10.3389/fnut.2022.995250.

Gray, D.A., Payne, G., McClements, D.J., Decker, E.A. and Lad, M. (2010) 'Oxidative stability of *Echium plantagineum* seed oil bodies', *European Journal of Lipid Science and Technology*, 112 (7), pp. 741–749. doi:10.1002/ejlt.200900280.

Grinberg, V.Y. and Tolstoguzov, V.B. (1997) 'Thermodynamic incompatibility of proteins and polysaccharides in solutions', *Food Hydrocolloids*, 11 (2), pp. 145–158.

doi:10.1016/S0268-005X(97)80022-7.

Grossmann, L. and McClements, D.J. (2023) 'Current insights into protein solubility: a review of its importance for alternative proteins', *Food Hydrocolloids*, 137, pp. 108416. doi:10.1016/j.foodhyd.2022.108416.

Grundy, M.M.L., Carrière, F., Mackie, A.R., Gray, D.A., Butterworth, P.J. and Ellis, P.R. (2016) 'The role of plant cell wall encapsulation and porosity in regulating lipolysis during the digestion of almond seeds', *Food and Function*, 7 (1), pp. 69–78. doi:10.1039/c5fo00758e.

Guerreo-Ochoa, M.R., Pedreschi, R. and Chirinos, R. (2015) 'Optimised methodology for the extraction of protein from quinoa (*Chenopodium quinoa* Willd.)', *International Journal of Food Science and Technology*, 50 (8), pp. 1815–1822. doi:10.1111/ijfs.12834.

Guo, Q., Su, J., Yuan, F., Mao, L. and Gao, Y. (2019) 'Preparation, characterization and stability of pea protein isolate and propylene glycol alginate soluble complexes', *LWT - Food Science and Technology*, 101, pp. 476–482. doi:10.1016/j.lwt.2018.11.057.

Hao, J., Li, X., Wang, Q., Lv, W., Zhang, W. and Xu, D. (2022) 'Recent developments and prospects in the extraction, composition, stability, food applications, and in vitro digestion of plant oil bodies', *Journal of the American Oil Chemists' Society*, 99 (8), pp. 635–653. doi:10.1002/aocs.12618.

Hao, L., Chen, F., Xia, Y., Zhang, L. and Xin, Y. (2016) 'Size and charge stability of oil bodies from peanut', *Journal of Chemistry*, 2016, pp. 16–18. doi:10.1155/2016/5808172.

He, X., Wang, B., Zhao, B. and Yang, F. (2022) 'Ultrasonic assisted extraction of quinoa (*Chenopodium quinoa* Willd.) protein and effect of heat treatment on its in vitro digestion characteristics', *Foods*, 11 (5), pp. 771. doi:10.3390/foods11050771.

Hofmeister, F. (1888) 'Zur Lehre von der Wirkung der Salze - Zweite Mittheilung', *Archiv für Experimentelle Pathologie und Pharmakologie*, 24 (4–5), pp. 247–260. doi:doi.org/10.1007/BF01838161.

Höhne, G.W.H., Hemminger, W.F. and Flammersheim, H.-J. (2003) *Differential Scanning Calorimetry*. 2nd ed. Springer. doi:10.1007/978-3-662-06710-9_1.

Hopf, A., Dehghani, F. and Buckow, R. (2023) 'Dry fractionation of plant-based proteins for better meat analogue applications', *Current Food Science and Technology Reports*, 1 (2), pp. 91–98. doi:10.1007/s43555-023-00009-1.

Horton, J.C., Harding, S.E. and Mitchell, J.R. (1991) 'Gel permeation chromatography-multi-angle laser light scattering characterization of the molecular mass distribution of 'Pronova' sodium alginate', *Biochemical Society Transactions*, 19 (2), pp. 510–511. doi:10.1042/bst0190510.

Houde, M., Khodaei, N., Benkerroum, N. and Karboune, S. (2018) 'Barley protein concentrates: extraction, structural and functional properties', *Food Chemistry*, 254, pp. 367–376. doi:10.1016/j.foodchem.2018.01.156.

Huang, A.H.C. (2018) 'Plant lipid droplets and their associated proteins: potential for rapid advances', *Plant Physiology*, 176 (3), pp. 1894–1918. doi:10.1104/pp.17.01677.

Huang, T., Yang, B., Zheng, J., Li, G., Wahlqvist, M.L. and Li, D. (2012) 'Cardiovascular disease mortality and cancer incidence in vegetarians: a meta-analysis and systematic review', *Annals of Nutrition and Metabolism*, 60 (4), pp. 233–240. doi:10.1159/000337301.

Iwanaga, D., Gray, D.A., Decker, E.A., Weiss, J. and McClements, D.J. (2008) 'Stabilization of soybean oil bodies using protective pectin coatings formed by electrostatic deposition', *Journal of Agricultural and Food Chemistry*, 56 (6), pp. 2240–2245. doi:10.1021/jf073060y.

Iwanaga, D., Gray, D.A., Fisk, I.D., Decker, E.A., Weiss, J. and McClements, D.J. (2007) 'Extraction and characterization of oil bodies from soy beans: a natural source of pre-emulsified soybean oil', *Journal of Agricultural and Food Chemistry*, 55 (21), pp. 8711–8716. doi:10.1021/jf071008w.

Jahaniaval, F., Kakuda, Y. and Marcone, M.F. (2000) 'Fatty acid and triacylglycerol compositions of seed oils of five *Amaranthus* accessions and their comparison to other oils', *JAOCS, Journal of the American Oil Chemists' Society*, 77 (8), pp. 847–852. doi:10.1007/s11746-000-0135-0.

Jan, N., Hussain, S.Z., Naseer, B. and Bhat, T.A. (2023) 'Amaranth and quinoa as potential nutraceuticals: a review of anti-nutritional factors, health benefits and their applications in food, medicinal and cosmetic sectors', *Food Chemistry: X*, 18, pp. 100687. doi:10.1016/j.fochx.2023.100687.

Janssen, F., Pauly, A., Rombouts, I., Jansens, K.J.A., Deleu, L.J. and Delcour, J.A. (2017) 'Proteins of amaranth (*Amaranthus* spp.), buckwheat (*Fagopyrum* spp.), and quinoa (*Chenopodium* spp.): a food science and technology perspective', *Comprehensive Reviews in Food Science and Food Safety*, 16 (1), pp. 39–58. doi:10.1111/1541-4337.12240.

Jayaram, S. and Bal, A.K.K. (1991) 'Oleosomes (lipid bodies) in nitrogen-fixing peanut nodules', *Plant, Cell & Environment*, 14 (2), pp. 195–203. doi:10.1111/j.1365-3040.1991.tb01336.x.

Johansson, M., Johansson, D., Ström, A., Rydén, J., Nilsson, K., Karlsson, J., Moriana, R. and Langton, M. (2022) 'Effect of starch and fibre on faba bean protein gel characteristics', *Food Hydrocolloids*, 131, pp. 107741. doi:10.1016/j.foodhyd.2022.107741.

Kanyuck, K.M., Mills, T.B., Norton, I.T. and Norton-Welch, A.B. (2019) 'Temperature influences on network formation of low DE maltodextrin gels', *Carbohydrate Polymers*, 218, pp. 170–178. doi:10.1016/j.carbpol.2019.04.039.

Karefyllakis, D., van der Goot, A.J. and Nikiforidis, C. V. (2019) 'The behaviour of sunflower oleosomes at the interfaces', *Soft Matter*, 15 (23), pp. 4639–4646. doi:10.1039/c9sm00352e.

Karoui, R. (2018) *Spectroscopic technique: mid-infrared (MIR) and Fourier transform mid-infrared (FT-MIR) spectroscopies*. 2nd ed. Elsevier Inc. doi:10.1016/b978-0-12-814264-6.00002-5.

Kasapis, S., Morris, E.R., Norton, I.T. and Brown, C.R.T. (1993a) 'Phase equilibria and gelation in gelatin/maltodextrin systems - Part III: phase separation in mixed gels',

Carbohydrate Polymers, 21 (4), pp. 261–268. doi:10.1016/0144-8617(93)90057-B.

Kasapis, S., Morris, E.R., Norton, I.T. and Clark, A.H. (1993b) 'Phase equilibria and gelation in gelatin/maltodextrin systems - Part I: gelation of individual components', *Carbohydrate Polymers*, 21 (4), pp. 243–248. doi:10.1016/0144-8617(93)90055-9.

Kasapis, S., Morris, E.R., Norton, I.T. and Gidley, M.J. (1993c) 'Phase equilibria and gelation in gelatin/maltodextrin systems - Part II: polymer incompatibility in solution', *Carbohydrate Polymers*, 21 (4), pp. 249–259. doi:10.1016/0144-8617(93)90056-A.

Kaspchak, E., Oliveira, M.A.S. de, Simas, F.F., Franco, C.R.C., Silveira, J.L.M., Mafra, M.R. and Igarashi-Mafra, L. (2017) 'Determination of heat-set gelation capacity of a quinoa protein isolate (*Chenopodium quinoa*) by dynamic oscillatory rheological analysis', *Food Chemistry*, 232, pp. 263–271. doi:10.1016/j.foodchem.2017.04.014.

Katiyar, N.K., Biswas, K. and Tiwary, C.S. (2021) 'Cryomilling as environmentally friendly synthesis route to prepare nanomaterials', *International Materials Reviews*, 66 (7), pp. 493–532. doi:10.1080/09506608.2020.1825175.

Khanmohammadi, M. and Garmarudi, A.B. (2010) "Application of chemometric modeled Fourier transform infrared spectrometric data for diagnostic investigation of cancer via tissue and blood analysis." In Rees, O.J. (ed.) *Fourier transform infrared spectroscopy: developments, techniques and applications*. Nova Science Publishers.

Kharlamova, A., Inthavong, W., Nicolai, T. and Chassenieux, C. (2016) 'The effect of aggregation into fractals or microgels on the charge density and the isoionic point of globular proteins', *Food Hydrocolloids*, 60, pp. 470–475. doi:10.1016/j.foodhyd.2016.04.013.

Kierulf, A., Whaley, J., Liu, W., Enayati, M., Tan, C., Perez-Herrera, M., You, Z. and Abbaspourrad, A. (2020) 'Protein content of amaranth and quinoa starch plays a key role in their ability as Pickering emulsifiers', *Food Chemistry*, 315, pp. 126246. doi:10.1016/j.foodchem.2020.126246.

Kim, H.-J., Decker, E. and McClements, D.J. (2006) 'Preparation of multiple emulsions based on thermodynamic incompatibility of heat-denatured whey protein and pectin solutions', *Food Hydrocolloids*, 20 (5), pp. 586–595. doi:10.1016/j.foodhyd.2005.06.007.

Klinjapo, R. and Krasaekoopt, W. (2018) "Microencapsulation of color and flavor in confectionery products." In Grumezescu, A.M. and Holban, A.M. (eds.) *Natural and artificial flavoring agents and food dyes*. Academic Press. pp. pp. 457–494. doi:10.1016/B978-0-12-811518-3/00014-4.

Klost, M. and Drusch, S. (2019) 'Structure formation and rheological properties of pea protein-based gels', *Food Hydrocolloids*, 94, pp. 622–630. doi:10.1016/j.foodhyd.2019.03.030.

Konishi, Y., Hirano, S., Tsuboi, H. and Wada, M. (2004) 'Distribution of minerals in quinoa (*Chenopodium quinoa* Willd.) seeds', *Bioscience, Biotechnology and Biochemistry*, 68 (1), pp. 231–234. doi:10.1271/bbb.68.231.

Kornet, R., Shek, C., Venema, P., Jan van der Goot, A., Meinders, M. and van der Linden, E. (2021) 'Substitution of whey protein by pea protein is facilitated by specific fractionation routes', *Food Hydrocolloids*, 117, pp. 106691.

doi:10.1016/j.foodhyd.2021.106691.

Koziol, M.J. (1992) 'Chemical composition and nutritional evaluation of quinoa (*Chenopodium quinoa* Willd.)', *Journal of Food Composition and Analysis*, 5, pp. 35–68.

Krintiras, G.A., Göbel, J., van der Goot, A.J. and Stefanidis, G.D. (2015) 'Production of structured soy-based meat analogues using simple shear and heat in a Couette Cell', *Journal of Food Engineering*, 160, pp. 34–41. doi:10.1016/j.jfoodeng.2015.02.015.

Kumar, A. and Venkatesu, P. (2014) 'Does the stability of proteins in ionic liquids obey the Hofmeister series?', *International Journal of Biological Macromolecules*, 63, pp. 244–253. doi:10.1016/j.ijbiomac.2013.10.031.

Kumar, M., Tomar, M., Potkule, J., Verma, R., Punia, S., Mahapatra, A., Belwal, T., Dahuja, A., Joshi, S., Berwal, M.K., Satankar, V., Bhoite, A.G., Amarowicz, R., Kaur, C. and Kennedy, J.F. (2021) 'Advances in the plant protein extraction: mechanism and recommendations', *Food Hydrocolloids*, 115, pp. 106595. doi:10.1016/j.foodhyd.2021.106595.

Kumar, P., Chatli, M.K., Mehta, N., Singh, P., Malav, O.P. and Verma, A.K. (2017) 'Meat analogues: health promising sustainable meat substitutes', *Critical Reviews in Food Science and Nutrition*, 57 (5), pp. 923–932. doi:10.1080/10408398.2014.939739.

Kunz, W., Henle, J. and Ninham, B.W. (2004) '"Zur Lehre von der Wirkung der Salze" (about the science of the effect of salts): Franz Hofmeister's historical papers', *Current Opinion in Colloid and Interface Science*, 9 (1–2), pp. 19–37. doi:10.1016/j.cocis.2004.05.005.

Kurien, B.T. and Scofield, R.H. (2019) *Electrophoretic Separation of Proteins: Methods and Protocols*. Humana Press. Available at: http://www.springer.com/series/7651.

Kyriakopoulou, K., Keppler, J.K. and van der Goot, A.J. (2021) 'Functionality of ingredients and additives in plant-based meat analogues', *Foods*, 10 (3), pp. 600. doi:10.3390/foods10030600.

Kyriakopoulou, K., Keppler, J.K., Van Der Goot, A.J. and Boom, R.M. (2021) "Alternatives to meat and dairy." In *Annual Review of Food Science and Technology*. pp. pp. 29–50. doi:10.1146/annurev-food-062520-101850.

Lam, A.C.Y., Can Karaca, A., Tyler, R.T. and Nickerson, M.T. (2018) 'Pea protein isolates: structure, extraction, and functionality', *Food Reviews International*, 34 (2), pp. 126–147. doi:10.1080/87559129.2016.1242135.

Lan, Y., Chen, B. and Rao, J. (2018) 'Pea protein isolate–high methoxyl pectin soluble complexes for improving pea protein functionality: effect of pH, biopolymer ratio and concentrations', *Food Hydrocolloids*, 80, pp. 245–253. doi:10.1016/j.foodhyd.2018.02.021.

Lan, Y., Ohm, J.-B., Chen, B. and Rao, J. (2020a) 'Phase behavior, thermodynamic and microstructure of concentrated pea protein isolate-pectin mixture: effect of pH, biopolymer ratio and pectin charge density', *Food Hydrocolloids*, 101, pp. 105556. doi:10.1016/j.foodhyd.2019.105556.

Lan, Y., Ohm, J.B., Chen, B. and Rao, J. (2020b) 'Phase behavior and complex

coacervation of concentrated pea protein isolate-beet pectin solution', *Food Chemistry*, 307, pp. 125536. doi:10.1016/j.foodchem.2019.125536.

Li, G., Xu, X. and Zhu, F. (2019) 'Physicochemical properties of dodecenyl succinic anhydride (DDSA) modified quinoa starch', *Food Chemistry*, 300, pp. 125201. doi:10.1016/j.foodchem.2019.125201.

Li, G. and Zhu, F. (2018) 'Quinoa starch: structure, properties, and applications', *Carbohydrate Polymers*, 181, pp. 851–861. doi:10.1016/j.carbpol.2017.11.067.

Li, S., Li, C., Yang, Y., He, X., Zhang, B., Fu, X., Tan, C.P. and Huang, Q. (2019a) 'Starch granules as Pickering emulsifiers: role of octenylsuccinylation and particle size', *Food Chemistry*, 283, pp. 437–444. doi:10.1016/j.foodchem.2019.01.020.

Li, S., Zhang, B., Li, C., Fu, X. and Huang, Q. (2020a) 'Pickering emulsion gel stabilized by octenylsuccinate quinoa starch granule as lutein carrier: role of the gel network', *Food Chemistry*, 305, pp. 125476. doi:10.1016/j.foodchem.2019.125476.

Li, S., Zhang, B., Tan, C.P., Li, C., Fu, X. and Huang, Q. (2019b) 'Octenylsuccinate quinoa starch granule-stabilized Pickering emulsion gels: preparation, microstructure and gelling mechanism', *Food Hydrocolloids*, 91, pp. 40–47. doi:10.1016/j.foodhyd.2019.01.001.

Li, X., Cheng, Y., Yi, C., Hua, Y., Yang, C. and Cui, S. (2009) 'Effect of ionic strength on the heat-induced soy protein aggregation and the phase separation of soy protein aggregate/dextran mixtures', *Food Hydrocolloids*, 23 (3), pp. 1015–1023. doi:10.1016/j.foodhyd.2008.07.024.

Li, X., Deng, F., Hua, Y., Qiu, A., Yang, C. and Cui, S. (2008a) 'Effect of molecular weight of dextran on the phase behavior and microstructure of preheated soy protein/dextran mixtures', *Carbohydrate Polymers*, 72 (1), pp. 160–168. doi:10.1016/j.carbpol.2007.07.037.

Li, X., Hua, Y., Qiu, A., Yang, C. and Cui, S. (2008b) 'Phase behavior and microstructure of preheated soy proteins and κ-carrageenan mixtures', *Food Hydrocolloids*, 22 (5), pp. 845–853. doi:10.1016/j.foodhyd.2007.04.008.

Li, Y., Han, K., Wan, Z. and Yang, X. (2020b) 'Salt reduction in semi-solid food gel via inhomogeneous distribution of sodium-containing coacervate: effect of gum arabic', *Food Hydrocolloids*, 109, pp. 106102. doi:10.1016/j.foodhyd.2020.106102.

Lie-Piang, A., Yang, J., Schutyser, M.A.I., Nikiforidis, C. V. and Boom, R.M. (2023) 'Mild fractionation for more sustainable food ingredients', *Annual Review of Food Science and Technology*, 14, pp. 473–493. doi:10.1146/annurev-food-060721-024052.

Lin, X., Li, S., Yin, J., Chang, F., Wang, C., He, X., Huang, Q. and Zhang, B. (2020) 'Anthocyanin-loaded double Pickering emulsion stabilized by octenylsuccinate quinoa starch: preparation, stability and in vitro gastrointestinal digestion', *International Journal of Biological Macromolecules*, 152, pp. 1233–1241. doi:10.1016/j.ijbiomac.2019.10.220.

Liu, H., Zheng, J., Liu, P. and Zeng, F. (2018) 'Pulverizing processes affect the chemical quality and thermal property of black, white, and green pepper (*Piper nigrum* L.)', *Journal of Food Science and Technology*, 55 (6), pp. 2130–2142. doi:10.1007/s13197-018-3128-8.

Liu, S., Xie, Y., Li, B., Li, S., Yu, W., Ye, A. and Guo, Q. (2023) 'Structural properties of quinoa protein isolate: impact of neutral to high alkaline extraction pH', *Foods*, 12 (13), pp. 1–12. doi:10.3390/foods12132589.

Liu, Y., Li, X., Liu, J., Wei, L., Liu, Y., Lu, F., Wang, W., Li, Q. and Li, Y. (2022) 'Focusing on Hofmeister series: composition, structure and functional properties of pea protein extracted with food-related anions', *Food Hydrocolloids*, 133, pp. 107976. doi:10.1016/j.foodhyd.2022.107976.

Al Loman, A., Callow, N. V., Islam, S.M.M. and Ju, L.K. (2018) 'Single-step enzyme processing of soybeans into intact oil bodies, protein bodies and hydrolyzed carbohydrates', *Process Biochemistry*, 68, pp. 153–164. doi:10.1016/j.procbio.2018.02.015.

Lonnie, M., Hooker, E., Brunstrom, J.M., Corfe, B.M., Green, M.A., Watson, A.W., Williams, E.A., Stevenson, E.J., Penson, S. and Johnstone, A.M. (2018) 'Protein for life: review of optimal protein intake, sustainable dietary sources and the effect on appetite in ageing adults', *Nutrients*, 10 (3), pp. 1–18. doi:10.3390/nu10030360.

Lorén, N. and Hermansson, A.M. (2000) 'Phase separation and gel formation in kinetically trapped gelatin/maltodextrin gels', *International Journal of Biological Macromolecules*, 27 (4), pp. 249–262. doi:10.1016/S0141-8130(00)00127-6.

Loret, C., Meunier, V., Frith, W.J. and Fryer, P.J. (2004) 'Rheological characterisation of the gelation behaviour of maltodextrin aqueous solutions', *Carbohydrate Polymers*, 57 (2), pp. 153–163. doi:10.1016/j.carbpol.2004.03.026.

Loret, C., Schumm, S., Pudney, P.D.A., Frith, W.J. and Fryer, P.J. (2005) 'Phase separation and molecular weight fractionation behaviour of maltodextrin/agarose mixtures', *Food Hydrocolloids*, 19 (3), pp. 557–565. doi:10.1016/j.foodhyd.2004.10.030.

Loret, C.L., Frith, W.J. and Fryer, P.J. (2004) "Mechanical properties of maltodextrin gels: small and large deformation." In *Gums and Stabilisers for the Food Industry 12*. The Royal Society of Chemistry. doi:10.1039/9781847551214-00116.

Loveday, S.M. (2020) 'Plant protein ingredients with food functionality potential', *Nutrition Bulletin*, 45 (3), pp. 321–327. doi:10.1111/nbu.12450.

Luo, L., Cheng, L., Zhang, R. and Yang, Z. (2022a) 'Impact of high-pressure homogenization on physico-chemical, structural, and rheological properties of quinoa protein isolates', *Food Structure*, 32, pp. 100265. doi:10.1016/j.foostr.2022.100265.

Luo, L., Yang, Z., Wang, H., Ashokkumar, M. and Hemar, Y. (2022b) 'Impacts of sonication and high hydrostatic pressure on the structural and physicochemical properties of quinoa protein isolate dispersions at acidic, neutral and alkaline pHs', *Ultrasonics Sonochemistry*, 91, pp. 106232. doi:10.1016/j.ultsonch.2022.106232.

Mäkinen, O.E., Zannini, E. and Arendt, E.K. (2015) 'Modifying the cold gelation properties of quinoa protein isolate: influence of heat-denaturation pH in the alkaline range', *Plant Foods for Human Nutrition*, 70 (3), pp. 250–256. doi:10.1007/s11130-015-0487-4.

Mäkinen, O.E., Zannini, E., Koehler, P. and Arendt, E.K. (2016) 'Heat-denaturation and aggregation of quinoa (*Chenopodium quinoa*) globulins as affected by the pH value',

Food Chemistry, 196, pp. 17–24. doi:10.1016/j.foodchem.2015.08.069.

Maksimovic, V.R., Varkonji-Gasic, E.I., Radovic, S.R. and Savic, A.P. (1996) 'The biosynthesis of 13S buckwheat seed storage protein', *Journal of Plant Physiology*, 147 (6), pp. 759–761. doi:10.1016/S0176-1617(11)81490-2.

Manoj, P., Kasapis, S. and Chronakis, I.S. (1996) 'Gelation and phase separation in maltodextrin-caseinate systems', *Food Hydrocolloids*, 10 (4), pp. 407–420. doi:10.1016/S0268-005X(96)80019-1.

Manski, J.M., van der Goot, A.J. and Boom, R.M. (2007) 'Advances in structure formation of anisotropic protein-rich foods through novel processing concepts', *Trends in Food Science & Technology*, 18 (11), pp. 546–557. doi:10.1016/j.tifs.2007.05.002.

Marčac, N., Balbino, S., Tonković, P., Medved, A.M., Cegledi, E., Dragović, S., Dragović-Uzelac, V. and Repajić, M. (2023) 'Hydrodistillation and steam distillation of fennel seeds essential oil: parameter optimization and application of cryomilling pretreatment', *Processes*, 11 (8), pp. 2354. doi:10.3390/pr11082354.

Martínez-Villaluenga, C., Gulewicz, P., Frias, J., Gulewicz, K. and Vidal-Valverde, C. (2008) 'Assessment of protein fractions of three cultivars of *Pisum sativum* L.: effect of germination', *European Food Research and Technology*, 226 (6), pp. 1465–1478. doi:10.1007/s00217-007-0678-9.

Martínez, E.N. and Añón, M.C. (1996) 'Composition and structural characterization of amaranth protein isolates. an electrophoretic and calorimetric study', *Journal of Agricultural and Food Chemistry*, 44 (9), pp. 2523–2530. doi:10.1021/jf960169p.

Matalanis, A., Jones, O.G. and McClements, D.J. (2011) 'Structured biopolymer-based delivery systems for encapsulation, protection, and release of lipophilic compounds', *Food Hydrocolloids*, 25 (8), pp. 1865–1880. doi:10.1016/j.foodhyd.2011.04.014.

Matos, M., Timgren, A., Sjöö, M., Dejmek, P. and Rayner, M. (2013) 'Preparation and encapsulation properties of double Pickering emulsions stabilized by quinoa starch granules', *Colloids and Surfaces A: Physicochemical and Engineering Aspects*, 423, pp. 147–153. doi:10.1016/j.colsurfa.2013.01.060.

Matsumoto, H., Haniu, H. and Komori, N. (2019) “Determination of protein molecular weights on SDS-PAGE.” In Kurien, B.T. and Scofield, R.H. (eds.) *Electrophoretic Separation of Proteins*. Humana Press. pp. pp. 101–106.

Mattice, K.D. and Marangoni, A.G. (2019) 'Comparing methods to produce fibrous material from zein', *Food Research International*, 128, pp. 108804. doi:10.1016/J.FOODRES.2019.108804.

Maurer, S., Waschatko, G., Schach, D., Zielbauer, B.I., Dahl, J., Weidner, T., Bonn, M. and Vilgis, T.A. (2013) 'The role of intact oleosin for stabilization and function of oleosomes', *Journal of Physical Chemistry B*, 117 (44), pp. 13872–13883. doi:10.1021/jp403893n.

McClements, D.J. (2000) 'Comments on viscosity enhancement and depletion flocculation by polysaccharides', *Food Hydrocolloids*, 14 (2), pp. 173–177. doi:10.1016/S0268-005X(99)00065-X.

McClements, D.J. and Grossmann, L. (2021) 'The science of plant-based foods: constructing next-generation meat, fish, milk, and egg analogs', *Comprehensive Reviews*

in Food Science and Food Safety, 20 (4), pp. 4049–4100. doi:10.1111/1541-4337.12771.

McClements, D.J. and Grossmann, L. (2022) *Next-generation plant-based foods: design, production, and properties*. Springer. doi:10.1007/978-3-030-96764-2.

McSwiney, M., Singh, H. and Campanella, O.H. (1994) 'Thermal aggregation and gelation of bovine β-lactoglobulin', *Topics in Catalysis*, 8 (5), pp. 441–453. doi:10.1016/S0268-005X(09)80087-8.

Medina, E., Caro, N., Abugoch, L., Gamboa, A., Díaz-Dosque, M. and Tapia, C. (2019) 'Chitosan thymol nanoparticles improve the antimicrobial effect and the water vapour barrier of chitosan-quinoa protein films', *Journal of Food Engineering*, 240, pp. 191–198. doi:10.1016/j.jfoodeng.2018.07.023.

Mékaoui, R., Benkaci-Ali, F., Scholl, G. and Eppe, G. (2016) 'Effect of the extraction technique, heating time and cryogenic grinding (N2 at -196°C) on the composition of cumin seeds volatile oil', *Journal of Essential Oil Bearing Plants*, 19 (8), pp. 1903–1919. doi:10.1080/0972060X.2016.1235994.

Meng, G.T. and Ma, C.Y. (2001) 'Thermal properties of *Phaseolus angularis* (red bean) globulin', *Food Chemistry*, 73 (4), pp. 453–460. doi:10.1016/S0308-8146(00)00329-0.

Mession, J.L., Assifaoui, A., Cayot, P. and Saurel, R. (2012a) 'Effect of pea proteins extraction and vicilin/legumin fractionation on the phase behavior in admixture with alginate', *Food Hydrocolloids*, 29 (2), pp. 335–346. doi:10.1016/j.foodhyd.2012.03.003.

Mession, J.L., Assifaoui, A., Lafarge, C., Saurel, R. and Cayot, P. (2012b) 'Protein aggregation induced by phase separation in a pea proteins-sodium alginate-water ternary system', *Food Hydrocolloids*, 28 (2), pp. 333–343. doi:10.1016/j.foodhyd.2011.12.022.

Mession, J.L., Sok, N., Assifaoui, A. and Saurel, R. (2013) 'Thermal denaturation of pea globulins (*Pisum sativum* L.) - Molecular interactions leading to heat-induced protein aggregation', *Journal of Agricultural and Food Chemistry*, 61 (6), pp. 1196–1204. doi:10.1021/jf303739n.

Metrick, M.A. and MacDonald, G. (2015) 'Hofmeister ion effects on the solvation and thermal stability of model proteins lysozyme and myoglobin', *Colloids and Surfaces A: Physicochemical and Engineering Aspects*, 469, pp. 242–251. doi:10.1016/j.colsurfa.2015.01.038.

Mezger, T.G. (2014) *The Rheology Handbook*. 4th ed. Vincentz Network.

Mihoc, M., Pop, G., Alexa, E. and Radulov, I. (2012) 'Nutritive quality of romanian hemp varieties (*Cannabis sativa L.*) with special focus on oil and metal contents of seeds', *Chemistry Central Journal*, 6 (1). doi:10.1186/1752-153X-6-122.

Mir, N.A., Riar, C.S. and Singh, S. (2018) 'Nutritional constituents of pseudo cereals and their potential use in food systems: a review', *Trends in Food Science and Technology*, 75, pp. 170–180. doi:10.1016/j.tifs.2018.03.016.

Mir, N.A., Riar, C.S. and Singh, S. (2019a) 'Effect of pH and holding time on the characteristics of protein isolates from *Chenopodium* seeds and study of their amino acid profile and scoring', *Food Chemistry*, 272, pp. 165–173. doi:10.1016/j.foodchem.2018.08.048.

Mir, N.A., Riar, C.S. and Singh, S. (2019b) 'Structural modification of quinoa seed protein isolates (QPIs) by variable time sonification for improving its physicochemical and functional characteristics', *Ultrasonics Sonochemistry*, 58, pp. 104700. doi:10.1016/j.ultsonch.2019.104700.

Mir, N.A., Riar, C.S. and Singh, S. (2020) 'Structural modification in album (*Chenopodium album*) protein isolates due to controlled thermal modification and its relationship with protein digestibility and functionality', *Food Hydrocolloids*, 103, pp. 105708. doi:10.1016/j.foodhyd.2020.105708.

Mir, N.A., Riar, C.S. and Singh, S. (2021a) 'Improvement in the functional properties of quinoa (*Chenopodium quinoa*) protein isolates after the application of controlled heat-treatment: effect on structural properties', *Food Structure*, 28, pp. 100189. doi:10.1016/j.foostr.2021.100189.

Mir, N.A., Riar, C.S. and Singh, S. (2021b) 'Rheological, structural and thermal characteristics of protein isolates obtained from album (*Chenopodium album*) and quinoa (*Chenopodium quinoa*) seeds', *Food Hydrocolloids for Health*, 1, pp. 100019. doi:10.1016/j.fhfh.2021.100019.

Mir, N.A., Riar, C.S. and Singh, S. (2023) 'Effect of film forming solution pH on antibacterial, antioxidant and structural characteristics of edible films from modified quinoa protein', *Food Hydrocolloids*, 135, pp. 108190. doi:10.1016/j.foodhyd.2022.108190.

Moll, P., Salminen, H., Seitz, O., Schmitt, C. and Weiss, J. (2023) 'Characterization of soluble and insoluble fractions obtained from a commercial pea protein isolate', *Journal of Dispersion Science and Technology*, 44 (13), pp. 2417–2428. doi:10.1080/01932691.2022.2093214.

Morris, V.J. (1986) “Multicomponent gels.” In Phillips, G.O., Williams, P.A. and Wedlock, D.J. (eds.) *Gums and stabilisers for the food industry*. pp. pp. 87–99.

Moschakis, T. and Biliaderis, C.G. (2017) 'Biopolymer-based coacervates: structures, functionality and applications in food products', *Current Opinion in Colloid and Interface Science*, 28, pp. 96–109. doi:10.1016/j.cocis.2017.03.006.

Mudgil, P., Omar, L.S., Kamal, H., Kilari, B.P. and Maqsood, S. (2019) 'Multi-functional bioactive properties of intact and enzymatically hydrolysed quinoa and amaranth proteins', *LWT - Food Science and Technology*, 110, pp. 207–213. doi:https://doi.org/10.1016/j.lwt.2019.04.084.

Mufari, J.R., Gorostegui, H.A., Miranda-Villa, P.P., Bergesse, A.E. and Calandri, E.L. (2020) 'Oxidative stability and characterization of quinoa oil extracted from wholemeal and germ flours', *Journal of the American Oil Chemists' Society*, 97 (1), pp. 57–66. doi:10.1002/aocs.12308.

Murphy, K.M., Matanguihan, J.B., Fuentes, F.F., Gómez-Pando, L.R., Jellen, E.N., Maughan, P.J. and Jarvis, D.E. (2019) “Quinoa breeding and genomics.” In *Plant Breeding Reviews*. pp. pp. 257–320. doi:10.1002/9781119521358.ch7.

Nasrabadi, M.N., Doost, A.S. and Mezzenga, R. (2021) 'Modification approaches of plant-based proteins to improve their techno-functionality and use in food products', *Food Hydrocolloids*, 118, pp. 106789. doi:10.1016/j.foodhyd.2021.106789.

Nechyporuk-Zloy, V. (2022) *Principles of light microscopy: from basic to advanced*. Springer. doi:10.1007/978-3-031-04477-9.

Nguyen, T.D., Lafarge, C., Murat, C., Message, J., Cayot, N. and Saurel, R. (2014) 'Partition of volatile compounds in pea globulin–maltodextrin aqueous two-phase system', *Food Chemistry*, 164, pp. 406–412. doi:10.1016/j.foodchem.2014.05.008.

Nichele, S., Phillips, S.M. and Boaventura, B.C.B. (2022) 'Plant-based food patterns to stimulate muscle protein synthesis and support muscle mass in humans: a narrative review', *Applied Physiology, Nutrition and Metabolism*, 47 (7), pp. 700–710. doi:10.1139/apnm-2021-0806.

Nicolai, T. (2019) 'Gelation of food protein-protein mixtures', *Advances in Colloid and Interface Science*, 270, pp. 147–164. doi:10.1016/j.cis.2019.06.006.

Nikiforidis, C. V. (2019) 'Structure and functions of oleosomes (oil bodies)', *Advances in Colloid and Interface Science*, 274, pp. 102039. doi:10.1016/j.cis.2019.102039.

Nongonierma, A.B., Le Maux, S., Dubrulle, C., Barre, C. and FitzGerald, R.J. (2015) 'Quinoa (*Chenopodium quinoa* Willd.) protein hydrolysates with in vitro dipeptidyl peptidase IV (DPP-IV) inhibitory and antioxidant properties', *Journal of Cereal Science*, 65, pp. 112–118. doi:10.1016/j.jcs.2015.07.004.

Norton, I.T. and Frith, W.J. (2001) 'Microstructure design in mixed biopolymer composites', *Food Hydrocolloids*, 15 (4–6), pp. 543–553. doi:10.1016/S0268-005X(01)00062-5.

Norton, I.T., Smith, C.G., Frith, W.J. and Foster, T.J. (2000) "The production, properties and utilisation of fluid gels." In *Hydrocolloids*. Elsevier. pp. pp. 219–227. doi:10.1016/B978-044450178-3/50088-3.

Norton, J.E., Gonzalez Espinosa, Y., Watson, R.L., Spyropoulos, F. and Norton, I.T. (2015) 'Functional food microstructures for macronutrient release and delivery', *Food and Function*, 6 (3), pp. 663–678. doi:10.1039/c4fo00965g.

Nosworthy, M.G., Franczyk, A.J., Medina, G., Neufeld, J., Appah, P., Utioh, A., Frohlich, P. and House, J.D. (2017) 'Effect of processing on the in vitro and in vivo protein quality of yellow and green split peas (*Pisum sativum*)', *Journal of Agricultural and Food Chemistry*, 65 (35), pp. 7790–7796. doi:10.1021/acs.jafc.7b03597.

O'Kane, F.E., Happe, R.P., Vereijken, J.M., Gruppen, H. and van Boekel, M.A.J.S. (2004) 'Heat-induced gelation of pea legumin: comparison with soybean glycinin', *Journal of Agricultural and Food Chemistry*, 52 (16), pp. 5071–5078. doi:10.1021/jf035215h.

Ochoa-Rivas, A., Nava-Valdez, Y., Serna-Saldívar, S.O. and Chuck-Hernández, C. (2017) 'Microwave and ultrasound to enhance protein extraction from peanut flour under alkaline conditions: effects in yield and functional properties of protein isolates', *Food and Bioprocess Technology*, 10 (3), pp. 543–555. doi:10.1007/s11947-016-1838-3.

Okur, H.I., Hladílková, J., Rembert, K.B., Cho, Y., Heyda, J., Dzubiella, J., Cremer, P.S. and Jungwirth, P. (2017) 'Beyond the Hofmeister series: ion-specific effects on proteins and their biological functions', *Journal of Physical Chemistry B*, 121 (9), pp. 1997–2014. doi:10.1021/acs.jpcb.6b10797.

Olivera-Montenegro, L., Bugarin, A., Marzano, A., Best, I., Zabot, G.L. and Romero, H. (2022) 'Production of protein hydrolysate from quinoa (*Chenopodium quinoa* Willd.): economic and experimental evaluation of two pretreatments using supercritical fluids' extraction and conventional solvent extraction', *Foods*, 11 (7), pp. 1015. doi:10.3390/foods11071015.

Omta, A.W., Kropman, M.F., Woutersen, S. and Bakker, H.J. (2003) 'Negligible effect of ions on the hydrogen-bond structure in liquid water', *Science*, 301 (5631), pp. 347–349. doi:10.1126/science.1084801.

Ong, L., Dagastine, R.R., Kentish, S.E. and Gras, S.L. (2011) 'Microstructure of milk gel and cheese curd observed using cryo scanning electron microscopy and confocal microscopy', *LWT - Food Science and Technology*, 44 (5), pp. 1291–1302. doi:10.1016/j.lwt.2010.12.026.

Ong, L., Pax, A.P., Ong, A., Vongsvivut, J., Tobin, M.J., Kentish, S.E. and Gras, S.L. (2020) 'The effect of pH on the fat and protein within cream cheese and their influence on textural and rheological properties', *Food Chemistry*, 332, pp. 127327. doi:10.1016/j.foodchem.2020.127327.

Opazo-Navarrete, M., Freire, D.T., Boom, R.M., Janssen, A.E.M. and Schutyser, M.A.I. (2018a) 'Dry fractionation of quinoa sweet varieties Atlas and Riobamba for sustainable production of protein and starch fractions', *Journal of Food Composition and Analysis*, 74, pp. 95–101. doi:10.1016/j.jfca.2018.09.009.

Opazo-Navarrete, M., Schutyser, M.A.I., Boom, R.M. and Janssen, A.E.M. (2018b) 'Effect of pre-treatment on in vitro gastric digestion of quinoa protein (*Chenopodium quinoa* Willd.) obtained by wet and dry fractionation', *International Journal of Food Sciences and Nutrition*, 69 (1), pp. 1–11. doi:10.1080/09637486.2017.1332171.

Osborne, T.B. (1907) *'The proteins of the wheat kernel'*. Carnegie Institution of Washington. Available at: http://archive.org/details/cu31924024559167.

Patole, S., Cheng, L. and Yang, Z. (2022) 'Impact of incorporations of various polysaccharides on rheological and microstructural characteristics of heat-induced quinoa protein isolate gels', *Food Biophysics*, 17 (3), pp. 314–323. doi:10.1007/s11483-022-09720-3.

Pax, A.P., Ong, L., Vongsvivut, J., Tobin, M.J., Kentish, S.E. and Gras, S.L. (2019) 'The characterisation of Mozzarella cheese microstructure using high resolution synchrotron transmission and ATR-FTIR microspectroscopy', *Food Chemistry*, 291, pp. 214–222. doi:10.1016/j.foodchem.2019.04.016.

Pelgrom, P.J.M., Vissers, A.M., Boom, R.M. and Schutyser, M.A.I. (2013) 'Dry fractionation for production of functional pea protein concentrates', *Food Research International*, 53 (1), pp. 232–239. doi:10.1016/j.foodres.2013.05.004.

Pernollet, J.C. (1978) 'Protein bodies of seeds: Ultrastructure, biochemistry, biosynthesis and degradation', *Phytochemistry*, 17 (9), pp. 1473–1480. doi:10.1016/S0031-9422(00)94623-5.

Pietsch, V.L., Emin, M.A. and Schuchmann, H.P. (2017) 'Process conditions influencing wheat gluten polymerization during high moisture extrusion of meat analog products', *Journal of Food Engineering*, 198, pp. 28–35.

doi:10.1016/j.jfoodeng.2016.10.027.

Piñuel, L., Boeri, P., Zubillaga, F., Barrio, D.A., Torreta, J., Cruz, A., Vásquez, G., Pinto, A. and Carrillo, W. (2019) 'Production of white, red and black quinoa (*Chenopodium quinoa* Willd Var. Real) protein isolates and its hydrolysates in germinated and non-germinated quinoa samples and antioxidant activity evaluation', *Plants*, 8 (8), pp. 257. doi:10.3390/plants8080257.

Planas, J., Lefebvre, D., Tjerneld, F. and Hahn-Hägerdal, B. (1997) 'Analysis of phase composition in aqueous two-phase systems using a two-column chromatographic method: application to lactic acid production by extractive fermentation', *Biotechnology and Bioengineering*, 54 (4), pp. 303–311. Available at: https://doi.org/10.1002/(SICI)1097-0290(19970520)54:4%3C303::AID-BIT2%3E3.0.CO;2-O.

Plati, F., Ritzoulis, C., Pavlidou, E. and Paraskevopoulou, A. (2021) 'Complex coacervate formation between hemp protein isolate and gum Arabic: formulation and characterization', *International Journal of Biological Macromolecules*, 182, pp. 144–153. doi:10.1016/j.ijbiomac.2021.04.003.

Post, M.J. (2012) 'Cultured meat from stem cells: challenges and prospects', *Meat Science*, 92 (3), pp. 297–301. doi:10.1016/j.meatsci.2012.04.008.

Prego, I., Maldonado, S. and Otegui, M. (1998) 'Seed structure and localization of reserves in *Chenopodium quinoa*', *Annals of Botany*, 82 (4), pp. 481–488. doi:10.1006/anbo.1998.0704.

Przybylski, R., Chauhan, G.S. and Eskin, N.A.M. (1994) 'Characterization of quinoa (*Chenopodium quinoa*) lipids', *Food Chemistry*, 51 (2), pp. 187–192. doi:10.1016/0308-8146(94)90255-0.

Purkrtova, Z., D'Andrea, S., Jolivet, P., Lipovova, P., Kralova, B., Kodicek, M. and Chardot, T. (2007) 'Structural properties of caleosin: a MS and CD study', *Archives of Biochemistry and Biophysics*, 464 (2), pp. 335–343. doi:10.1016/j.abb.2007.04.041.

Qi, B., Ding, J., Wang, Z., Li, Y., Ma, C., Chen, F., Sui, X. and Jiang, L. (2017) 'Deciphering the characteristics of soybean oleosome-associated protein in maintaining the stability of oleosomes as affected by pH', *Food Research International*, 100, pp. 551–557. doi:10.1016/j.foodres.2017.07.053.

Qin, X.-S., Luo, Z.-G., Peng, X.-C., Lu, X.-X. and Zou, Y.-X. (2018) 'Fabrication and characterization of quinoa protein nanoparticle-stabilized food-grade Pickering emulsions with ultrasound treatment: effect of ionic strength on the freeze–thaw stability', *Journal of Agricultural and Food Chemistry*, 66 (31), pp. 8363–8370. doi:10.1021/acs.jafc.8b02407.

Quintero, J., Torres, J.D., Corrales-Garcia, L.L., Ciro, G., Delgado, E. and Rojas, J. (2022) 'Effect of the concentration, pH, and Ca2+ ions on the rheological properties of concentrate proteins from quinoa, lentil, and black bean', *Foods*, 11 (19), pp. 3116. doi:10.3390/foods11193116.

Quiroga, A., Martínez, E.N., Rogniaux, H., Geairon, A. and Añón, M.C. (2010) 'Amaranth (*Amaranthus hypochondriacus*) vicilin subunit structure', *Journal of Agricultural and Food Chemistry*, 58 (24), pp. 12957–12963. doi:10.1021/jf103296n.

Rayner, M., Timgren, A., Sjöö, M. and Dejmek, P. (2012) 'Quinoa starch granules: a candidate for stabilising food-grade Pickering emulsions', *Journal of the Science of Food and Agriculture*, 92 (9), pp. 1841–1847. doi:10.1002/jsfa.5610.

Repo-Carrasco-Valencia, R.A.-M. and Serna, L.A. (2011) 'Quinoa (*Chenopodium quinoa*, Willd.) as a source of dietary fiber and other functional components', *Ciência e Tecnologia de Alimentos*, 31 (1), pp. 225–230. doi:10.1590/S0101-20612011000100035.

Repo-Carrasco, R., Espinoza, C. and Jacobsen, S.E. (2003) 'Nutritional value and use of the andean crops quinoa (*Chenopodium quinoa*) and kañiwa (*Chenopodium pallidicaule*)', *Food Reviews International*, 19 (1–2), pp. 179–189. doi:10.1081/FRI-120018884.

Reuther, F., Damaschun, G., Gernat, C., Schierbaum, F., Kettlitz, B., Radosta, S. and Nothnagel, A. (1984) 'Molecular gelation mechanism of maltodextrins investigated by wide-angle X-ray scattering', *Colloid & Polymer Science*, 262 (8), pp. 643–647. doi:10.1007/BF01452456.

Ries-Kautt, M.M. and Ducruix, A.F. (1989) 'Relative effectiveness of various ions on the solubility and crystal growth of lysozyme.', *The Journal of biological chemistry*, 264 (2), pp. 745–748. doi:10.1016/s0021-9258(19)85005-6.

Ritchie, H., Rosado, P. and Roser, M. (2020) 'Environmental impacts of food production', *Published online at OurWorldInData.org.* Available at: https://ourworldindata.org/environmental-impacts-of-food.

Romero-Guzmán, M.J., Jung, L., Kyriakopoulou, K., Boom, R.M. and Nikiforidis, C. V. (2020a) 'Efficient single-step rapeseed oleosome extraction using twin-screw press', *Journal of Food Engineering*, 276. doi:10.1016/j.jfoodeng.2019.109890.

Romero-Guzmán, M.J., Petris, V., de Chirico, S., di Bari, V., Gray, D.A., Boom, R.M. and Nikiforidis, C. V. (2020b) 'The effect of monovalent (Na+, K+) and divalent (Ca2+, Mg2+) cations on rapeseed oleosome (oil body) extraction and stability at pH 7', *Food Chemistry*, 306, pp. 125578. doi:10.1016/j.foodchem.2019.125578.

Ross-Murphy, S.B. (1994) 'Rheological characterization of polymer gels and networks', *Polymer Gels and Networks*, 2 (3–4), pp. 229–237. doi:10.1016/0966-7822(94)90007-8.

Ruales, J. and Nair, B.M. (1992) 'Nutritional quality of the protein in quinoa (*Chenopodium quinoa*, Willd) seeds', *Plant Foods for Human Nutrition*, 42 (1), pp. 1–11. doi:10.1007/BF02196067.

Ruales, J. and Nair, B.M. (1993) 'Content of fat, vitamins and minerals in quinoa (*Chenopodium quinoa*, Willd) seeds', *Food Chemistry*, 48 (2), pp. 131–136. doi:10.1016/0308-8146(93)90047-J.

Ruiz-Capillas, C. and Herrero, A.M. (2024) "Non-meat proteins." In *Encyclopedia of Meat Sciences*. 3rd ed. Elsevier. pp. pp. 368–381. doi:10.1016/b978-0-323-85125-1.00085-5.

Ruiz, G.A., Opazo-Navarrete, M., Meurs, M., Minor, M., Sala, G., van Boekel, M., Stieger, M. and Janssen, A.E.M. (2016a) 'Denaturation and in vitro gastric digestion of heat-treated quinoa protein isolates obtained at various extraction pH', *Food Biophysics*, 11 (2), pp. 184–197. doi:10.1007/s11483-016-9429-4.

Ruiz, G.A., Xiao, W., van Boekel, M., Minor, M. and Stieger, M. (2016b) 'Effect of extraction pH on heat-induced aggregation, gelation and microstructure of protein isolate from quinoa (*Chenopodium quinoa* Willd)', *Food Chemistry*, 209, pp. 203–210. doi:10.1016/j.foodchem.2016.04.052.

Saavedra-Leos, Z., Leyva-Porras, C., Araujo-Díaz, S.B., Toxqui-Terán, A. and Borrás-Enríquez, A.J. (2015) 'Technological application of maltodextrins according to the degree of polymerization', *Molecules*, 20 (12), pp. 21067–21081. doi:10.3390/molecules201219746.

Salminen, H., Sachs, M., Schmitt, C. and Weiss, J. (2022) 'Complex coacervation and precipitation between soluble pea proteins and apple pectin', *Food Biophysics*, 17 (3), pp. 460–471. doi:10.1007/s11483-022-09726-x.

Salt, D.J., Leslie, R.B., Lillford, P.J. and Dunnill, P. (1982) 'Factors influencing protein structure during acid precipitation: a study of soya proteins', *European Journal of Applied Microbiology and Biotechnology*, 14 (3), pp. 144–148. doi:10.1007/BF00497890.

Samard, S., Gu, B.Y. and Ryu, G.H. (2019) 'Effects of extrusion types, screw speed and addition of wheat gluten on physicochemical characteristics and cooking stability of meat analogues', *Journal of the Science of Food and Agriculture*, 99 (11), pp. 4922–4931. doi:10.1002/jsfa.9722.

Samard, S. and Ryu, G.H. (2019) 'Physicochemical and functional characteristics of plant protein-based meat analogs', *Journal of Food Processing and Preservation*, 43 (10), pp. 1–11. doi:10.1111/jfpp.14123.

Sánchez-Reséndiz, A.I., Escalante-Aburto, A., Andía-Ayme, V. and Chuck-Hernández, C. (2019) 'Structural properties, functional evaluation, and in vitro protein digestibility of black and yellow quinoa (*Chenopodium petiolare*) protein isolates', *CyTA - Journal of Food*, 17 (1), pp. 864–872. doi:10.1080/19476337.2019.1669714.

Sarbon, N.M., Badii, F. and Howell, N.K. (2015) 'The effect of chicken skin gelatin and whey protein interactions on rheological and thermal properties', *Food Hydrocolloids*, 45, pp. 83–92. doi:10.1016/j.foodhyd.2014.10.008.

Sarkar, A. and Dickinson, E. (2020) 'Sustainable food-grade Pickering emulsions stabilized by plant-based particles', *Current Opinion in Colloid and Interface Science*, 49, pp. 69–81. doi:10.1016/j.cocis.2020.04.004.

Sarkis, J.R., Boussetta, N., Blouet, C., Tessaro, I.C., Marczak, L.D.F. and Vorobiev, E. (2015) 'Effect of pulsed electric fields and high voltage electrical discharges on polyphenol and protein extraction from sesame cake', *Innovative Food Science and Emerging Technologies*, 29, pp. 170–177. doi:10.1016/j.ifset.2015.02.011.

Scarborough, P., Appleby, P.N., Mizdrak, A., Briggs, A.D.M., Travis, R.C., Bradbury, K.E. and Key, T.J. (2014) 'Dietary greenhouse gas emissions of meat-eaters, fish-eaters, vegetarians and vegans in the UK', *Climatic Change*, 125 (2), pp. 179–192. doi:10.1007/s10584-014-1169-1.

Schierbaum, F., Radosta, S., Vorwerg, W., Yuriev, V.P., Braudo, E.E. and German, M.L. (1992) 'Formation of thermally reversible maltodextrin gels as revealed by low resolution H-NMR', *Carbohydrate Polymers*, 18 (3), pp. 155–163. doi:10.1016/0144-

8617(92)90059-Y.

Schmitt, C., Bovetto, L., Buczkowski, J., De Oliveira Reis, G., Pibarot, P., Amagliani, L. and Dombrowski, J. (2021) 'Plant proteins and their colloidal state', *Current Opinion in Colloid and Interface Science*, 56, pp. 101510. doi:10.1016/j.cocis.2021.101510.

Scholten, E., Tuinier, R., Tromp, R.H. and Lekkerkerker, H.N.W. (2002) 'Interfacial tension of a decomposed biopolymer mixture', *Langmuir*, 18 (6), pp. 2234–2238. doi:10.1021/la0114373.

Schreuders, F.K.G., Dekkers, B.L., Bodnár, I., Erni, P., Boom, R.M. and van der Goot, A.J. (2019) 'Comparing structuring potential of pea and soy protein with gluten for meat analogue preparation', *Journal of Food Engineering*, 261, pp. 32–39. doi:10.1016/j.jfoodeng.2019.04.022.

Schutyser, M.A.I. and van der Goot, A.J. (2011) 'The potential of dry fractionation processes for sustainable plant protein production', *Trends in Food Science & Technology*, 22 (4), pp. 154–164. doi:10.1016/j.tifs.2010.11.006.

Scopes, R.K. (1994) *Protein purification: principles and practice*. 3rd ed. New York, NY: Springer Advanced Texts in Chemistry.

Semenova, M.G. (2007) 'Thermodynamic analysis of the impact of molecular interactions on the functionality of food biopolymers in solution and in colloidal systems', *Food Hydrocolloids*, 21, pp. 23–45. doi:https://doi.org/10.1016/j.foodhyd.2006.02.009.

Şen, A., Acevedo-Fani, A., Dave, A., Ye, A., Husny, J. and Singh, H. (2024) 'Plant oil bodies and their membrane components: new natural materials for food applications', *Critical Reviews in Food Science and Nutrition*, 64 (2), pp. 256–279. doi:10.1080/10408398.2022.2105808.

Sharma, L.K., Agarwal, D., Rathore, S.S., Malhotra, S.K. and Saxena, S.N. (2016) 'Effect of cryogenic grinding on volatile and fatty oil constituents of cumin (*Cuminum cyminum* L.) genotypes', *Journal of Food Science and Technology*, 53 (6), pp. 2827–2834. doi:10.1007/s13197-016-2258-0.

Shen, Y., Tang, X. and Li, Y. (2021) 'Drying methods affect physicochemical and functional properties of quinoa protein isolate', *Food Chemistry*, 339, pp. 127823. doi:10.1016/j.foodchem.2020.127823.

Shen, Z.-J., Xu, S.-X., Huang, Q.-Y., Li, Z.-Y., Xu, Y.-D., Lin, C.-S. and Huang, Y.-J. (2022) 'TMT proteomics analysis of a pseudocereal crop, quinoa (*Chenopodium quinoa* Willd.), during seed maturation', *Frontiers in Plant Science*, 13, pp. 1–17. doi:10.3389/fpls.2022.975073.

Sheppard, C.J.R. and Shotton, D.M. (1997) *Confocal Laser Scanning Microscopy*. BIOS Scientific Publishers.

Shimada, T.L. and Hara-Nishimura, I. (2015) 'Leaf oil bodies are subcellular factories producing antifungal oxylipins', *Current Opinion in Plant Biology*, 25, pp. 145–150. doi:10.1016/j.pbi.2015.05.019.

Silva, D.F.C., Azevedo, A.M., Fernandes, P., Chu, V., Conde, J.P. and Aires-Barros, M.R. (2014) 'Determination of aqueous two phase system binodal curves using a microfluidic device', *Journal of Chromatography A*, 1370, pp. 115–120.

doi:10.1016/j.chroma.2014.10.035.

Sim, S.Y.J., SRV, A., Chiang, J.H. and Henry, C.J. (2021) 'Plant proteins for future foods: a roadmap', *Foods*, 10 (8), pp. 1967. doi:10.3390/foods10081967.

Simeone, M., Alfani, A. and Guido, S. (2004) 'Phase diagram, rheology and interfacial tension of aqueous mixtures of Na-caseinate and Na-alginate', *Food Hydrocolloids*, 18 (3), pp. 463–470. doi:10.1016/j.foodhyd.2003.08.004.

Singh, K.K. and Goswami, T.K. (1999) 'Design of a cryogenic grinding system for spices', *Journal of Food Engineering*, 39 (4), pp. 359–368. doi:10.1016/S0260-8774(98)00172-1.

Singh, T.P., Siddiqi, R.A. and Sogi, D.S. (2021) 'Enzymatic modification of rice bran protein: impact on structural, antioxidant and functional properties', *LWT - Food Science and Technology*, 138, pp. 110648. doi:10.1016/j.lwt.2020.110648.

Smith, B.C. (2011) *Fundamentals of Fourier transform infrared spectroscopy*. Taylor & Francis Group.

Sperry, P.R. (1984) 'Morphology and mechanism in latex flocculated by volume restriction', *Journal of Colloid And Interface Science*, 99 (1), pp. 97–108. doi:10.1016/0021-9797(84)90089-4.

Spyropoulos, F., Portsch, A. and Norton, I.T. (2010) 'Effect of sucrose on the phase and flow behaviour of polysaccharide/protein aqueous two-phase systems', *Food Hydrocolloids*, 24 (2–3), pp. 217–226. doi:10.1016/j.foodhyd.2009.09.008.

Steffolani, M.E., Villacorta, P., Morales-Soriano, E.R., Repo-Carrasco, R., León, A.E. and Pérez, G.T. (2016) 'Physicochemical and functional characterization of protein isolated from different quinoa varieties (*Chenopodium quinoa* Willd.)', *Cereal Chemistry Journal*, 93 (3), pp. 275–281. doi:10.1094/CCHEM-04-15-0083-R.

Stokes, G.G. (1850) 'On the effect of the internal friction of fluids on the motion of pendulums', *Transactions of the Cambridge Philosophical Society*, 9 (1), pp. part ii: 8–106. doi:10.1007/BF03017698.

Sun, C., Ge, J., He, J., Gan, R. and Fang, Y. (2021) 'Processing, quality, safety, and acceptance of meat analogue products', *Engineering*, 7 (5), pp. 674–678. doi:10.1016/j.eng.2020.10.011.

Sun, X.D. and Arntfield, S.D. (2010) 'Gelation properties of salt-extracted pea protein induced by heat treatment', *Food Research International*, 43 (2), pp. 509–515. doi:10.1016/j.foodres.2009.09.039.

Sun, X.D. and Arntfield, S.D. (2011) 'Dynamic oscillatory rheological measurement and thermal properties of pea protein extracted by salt method: effect of pH and NaCl', *Journal of Food Engineering*, 105 (3), pp. 577–582. doi:10.1016/j.jfoodeng.2011.03.008.

Sun, X.D. and Arntfield, S.D. (2012) 'Molecular forces involved in heat-induced pea protein gelation: effects of various reagents on the rheological properties of salt-extracted pea protein gels', *Food Hydrocolloids*, 28 (2), pp. 325–332. doi:10.1016/j.foodhyd.2011.12.014.

Tang, C.-H. (2008) 'Thermal denaturation and gelation of vicilin-rich protein isolates

from three *Phaseolus* legumes: a comparative study', *LWT - Food Science and Technology*, 41 (8), pp. 1380–1388. doi:10.1016/j.lwt.2007.08.025.

Tang, Y., Li, X., Chen, P.X., Zhang, B., Hernandez, M., Zhang, H., Marcone, M.F., Liu, R. and Tsao, R. (2015) 'Characterisation of fatty acid, carotenoid, tocopherol/tocotrienol compositions and antioxidant activities in seeds of three *Chenopodium quinoa* Willd. genotypes', *Food Chemistry*, 174, pp. 502–508. doi:10.1016/j.foodchem.2014.11.040.

Tang, Y. and Tsao, R. (2017) 'Phytochemicals in quinoa and amaranth grains and their antioxidant, anti-inflammatory, and potential health beneficial effects: a review', *Molecular Nutrition and Food Research*, 61 (7), pp. 1–16. doi:10.1002/mnfr.201600767.

Tanger, C., Engel, J. and Kulozik, U. (2020) 'Influence of extraction conditions on the conformational alteration of pea protein extracted from pea flour', *Food Hydrocolloids*, 107, pp. 105949. doi:10.1016/j.foodhyd.2020.105949.

Tanger, C., Müller, M., Andlinger, D. and Kulozik, U. (2022) 'Influence of pH and ionic strength on the thermal gelation behaviour of pea protein', *Food Hydrocolloids*, 123, pp. 106903. doi:10.1016/j.foodhyd.2021.106903.

Taylor, G.I. (1934) 'The formation of emulsions in definable fields of flow', *Proceedings of the Royal Society of London. Series A, Containing Papers of a Mathematical and Physical Character*, 146 (858), pp. 501–523. doi:10.1098/rspa.1934.0169.

Timgren, A., Rayner, M., Dejmek, P., Marku, D. and Sjöö, M. (2013) 'Emulsion stabilizing capacity of intact starch granules modified by heat treatment or octenyl succinic anhydride', *Food Science & Nutrition*, 1 (2), pp. 157–171. doi:10.1002/fsn3.17.

Toapanta, A., Carpio, C., Vilcacundo, R. and Carrillo, W. (2016) 'Analysis of protein isolate from quinoa (*Chenopodium quinoa*)', *Asian Journal of Pharmaceutical and Clinical Research*, 9 (2), pp. 332–334.

Tolstoguzov, V. (2000a) 'Compositions and phase diagrams for aqueous systems based on proteins and polysaccharides', *International Review of Cytology*, 192.

Tolstoguzov, V. (2000b) 'Phase behaviour of macromolecular components in biological and food systems', *Nahrung - Food*, 44 (5), pp. 299–308. doi:10.1002/1521-3803(20001001)44:5<299::AID-FOOD299>3.0.CO;2-9.

Tolstoguzov, V. (2002) 'Thermodynamic aspects of biopolymer functionality in biological systems, foods, and beverages', *Critical Reviews in Biotechnology*, 22 (2), pp. 89–174. doi:10.1080/07388550290789478.

Tolstoguzov, V. (2003) 'Some thermodynamic considerations in food formulation', *Food Hydrocolloids*, 17, pp. 1.

Tolstoguzov, V.B., Mzhel'sky, A.I. and Gulov, V.Y. (1974) 'Deformation of emulsion droplets in flow', *Colloid and Polymer Science Kolloid-Zeitschrift & Zeitschrift für Polymere*, 252 (2), pp. 124–132. doi:10.1007/BF01555536.

Torres, M., Martínez, M., Pierantozzi, P., Albanese, M., Nasjleti, A. and Maestri, D. (2011) 'Contribution of compositional parameters to the oxidative stability of olive and walnut oil blends', *Journal of the American Oil Chemists' Society*, 88 (6), pp. 755–762. doi:10.1007/s11746-010-1735-2.

Tuinier, R., Dhont, J.K.G. and de Kruif, C.G. (2000) 'Depletion-induced phase separation of aggregated whey protein colloids by an exocellular polysaccharide', *Langmuir*, 16 (4), pp. 1497–1507. doi:10.1021/la990202c.

Tzen, J.T.C. (2012) 'Integral proteins in plant oil bodies', *ISRN Botany*, 2012, pp. 1–16. doi:10.5402/2012/173954.

Tzen, J.T.C., Cao, Y.Z., Laurent, P., Ratnayake, C. and Huang, A.H.C. (1993) 'Lipids, proteins, and structure of seed oil bodies from diverse species', *Plant Physiology*, 101 (1), pp. 267–276. doi:10.1104/pp.101.1.267.

Tzen, J.T.C. and Huang, A.H.C. (1992) 'Surface structure and properties of plant seed oil bodies', *Journal of Cell Biology*, 117 (2), pp. 327–335. doi:10.1083/jcb.117.2.327.

Tzen, J.T.C., Peng, C.C., Cheng, D.J., Chen, E.C.F. and Chiu, J.M.H. (1997) 'A new method for seed oil body purification and examination of oil body integrity following germination', *Journal of Biochemistry*, 121 (4), pp. 762–768. doi:10.1093/oxfordjournals.jbchem.a021651.

United Nations Department of Economic and Social affairs (2015) *World Population Prospects: The 2015 Revision*.

Uruakpa, F.O. and Arntfield, S.D. (2004) 'Rheological characteristics of commercial canola protein isolate-κ-carrageenan systems', *Food Hydrocolloids*, 18 (3), pp. 419–427. doi:10.1016/j.foodhyd.2003.07.001.

Valenzuela, C., Abugoch, L., Tapia, C. and Gamboa, A. (2013) 'Effect of alkaline extraction on the structure of the protein of quinoa (*Chenopodium quinoa* Willd.) and its influence on film formation', *International Journal of Food Science and Technology*, 48 (4), pp. 843–849. doi:10.1111/ijfs.12035.

Venkatachalan, M. and Sathe, S.K. (2006) 'Chemical composition of selected edible nut seeds', *Journal of Agricultural and Food Chemistry*, 54 (13), pp. 4705–4714. doi:10.1021/jf0606959.

Vera, A., Valenzuela, M.A., Yazdani-Pedram, M., Tapia, C. and Abugoch, L. (2019) 'Conformational and physicochemical properties of quinoa proteins affected by different conditions of high-intensity ultrasound treatments', *Ultrasonics Sonochemistry*, 51, pp. 186–196. doi:10.1016/j.ultsonch.2018.10.026.

Veraverbeke, W.S. and Delcour, J.A. (2002) 'Wheat protein composition and properties of wheat glutenin in relation to breadmaking functionality', *Critical Reviews in Food Science and Nutrition*, 42 (3), pp. 179–208. doi:10.1080/10408690290825510.

Verboven, P., Defraeye, T. and Nicolai, B. (2018) “Measurement and visualization of food microstructure: fundamentals and recent advances.” In *Food microstructure and its relationship with quality and stability*. Elsevier. pp. pp. 3–28. doi:10.1016/B978-0-08-100764-8.00001-0.

Vilcacundo, R. and Hernández-Ledesma, B. (2017) 'Nutritional and biological value of quinoa (*Chenopodium quinoa* Willd.)', *Current Opinion in Food Science*, 14, pp. 1–6. doi:10.1016/j.cofs.2016.11.007.

van de Vondel, J., Lambrecht, M.A. and Delcour, J.A. (2020) 'Osborne extractability and chromatographic separation of protein from quinoa (*Chenopodium quinoa* Willd.) wholemeal', *LWT - Food Science and Technology*, 126, pp. 109321.

doi:10.1016/j.lwt.2020.109321.

van de Vondel, J., Lambrecht, M.A. and Delcour, J.A. (2022) 'Heat-induced denaturation and aggregation of protein in quinoa (*Chenopodium quinoa* Willd.) seeds and whole meal', *Food Chemistry*, 372, pp. 131330. doi:10.1016/j.foodchem.2021.131330.

van de Vondel, J., Lambrecht, M.A., Housmans, J.A.J., Rousseau, F., Schymkowitz, J. and Delcour, J.A. (2021) 'Impact of hydrothermal treatment on denaturation and aggregation of water-extractable quinoa (*Chenopodium quinoa* Willd.) protein', *Food Hydrocolloids*, 115, pp. 106611. doi:10.1016/j.foodhyd.2021.106611.

de Vries, A., Gomez, Y.L., Jansen, B., van der Linden, E. and Scholten, E. (2017) 'Controlling agglomeration of protein aggregates for structure formation in liquid oil: a sticky business', *ACS Applied Materials and Interfaces*, 9 (11), pp. 10136–10147. doi:10.1021/acsami.7b00443.

Walls, H.J., Caines, S.B., Sanchez, A.M. and Khan, S.A. (2003) 'Yield stress and wall slip phenomena in colloidal silica gels', *Journal of Rheology*, 47 (4), pp. 847–868. doi:10.1122/1.1574023.

Wang, F., Zheng, J., Yang, B., Jiang, J., Fu, Y. and Li, D. (2015) 'Effects of vegetarian diets on blood lipids: a systematic review and meta-analysis of randomized controlled trials', *Journal of the American Heart Association*, 4 (10). doi:10.1161/JAHA.115.002408.

Wang, L., Dong, J. lin, Zhu, Y. ying, Shen, R. ling, Wu, L. gen and Zhang, K. yi (2021a) 'Effects of microwave heating, steaming, boiling and baking on the structure and functional properties of quinoa (*Chenopodium quinoa* Willd.) protein isolates', *International Journal of Food Science and Technology*, 56 (2), pp. 709–720. doi:10.1111/ijfs.14706.

Wang, W., Cui, C., Wang, Q., Sun, C., Jiang, L. and Hou, J. (2019a) 'Effect of pH on physicochemical properties of oil bodies from different oil crops', *Journal of Food Science and Technology*, 56 (1), pp. 49–58. doi:10.1007/s13197-018-3453-y.

Wang, X., Qiao, C., Song, K., Jiang, S. and Yao, J. (2021b) 'Hofmeister effect on the viscosity properties of gelatin in dilute solutions', *Colloids and Surfaces B: Biointerfaces*, 206, pp. 111944. doi:10.1016/j.colsurfb.2021.111944.

Wang, Y.J. and Wang, L. (2000) 'Structures and properties of commercial maltodextrins from corn, potato, and rice starches', *Starch/Staerke*, 52 (7–8), pp. 296–304. doi:10.1002/1521-379x(20009)52:8/9<296::aid-star296>3.0.co;2-a.

Wang, Z., Dekkers, B.L., Boom, R. and van der Goot, A.J. (2019b) 'Maltodextrin promotes calcium caseinate fibre formation through air inclusion', *Food Hydrocolloids*, 95, pp. 143–151. doi:10.1016/j.foodhyd.2019.04.028.

Westphalen, A.D., Briggs, J.L. and Lonergan, S.M. (2005) 'Influence of pH on rheological properties of porcine myofibrillar protein during heat induced gelation', *Meat Science*, 70 (2), pp. 293–299. doi:10.1016/j.meatsci.2005.01.015.

White, D.A., Fisk, I.D. and Gray, D.A. (2006) 'Characterisation of oat (*Avena sativa* L.) oil bodies and intrinsically associated E-vitamers', *Journal of Cereal Science*, 43 (2), pp. 244–249. doi:10.1016/j.jcs.2005.10.002.

White, D.A., Fisk, I.D., Makkhun, S. and Gray, D.A. (2009) 'In vitro assessment of the bioaccessibility of tocopherol and fatty acids from sunflower seed oil bodies', *Journal of Agricultural and Food Chemistry*, 57 (13), pp. 5720–5726. doi:10.1021/jf9003412.

White, D.A., Fisk, I.D., Mitchell, J.R., Wolf, B., Hill, S.E. and Gray, D.A. (2008) 'Sunflower-seed oil body emulsions: rheology and stability assessment of a natural emulsion', *Food Hydrocolloids*, 22 (7), pp. 1224–1232. doi:10.1016/j.foodhyd.2007.07.004.

WHO/FAO/UNU (2007) 'Protein and amino acid requirements in human nutrition', *WHO Technical Report Series*, 935.

Whole Grains Council, Food and Agriculture Organization of the United Nations (FAO) and Whole Grains Council (2020) *Quinoa*. Available at: https://wholegrainscouncil.org/ (Accessed: 21 January 2024).

Williams, C.M., Thomas, R.H., MacMillan, H.A., Marshall, K.E. and Sinclair, B.J. (2011) 'Triacylglyceride measurement in small quantities of homogenised insect tissue: comparisons and caveats', *Journal of Insect Physiology*, 57 (12), pp. 1602–1613. doi:10.1016/j.jinsphys.2011.08.008.

Williams, M.A.K., Fabri, D., Hubbard, C.D., Lundin, L., Foster, T.J., Clark, A.H., Norton, I.T., Lorén, N. and Hermansson, A.M. (2001) 'Kinetics of droplet growth in gelatin/maltodextrin mixtures following thermal quenching', *Langmuir*, 17 (11), pp. 3412–3418. doi:10.1021/la001811j.

Wilson, E.K. (2007) 'A renaissance for Hofmeister', *Chemical and Engineering News*, 85 (48), pp. 47–49. doi:10.1021/cen-v085n048.p047.

Wolf, B. and Frith, W.J. (2003) 'String phase formation in biopolymer aqueous solution blends', *Journal of Rheology*, 47 (5), pp. 1151–1170. doi:10.1122/1.1603238.

Wolf, B., Frith, W.J. and Norton, I.T. (2001) 'Influence of gelation on particle shape in sheared biopolymer blends', *Journal of Rheology*, 45 (5), pp. 1141–1157. doi:10.1122/1.1389312.

Wolf, B., Frith, W.J., Singleton, S., Tassieri, M. and Norton, I.T. (2001) 'Shear behaviour of biopolymer suspensions with spheroidal and cylindrical particles', *Rheologica Acta*, 40 (3), pp. 238–247. doi:10.1007/s003970000133.

Wolf, B., Scirocco, R., Frith, W.J. and Norton, I.T. (2000) 'Shear-induced anisotropic microstructure in phase-separated biopolymer mixtures', *Food Hydrocolloids*, 14 (3), pp. 217–225. doi:10.1016/S0268-005X(99)00062-4.

Wood, S.G., Lawson, L.D., Fairbanks, D.J., Robison, L.R. and Andersen, W.R. (1993) 'Seed lipid content and fatty acid composition of three quinoa cultivars'. *Journal of Food Composition and Analysis*. 6 (1) pp. pp. 41–44. doi:10.1006/jfca.1993.1005.

Xiong, Y.L. (2018) "Muscle proteins." In *Proteins in Food Processing*. 2nd ed. Elsevier. pp. pp. 127–148. doi:10.1016/B978-0-08-100722-8.00006-1.

Yang, J., Berton-Carabin, C.C., Nikiforidis, C. V., van der Linden, E. and Sagis, L.M.C. (2022a) 'Competition of rapeseed proteins and oleosomes for the air-water interface and its effect on the foaming properties of protein-oleosome mixtures', *Food Hydrocolloids*, 122, pp. 107078. doi:10.1016/j.foodhyd.2021.107078.

Yang, M.C., Scriven, L.E. and Macosko, C.W. (1986) 'Some rheological measurements on magnetic iron oxide suspensions in silicone oil', *Journal of Rheology*, 30 (5), pp. 1015–1029. doi:10.1122/1.549892.

Yang, Z., de Campo, L., Gilbert, E.P., Knott, R., Cheng, L., Storer, B., Lin, X., Luo, L., Patole, S. and Hemar, Y. (2022b) 'Effect of NaCl and CaCl2 concentration on the rheological and structural characteristics of thermally-induced quinoa protein gels', *Food Hydrocolloids*, 124, pp. 107350. doi:10.1016/j.foodhyd.2021.107350.

Yin, B., Zhang, R. and Yao, P. (2015) 'Influence of pea protein aggregates on the structure and stability of pea protein/soybean polysaccharide complex emulsions', *Molecules*, 20 (3), pp. 5165–5183. doi:10.3390/molecules20035165.

Yokoyama, Y., Barnard, N.D., Levin, S.M. and Watanabe, M. (2014) 'Vegetarian diets and glycemic control in diabetes: a systematic review and meta-analysis.', *Cardiovascular diagnosis and therapy*, 4 (5), pp. 373–82. doi:10.3978/j.issn.2223-3652.2014.10.04.

Yuan, C., Chen, M., Luo, J., Li, X., Gao, Q. and Li, J. (2017) 'A novel water-based process produces eco-friendly bio-adhesive made from green cross-linked soybean soluble polysaccharide and soy protein', *Carbohydrate Polymers*, 169, pp. 417–425. doi:10.1016/j.carbpol.2017.04.058.

Zaslavsky, B.Y. (1995) *Aqueous two-phase partitioning - Physical chemistry and bioanalytical applications*. New York: Marcel Dekker Inc.

Zayas, J.F. (1997) "Water holding capacity of proteins." In *Functionality of Proteins in Food*. Berlin, Heidelberg: Springer. pp. pp. 76–133. doi:10.1007/978-3-642-59116-7_3.

Zhang, P., Bari, V. Di, Briars, R., Taher, Z.M., Yuan, J., Liu, G. and Gray, D.A. (2017) 'Influence of pecan nut pretreatment on the physical quality of oil bodies', *Journal of Food Quality*, 2017, pp. 1–9. doi:10.1155/2017/3864126.

Zhang, Y. and Cremer, P.S. (2009) 'The inverse and direct Hofmeister series for lysozyme', *Proceedings of the National Academy of Sciences of the United States of America*, 106 (36), pp. 15249–15253. doi:10.1073/pnas.0907616106.

Zhang, Y. and Cremer, P.S. (2010) 'Chemistry of hofmeister anions and osmolytes', *Annual Review of Physical Chemistry*, 61, pp. 63–83. doi:10.1146/annurev.physchem.59.032607.093635.

Zhao, Y., Yuan, Y., Yuan, X., Zhao, S., Kang, Z., Zhu, M., He, H. and Ma, H. (2023) 'Physicochemical, conformational and functional changes of quinoa protein affected by high-pressure homogenization', *LWT - Food Science and Technology*, 173, pp. 114343. doi:10.1016/j.lwt.2022.114343.

Zheng, B., Zhang, X., Peng, S. and Julian McClements, D. (2019) 'Impact of curcumin delivery system format on bioaccessibility: nanocrystals, nanoemulsion droplets, and natural oil bodies', *Food & Function*, 10 (7), pp. 4339–4349. doi:10.1039/C8FO02510J.

Zheng, M., Jin, Z. and Zhang, Y. (2007) 'Effect of cross-linking and esterification on hygroscopicity and surface activity of cassava maltodextrins', *Food Chemistry*, 103 (4), pp. 1375–1379. doi:10.1016/j.foodchem.2006.10.053.

Zhou, K., Slavin, M., Lutterodt, H., Whent, M., Eskin, N.A.M. and Yu, L. (2012) *Cereals and Legumes*. Third Edit. Elsevier. doi:10.1016/B978-0-08-091809-9.00001-7.

Zhou, L. zheng, Chen, F. sheng, Hao, L. hua, Du, Y. and Liu, C. (2019) 'Peanut oil body composition and stability', *Journal of Food Science*, 84 (10), pp. 2812–2819. doi:10.1111/1750-3841.14801.

Zhou, X., Liu, Z., Wang, W., Miao, Y., Gu, L., Li, Y., Liu, X., Jiang, L., Hou, J. and Jiang, Z. (2022) 'NaCl induces flocculation and lipid oxidation of soybean oil body emulsions recovered by neutral aqueous extraction', *Journal of the Science of Food and Agriculture*, 102 (9), pp. 3752–3761. doi:10.1002/jsfa.11723.

Zhu, F. and Li, H. (2019) 'Effect of high hydrostatic pressure on physicochemical properties of quinoa flour', *LWT - Food Science and Technology*, 114, pp. 108367. doi:10.1016/j.lwt.2019.108367.

Appendices

Appendix A

Phase diagrams: total protein concentration

The following phase diagrams correspond to data presented in Figure 4-2 in the main text but are here presented with total protein concentration on the x-axis.

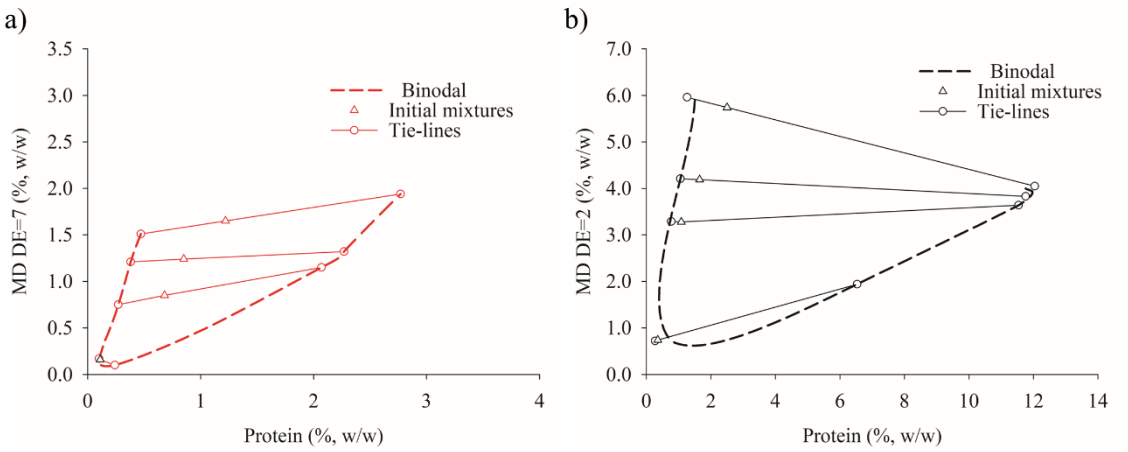

Figure A.1. Experimental phase diagrams between QPI and MD DE 7 and DE 2 at pH 7.0, 22°C and 0.1 M NaCl, showing total protein content in the x-axis: a) QPI-MD DE 7 and b) QPI-MD DE 2. Calculated considering the total protein content of QPI (obtained by total nitrogen analysis) in the UV-Vis spectrophotometer calibration curves.

Increase in the physical height of QPI-rich (bottom) phases in phase separated mixtures with an increase in MD concentration

The effect of increasing MD concentration on the physical height of bottom phases formed by phase separated QPI-MD mixtures was examined to allow comparison to other systems previously studied in the literature. Data shows that the bottom phase height increased with MD concentration.

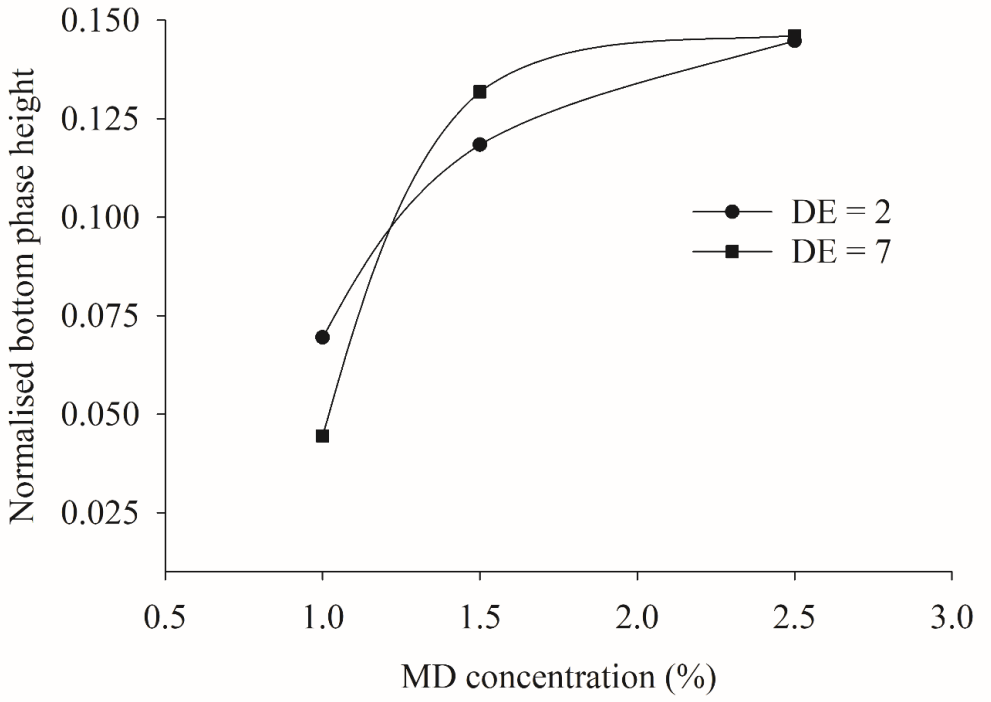

Figure A.2. Normalised bottom phase (QPI-rich) height of 1.5% QPI and *x*% MD mixtures, where *x* = 1, 1.5 and 2.5. The lines in the figure are guides for the eye. The normalised bottom phase height was calculated by dividing the bottom phase height (cm) by the total mixture height (cm) in the graduated centrifuge tubes.

Micrograph of QPI stock solution

The QPI stock solution was observed by phase contrast light microscopy prior to mixture with MD. Large fractal aggregates appeared as bright structures, as shown in Figure A.3 below.

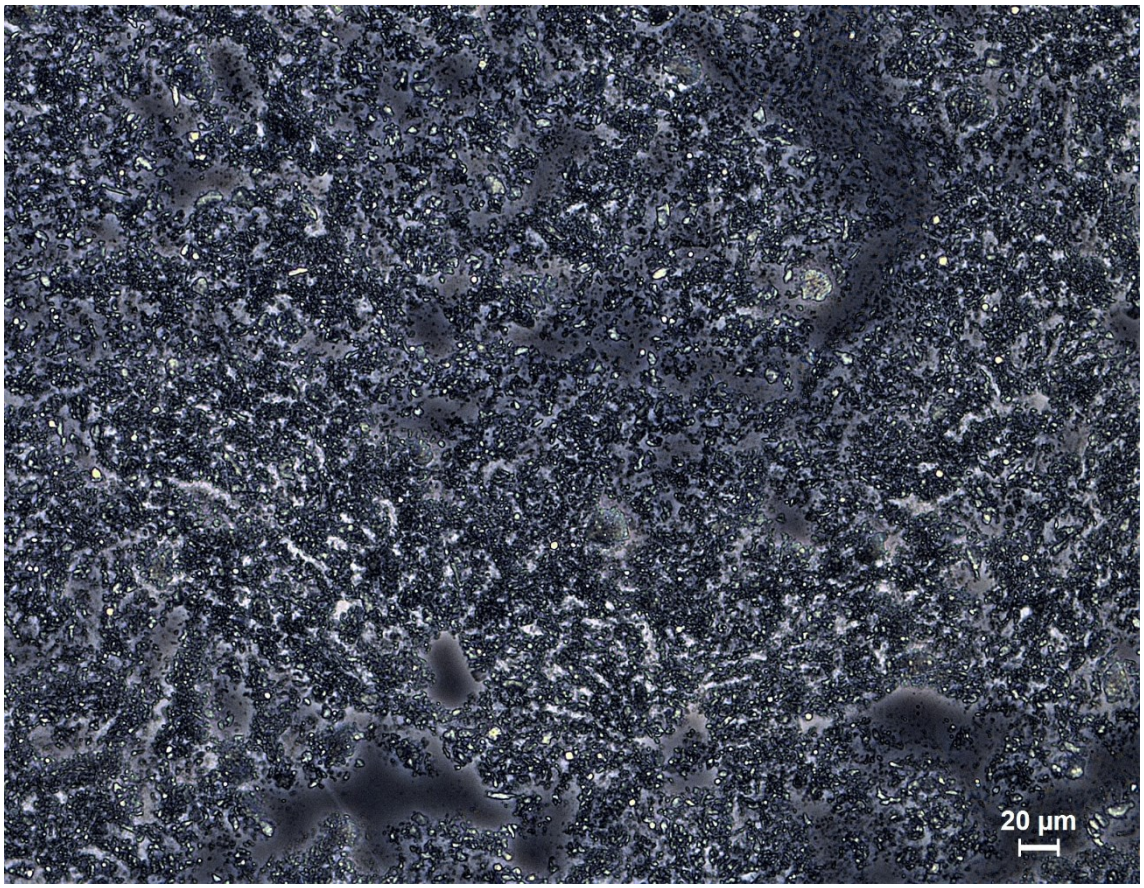

Figure A.3. Light micrograph of QPI stock solution.

Effect of the absence of salt on the phase behaviour or QPI-MD mixtures

Salt can alter phase segregation, so the effect of the removal of salt from QPI-MD mixtures was examined. Large heterogeneous structures ~50 – 100 μm in diameter, corresponding to protein, were observed in both mixtures of QPI-MD DE 7 and QPI-MD DE 2, as well as HTQPI-MD DE 2 in the absence of salt (Figure A.4). Under these conditions, the absence of salt appears to result in lower initial protein aggregation in comparison to the initial mixtures of QPI-MD in the presence of NaCl (Figure 4-4b and e), although small protein clusters can still be observed (Figures A.4a and b). In contrast, the initial mixture of HTQPI-MD DE 2 in the absence of salt (Figure A.4c), where the protein was heat-treated, showed similar initial protein self-association both in the absence and presence of salt (Figure 4-6c).

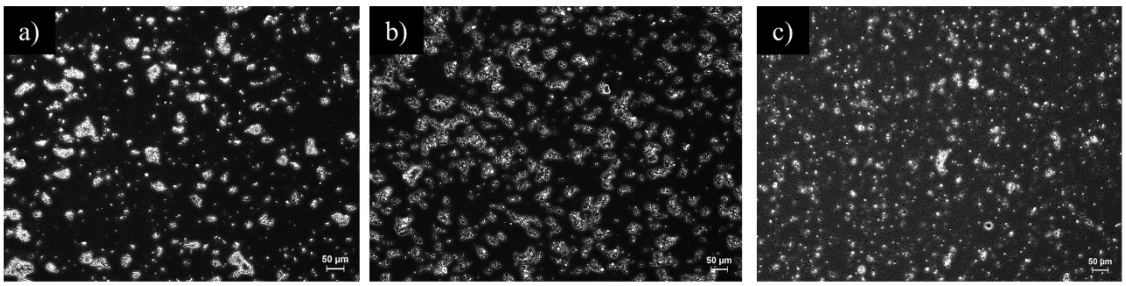

Figure A.4. Light micrographs of the initial mixtures of each QPI-MD system in the absence of salt: a) QPI-MD DE 7 (1.6% QPI + 1.4% MD); b) QPI-MD DE 2 (2.7% QPI + 4.6% MD); c) HTQPI-MD DE 2 (0.8% QPI + 2.2% MD). Bright structures correspond to protein. The scale bar represents 50 μm.

Appendix B

Soluble protein content

Table B.1 and B.2 correspond to data presented in Figure 5-1 in the main text, to facilitate data visualisation and analysis.

Table B.1. Soluble protein content (%) at different pH values for QPI precipitated with HCl (QPI-H), acetic acid (QPI-A) or citric acid (QPI-C).

	Protein isolates (1%, w/w)		
pH	QPI-H	QPI-A	QPI-C
6	$30.8 \pm 3.6^{b,C}$	$63.5 \pm 3.2^{a,B}$	$62.7 \pm 2.3^{a,B}$
7	$42.3 \pm 3.0^{b,B}$	$71.8 \pm 2.3^{a,A}$	$66.8 \pm 2.6^{a,AB}$
8	$50.4 \pm 3.6^{b,AB}$	$72.2 \pm 0.6^{a,A}$	$71.2 \pm 1.0^{a,A}$
9	$55.8 \pm 2.2^{b,A}$	$69.8 \pm 2.1^{a,A}$	$68.9 \pm 3.9^{a,AB}$

Equal lowercase letters in the same row and equal uppercase letters in the same column indicate that there is no significant difference between the means (Tukey's test, $p > 0.05$).

Table B.2. Soluble protein content (%) for different concentrations of QPI precipitated with HCl (QPI-H), acetic acid (QPI-A) or citric acid (QPI-C).

	Protein isolates (pH 6.8 ± 0.2)		
Concentration (%, w/w)	QPI-H	QPI-A	QPI-C
1	$42.3 \pm 3.0^{b,A}$	$71.8 \pm 2.3^{a,A}$	$66.8 \pm 2.6^{a,AB}$
5	$42.6 \pm 1.7^{b,A}$	$68.5 \pm 6.1^{a,A}$	$71.5 \pm 2.8^{a,A}$
10	$39.1 \pm 1.3^{b,AB}$	$58.6 \pm 2.8^{a,B}$	$63.3 \pm 3.1^{a,BC}$
15	$33.9 \pm 4.3^{c,B}$	$48.8 \pm 1.2^{b,C}$	$57.0 \pm 1.9^{a,C}$
20	$19.6 \pm 0.4^{c,C}$	$29.7 \pm 1.9^{b,D}$	$37.3 \pm 3.3^{a,D}$

Equal lowercase letters in the same row and equal uppercase letters in the same column indicate that there is no significant difference between the means (Tukey's test, $p > 0.05$).

Microstructure of QPI gels

Figures B.1 and B.2 correspond to the confocal laser scanning microscopy images of heat-induced 10% (w/w) and 20% (w/w) QPI gels shown in Figure 5-5 in the main text. Here, the images show the microstructure of each gel stained for either the protein or lipid alone to allow separate visualisation and analysis.

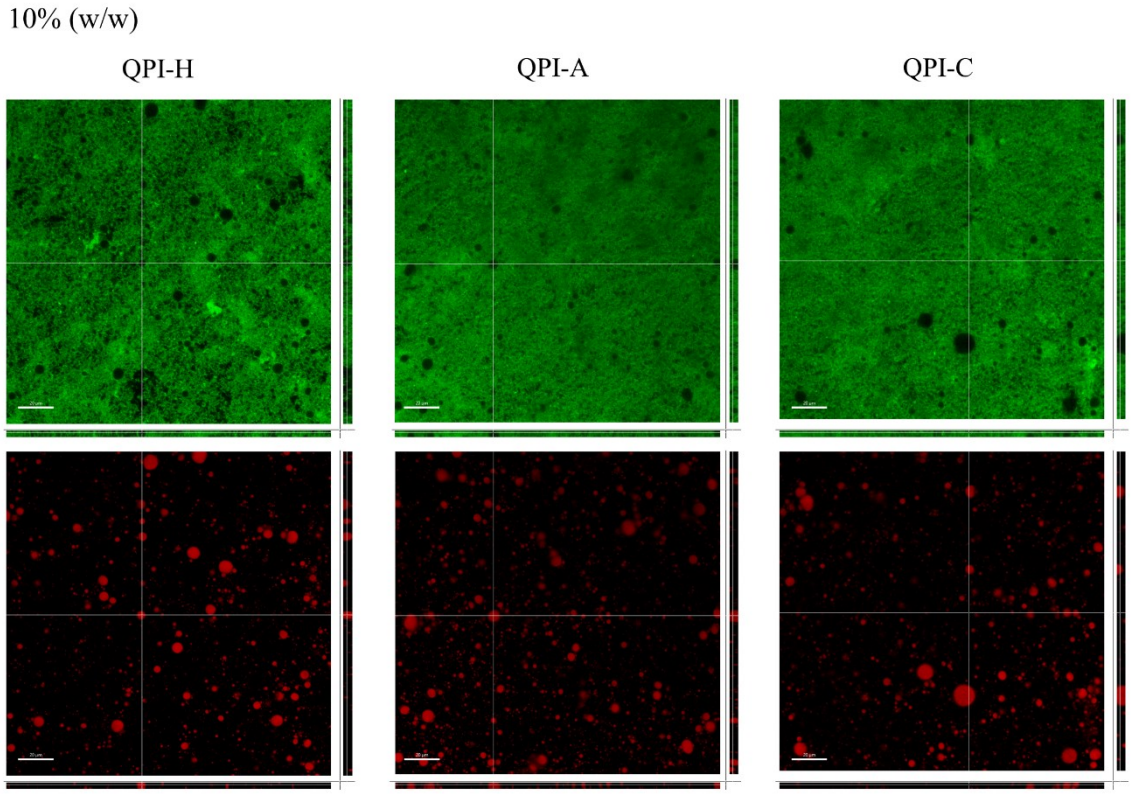

Figure B.1. Confocal laser scanning microscopy images showing the cross-sections of heat-induced gels of 10% (w/w) QPI precipitated with HCl (QPI-H), acetic acid (QPI-A) or citric acid (QPI-C). Protein structures are stained green and lipid droplets are stained red. The scale bars represent 20 μm. The samples are shown in cross section, where the projection in the x-z and y-z direction is shown adjacent to the x-y image.

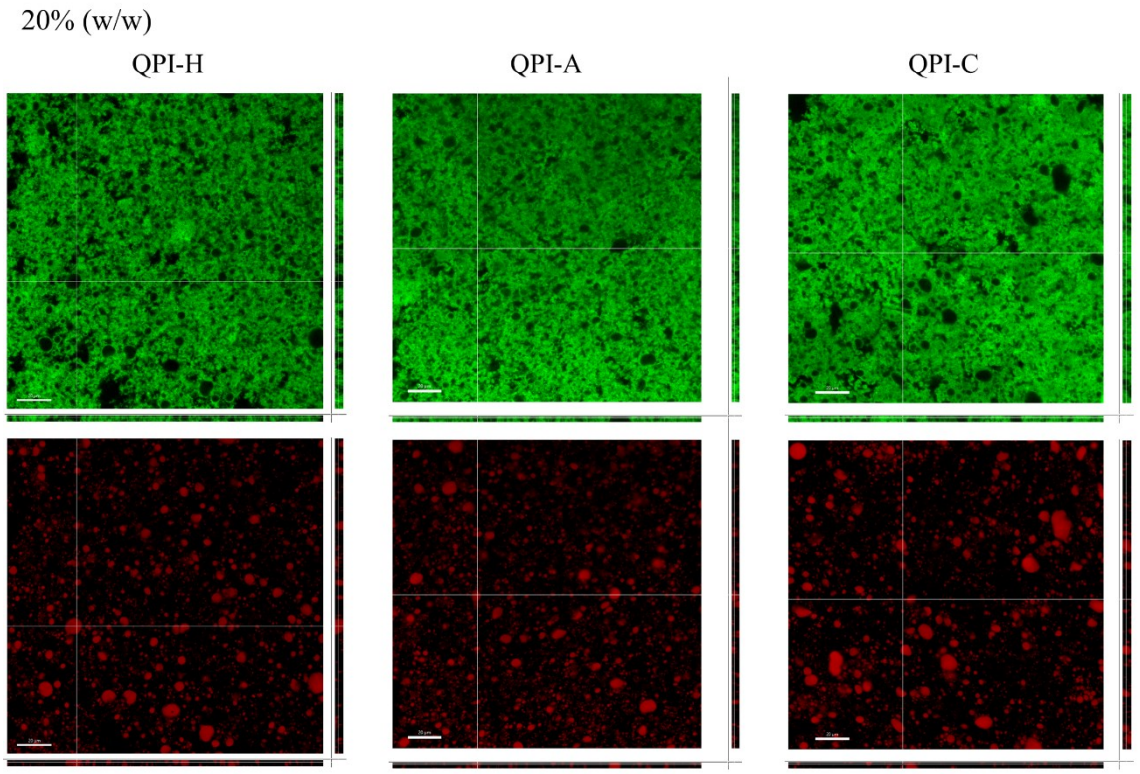

Figure B.2. Confocal laser scanning microscopy images showing the cross-sections of heat-induced gels of 20% (w/w) QPI precipitated with HCl (QPI-H), acetic acid (QPI-A) or citric acid (QPI-C). Protein structures are stained green and lipid droplets are stained red. The scale bars represent 20 µm. The samples are shown in cross section, where the projection in the x-z and y-z direction is shown adjacent to the x-y image.

Rheological properties of QPI gels

The gelation properties of 10% (w/w) and 20% (w/w) QPI were investigated by temperature sweeps recording the storage (G') and loss (G") modulus by heating the samples from 20 °C to 90 °C at a heating rate of 1 °C/min, holding for 5 min at 90 °C, followed by cooling to 20 °C at 1 °C/min, using 1% strain and an angular frequency of 10 rad/s (Figure 5-7 in the main text). Immediately afterwards, without removing the sample from the gap, a time sweep (1% strain and 10 rad/s frequency) of 5 min at 20 °C, was performed, and the results are shown in Figure B.3. G' and G" values remained

relatively constant throughout the time sweeps, showing that gel formation and restructuring reached steady state at 20 °C.

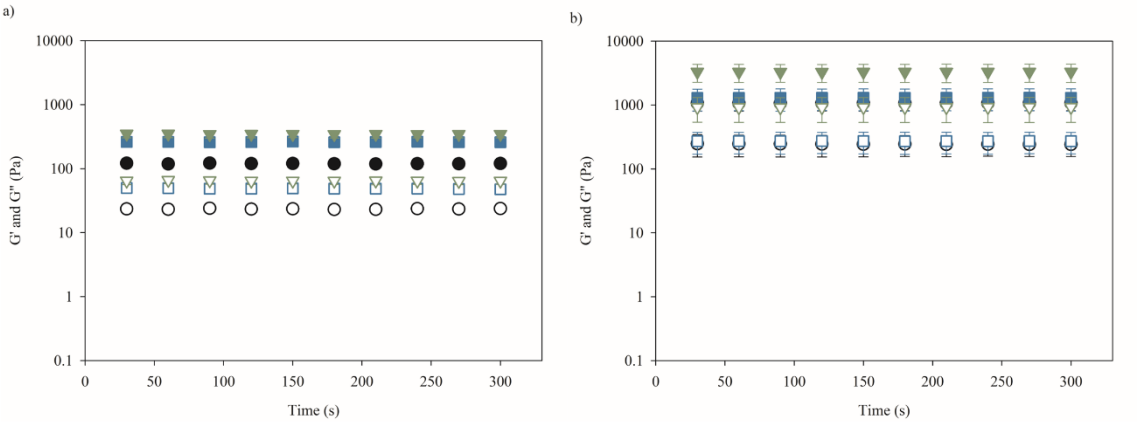

Figure B.3. Time sweeps of gels of (a) 10% and (b) 20% (w/w) QPI precipitated with HCl (QPI-H, ● black), acetic acid (QPI-A, ■ blue) and citric acid (QPI-C, ▼ green). Closed symbols represent the elastic modulus (G'), open symbols represent the viscous modulus (G").

Figure B.4 shows the correlations between final gel strength (G'_{20}) values (Table 5-4 in the main text) and soluble protein content (Figure 5-1b in the main text) of QPI samples at 10% (w/w) and 20% (w/w) concentrations. Results show that G'_{20} is strongly positively correlated ($R^2 = 0.99$) to soluble protein content at 10% (w/w) concentration, while the correlation is lower ($R^2 = 0.73$) at 20% (w/w) concentration. At this higher concentration, however, QPI-C showed significantly higher ($p < 0.05$) gel strength and soluble protein content than QPI-H and QPI-A, which agrees with the contribution of native protein content to gel network formation observed for 10% (w/w) QPI samples.

Figure B.5 shows the frequency sweeps (0.1 – 100 rad/s) at 1% strain of QPI gels following the temperature sweeps and time sweeps. All samples showed a gel-like behaviour and low frequency dependences (n = 0.1 – 0.2, Table 5-4 in the main text), regardless of concentration and extraction acid.

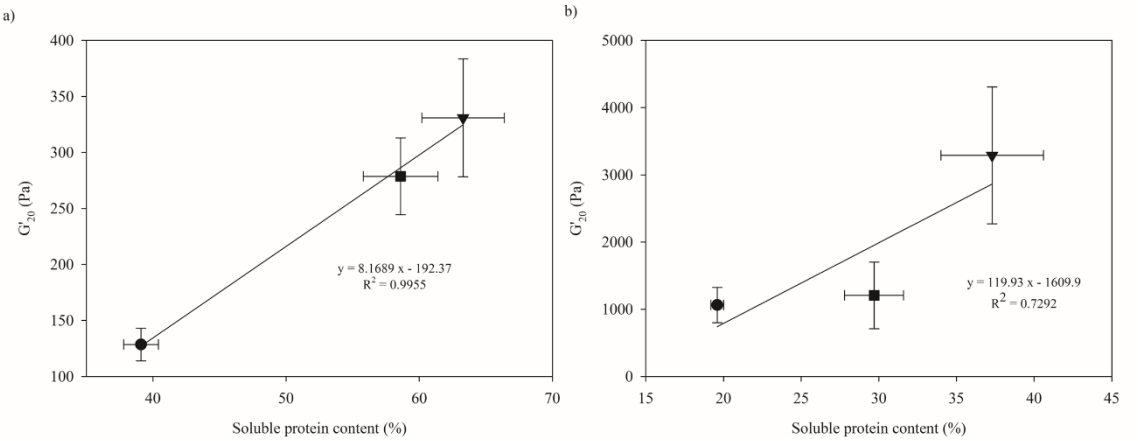

Figure B.4. Correlation between final elastic modulus (G'_{20}, Pa) and soluble protein content (%) of gels formed from (a) 10% (w/w) or (b) 20% (w/w) QPI precipitated with HCl (QPI-H, ●), acetic acid (QPI-A, ■) or citric acid (QPI-C, ▼).

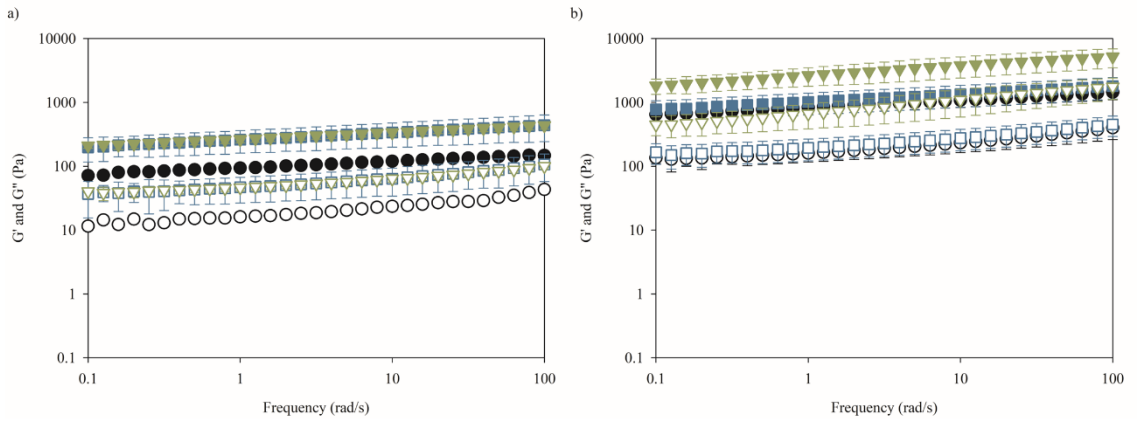

Figure B.5. Frequency sweeps for gels formed from (a) 10% (w/w) or (b) 20% QPI precipitated with HCl (QPI-H, ● black), acetic acid (QPI-A, ■ blue) and citric acid (QPI-C, ▼ green): elastic (G', closed symbols) and viscous (G", open symbols) moduli as a function of frequency.

Figure B.6 shows the amplitude sweeps (0.1 – 1000%) at 10 rad/s of QPI gels performed after frequency sweeps. All samples displayed similar linear viscoelastic (LVE) regions until the point where the structures ruptured at ~40% strain for 10% (w/w) gels and ~12% strain for 20% (w/w) gels.

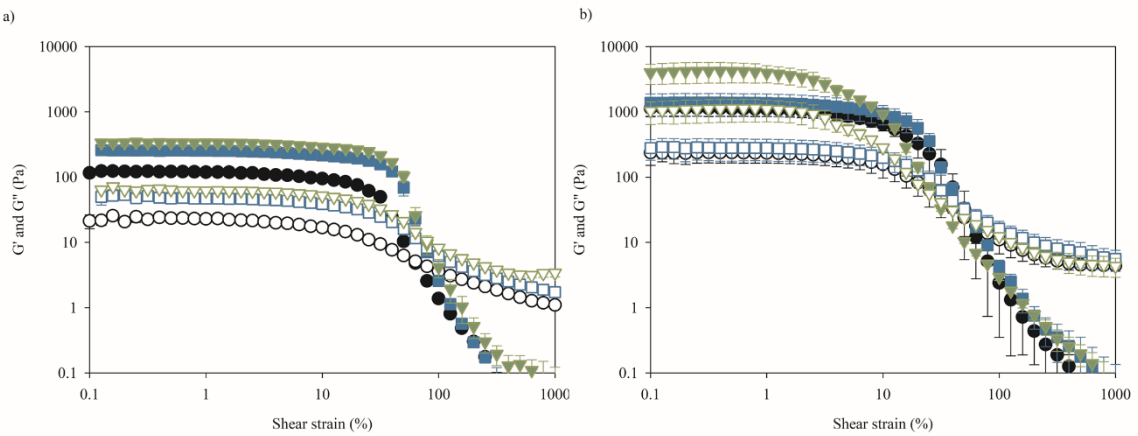

Figure B.6. Amplitude sweeps for gels formed from (a) 10% (w/w) or (b) 20% (w/w) gels of QPI protein precipitated with HCl (QPI-H, ● black), acetic acid (QPI-A, ■ blue) and citric acid (QPI-C, ▼ green): elastic (G', closed symbols) and viscous (G", open symbols) moduli as a function of shear strain.

Appendix C

Soluble protein content

Table C.1 corresponds to data presented in Figure 6-1 in the main text, to facilitate data visualisation and analysis.

Table C.1. Soluble protein content (%) in different conditions of QPI precipitated with HCl (QPI-H), acetic acid (QPI-A) and citric acid (QPI-C).

Dispersion conditions	Soluble protein content (%, w/w)		
	QPI-H	QPI-A	QPI-C
Solubilised 1h	$45.3 \pm 3.0^{b,B}$	$71.8 \pm 2.3^{a,A}$	$66.8 \pm 2.6^{a,B}$
Solubilised 24h	$76.9 \pm 3.7^{a,A}$	$71.5 \pm 2.3^{a,A}$	$75.0 \pm 2.3^{a,A}$
0.1 M NaCl	$49.3 \pm 2.1^{b,B}$	$65.5 \pm 4.8^{a,A}$	$74.8 \pm 3.9^{a,A}$
Dialysed	$11.6 \pm 2.2^{a,C}$	$14.3 \pm 1.3^{a,B}$	$13.7 \pm 2.6^{a,C}$
Dialysed + 0.1 M NaCl	$15.4 \pm 0.8^{ab,C}$	$16.2 \pm 0.7^{a,B}$	$12.7 \pm 1.7^{b,C}$

QPI-H, QPI-A and QPI-C refer to QPI precipitated with HCl, acetic acid and citric acid, respectively. Equal lowercase letters in the same row and equal uppercase letters in the same column indicate that there is no significant difference between the means (Tukey's test, $p > 0.05$).

Protein profile

Figure C.1 shows the protein profile of all non-dialysed and dialysed QPI-H, QPI-A and QPI-C under different dispersion conditions analysed by Native-PAGE and SDS-PAGE under reducing and non-reducing conditions. Figure C.1a corresponds to Figure 6-2b in the main text; Figure C.1c corresponds to Figure 6-2c in the main text and Figure C.1d corresponds to Figure 6-2d in the main text. Independently of dispersion condition, all non-dialysed samples showed intense protein bands expected from the high soluble protein content of these samples (Figure 6-1 in the main text). In contrast, all dialysed samples showed faint bands consistent with the low soluble protein content of these

samples (Figure 6-1 in the main text). The bands in dialysed samples corresponded only to globulin 11S, which indicates that globulin 7S and albumin 2S were completely denatured during dialysis.

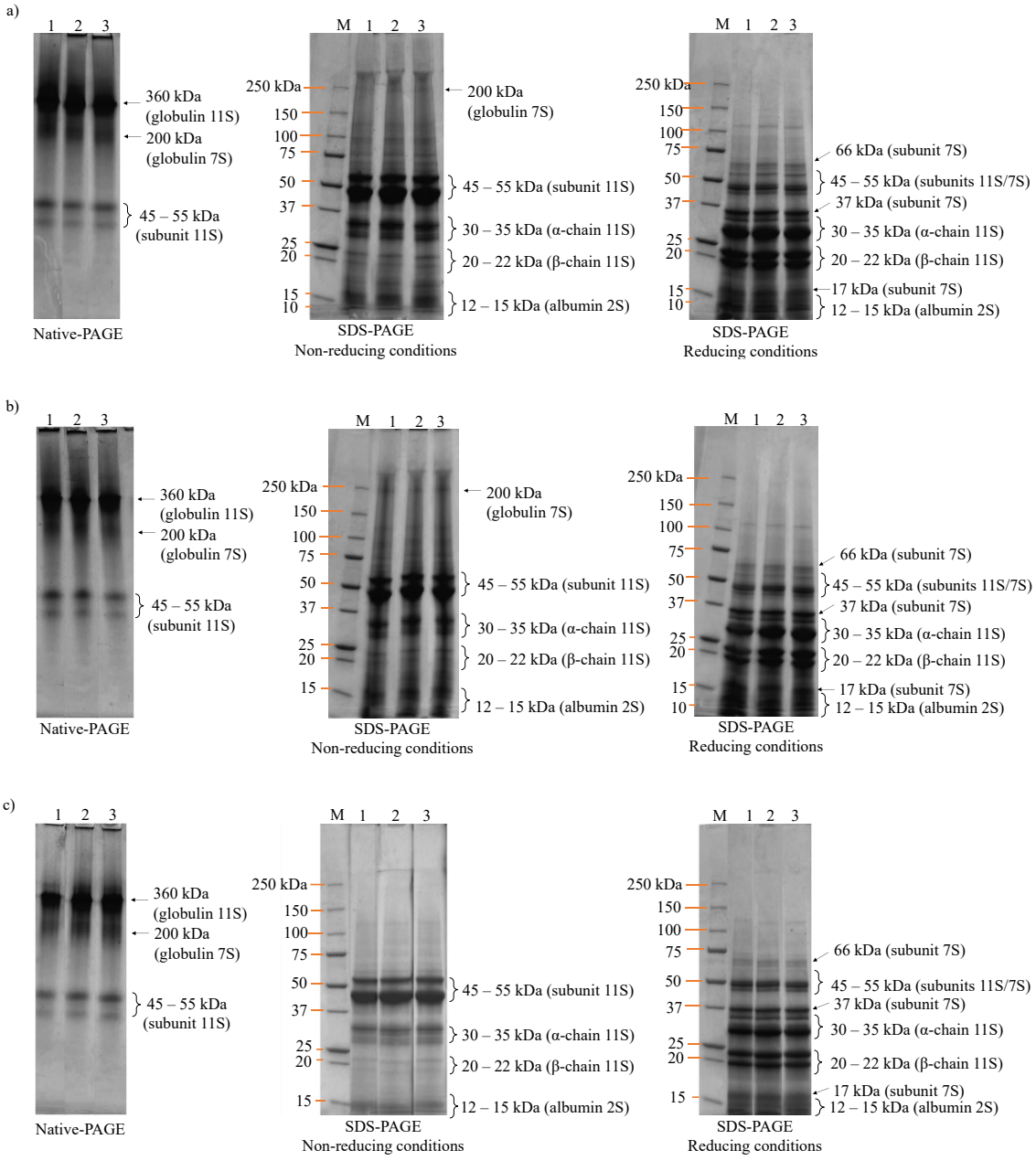

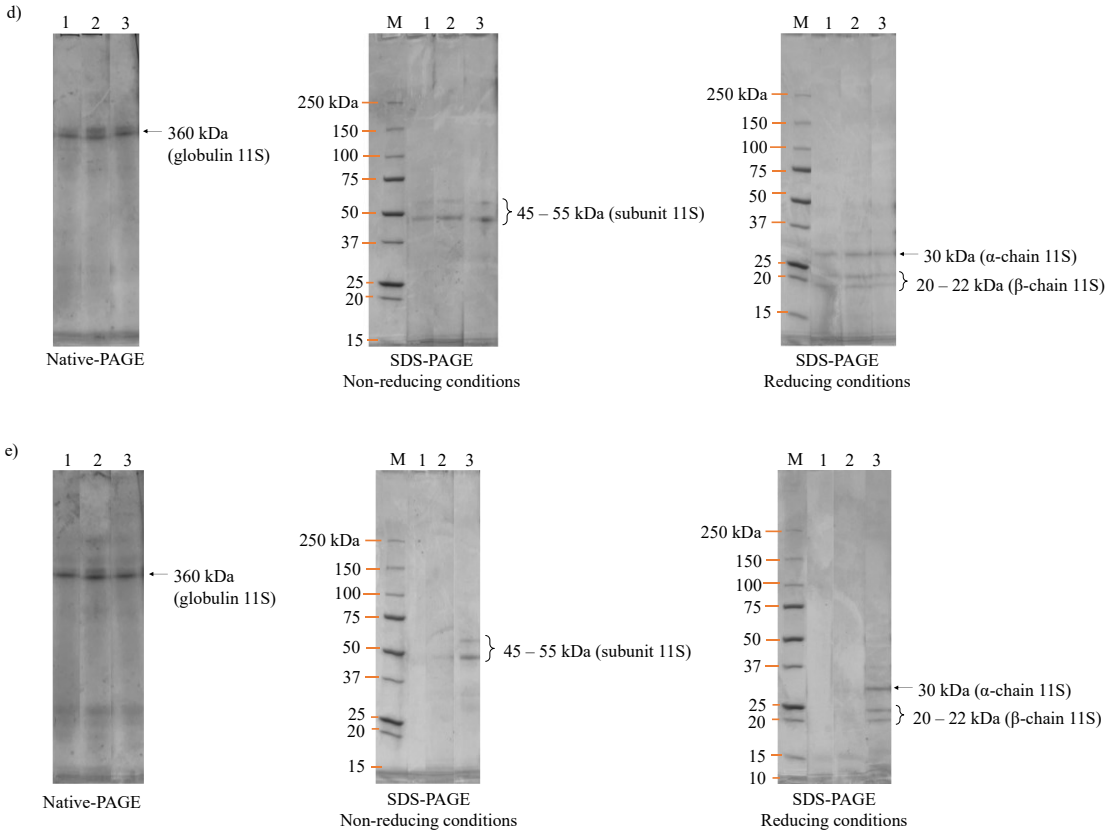

Figure C.1. Gel electrophoresis of QPI precipitated with HCl (QPI-H), acetic acid (QPI-A) and citric acid (QPI-C): a) dispersed in water for 1 h; b) dispersed in water for 24 h; c) dispersed in 0.1 M NaCl for 1 h; d) dialysed and dispersed in water for 1 h; e) dialysed and dispersed in 0.1 M NaCl for 1 h. M- protein markers; 1- QPI-H; 2- QPI-A; 3- QPI-C.

Rheological properties of QPI gels

The gelation properties of 10% (w/w) QPI samples dispersed under different conditions were monitored by temperature sweeps by heating the samples from 20 °C to 90 °C at a heating rate of 1 °C/min, holding for 5 min at 90 °C, followed by cooling to 20 °C at 1 °C/min, using 1% strain and an angular frequency of 10 rad/s while recording the storage (G') and loss (G") modulus (Figure 6-6 in the main text). Immediately afterwards, a time sweep (1% strain and 10 rad/s frequency) of 5 min at 20 °C, was performed, and the results are shown in Figure C.2. For non-dialysed samples (Figure C.2a-c), G' and G"

values remained relatively constant throughout the time sweeps, indicating that gel formation and restructuring reached steady state. For dialysed samples, G' and G" did not developed during temperature sweeps (Figure 6-6d-e in the main text), and variability was high during time sweeps (Figure C.2d-e), showing the poor gel formation in these samples.

Figure C.3 shows the frequency sweeps (0.1 – 100 rad/s) at 1% strain of QPI gels following the temperature sweeps and time sweeps. G' and G" were parallel to each other throughout the range of frequencies for all non-dialysed QPI samples, demonstrating the gel-like behaviour and low frequency dependences (n = 0.1 – 0.2, Table 6-4 in the main text) of these samples (Figure C.3a-c). Again, the frequency sweeps of dialysed samples showed large variability in G' and G" values, confirming the lack of gel formation in these samples (Figure C.3d-e). Due to this high variability, the frequency dependence was not determined for dialysed samples.

Figure C.4 shows the amplitude sweeps (0.1 – 1000%) at 10 rad/s of QPI gels following the frequency sweeps. Non-dialysed samples dispersed in water for either 1 h or 24 h showed linear viscoelastic regions (LVR) of similar lengths, with gel structures breaking at ~30% strain (Figure C.4a-b). When dispersed in 0.1 M NaCl solution, QPI-H gels presented a smaller LVR than QPI-A and QPI-C, with gel structures starting to break at ~5% strain vs ~17% (Figure C.4c). For dialysed samples, the LVR or yield stress values were not determined due to the lack of gel network formation (Figure C.4d-e).

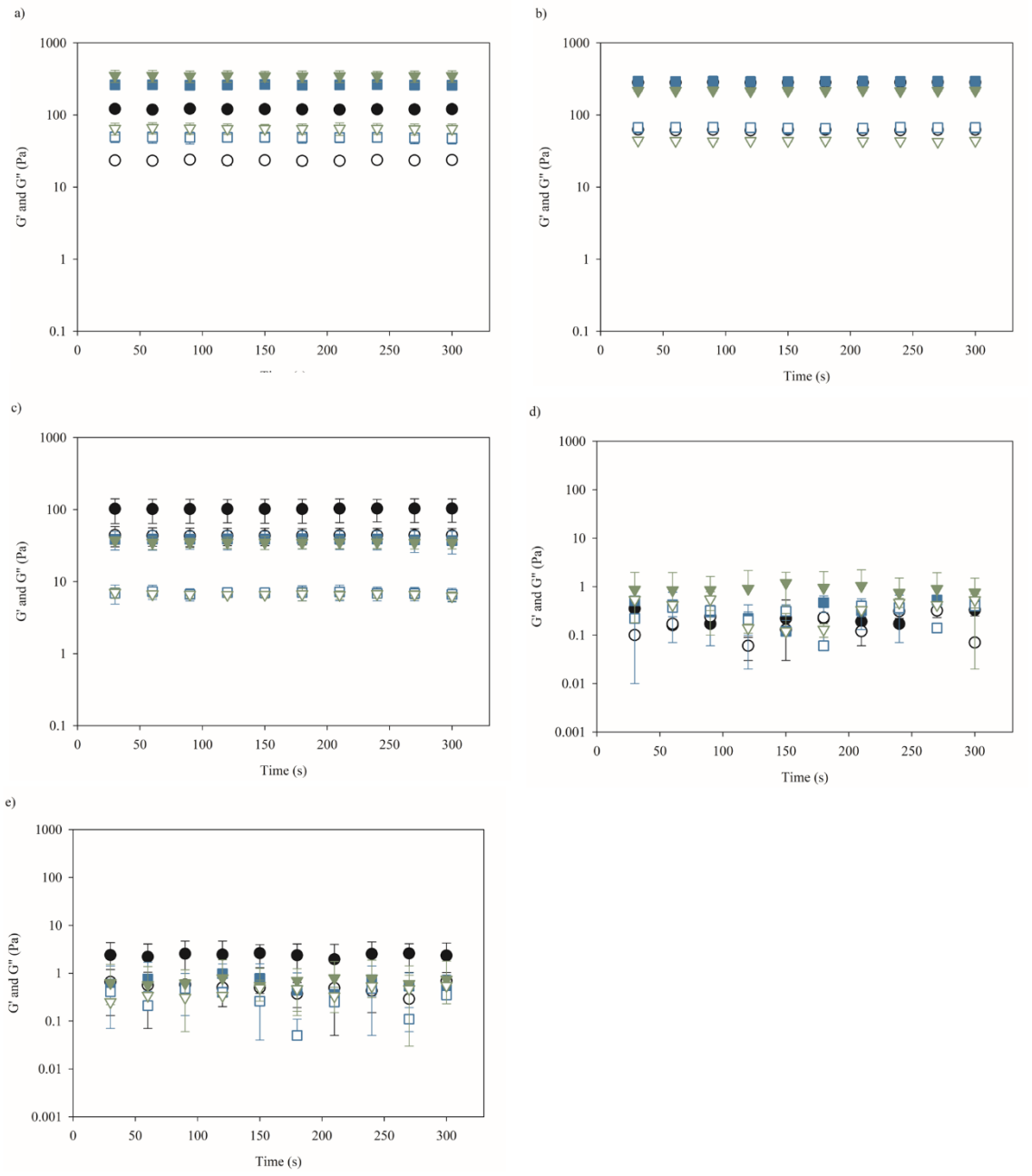

Figure C.2. Time sweeps of gels of 10% (w/w) QPI precipitated with HCl (QPI-H, ●), acetic acid (QPI-A, ■) and citric acid (QPI-C, ▼): a) solubilised for 1h; b) solubilised for 24h; c) solubilised in 0.1 M NaCl; d) dialysed and solubilised in water for 1 h; e) dialysed and solubilised in 0.1 M NaCl for 1 h. Closed symbols represent the elastic modulus (G'), open symbols represent the viscous (G") modulus. Note differences in y-axis scales.

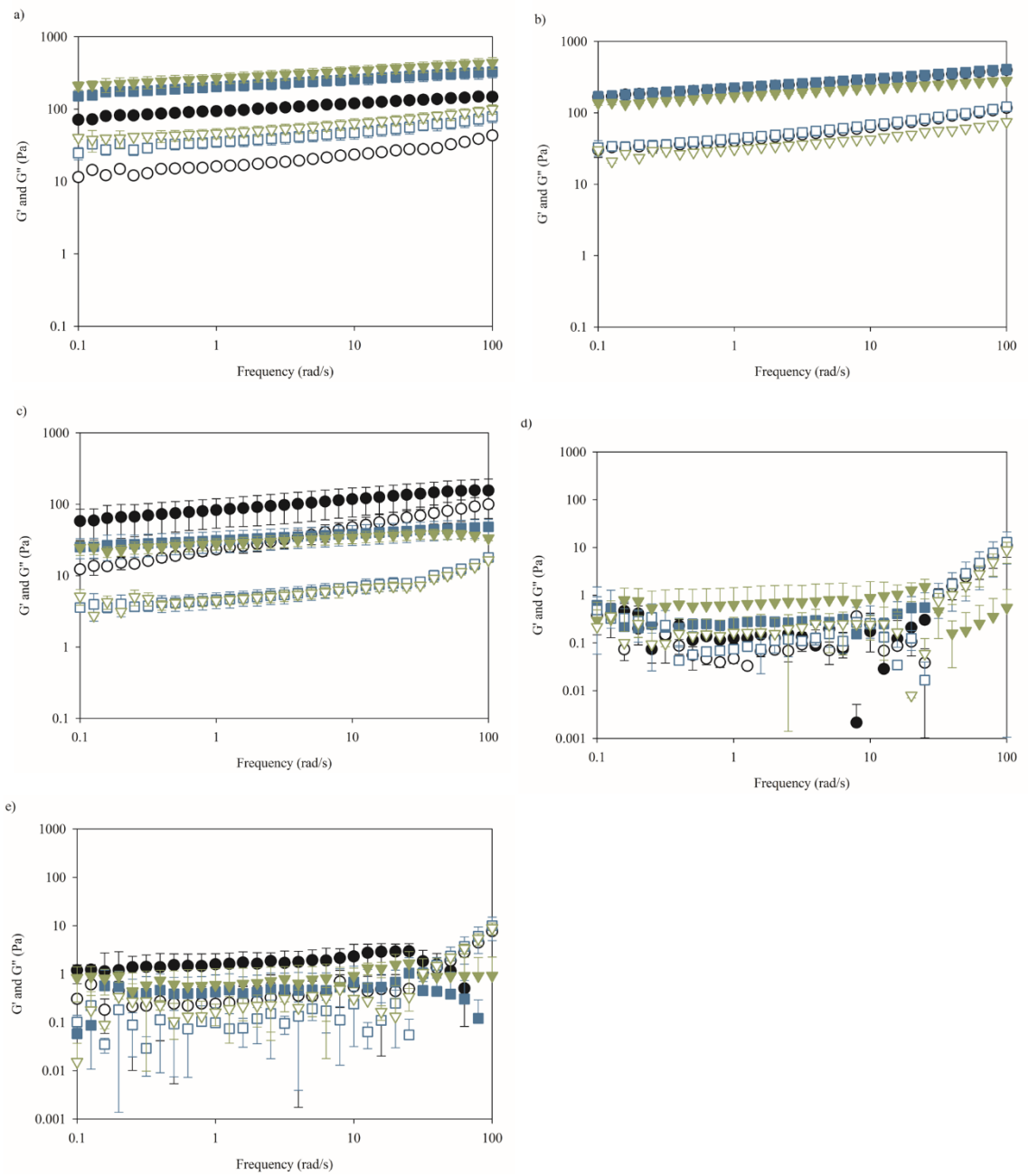

Figure C.3. Frequency sweeps of 10% (w/w) QPI precipitated with HCl (QPI-H, ● black), acetic acid (QPI-A, ■ blue) and citric acid (QPI-C, ▼ green): a) dispersed for 1 h; b) dispersed for 24 h; c) dispersed in 0.1 M NaCl; d) dialysed and dispersed in water for 1 h; e) dialysed and dispersed in 0.1 M NaCl for 1 h. Closed symbols represent the elastic modulus (G'), open symbols represent the viscous (G") modulus. Note differences in y-axis scales.

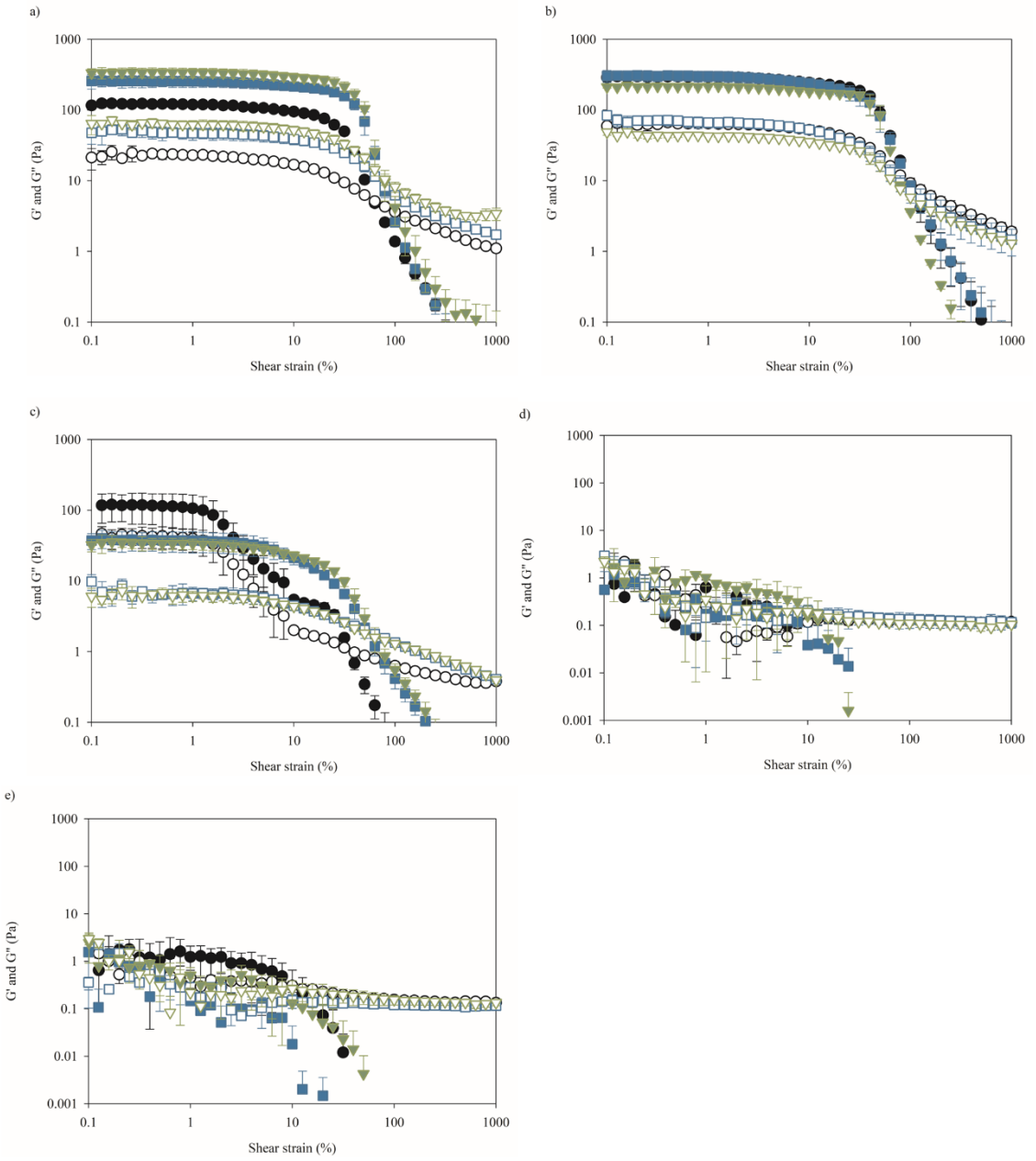

Figure C.4. Amplitude sweeps of 10% (w/w) QPI samples precipitated with HCl (QPI-H, ● black), acetic acid (QPI-A, ■ blue) and citric acid (QPI-C, ▼ green): a) dispersed for 1 h; b) dispersed for 24 h; c) dispersed in 0.1 M NaCl; d) dialysed and dispersed in water for 1 h; e) dialysed and dispersed in 0.1 M NaCl for 1 h. Closed symbols represent the elastic modulus (G'), open symbols represent the viscous (G") modulus. Note differences in y-axis scales.

Appendix D

Fatty acids composition of QPI and oil body emulsion

The fatty acid composition of the oil body (OB) emulsion produced after cryo-milling and of the lipids extracted in the QPI precipitated with three different acids, as determined by GC-MS (Table D.1).

Table D.1. Fatty acid composition of the oil body (OB) emulsion after cryo-milling and QPI precipitated with HCl (QPI-H), acetic acid (QPI-A) or citric acid (QPI-C).

Fatty acids		Composition (%, w/w)			
		OB emulsion	QPI-H	QPI-A	QPI-C
Palmitic acid	C16:0	9.6 ±< 0.1[a]	9.5 ± 0.1[a]	9.9 ± 0.1[a]	9.7 ±< 0.1[a]
Stearic acid	C18:0	0.0 ±< 0.1[a]	0.3 ± 0.2[a]	0.6 ±< 0.1[a]	0.4 ± 0.2[a]
Isooleic acid	C18:1 (10)	23.3 ± 0.1[a]	23.3 ± 0.2[a]	23.6 ±< 0.1[a]	23.2 ±< 0.1[a]
Linoleic acid	C18:2 (9, 12)	53.6 ±< 0.1[a]	53.1 ± 0.4[a]	53.1 ±< 0.1[a]	53.2 ± 0.2[a]
α-linolenic acid	C18:3 (9, 12, 15)	5.9 ± 0.1[a]	5.9 ± 0.1[a]	5.7 ±< 0.1[a]	5.9 ±< 0.1[a]
Gondoic acid	C20:1	1.7 ±< 0.1[a]	1.5 ± 0.1[a]	1.7 ±< 0.1[a]	1.8 ± 0.1[a]
Erucic acid	C22:1	2.4 ±< 0.1[a]	2.3 ± 0.2[a]	2.4 ± 0.1[a]	2.8 ± 0.1[a]
Squalene	C30:6	3.5 ±< 0.1[a]	4.2 ± 0.6[a]	3.0 ± 0.1[a]	3.1 ± 0.1[a]
Total unsaturated FAME		90.4 ±< 0.1[a]	90.2 ± 0.1[a]	89.4 ± 0.1[a]	89.9 ± 0.3[a]
Total saturated FAME		9.6 ±< 0.1[a]	9.8 ± 0.1[a]	10.6 ± 0.1[a]	10.1 ± 0.3[a]

Equal lowercase letters in the same row indicate that there is no significant difference among the means (Tukey's test, $p > 0.05$).